

Establishment and survival of coastal mangrove trees under mechanical disturbances

Rosanna van Hespén

ISBN number: 978-90-6266-646-1

USES Series number: 277

Copyright © 2023 Rosanna van Hespen. All rights reserved. No part of this publication may be reproduced in any form, by print or photo print, microfilm or any other means, without written permission by the publisher.

The research presented in this thesis was carried out at the Department of Estuarine and Delta Systems (EDS) of the Royal Netherlands Institute for Sea Research (NIOZ) in Yerseke, the Netherlands, and at the School of Marine Science at the Sun Yat-Sen University in Zhuhai, China, and was financially supported by the Joint Research Project Sustainable Deltas by the Dutch Research Council (NWO), the National Natural Science Foundation of China (NSFC), and the Engineering and Physical Sciences Research Council (EPSRC) as part of the project “Applying nature-based coastal defence to the world’s largest urban area” (ANCODE), with project numbers ALWSD.2016.026 (NWO), 51761135022 (NSFC), and EP/R024537/1 (EPSRC). Printing this thesis was financially supported by NIOZ.

This thesis is printed on recycled paper.

Cover illustration: Rosanna van Hespen

Cover formatting: Margot Stoete

Printed by: Ipskamp Printing, Enschede, The Netherlands

Author contact: rosannavanhespen@gmail.com

Establishment and survival of coastal mangrove trees under mechanical disturbances

Vestiging en overleving van mangrovebomen bij mechanische verstoringen aan de kust

(met een samenvatting in het Nederlands)

Proefschrift

ter verkrijging van de graad van doctor aan de
Universiteit Utrecht
op gezag van de
rector magnificus, prof.dr. H.R.B.M. Kummeling,
ingevolge het besluit van het college voor promoties
in het openbaar te verdedigen op

woensdag 12 april 2023 des middags te 2.15 uur

door

Rosanna van Hespen

geboren op 13 maart 1992
te Enschede

Promotoren:

Prof. dr. T.J. Bouma

Prof. dr. Z. Hu

Copromotor:

Dr. T.J.W. Ysebaert

Beoordelingscommissie:

Dr. ir. E.M. Horstman

Prof. dr. ir. L. Poorter

Dr. M.W. Skov

Prof. dr. M.B. Soons

Prof. dr. D. van der Wal

Contents

General introduction	1
1 <i>Introduction</i>	
Mangrove forests as a nature-based solution for coastal flood protection: biophysical and ecological considerations	6
2 Identifying trait-based tolerance to sediment dynamics during seedling establishment across eight mangrove species	28
3 Unravelling mangrove tree stability as a function of root morphology and sediment type using 3D-printed mimics	66
4 Analysis of coastal storm damage resistance in successional mangrove species	100
5 <i>Synthesis</i>	136
A How can nature protect people against sea-level rise?	148
Summary Samenvatting	155
Acknowledgements	162
Curriculum Vitae	166
References	168

General introduction

Under the unprecedented consequences of anthropogenic global change, including sea-level rise and changing storm patterns, our world needs innovative solutions to warrant flood safety along our coasts (Hinkel et al., 2014; IPCC, 2022). Nature-based flood defence is such a possible solution, and uses coastal ecosystems as part of a flood defence scheme (Borsje et al., 2011; Temmerman et al., 2013). Along sub- and tropical coastlines mangrove forests have gained particular interest for nature-based flood defence. The sturdy mangrove tree structures can reduce the flow energy of waves and may potentially lower storm surges (McIvor et al., 2015), thereby substantially reducing damage on the landward side of the forest (Del Valle et al., 2019). Accordingly, wider and denser mangrove forests that contain more trees can provide more flood safety (Mazda et al., 1997; Quang Bao, 2011). However, integrating mangrove forests in a nature-based flood defence, i.e. partially relying on trees for flood safety, requires in-depth knowledge of mangrove presence and functioning over multiple decades (CIRIA et al., 2013). Yet, estimating the decadal size and resilience of mangrove forests is currently challenging, as seedling establishment and tree mortality cause mangrove forests to fluctuate in size across space and time, and massive disturbances like storms can reduce the structural integrity of the forest.

At the seaward forest fringe, establishment and survival are, among other physical drivers, affected strongly by exposure to wind, waves, tides and sediment dynamics (Balke et al., 2015; Jimenez et al., 1985; Krauss and Osland, 2020, Figure 1). At a small, daily scale, these processes comprise a challenging environment for mangrove seedlings that are trying to anchor their tiny roots in the seabed without being washed away (Balke et al., 2011, 2013). At larger timescales, coastal storms can generate strong wind gusts and storm waves and erode large amounts of sediment, damaging or even uprooting entire trees (Baldwin et al., 1995; Kauffman & Cole, 2010; Smith et al., 2009) and resulting in massive mortality events (Jimenez et al., 1985; Sippo et al., 2018). Hence, to understand expansion and retreat of mangrove

width at the seaward fringe, we must quantify the impact of mechanical disturbance from hydrodynamic and wind forces and sediment dynamics on establishment and survival of mangrove trees. Moreover, with 72 mangrove species known globally, that differ in their environmental tolerances (e.g. salinity, Ball and Pidsley, 1988; Kodikara, Jayatissa, et al., 2017; Tomlinson, 2016), there is need to study species-specific tolerances to mechanical disturbances.

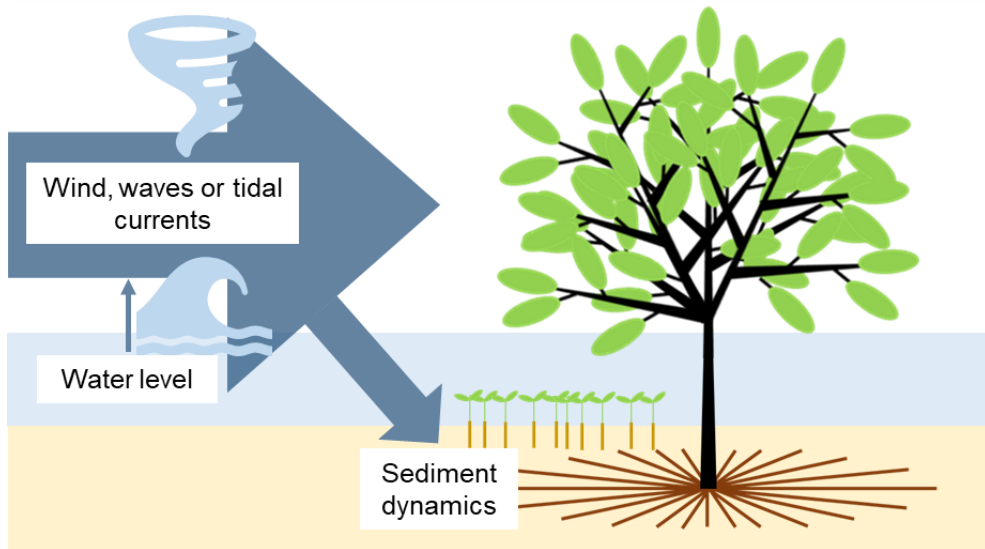


Figure 1: Mechanical disturbances that can act on mangrove seedlings and trees at the exposed seaward forest fringe. Wind, waves or tidal currents can impact the seedling or tree, depending on the water level. At low tide, wind will be at play, whereas at high tide waves and currents will be in action. The latter two can also impose sediment dynamics (accretion and erosion of the seabed). The intensity of wind or waves (e.g. a calm day versus a massive storm) will determine the intensity of the mechanical disturbance on the mangrove seedling or tree.

This thesis aims to identify (Chapter 1) and address (Chapter 2, 3, and 4) the challenges in estimating long-term mangrove functioning by uncovering how mechanical disturbances from wind, and waves and sediment dynamics affect seedling establishment, cause canopy damage and can lead to uprooting across mangrove species. In Chapter 1, I start with a perspective paper that serves as an in-depth introduction to the topic, while Chapter 2, 3 and 4 describe experimental work which is combined and discussed in Chapter 5 (Figure 2). Given the societal relevance of my research, I add an outreach paper in Appendix A that explains nature-based flood defence, and is written for an audience of age of 10 years and older. In the scientific part of my thesis I aim to answer the following questions:

General introduction

- i What is the current state of knowledge on the processes that determine long-term resilience and functioning of mangroves as part of a nature-based flood defence? (**Chapter 1**)
- ii How does tolerance to sediment dynamics differ in establishing seedlings for eight species with three diverging propagule traits? (**Chapter 2**)
- iii How do sediment properties and belowground root morphology determine the stability of a mangrove tree? (**Chapter 3**)
- iv How does a species' tidal elevation affect the mechanical properties that make up its aboveground damage resistance? (**Chapter 4**)

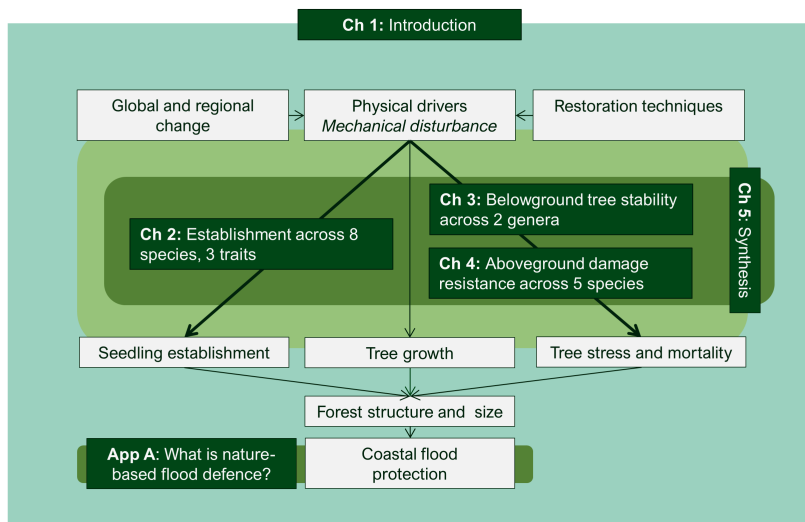


Figure 2: Relationships between the chapters in this thesis. Chapter 1 provides a perspective on all bio-physical and ecological drivers relevant for designing nature-based flood defences with mangroves forests. Chapter 2, 3 and 4 present experimental work on seedling establishment (Chapter 2), belowground tree stability (Chapter 3) and aboveground crown damage (Chapter 4), which is synthesised in Chapter 5. Appendix A provides a brief introduction into the topic of nature-based flood defence.

Chapter 1 (introduction) is a perspective paper that serves as an introduction to the topic of using mangroves in nature-based flood defence. It provides an overview of the physical and ecological processes that make up survival and establishment, and consequently the shape and size of a mangrove forest. It provides an overview of the

General introduction

current state of knowledge and identifies the most urgent and important biophysical questions that must be answered to use mangroves for nature-based flood defence.

Chapter 2 focuses on small, daily disturbances that can affect the establishment of mangrove seedlings. It presents an open-air mesocosm study with eight mangrove species that diverge in the traits vivipary, propagule size and successional stage. The study tests the impact of sediment dynamics on the survival, growth and critical erosion depth of the eight species, and tries to uncover if, and how these traits may contribute to successful establishment.

Chapter 3 focuses on tree stability in relation to belowground processes. Large disturbances such as storms can generate so much flow energy that the resulting drag forces can uproot entire trees. This chapter tests how sediment properties, root mass distribution and root breakage (as a proxy for root strength) affect the mechanical stability of mangrove trees. To allow for rapid and non-invasive testing, I used 3D-printed, scaled mangrove mimics to carry out pulling tests. The experiments consider five root mass distributions that represent the belowground root systems of two mangrove genera, *Avicennia* and *Rhizophora*.

Chapter 4 focuses on the aboveground damage that storms can impose on the mangrove tree canopy. It presents a field campaign where branches and leaves of five mangrove species were sampled across seven different sites that diverge in salinity. The species differ in tidal elevation, which can be considered a proxy for exposure to mechanical stresses. That is, a tree right at the seaward fringe is more exposed to wind, waves and sediment dynamics than a tree closer to the landward fringe. The branches and leaves were tested to obtain measures of branch mechanical strength, branch mechanical flexibility, a drag coefficient and leaf attachment strength.

Chapter 5 (synthesis) provides a synthesis of the findings. It reviews the mechanisms that have been uncovered or elaborated upon in this thesis, with which mangrove trees overcome mechanical stresses. Furthermore, it examines the extent of species differences in overcoming small and large mechanical stresses, and considers how these findings contribute to a better understanding of designing nature-based flood defences with mangroves.

Appendix A provides a brief and gentle introduction to the general topic of nature-based flood defence aimed at an audience of 10 years and older, and is not a part of the scientific contents of this thesis.



Chapter 1

Introduction

Mangrove forests as a nature-based solution for coastal flood protection: biophysical and ecological considerations

R. van Hespen, Z. Hu, B.W. Borsje, M. De Dominicis, D.A. Friess, S. Jevrejava, M.G. Kleinhans, M. Maza, C.E.J. van Bijsterveldt, T. Van der Stocken, B. van Wesenbeeck, D. Xie, T.J. Bouma

Water Science and Engineering (In Press)

1 | *Introduction*

Mangrove forests as a nature-based solution for coastal flood protection: biophysical and ecological considerations

Abstract

Nature-based coastal protection, where ecosystems are used to create resilient designs for coastal flood protection, is increasingly recognised as a potentially sustainable and cost-effective solution to reduce coastal flood risk. Mangrove forests have gained particular interest as a nature-based solution along (sub)tropical coastlines, but to use them effectively we must understand their coastal protection capacity, and the biophysical processes that govern ecosystem size and structure. In this perspective, we evaluate the current state of knowledge on local physical drivers and ecological processes that determine mangrove functioning as part of a nature-based flood defence. We investigate which processes are well-known, require a better mechanistic understanding, better quantification of parameters or of modelling tools to estimate forest resilience and functioning over time. The forest properties that make up coastal flood protection are well-known but refinement of modelling tools is needed to pinpoint the sensitivity of wave or surge attenuation capacity to spatial heterogeneity of forest structure. There is relatively good understanding of the ecological processes and tolerances that drive forest structure and size, but there is a lack of knowledge on the link between daily and long-term bed level dynamics, field application of restoration techniques, and the role of combined stressors particularly in forest retreat. Integrating simulation models of forest structure under changing physical (e.g. due to sea-level change) and ecological drivers with numerical hydrodynamic attenuation models will allow to project the development of natural coastal protection capacity.

1.1 Introduction

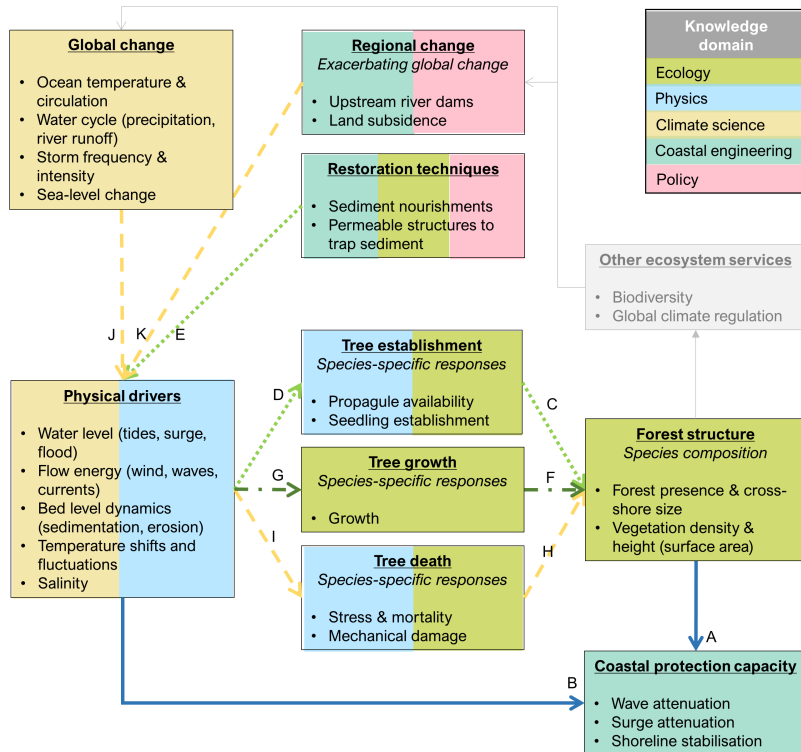
Coastal flood risk is increasing globally, as sea-level rise is further accelerating and coastal storms are predicted to increase in both frequency and intensity in this century (IPCC, 2022). Growing populations and increasing urban development along the coast raise the demand for flood protection measures (Kulp & Strauss, 2019). Coastal areas are generally protected by traditional structures such as breakwaters, levees and seawalls, but increasing flood risk poses unprecedented challenges. Accelerating sea-level rise requires expensive strengthening and heightening (Hinkel et al., 2014), while unlikely but potential structural failure may have devastating consequences (Zhu et al., 2020). Nature-based coastal protections – where coastal ecosystems such as mangroves are used to create more resilient flood defence designs – are increasingly recognised as a solution to reducing these challenges (Borsje et al., 2011; Temmerman et al., 2013). For instance, the wave attenuating capacity of mangroves can reduce the risk of overtopping of these structures and lower direct wave impact, allowing for lower structures and consequently lower construction costs (van Zelst et al., 2021). Furthermore, a benefit of nature-based solutions over traditionally engineered structures is their potential for multi-functionality (i.e. providing additional ecosystem services beyond coastal protection, such as carbon sequestration; Lee et al., 2014). However, implementing nature-based coastal protections is complex (Bouma et al., 2014). Although at a global scale, mangrove presence has prevailed over millions of years and numerous catastrophic climate events (Alongi, 2015), nature-based flood defence requires that mangrove presence is known locally. Coastal protection structures are typically designed with a life-span of 50-100 years, requiring in-depth knowledge of long-term functioning (CIRIA et al., 2013). Estimating this for coastal mangrove ecosystems is currently challenging as mangrove forests are not uniform, but fluctuate in space (e.g. species distributions within the forest, presence of creeks) and time (e.g. forest expansion and retreat; Koch et al., 2009), and these fluctuations take place over various timescales (e.g. daily bed level dynamics vs. long-term changes in elevation). These spatiotemporal fluctuations in forest structure and size are caused by natural and anthropogenic drivers (e.g. Alongi, 2008; Sherman et al., 2000), and recent work has highlighted the importance of untangling the physical drivers and ecological processes that affect mangrove resilience and structure (Gijssman, Horstman, van der Wal, Friess, et al., 2021).

In this perspective, we evaluate the current state of knowledge on the processes that determine long-term resilience and functioning of mangroves as part of a nature-based flood defence (Figure 1.1). We write the perspective from an eco-engineering design point of view, and use knowledge from relevant domains (ecology, physics,

Chapter 1

climate science and coastal engineering). Hence, we assume there are local socio-political motivation and means to implement a nature-based flood defence (but point out when policy may be used to improve physical conditions for mangrove forest resilience). First, we first identify which aspects of mangrove forest structure are most important for nature-based flood defence, and at what spatial scale. Then, we assess how local physical drivers affect these aspects of forest structure. We examine the physical drivers that govern increase in forest size (forest expansion) through seedling establishment and how this can be improved with restoration techniques. Next, we assess how physical drivers, which are affected by global change, govern decrease in forest size (forest retreat). Then we look at how establishment, growth and mortality of trees lead to changes in forest vegetation density and height.

Introduction



Arrows	Processes	Section
→ A, B	Mangrove forest structure determines fluid defence capacity of a forest (A), depending on the water level and flow energy generated (B).	2
→ C, D, E	Forest size increases when seedlings establish (C), which depends on species-specific tolerances to local physical drivers (D) that can be improved with restoration techniques (E).	3
→ H, I, J, K	Forest size and presence may reduce when trees damage and die (H). Trees die if stress from physical drivers (I) exceeds the tolerance limit, or damage e.g. from storm wind and waves (I). Global change , and regional change that exacerbates global change can worsen physical drivers (J, K).	4
→ C, F, H, D, G, I	Vegetation height and density are driven by establishment, growth, and death of trees (C, F, H), which in turn are affected by physical drivers (D, G, I).	5

Figure 1.1: Processes (boxes) and interactions (arrows) discussed in this perspective for assessing the coastal protection capacity of coastal mangroves, showing the relevant knowledge domain (box colour) and the section in which each arrow is discussed. Other ecosystem services are grey as they are mentioned but not explicitly discussed in this perspective.

1.2 Forest properties for optimal coastal protection capacity

Mangrove forests can be effective in reducing energy of wind and swell waves (McIvor et al., 2015; Sánchez-Núñez et al., 2019), and attenuating storm surges (McIvor et al., 2012; Menéndez et al., 2020; Figure 1.2). Although mangroves can not block water, in the absence of levees or seawalls they may still reduce the extent of flooding by reducing direct wave impact and surge water levels (Horstman et al., 2014; Maza et al., 2021; Van Coppenolle et al., 2018). Furthermore, mangroves can contribute to coastal flood protection through shoreline stabilisation Lee et al., 2014, which might contribute to reduction of dike breaches, as can be the case in saltmarshes (Zhu et al., 2020). Inside a forest, the presence of mangrove vegetation attenuates hydrodynamic energy (Mazda et al., 1997), enhancing sediment deposition and preventing resuspension (Scoffin, 1970), particularly in minerogenic systems. These processes are controlled by density of stems and roots (Fromard et al., 1998; Krauss et al., 2003; Pinsky et al., 2013; Roskoden et al., 2020) and plant traits such as morphology and flexibility (Bouma et al., 2005). In this section, we focus mainly on wave and surge attenuation.

1.2.1 Forest width, density and height are important for wave attenuation

The mangrove forest properties that are relevant for wave attenuation are relatively well understood and include the forest width, and density and height of the vegetation (Figure 1.3), as well as the incoming hydraulic conditions. Here, a wider (cross-shore) forest provides more wave attenuation, although waves do not attenuate linearly along the forest (Lee et al., 2021; Quang Bao, 2011). Instead, the greatest attenuation of wave height is found in the first few meters of the forest and the attenuation rate decreases along the forest (Barbier et al., 2008; Dalrymple et al., 1984). A denser, taller forest also provides more wave attenuation. Specifically, the vegetation density and height together make up the frontal surface area of 'structures' that are met by waves, which determine the amount of energy transferred from waves to trees (Figure 1.3; Horstman et al., 2014; Mazda et al., 1997, 2006). Here, we define density as vegetation density, because it is not just the stem density (i.e. how many trees per area), but the entire vegetation density that contributes to wave attenuation. The latter increases as trees mature and stem diameters thicken, trees grow taller and develop more side branches and leaves, while the former decreases as the forest matures and self-thinning takes place (Azman et al., 2021; Jimenez et al., 1985). Vegetation height is also important for wave attenuation, and should be considered relative to the water level. In any coastal ecosystem, emerged canopies that match or exceed the water level dissipate more wave energy than submerged short canopies (e.g. Maza et al., 2015; Yang et al., 2012; Ysebaert et al., 2011). It also matters what vertical layer of the vegetation is submerged exactly, as root layers, trunk layers and

Introduction

canopies differ in geometry, resulting in different wave energy attenuation rates depending on the water level (e.g. Horstman et al., 2014; Maza et al., 2021; Mazda et al., 1997). Finally, the prevailing hydraulic conditions also affect vegetation-induced wave height reduction, including incoming wave height and period (Horstman et al., 2018; Maza et al., 2019), and the combined current-wave flow (Hu et al., 2014; Li & Yan, 2007; Paul et al., 2012; Zhang & Nepf, 2021; Zhao et al., 2021).

1.2.2 Modelling wave attenuation

Over the decades, numerical models have improved at capturing the interaction between vegetation and flow to predict wave attenuation. The first analytical model that explicitly expressed vegetation-induced drag force used the Morison equation and schematised forests as arrays of vertical cylinders (Dalrymple et al., 1984; Morison et al., 1950). It has paved the way for modelling advanced physics in wave propagation, such as wave breaking, wave randomness and wave-current interaction (Hu et al., 2022; Hu et al., 2014; Losada et al., 2016; Mendez & Losada, 2004), and somewhat more complex forest configurations such as horizontal roots and extremely dense vegetation (Suzuki et al., 2012, 2019). Further advancements that use a novel measuring approach can obtain generic drag coefficient equations for various flow and wave conditions and different vegetation types (Chen, Ni, et al., 2018; Hu, Lian, et al., 2021; van Wesenbeeck et al., 2022; Yao et al., 2018), and have successfully been applied in several modelling studies (Hu et al., 2019; Liu et al., 2015; van Veelen et al., 2020, 2021; Wang et al., 2015). This is an improvement of previous models, which required experimental or field data to correctly estimate drag coefficients (which depend on hydraulic conditions and flexibility of stems and branches). Furthermore, experimental studies have accounted for the complex structure of mangrove forests to better understand flow interaction with these ecosystems (e.g. Maza et al., 2017; Zhang et al., 2015, which led to development of a predictive approach that uses empirical relations between wave height attenuation and forest submerged solid volume fraction (Maza et al., 2019). As the tree architecture of most mangrove species is known (Tomlinson, 2016), this approach can reliably account for the complex structure of mangroves forests – given that field validation is possible. Finally, although models can account for complex forest structures, there is still high uncertainty in the effect of flexible vegetation on wave attenuation. Currently, model approaches assume that vegetation is considered rigid under flow action (e.g. Maza et al., 2021). However, at high velocities, stems, branches and leaves bend to realign in the water stream (van Wesenbeeck et al., 2022; Vollsinger et al., 2005), or even break, likely as a protection mechanism to reduce drag forces acting on the tree (Gardiner et al., 2016). The resulting reduction in frontal surface area can differ between mangroves species, that vary in flexibility and strength of branches and

leaves (Chapter 4). Realigned vegetation still contributes to wave attenuation, yet to what extent is complex to quantify (Kalloe et al., 2022). Ultimately, further model development that allows for increasingly complex forest structures can help resolve the remaining uncertainty around the sensitivity of wave attenuation capacity to changes in spatial forest configuration.

1.2.3 Estimating mangrove surge attenuation requires capturing the surrounding landscape
Mangrove forests can reduce surge water levels during tropical storms by decreasing current velocities through increased roughness and by slowing down the water that is pushed toward the shore by the force of winds (De Dominicis et al., In Review). This ability depends on the forest structure, storm properties (intensity, duration, forward speed and track) and the surrounding landscape (McIvor et al., 2012). The relevant forest properties are similar to those for wave attenuation; wider, denser and taller forests are more effective (Maza et al., 2017; Montgomery et al., 2018; Sheng et al., 2012; Zhang et al., 2012). However, the exact contribution of mangroves to surge attenuation is poorly understood. For example, mangrove fragmentation by local creeks may actually increase storm surges, when the creeks work as a conveyer (reviewed in McIvor et al., 2015). In the past decade, surge attenuation modelling with mangroves has started to emerge, with models that include the effect of vegetation by an enhanced bottom friction (Dasgupta et al., 2019; Kiesel et al., 2022; Liu et al., 2013; Xu et al., 2010) or more accurately by including the vegetative drag force at the depths spanned by the mangroves in the water column (De Dominicis et al., In Review). However, resolving the contribution of mangroves to surge attenuation is complicated and requires detailed spatially explicit modelling, as surge effects are strongly dependent on the interaction with the surrounding topography and landscape and storm properties (Hu, Chen, & Wang, 2015; Liu et al., 2013). Further model developments, together with collection of observations of surge attenuation during extreme events, could help resolve the current uncertainty around the role of mangrove forest properties in surge attenuation.

Introduction

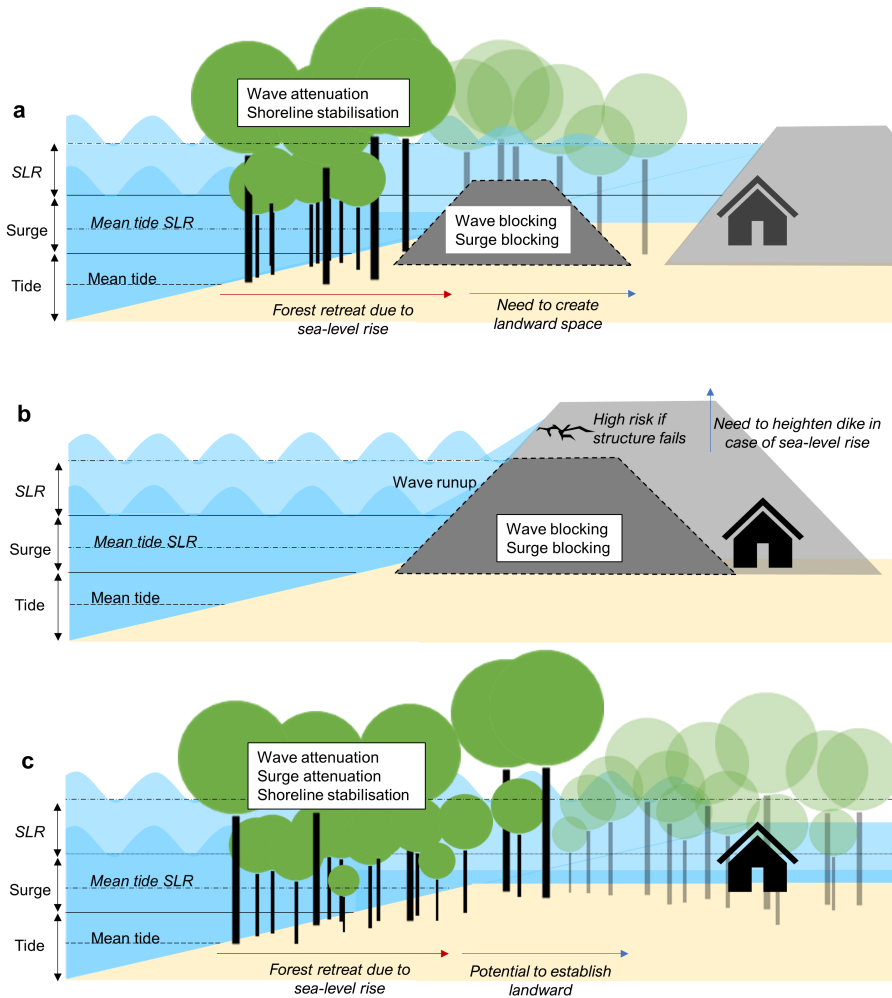


Figure 1.2: Simplified overview of coastal protection functions by mangroves and engineering structures, and potential consequences of sea-level rise. NOT to scale. (a) Mangrove forest and dike, where in case of sea-level rise landward space may be necessary to allow landward migration of mangrove forests, (b) traditionally engineering structure that may need to be heightened in case of sea-level rise, and (c) only a mangrove forest, that may need to move landward in case of sea-level rise.

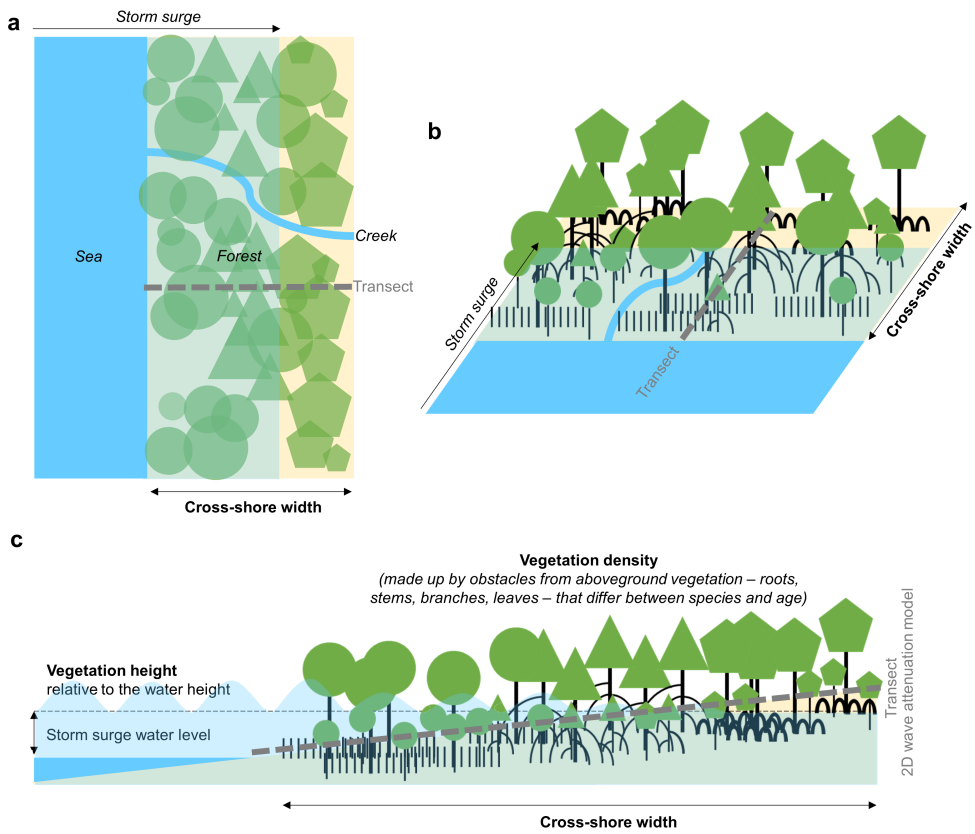


Figure 1.3: Simplified overview of relevant mangrove properties for wave attenuation, with (a) top-down (b) 3D frontal view and (c) cross-shore side view.

1.3 Forest expansion requires space and successful seedling establishment

Expansion of cross-shore mangrove forest width is driven by successful seedling establishment (Figure 1.4), while reduction in width from forest retreat is driven by tree mortality (Section 1.4). The maximum cross-shore width a mangrove forest can reach can be limited at both the landward and seaward fringes. At the landward side, factors such as presence of dikes or alternative land use can be limiting (van Bijsterveldt et al., 2022). At the seaward side, space is mainly limited by physical drivers that determine how suitable the local biophysical conditions are for seedling establishment, most obviously the hydroperiod and wave action (Balke et al., 2015).

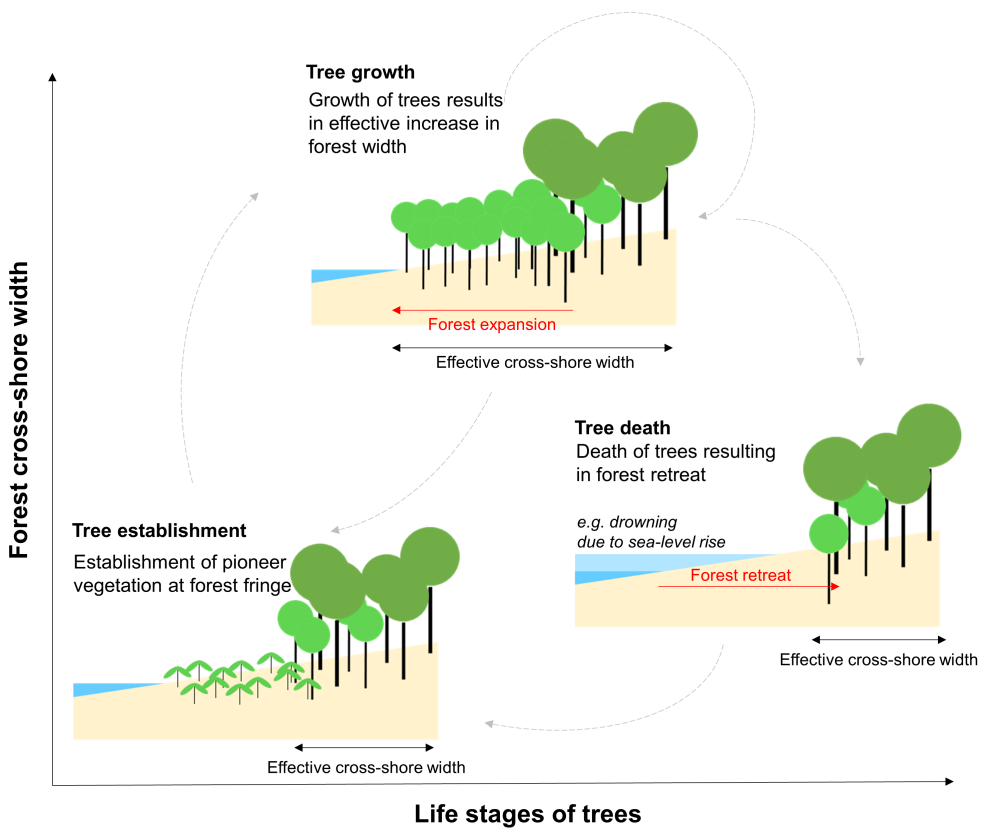


Figure 1.4: Simplified overview of how forest expansion and retreat (cross-shore width) change as a function of tree development (life stages). Initial tree establishment does not affect the effective forest width immediately, as seedlings can not yet provide coastal protection but are the essential basis for forest expansion (Section 1.3). Forest retreat takes place when trees at the forest edge die (Section 1.4). Life stage progression (establishment, growth and mortality) is species-specific and depends on environmental settings such as physical drivers. Arrows suggest possible directions in which forest changes can take place.

1.3.1 Propagule availability and seedling establishment

The biophysical processes that are common at the seaward fringe and drive forest expansion through seedling establishment are relatively well-known. To be colonised, suitable habitat should be within reach of propagules dispersing from existing mangrove stands. Propagule availability in potential source populations depends on i) the number of reproducing trees in a forest and ii) the fecundity (i.e. the number of propagules produced per tree) of these trees (Clarke, 1995). Fecundity increases with tree age, and with species that have smaller propagules (Alleman & Hester, 2011; Clarke, 1992). Furthermore, fecundity varies greatly among individual trees (Clarke, 1992), and increases with environmental conditions such as temperature (Duke, 1990). Furthermore, fecundity tends to be higher in years after tropical storms (Alleman & Hester, 2011), unless there was large canopy damage (Proffitt et al., 2006). While reproductive trees ensure propagule production, propagules need to disperse, establish, and grow beyond the forest edge to expand forest size. Mangrove propagules disperse via water, a process mediated by propagule traits, tidal currents, wind, waves and the landscape features such as vegetation and (micro)topography (see Van der Stocken et al., 2019 for a review). Physical structures may impact the spatial distribution of propagules by either interacting with the propagules directly or through the effects of vegetation-induced drag force on local hydrodynamics (Maza et al., 2017). Previous studies suggested that physical structures encountered by dispersing propagules, such as saltmarsh vegetation, enable stranding and may facilitate mangrove recruitment beyond the established tree line, particularly during high water events, such as spring or storm tides (Peterson & Bell, 2012, 2015). When a propagule has reached a suitable spot at the seaward forest fringe, establishment success will typically depend on the presence of a so-called 'window of opportunity', where disturbance from hydrodynamic forces is absent (Balke et al., 2011). During this window of opportunity a seedling must grow roots fast enough to anchor and overcome the forces exerted by (1) buoyancy during high tide, (2) wave drag, and (3) hydrodynamic drag during events causing sediment erosion (Balke et al., 2011). It must also grow a shoot fast enough to overcome suffocation from sediment burial (Balke et al., 2013). Thus, the seaward space available for successful establishment is determined by the ability of seedlings to overcome physical disturbances: tidal inundation, wave drag and bed level dynamics, and the prevalence of a window of opportunity. This ability varies across species and environmental settings, as root and shoot initiation (germination) and extension rates depend on species-specific tolerances to environmental drivers such as salinity, temperature, waterlogging, sediment type and light availability (Krauss et al., 2008; Sloey et al., 2022; van Bijsterveldt et al., 2020).

1.3.2 Modelling forest expansion

To estimate changes in forest cross-shore width, mechanistic models may be used that can predict seedling establishment using the window of opportunity framework. For example, the mechanistic approach by Balke et al. (Balke et al., 2015) compares tidal data and sediment erosion depth to seedling root length to predict population survival rates of establishing mangrove seedlings. The simulation model by Hu et al. (2015) predicts establishment of saltmarsh pioneer species and explicitly considers spatial and temporal variability, while the model by Hu et al. (2021) uses machine-learning of saltmarsh seedling tolerance to erosion to reproduce the presence and absence of marsh establishment in different intertidal environments. Further developing these saltmarsh models to estimate mangrove forest expansion requires experimental data on (i) mangrove species and environment-specific seedling root growth rates and uprooting tolerance, and (ii) daily bed level dynamics. The former can be obtained from studies specifically on establishment under sediment dynamics (Balke et al., 2011, 2013; Chapter 2) and other seedling establishment studies (reviewed in Krauss et al., 2008). Up until recently, daily bed level dynamics have been more challenging to obtain due to the labour-intensiveness of measuring at daily temporal resolution. However, new tools are emerging. Surface Elevation Dynamic (SED) sensors provide a new, cheap and reliable way to collect long-term measurements of daily bed level dynamics at many locations simultaneously (Hu et al., 2020; Hu, Lenting, et al., 2015; Willemsen et al., 2018). This allows for studying both daily and long-term natural dynamics at high resolution and gaining understanding of the role of daily bed-level dynamics in long-term mangrove development and seedling establishment at the forest fringe.

1.3.3 Boosting establishment with restoration techniques

If the local conditions set by physical drivers (like inundation frequency or bed level dynamics) are unfavourable, restoration techniques can aid seedling establishment. Some of these techniques have been tested extensively in mangroves forests, while others require more field testing or have not yet been implemented specially for mangrove forests. At the seaward edge, permeable structures designed to attenuate waves can create a calm hydrodynamic environment while allowing sediment-loaded water to pass. The calm environment allows the sediment in the water column to sink on the bed and thereby increase the bed level, creating potentially favourable elevations for seedling establishment (Winterwerp et al., 2020). Alternatively, restoration of a cascade of connected facilitating ecosystems such coral reefs and seagrasses can also dampen wave energy and facilitate seedling establishment (Gillis et al., 2014; Gillis et al., 2017; Guannel et al., 2016). If suspended sediment is limited (for example from limited runoff due to upstream dams), active sediment

nourishment could be used, a technique that has been tested in saltmarshes (Baptist et al., 2019). Active sediment nourishment can elevate the bed level and increase the local suspended sediment concentration to create a depositional environment that is beneficial for seedling root anchorage. Finally, planting of nursery-raised seedlings can be used if a lack of windows of opportunity or a lack of propagules are a bottleneck to new establishment (van Bijsterveldt et al., 2022). At the landward edge, presence of dikes or land use (such as aquaculture) can limit the potential space available for landward forest expansion. Creating landward space is expected to be essential to maintain forest width if accelerating sea-level rise becomes limiting to forest presence at the seaward edge (Section 1.4.1; (Saintilan et al., 2020; Schuerch et al., 2018). To allow for landward space, the original local hydrology often needs to be restored (Lewis, 2005). For instance, in non-productive aquaculture ponds, dikes can impede flushing with fresh or sea water, hampering sediment supply, sediment drainage, and propagule supply. Breaching of pond dikes and digging of canals is then a useful measure (Lewis & Brown, 2014). Setting back large dikes or seawalls (managed realignment) has been implemented in some cases for saltmarshes (Kiesel et al., 2022), and besides space may also allow the tidal prism, and thus the sediment supply to the forest, to increase (Winterwerp et al., 2013). Such measures will likely require not only a strong hydrological, ecological and engineering design, but also careful consideration of socio-political barriers.

1.4 Forest retreat under global change

Mangrove forest retreat at the seaward fringe takes place when local physical drivers become too unfavourable for seedling establishment or tree survival. Unsuitable physical drivers lead to tree mortality if they cause stress too much, too frequently or for too long (Figure 1.4), leading to loss of effective biomass for coastal flood protection (Figure 1.5). If too much forest is lost during forest retreat, forest width can even reach beyond a point of no return (tipping point; Scheffer et al., 2001). In the coming century, massive mangrove tree mortality events are expected to be exacerbated by global change, in particular extreme weather events including storms, heatwaves, droughts and oscillating sea levels (Sippo et al., 2018), with sea-level rise expected to have the biggest impact globally (Friess et al., 2022). These risks will vary regionally (Ward et al., 2016), and are subject to uncertainty in future human choices (captured in for example Representative Concentration Pathways or Shared Socioeconomic Pathway scenarios; IPCC, 2022). Furthermore, general shifts such as changes in mean temperature or rainfall patterns may affect the survival of mangroves at the geographic edge of their tolerances (Ward et al., 2016).

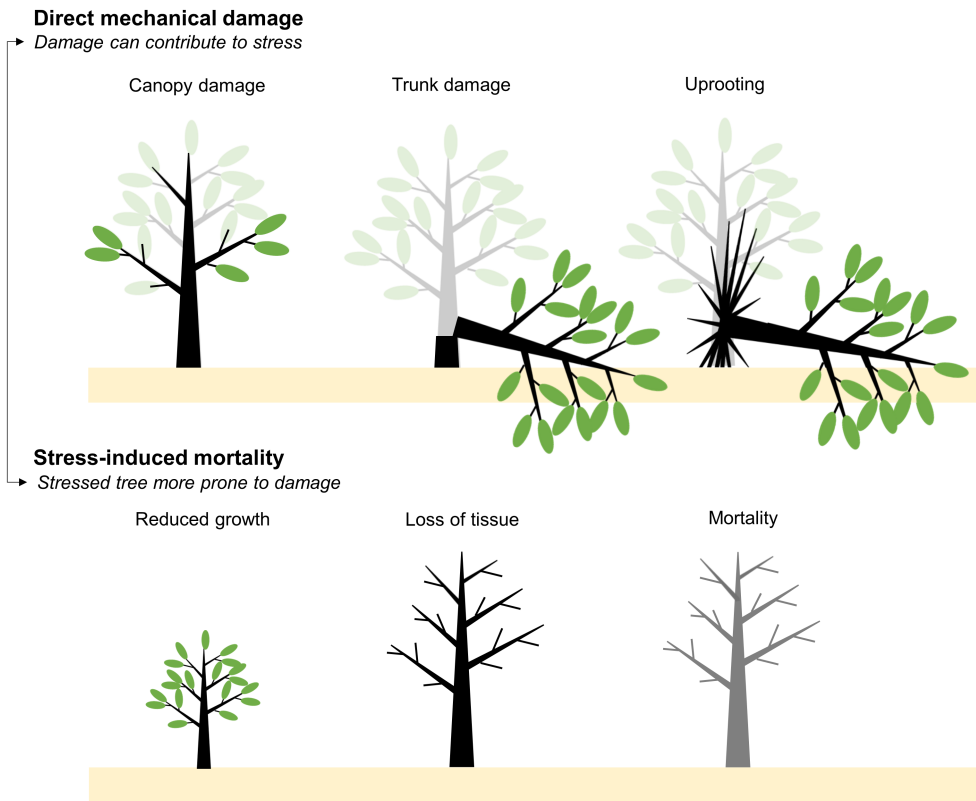


Figure 1.5: Loss of effective biomass for coastal flood protection, where mechanical damage (i.e. from storms) directly reduces the effective forest biomass for wave and surge attenuation, and stress (e.g. from prolonged inundation, salinity) can cause reduced growth (Lovelock et al., 2006) and mortality, which can also affect coastal protection capacity. Stress may make trees more prone to damage, and damage may cause stress.

1.4.1 Keeping up with relative sea-level rise

The mechanisms that drive forest retreat under relative sea-level rise are quite well understood. Relative sea-level rise is the outcome of the combination of large-scale sea level changes and vertical land movement, such as regional land subsidence from geological movements and anthropogenic activities like groundwater extraction (Woodroffe et al., 2016). Relative sea-level rise can result in an altered tidal regime and if inundation becomes too frequent or too long this can lead to stress and drowning of mangrove trees (He et al., 2007; Sippo et al., 2018). At the same time, windows of opportunity where tides and waves are absent may become very rare, hampering seedling establishment (Section 1.3.1). The risk of drowning is higher in mangroves in microtidal settings, where any relative sea-level rise represents a much bigger

proportion of the tidal range than in a macrotidal setting (Lovelock et al., 2015). Under the right circumstances, the sea-level induced worsening of the tidal regime for mangroves can be overcome, as mangrove vegetation can promote sediment accretion. Indeed, several studies have indicated that minerogenic mangroves can keep pace with (relative) sea-level rise if their surface elevation change rates exceed the rate of sea-level rise (Kirwan et al., 2016; Schuerch et al., 2018; Woodroffe et al., 2016). The ability of mangrove vegetation to accrete sediment may vary with factors such as tidal range and vegetation density. For example, a numerical simulation study indicated that sediment accretion may be less for mangrove forests with a small tidal range, as sediment deposition remains limited in such tidal systems (Xie et al., 2022). Furthermore, even if the forest surface elevation is able to keep up with sea-level rise, the increased water depths in front of the mangrove forest may deepen the foreshore and larger waves may hamper seedling establishment (van Bijsterveldt et al., 2020). If a mangrove forest is not able to overcome relative-sea level rise, alternative measures are needed to maintain enough forest biomass for nature-based flood defence. Those measures may include restoration techniques to improve conditions for seedling establishment at the seaward fringe or developing suitable space at the landward forest fringe (Section 1.3.3).

1.4.2 Extreme weather events and mangrove forest resilience

The general mechanisms of extreme weather impact on mangrove forests are quite well-known. Coastal storms can impose two types of stresses to mangroves: *i*) stress from reduced oxygen supply to roots, caused by prolonged flooding or burial of roots by large volumes of sediment (Jimenez et al., 1985), and *ii*) mechanical damage (canopy damage, trunk damage, Figure 1.5) due to drag forces from strong storm winds (Krauss & Osland, 2020), large waves and enhanced tidal currents (Tanaka, 2008). The chance that these stresses lead to mortality or structural damage can vary across species, depending on their stress tolerance, size and mechanical properties such as strength and flexibility (Aung et al., 2013; Chapter 4). Furthermore, previous storm history or pre-existing conditions such as long-term shoreline erosion trends can also affect the impact of future storms (Bhargava & Friess, 2022; Taillie et al., 2020). Extreme weather events such as El Niño Southern Oscillation (ENSO) can lead to heatwaves, drought and temporary drops in sea level (Sippo et al., 2018). Heatwaves may lead to desiccation as evaporation increases with high temperatures, leading to water loss (Rennenberg et al., 2006). Droughts, as a result of low rainfall and groundwater inputs combined with high temperature, can lead to development of hypersaline soils and cause hydraulic failure and desiccation in mangrove trees (Hoppe-Speer et al., 2013; Ward et al., 2016). Temporary drops in sea level may result in forest diebacks comprising of canopy loss due to desiccation and

reduced recruitment (Lovelock et al., 2017). Finally, combined stressors can lead to widespread mangrove dieback, and subsequent storms can limit the reestablishment of mangrove seedlings. While some studies have investigated this (Asbridge et al., 2019; Duke et al., 2021), research and quantification generally remain limited. Field experiments, such as testing the impact of storm waves with wave-generating field flumes (de Smit et al., 2020) could be used to test mangrove resilience to repeated storms, and could even be combined with drought or heatwave experiments to test resilience of mangrove trees to multiple stressors.

Although there is relatively good understanding of the mechanisms that drive forest mortality, there are few tools to estimate the long-term resilience of a specific forest (particularly its cross-shore width; but see (Asbridge et al., 2015)). However, such tools are necessary, as impacts can vary widely depending on environmental settings (e.g. Krauss and Osland, 2020). For example, the direct impact of coastal storms could be predicted by using models developed in forestry, that predict damage during storms from winds using average canopy height, frontal surface area and local wind speeds (Gardiner et al., 2008). Similar mechanical models could be developed for the mangrove environment by quantifying mechanical properties of mangrove trees Chapter 4, the sediment they are rooted in and their surrounding environment (Vovides et al., 2021).

1.4.3 Modelling forest retreat under global change

Understanding the consequences of global change on forest retreat requires translating the consequences to local scale. This can be done by downscaling of global climate models to local estuary models. Application of this method is currently still limited, but certainly possible. Global climate models (such as CMIP6; Eyring et al., 2016) are used to project future atmospheric and ocean conditions (e.g. wind, temperature, salinity, sea surface height) at large spatial scales (25-100 km) using various emission scenarios to account for uncertainty in future human choices (e.g. Representative Concentration Pathway or Shared Socioeconomic Pathways scenarios). Those global predictions are not suitable for coastal application as their resolution is too coarse and they lack representation of the physical mechanism for ocean dynamics in shallow coastal areas, e.g. tides, local winds, and surface and internal waves (Jevrejeva et al., 2019). Instead, they are downscaled to produce regional climate projections, that use the global predictions as boundary conditions (e.g. Gutowski et al., 2016; Hermans et al., 2020; Lewis et al., 2019). Those regional climate projections can then force (i.e. provide boundary conditions for) very high-resolution models for specific coastlines. They can, for example, be used to understand how global sea-level rise will affect local water levels (which is the sum of sea-level rise, surges,

tides and river runoff changes; e.g. De Dominicis et al., 2020). Such high-resolution models may then be combined with the local forest structure and species-specific stress tolerances to obtain predictions of forest retreat at local scale (for example forest-specific responses to sea-level rise or storms (Gardiner et al., 2008; Xie et al., 2020, 2022).

1.5 Forest structure depends on species composition and biophysical interactions

Vegetation density and height are determined by establishment, growth and damage and mortality of mangrove trees (Figure 1.6). The initial density of young mangrove trees is determined by the amount of seedlings that is able to establish in an area, either at the forest edge (Section 1.3, Figure 1.4) or inside a forest gap. The seedlings that survive and make it to maturity grow larger and taller. Then, trees may damage or die, reducing the vegetation density and/or height. Such mortality may take place in massive mortality events at the forest edge (Section 1.4), or can take place inside the forest (gaps dynamics) such as the result of senescence, competition, or lightning strikes (Duke, 2001; Jimenez et al., 1985; Sherman et al., 2000). Besides the age of a forest, forest structure also depends on species composition and species diversity. For example, wood volume increases with mangrove species diversity (Njana, 2020). Due to expected shifts in for example mean temperature or precipitation patterns, species compositions can shift (Ward et al., 2016), potentially resulting in altered coastal protection capacity.

1.5.1 Effect of shifts in species composition on wave attenuation capacity

Variation in vegetation density and height comes from environmental and species-specific differences. The height a tree can reach, and how long it takes to reach this, depends on the environment it grows in and the species it belongs to. Globally, mangrove canopy height is related to precipitation, temperature and potentially cyclone frequency (Simard et al., 2019). Locally, salinity, nutrients, hydrology and light availability can be major drivers of growth (Castañeda-Moya et al., 2011; Krauss et al., 2007; Lovelock et al., 2006; Naidoo, 2009; Peters et al., 2014). Between mangrove species, there are differences in the maximum heights species can reach, ranging between 3 and 40 meters (Quadros & Zimmer, 2017) and depending on climate and geomorphic setting (Rovai et al., 2021). In addition to tree height, tree architecture can also vary widely between mangrove species (Hallé et al., 1978), and environment (Clough et al., 1997). The most remarkable differences are probably found in the shapes of the specialised aerial root systems (Tomlinson, 2016). Architectural differences may not only affect wave and surge attenuation, but also sediment transport and resulting bed level dynamics, as some aerial root systems may reduce the water flow more strongly, causing more sediment deposition or preventing more resuspension (Xie et al., 2020).

Introduction

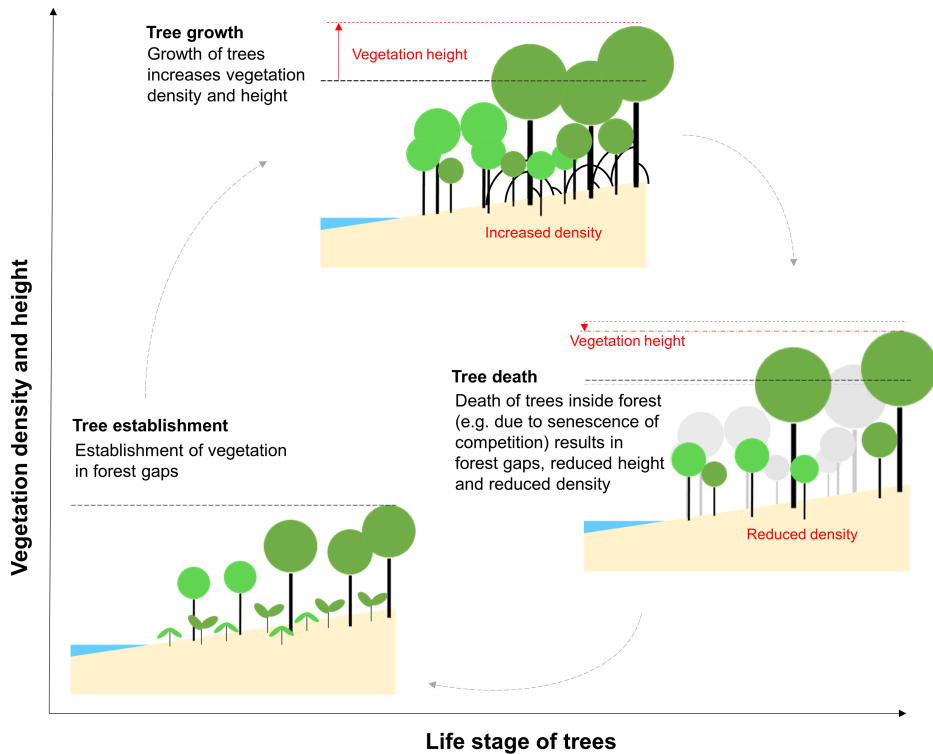


Figure 1.6: Simplified overview of how vegetation density and height change as a function of tree development (life stages). Initial establishment does not affect the effective vegetation density and height immediately, as seedlings can not yet provide coastal protection. When seedlings mature, the effective vegetation density and height increase, while this can decrease when trees die. Life stage progression (establishment, growth and mortality) is species-specific and depends on environmental setting such as physical drivers. Arrows suggest possible directions in which forest changes can take place.

Over time, the species composition of a forest may change, potentially altering its capacity for coastal protection (Koch et al., 2009). This will in large part be determined by (1) which species is currently present, and (2) which of those are able to establish and survive in the future. Global change that imposes major shifts in physical drivers (such as temperature or salinity) can affect local species compositions, as some species are no longer able to establish (Record et al., 2013). For example, it is well-known that mangrove species distribution is controlled by biophysical gradients, and particularly tidal inundation (Cruse et al., 2013; Leong et al., 2018; Ma et al., 2020; Watson, 1928). Therefore, shifts in inundation regime can also result in shifts in species composition, where species with wider tolerances are more likely to tolerate sea-level rise (Ellison et al., 2022). Similarly, increases in soil salinity can cause more stress for some species than others (Eswar et al., 2021; Rahman, 2020),

where a wider salinity tolerance may facilitate a species' response to global change induced salinity shifts (Lovelock et al., 2016). Furthermore, recovery from storm damage varies between species, possibly resulting in changes in species composition particularly if storms increase in frequency or intensity (Krauss & Osland, 2020).

1.5.2 Modelling forest development with individual-based models

Despite being important drivers of wave and surge attenuation, vegetation height and density have not been studied in much detail in the context of nature-based coastal protection. However, there is potential to do so. There is a wealth of long-term ecophysiological data on mangroves (Goessens et al., 2014; Putz & Chan, 1986; Sillanpää et al., 2017; Uddin et al., 2022; Walcker et al., 2018). These data can be combined with models that can simulate mangrove forest dynamics, to obtain increasingly realistic projections of forest structure. These simulations models (also known as individual-based models; IBMs) allow for simulating tree recruitment, establishment, growth and allometry, productivity and mortality, and can account for light and nutrient availability, soil pore water salinity, and competition between individuals, among others (Berger et al., 2008). Many IBMs assume that these abiotic factors are constant in time, but a push is expected towards models that can consider dynamic environmental conditions (Peters et al., 2020), which will allow for more realistic prediction of forest structure under changing environmental conditions.

1.6 Conclusions and outlook

This perspective evaluated the current state of science on the processes that determine long-term resilience and functioning of mangroves as part of a nature-based flood defence. We aimed to uncover the most important forest properties for coastal protection, and how biophysical and ecological processes drive the vegetation dynamics that alter these properties. While the forest properties relevant for coastal flood protection are well-known, it is currently still unclear how sensitive the (modelled) wave attenuation capacity is to changes in forest structure. Furthermore, the capacity of mangroves to contribute to surge attenuation is still poorly understood, because the surrounding landscape plays an important role. Development of increasingly accurate surge attenuation models that can represent the specific morphology and vegetation patterns inside an estuary or delta, combined with field observations of storm surges across a variety of forest structures, might help to fill in this knowledge gap.

The mechanisms that drive forest expansion are generally well understood, with a wide knowledge base on the tolerance of mangrove seedlings in a range of environmental settings. However, further mechanistic model development specifically for mangroves is needed to predict forest expansion in increasingly detailed environ-

Introduction

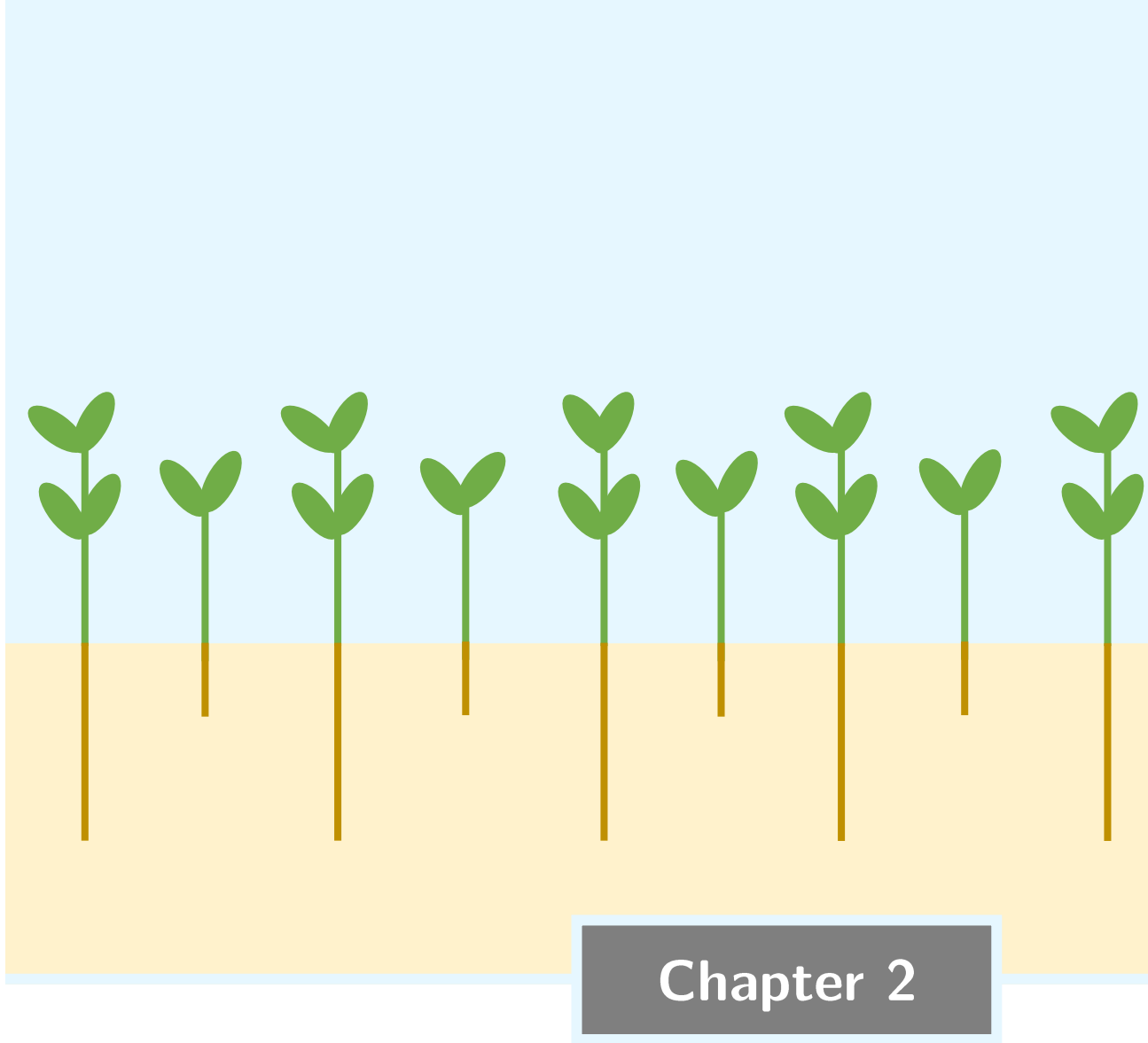
mental scenarios, such as changing tidal regimes, variable bed-level dynamics and changing salinities. Furthermore, new monitoring tools (SED-sensors) could be used to better understand the link between daily and long-term bed level dynamics and improve understanding of seedling establishment at the forest fringe. While theoretically, restoration techniques are well understood, more field testing of restoration techniques specifically in mangrove forests is needed, such as active sediment nourishments or preparing suitable land for landward forest migration. Forest retreat processes are relatively well understood, and can even be modelled for a range of sea-level rise scenarios. Moreover, empirical studies have greatly contributed to understanding the mechanisms of how extreme weather fluctuations can cause tree mortality. This can aid development of simulation models that can predict the extent of mangrove forest retreat under for example repeated storms or combined stressors such as heatwaves and sea-level rise. Finally, there are increasingly detailed datasets on the processes that determine mangrove forest structure (i.e. vegetation density and height). Combining these with development of individual-based models that can simulate forest structure under changing physical drivers could allow for predicting forest structural development over time under variable global change.

Ultimately, the current state of science allows for the development of modelling tools that can estimate how the cross-shore width and structure of a specific forest will develop over time. Such models need to capture the biophysical and ecological processes that drive establishment, growth and mortality of mangrove trees, and allow for uncertainty in global change pathways due to uncertainty in future human choices. For example, individual-based models (Berger et al., 2008; Peters et al., 2020) could be combined with mechanistic simulation models that capture how physical drivers determine forest expansion (Balke et al., 2015; Hu, Borsje, et al., 2021; Hu, van Belzen, et al., 2015) and retreat (Asbridge et al., 2015; Xie et al., 2020, 2022), to estimate changes in forest structure and size. Such forest simulation models require input on relevant physical drivers under global change, which can be achieved by downscaling of global climate models to provide local estimates, for example of sea-level change or shifts in salinity. The predicted forest structure and size could then be combined with models, such as the one presented in Maza. et al. (2021), to predict changes in the hydrodynamic attenuation capacity of a forest over time.

This paper provides a perspective on the current state of science of predicting future coastal protection capacity of a mangrove forest. Nevertheless, implementing nature-based flood defence requires more than a theoretical understanding of physical drivers and ecological processes alone. Mangrove forests sit in a socio-political and socio-economic environment, where local pressures, such as land use or plastic

Chapter 1

pollution (Bryan-Brown et al., 2020; van Bijsterveldt et al., 2021), as well as the triple planetary crisis (climate change, biodiversity loss and air pollution; UNEP, 2020) may need to be addressed. Mangrove forests offer multifunctionality by providing ecosystem services beyond flood protection, such as global climate regulation or trapping pollutants (Temmink et al., 2022; Waryszak et al., 2021), and have been perceived by fishers to increase fisheries yields after their establishment (Debrot et al., 2022). Hence, it is worthwhile to consider whether nature-based solutions should, or should not, be designed to provide multiple services at the same time. Finally, important constraints to the deployment of nature-based solutions in tropical coasts are practical in nature, such as a lack of guidelines or on the ground experience. Adaptive management can be used to obtain practical knowledge about mangrove functioning in coastal flood protection and developing field experience in restoring and protecting mangrove forests (Gijsman, Horstman, van der Wal, Friess, et al., 2021; Walters, 1986). Further research should focus on advancing interdisciplinary scientific understanding through development of open-source models and accessible science that can be translated to applicable guidelines.



Chapter 2

Identifying trait-based tolerance to sediment dynamics during seedling establishment across eight mangrove species

R. van Hesperen, Z. Hu, Y. Peng, Z. Zhu, T. Ysebaert, T.J. Bouma

Limnology & Oceanography (2022)

2 | Identifying trait-based tolerance to sediment dynamics during seedling establishment across eight mangrove species

Abstract

Mechanical disturbance from waves and sediment dynamics is a key bottleneck to mangrove seedling establishment. Yet, how species vary in tolerance to sediment dynamics has not been quantified. We identified how tolerance to sediment dynamics differs for three mangrove propagule traits: propagule size, successional stage and type of embryo development. We selected eight mangrove species growing in south China that vary from small seeds to large elongated propagules, pioneer to climax species and non-viviparous to viviparous. In a mesocosm set-up, we applied bed level treatments to establishing seedlings: erosion, control, or accretion, by removing 2 cm, 0 cm, or adding 1 cm of sediment per week over three weeks. We measured seedling survival, shoot and root lengths, and the critical erosion depth that leads to toppling or dislodgement. We identified five relationships between seedling morphology and accretion and erosion thresholds: (1) tall (viviparous) propagules likely had highest accretion thresholds, (2) small pioneer propagules grew relatively fast to increase accretion thresholds, (3) there was a strong correlation between the erosion threshold and root length, and (4) climax species grew longest roots overall, (5) while pioneer species grew longer roots fast in response to sediment erosion. We identify distinct strategies for successful establishment in sediment dynamics that contribute to understanding mangrove zonation and underpin the importance of restoring diverse forests containing not just robust climax species, but also adaptable pioneers. Furthermore, this study reveals maximum shoot and root length as key determinants for seedling stability across species, providing a simple proxy for modelling establishment events.

2.1 Introduction

Seedling establishment is a vital stage in a plant's life and a primary bottleneck to maintaining and establishing new forest biomass (Leck et al., 2008). Establishment of seedlings can be particularly challenging in environments with mechanical disturbances, such as sediment erosion or accretion in coastal marshes, sand dunes and snowdrift areas (Facelli, 2008; Friess et al., 2012). Though variable success in seedling establishment is a natural part of ecosystem functioning, it can limit access to key resources and services that societies rely on. Such is the case with mangrove forests, that provide critical ecosystem services at global (carbon storage) and local scales (fish nurseries, coastal flood defence; Lee et al., 2014). For optimal functioning, mangrove forests need to have a certain minimal size, particularly when the consequences of size reduction are directly linked to human survival, such as when mangrove forests are used for flood defence, where a wider forest will reduce waves and water levels more effectively (Cao et al., 2015; Horstman et al., 2014; Suzuki et al., 2019). To rely on mangrove ecosystem services, it is important to predict and maintain forest presence via seedling establishment. Yet, there is currently limited knowledge available to develop reliable models that can predict seedling establishment and forest expansion (Bouma et al., 2014; Gijsman, Horstman, van der Wal, & Wijnberg, 2021; Hu, Borsje, et al., 2021). If natural forest size is reduced too much, forest width can be increased through restoration efforts. However, such efforts are not always successful (Ellison, 1999; Erftemeijer & Lewis III, 2000; Lee et al., 2019; Primavera & Esteban, 2008; Terrados et al., 1997), often due to inadequate on-site knowledge of drivers affecting seedlings establishment like salinity, hydrology and appropriate species composition (Kodikara, Mukherjee, et al., 2017). Thus, it is important to understand what mangrove seedlings need for successful establishment for both modelling and restoration efforts.

While the impacts of abiotic drivers such as salinity and inundation on seedling establishment have been studied for numerous mangrove species (Ball & Pidsley, 1988; Krauss et al., 2008; Ye et al., 2005), impact of mechanical disturbance from sediment dynamics has only been quantified for two mangrove species, namely the pioneer species *Avicennia alba* and *Sonneratia alba* (Balke et al., 2013; but see Cao et al., 2018 and Redelstein et al., 2018 for saltmarsh species). Natural forest expansion as well as restoration often take place at the forest fringe where seedlings are exposed to mechanical disturbance from tides, waves and sediment dynamics (Balke et al., 2011, 2013; Chen, Li, et al., 2018). The latter can result in sediment accretion or erosion, with an order of magnitude of 1 cm day^{-1} in the pioneer zone (Hu et al., 2020), and strongly affect seedling survival (Ellison, 1999; Terrados et al., 1997). Sediment erosion can expose a seedling's roots, potentially reducing seedling stability or even

completely uprooting seedlings (Balke et al., 2011). Sediment accretion can result in partial or complete burial of seedlings, leading to etiolation and ultimately mortality (Maun, 1998; Thampanya et al., 2002). Improving the knowledge of tolerance to these mechanical disturbances could improve restoration attempts and enable accurate predictions of future mangrove presence. Balke et al. (2013) showed that there are large differences in tolerance to sediment dynamics between two pioneer species *A. alba* and *S. alba* that differ in traits like size and type of embryo development. It is likely that more such differences exist, as there are 72 mangrove species known to humankind, that vary in shape, type of embryo development, and successional stage (Tomlinson, 2016), and range from tiny seeds weighing less than a milligram up to large, elongate propagules weighing up to 23 g (Wang et al., 2019). Moreover, some mangrove species are pioneers that survive well in the exposed lower intertidal zone, whereas others are climax species that generally occur at less exposed, higher elevations (Friess et al., 2012). This can result in patterns such as observed between *Ceriops tagal* and *Rhizophora mucronata*, where the latter generally occur lower in the intertidal zone and establish root anchorage more quickly to overcome disturbance by waves (Robert et al., 2015). Following this, it is likely that tolerance to sediment dynamics will differ between the diverse group of mangrove species, and studying tolerance across species could advance our understanding of mangrove zonation and increase successful seedling establishment in the mangrove habitat.

Here, we aim to identify traits that contribute to successful establishment under sediment dynamics in the first month of a seedling's life, where we define trait in a broad sense, as a distinguishing quality or characteristic. We use a mesocosm experiment to create sediment accretion and erosion rates that are common in the forest fringe pioneer zone and measure how these treatments impact the growth and survival of eight mangrove species that co-occur in south China. The species cover a range of three propagule traits: successional stage (ranging from low-elevation pioneers to high-elevation climax species), propagule size, and type of embryo developments (non-viviparous, cryptoviviparous or viviparous, where vivipary is the process where the embryo grows first out of the seed coat and then out of the fruit while still attached to the parent tree – or only the seed coat in the case of cryptovivipary; Tomlinson, 2016). Specifically, we set out to learn if species have different accretion and erosion thresholds, and if the three traits provide an advantage in establishing in a sedimentary dynamic environment. For the three traits (successional stage, propagule size, and type of embryo development) we expect that being a pioneer, having a large propagule, and/or being viviparous respectively, contribute most to successful seedling establishment. By generating an extensive dataset, this re-

Seedling establishment

search provides valuable new knowledge on seedling establishment in mechanically stressful environments.

2.2 Methods

2.2.1 Species selection and traits

We selected eight mangrove species common in South China (Figure 2.1): *Avicennia marina*, *Laguncularia racemosa*, *Sonneratia apetala*, *Aegiceras corniculatum*, *Rhizophora stylosa*, *Kandelia obovata*, *Bruguiera gymnorrhiza* and *Bruguiera sexangula*. These species are native to the Pearl River Delta region in south China, with three exceptions: i) *S. apetala* was introduced from Bangladesh for mangrove afforestation in the mid-1980's (Xin et al., 2013), ii) *L. racemosa* was introduced from Mexico in the early 2000s (Zhong et al., 2011), and iii) *B. sexangula* was introduced to Guangdong regionally but is common in the southern tropical areas, i.e. Hainan island (Duke et al., 2010; GBIF, 2021). We categorised each species for the following ordinal or quantitative traits:

- successional stage: pioneer, mid-successional, climax
- type of embryo development: non-viviparous, cryptoviviparous or viviparous
- propagule size: length (cm) and fresh weight (g).

The species had diverging traits, such that we had at least two species in each trait group (Figure 2.1, Table S2.1).

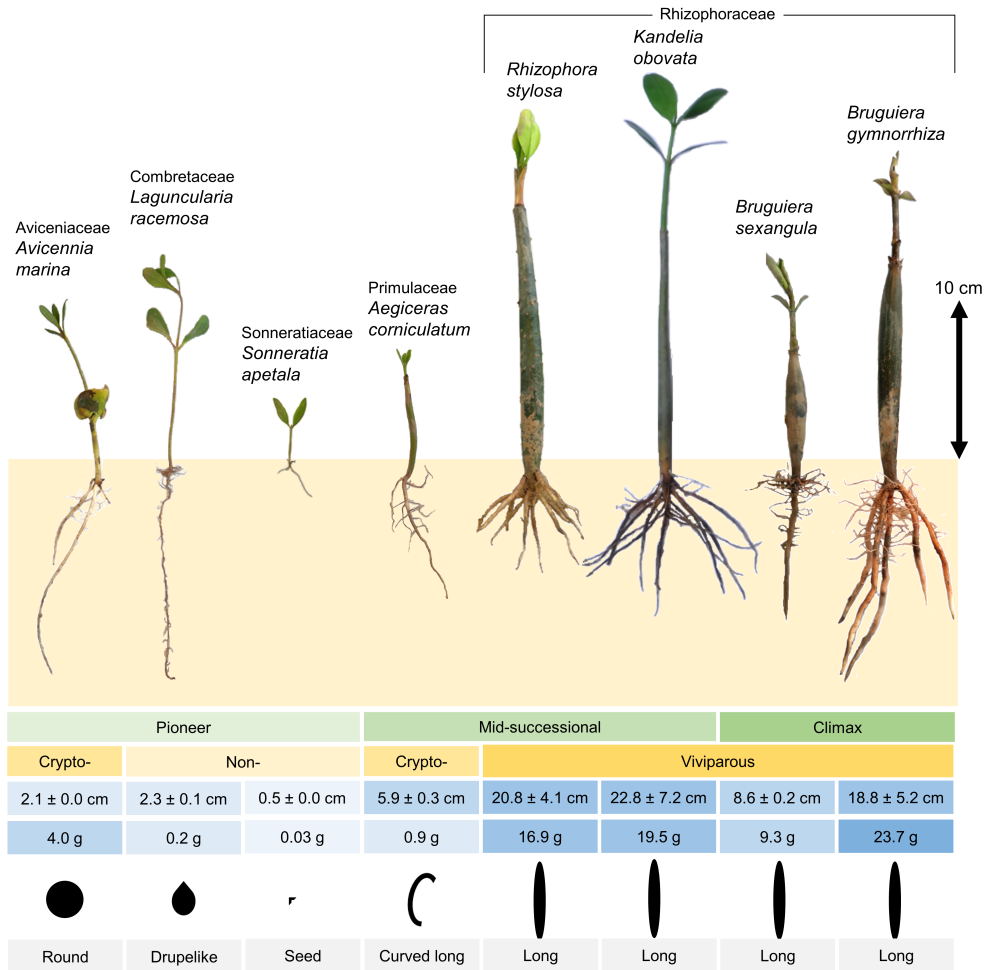


Figure 2.1: Overview of species studied, with a photo (to scale) of a seedling that survived the experiment and a classification for each of the traits: successional stage, type of embryo development, propagule length (cm, mean ± variance) and propagule fresh weight (g, mean values from literature, variability can be found in Table S2.1). For background information, propagule/seed shape is also shown (NOT to scale).

Seedling establishment

2.2.2 Experimental design and growth conditions

The study was carried out in three phases, based on propagule availability. Each phase lasted 34 days. The first phase was carried out with *K. obovata* from 15 April 2019 – 19 May 2019, for which propagules were collected at the Guangzhou Nansha Binhai Wetland, Guangdong, China 22°36'53.8"N 113°38'49.7"E in April 2019. The second phase was carried out with *L. racemosa*, *A. marina*, *R. stylosa*, *A. corniculatum*, *B. gymnorhiza* and *B. sexangula* from 19 July 2019 – 23 August 2019, for which propagules were collected at Hai Nan Dong Zhai Gang National Nature Reserve, Hainan, China (110°32' – 110°37'E, 19°51' – 20°1'N) in July 2019, and the third with *S. apetala* from 18 October 2019 – 21 November 2019, for which propagules were collected at 23°06'49.8"N 113°15'36.6"E in October 2019.

For each species and each sediment treatment we used 12 replicates, so that we tested 288 seedlings in total: 8 species × 3 treatments × 12 replicates. Propagules were sowed on day 1 (Figure 2.2) into pots filled with silty sediment (D50 = 1.8 µm) collected in the Pearl River Estuary at 22°36'19.6"N 113°35'52.3"E and at Qi'ao Island. The pots were placed in outdoor mesocosms that were constructed following the same method as in Balke et al. (2013; Figure S2.1). We selected ripe propagules and, except for *S. apetala*, all propagules were sowed by gently pushing until 2.5 cm into the sediment to ensure they would not float up when inundation started (same depth as in Tomlinson and Cox, 2000). Seedlings were watered daily with fresh water until inundation started. We used an alternative method for *S. apetala* because of complications we encountered with germination. Instead, ripe fruits were opened to extract seeds that were soaked in fresh water for two weeks; after this we selected germinated seeds and planted them with their tiny root (0.5-3 mm) in the soil to avoid desiccation.

Seedlings were inundated twice daily for 2.5 hours each time (5 h day⁻¹) starting a week after sowing (Figure 2.2). This inundation regime mimics a semidiurnal tidal cycle that is generally acceptable for mangroves (Lewis III & Estevez, 1988; Yang et al., 2013), and is consistent with a similar experiment described in Balke et al. (2013). During inundation, water was still. Water had a salinity of 3 psu to allow all seedlings to germinate. This salinity was achieved by mixing water with salt to create artificial seawater. Mean water temperatures were 26.4 °C in phase 1, 30.7 °C in phase 2 and 22.6 °C in phase 3.

2.2.3 Sediment treatments and Critical Erosion Depth

Sediment treatments were applied two, three and four weeks after sowing and carried out over two days due to labour intensiveness (Figure 2.2). For erosion treatment 2 cm was removed around seedlings, for control 0 cm, and for accretion

Chapter 2

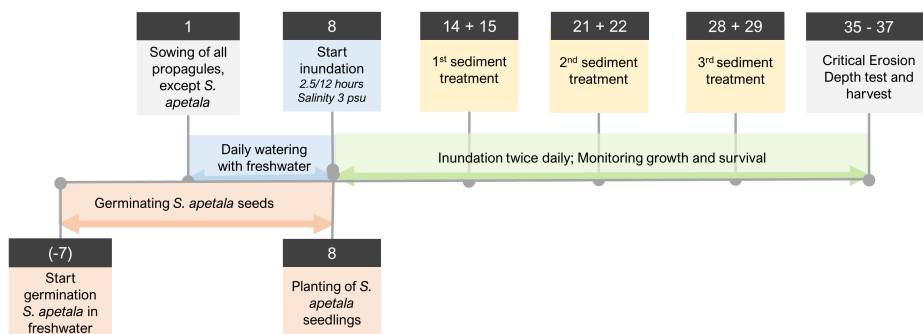


Figure 2.2: Timeline showing on which days experimental steps were carried out. All three phases followed this timeline, where day 1 started on 15 April, 19 July and 18 October 2019. *S. apetala* was sowed in a different manner than the other species, hence the separate experimental steps.

treatment 1 cm was added (cumulative -6, 0 and +3 cm, respectively; see Section S2.2). These sediment treatments were based on sediment dynamics generally found in the mangrove pioneer zone; a net change of about 1 cm week⁻¹ (Hu et al., 2020). Initially, we opted for an erosion treatment -1 cm per week but decided to change this to -2 cm during the first sediment treatment, because eroding only 1 cm was within the tolerance range of most seedlings and would not have resulted in useful results (i.e. all seedlings were likely to survive, which would make it hard to compare the effect of erosion between species). The extent of the sediment treatment could not be changed for the accretion treatment because this treatment required the pre-placement of discs before sowing (see Supplementary Information), which was not possible anymore since the seedlings were already present in the pots. Shoot growth and seedling survival were measured twice per week. Shoot growth was measured from the top of the sediment layer to the tip of the plant. Survival was monitored by visually assessing the state of a seedling: alive, toppled, or dead. Plants that were considered toppled had fallen over thus far that they were resting on the side of the pot. As biological death did not occur, death was defined by the erosion treatment having removed sediment over the full length of the roots such that the seedling had become fully dislodged (and the seedling would float away when inundated), or the accretion treatment having completely buried a seedling and it did not re-emerge.

At the end of each experiment phase, a final test was carried out to measure critical erosion depth. We measured two types: toppling and dislodgement, as these might have different consequences for a seedling's survival (e.g. if a seedling is toppled its roots still have access to nutrients in the soil and may re-erect). Critical erosion depth (CED) was measured as follows: first, we subjected each seedling to a wave treatment by placing it in a flume with a water depth of 15 cm and generating waves

Seedling establishment

with a wave height of 7-8 cm for approximately 1 minute or 7 waves, such that the maximum wave orbital velocity was 0.26 m s^{-1} and the bed shear stress 0.26 Pa (Infantes et al., 2021; Section S2.2). If the seedling did not topple, we removed a 0.5 cm layer of sediment and subjected the seedling to another wave treatment, until a seedling was toppled, upon which the erosion depth $\text{CED}_{\text{topple}}$ was noted. We then repeated the procedure again until a seedling was dislodged. When a seedling became dislodged, the erosion depth $\text{CED}_{\text{dislodge}}$ was again noted, as well as the number of roots and the maximum root length (length of longest root) of the seedling, the latter which has been found to be a good predictor of seedling stability in previous studies (e.g. Balke et al., 2011).

2.2.4 Data analysis

We used survival analysis to analyse the differences in the survival data (alive, toppled or dead) first between sediment treatments, and second between species. Survival data allows for the inclusion of right-censored data, meaning that the event of interest (toppled or dead) did not take place in the study time frame (Bland & Altman, 1998). Data were analysed twice using a Kaplan–Meier Mantel–Cox log-rank test, where we categorised toppling once as alive and once dead (R version 4.1.1 – used in all data analyses – with package ‘survival’ version 3.2.13), and we used a post-hoc analysis to make pairwise comparisons between species (R package ‘survminer’ version 0.4.9). The Kaplan–Meier Mantel–Cox log-rank test assumes that censoring is unrelated to study outcome, that events happened at the time specified, and that survival probabilities are the same for subjects that were added earlier or later to the study (Bland & Altman, 2004). None of these assumptions were violated in our experimental set-up. We used ANCOVA with sediment treatment as the continuous variables, and species as a categorical variable to analyse differences between species and treatments for variables measured at the end of the experiment: maximum shoot length (cm), longest root length (cm), total shoot growth (cm), and relative shoot growth rate. We used a significance level of $\alpha = 0.05$ and set treatment as an interaction term, so that the effect of sediment treatment could vary between species. Relative shoot growth rate (cm day^{-1}) was calculated as follows (Hoffmann & Poorter, 2002)

$$\frac{\ln H_1 - \ln H_0}{t_1 - t_0} \quad (2.1)$$

where H_0 was the initial propagule length (cm) at time t_0 (days) and H_1 was the max. shoot length (cm) measured at the end of the experiment at time t_1 (days), which was day 34. We used the absolute $\text{CED}_{\text{topple}}$ and $\text{CED}_{\text{dislodge}}$ measurements to obtain net $\text{CED}_{\text{topple}}$ and $\text{CED}_{\text{dislodge}}$ measurements: cumulative treatment + absolute CED = net CED (Balke et al., 2013), so that the CED of a seedling with a cumulative sediment

removal of 6 cm could be compared to a seedling with a cumulative addition of 3 cm sediment. We carried out Pearson correlations (with significance level $\alpha = 0.05$) to identify potentially relevant correlations between absolute and net CED_{topple} and CED_{dislodge} , seedling size (maximum shoot length (cm), longest root length (cm), total shoot growth (cm), and relative shoot growth rate (cm day^{-1})), and traits (successional stage, type of embryo development, and propagule length (cm) and fresh weight (g)). We then further analysed the most relevant Pearson correlations (R package 'corrplot' version 0.92).

2.3 Results

2.3.1 Survival and growth response to sediment treatments

Generally, seedling survival was more sensitive to sediment erosion than to accretion. For all species, significantly more seedlings died under erosion than accretion treatments (Figure 2.3, Table S2.2, S2.3). In fact, all species survived accretion except the seedling of the small pioneer *S. apetala* (2/12 died) that had grown significantly shorter shoots than the other species over the course of the 34-day experiment (Figure 2.3, Table S2.4, S2.5). In the erosion treatment group, we observed significant differences between the survival and growth of the eight species (Figure 2.3, 2.4, Table S2.2, Table S2.4). The pioneer species *A. marina* and *L. racemosa* had comparable survival outcomes (pairwise comparisons revealed no significant difference between Kaplan-Meier survival curves at $\alpha = 0.05$; Table S2.2), with some seedlings toppled (17% and 42% respectively), some dead (33% in both species), and some alive (50% and 25% respectively; Figure 2.3). Meanwhile, the pioneer *S. apetala* seedlings, that had the smallest seeds and grew the shortest roots (Figure 2.1, 2.4), had significantly lower survival, as all seedlings died (Figure 2.3, Table S2.3). It is noted that the *S. apetala* seedlings grew in the relatively coldest experimental phase (22.6 °C), as that is when the species is naturally establishing. This may have affected the root growth slightly (Figure S2.2). Mid-successional species *R. stylosa* and *K. obovata* produced significantly more roots than other species, yet those roots were also shorter, significantly in the case of *R. stylosa* (Figure 2.4, S2.6, Table S2.5). Accordingly, they had similar, low survival outcomes, especially when toppling was assumed to be deadly (Fig 3; no significant difference between Kaplan-Meier survival curves at $\alpha = 0.05$; Table S2.3). The mid-successional *A. corniculatum* seedlings germinated too slowly and were eroded before growing anchoring roots (Figure 2.3). The climax species *B. sexangula* and *B. gymnorhiza* had high survival outcomes (Figure 2.3; Table S2.3). In fact, *B. sexangula* survived all erosion treatments (Figure 2.3). It also had the highest mean max. root length (13.72 cm; Figure 2.4, Table S2.3). *B. gymnorhiza* had survival outcomes similar to *A. marina* and *L. racemosa* (Figure 2.3; no significant difference between Kaplan-Meier survival curves at $\alpha = 0.05$; Table S2.3). It also grew similar

Seedling establishment

root lengths over the 34 days of the experiment (10.19 cm; Figure 2.4, Table S2.5). Root and shoot lengths of seedlings that died during the experiment can be found in Figure S2.3.

Pioneer species *A. marina* and *L. racemosa* grew significantly longer roots under erosion; 0.61 and 0.92 cm per cm erosion, respectively (Table S2.5). At the same time, we observed a significant decrease in relative shoot growth rate ($-0.02 \text{ mm day}^{-1}$) towards sediment accretion in *A. marina* and *L. racemosa* (Table S2.5). This may be because some seedlings of these pioneer species only developed roots in the accretion treatment groups. For the mid-successional *K. obovata* and climax seedlings *B. sexangula* and *B. gymnorhiza* we observed a significant increase in shoot length and relative shoot growth rate under accretion treatments (Figure 2.4, Table S2.5), though the positive pattern is less obvious for *K. obovata* in Figure 2.4. Shoot growth over time can be found in Figure S2.4.

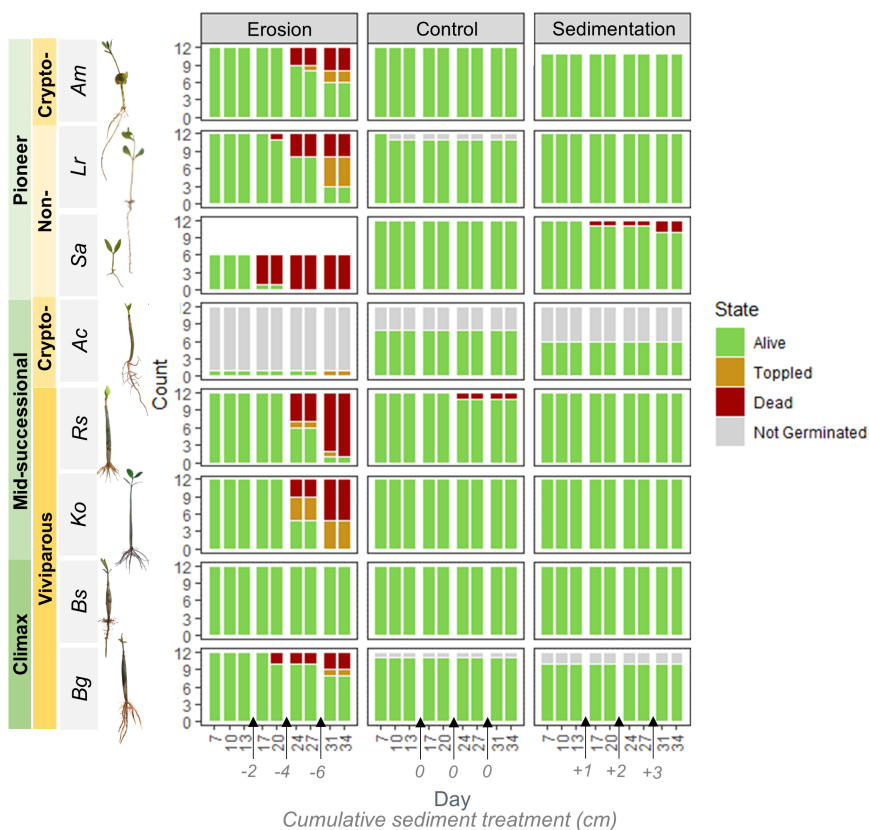


Figure 2.3: Survival of the seedlings under the erosion, control, and accretion sediment treatments over the course of the 34-day experiment, with dotted vertical lines representing treatments (full timeline in Figure 2). The traits successional stage and vivipary are indicated, and an image of a seedling of each species is shown, NOT to scale. Due to a lack of germinating *S. apetala* seedlings only six were tested in the erosion treatment. In the *A. marina* accretion group one seedling went missing. One *R. stylosa* seedling died in the control group for unknown reasons.

Seedling establishment

2.3.2 Erosion tolerance correlates with root length

We identified a strong correlation between maximum root length and net CED_{dislodge} across species ($r = 0.84$, $p < 0.01$, Figure 2.5, 2.6a, S2.5). Interestingly, a correlation between maximum root length and net CED_{topple} was much weaker ($r = 0.55$, $p < 0.01$; Figure 2.5; Figure 2.6b), suggesting a different mechanism driving CED_{topple} than CED_{dislodge} . There were weak significant negative correlations between the number of primary roots and net CED_{topple} and net CED_{dislodge} (-0.17 and -0.42 respectively; Figure 2.5), largely due to the significantly higher number of roots counted on the mid-successional *K. obovata* and *R. stylosa* seedlings (Figure S2.6), which were not the most stable species (Figure 2.4). When these two species were excluded, only a (weaker) significant correlation between the number of primary roots and net CED_{dislodge} remained ($r = -0.27$, $p < 0.01$).

With maximum root length as a likely mechanical predictor of net CED_{dislodge} , we subsequently identified which trait correlated most with maximum root length. We found that successional stage best explained variation in maximum root length, which captures the strong response in maximum root length to sediment treatment in the pioneer species, compared to mid-successional and climax species (Figure 2.7a). The pattern is not so apparent for the pioneer *S. apetala*, likely because we have no data for their root lengths in the erosion treatment. It is noted that although the pioneer species have higher root length plasticity under sediment erosion, the sediment erosion itself may lower their absolute CED_{dislodge} , cancelling each other out if erosion is deeper than root length. To find a better mechanical predictor for net CED_{topple} than only root length, we considered also shoot length (there was no significant collinearity between max. root length and max. shoot length; Figure 2.5). Such a model explained the variation in the data slightly better (net $CED_{\text{topple}} \sim \text{root}$: adj. $R^2 = 0.27$, net $CED_{\text{topple}} \sim \text{root} + \text{shoot}$: adj. $R^2 = 0.32$, Figure S2.7a), indicating that toppling tolerance is possibly driven by above- and belowground seedling morphology. Alternatively, we considered the root/shoot ratio (max. root length (cm)/shoot length (cm)), above and belowground oven-dried dry weight (g) and a below/aboveground ratio (Figure S2.7). For those, we did not find significant correlations with net CED_{topple} . Because the mechanical predictor for net CED_{topple} was not so clear as it was for net CED_{dislodge} , we also analysed the correlations between traits and net CED_{topple} directly (Figure 2.5). We found that successional stage best explained variation in net CED_{topple} , where climax species had highest net CED_{topple} (Figure 2.7b). Furthermore, net CED_{topple} had a stronger inverse correlation with sediment treatment (i.e. a more rapid increase in net CED_{topple} towards erosion) for pioneers than for mid-successional and climax species, suggesting a morphological response beyond root length and dry weight (Figure 2.7b).

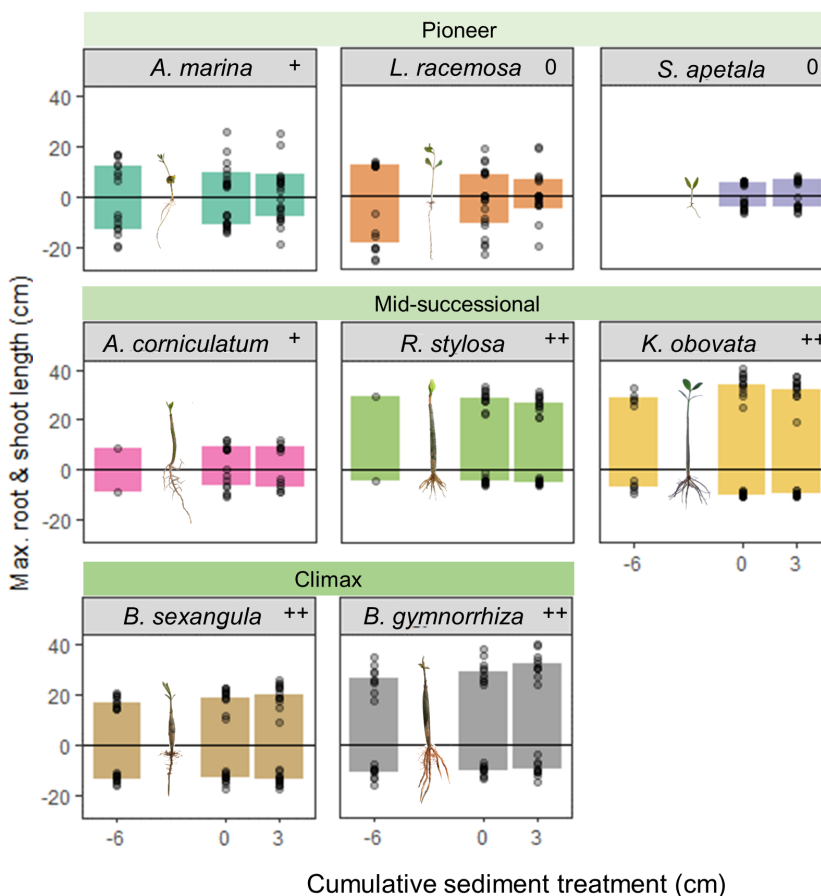


Figure 2.4: Max. shoot and root length of the surviving seedlings after 34 days under the erosion, control, and accretion sediment treatments, showing the means and underlying data of the shoot lengths and maximum root lengths (cm) for surviving seedlings of each species, where shoot length is depicted on the positive y-axis and root length on the negative y-axis. Successional stage is indicated and an image of a seedling of each species is shown, NOT to scale. Type of embryo development is indicated with 0 = non-viviparous, + = cryptoviviparous, ++ = viviparous.

Seedling establishment

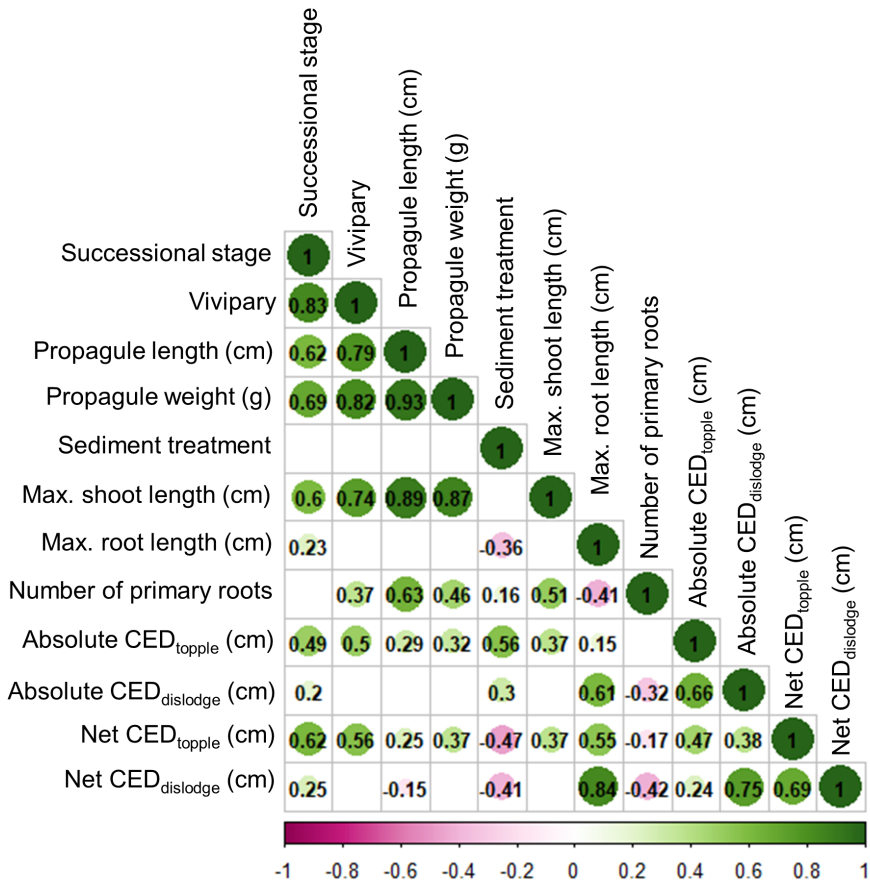


Figure 2.5: Pearson correlations between propagule traits and the measurements of the surviving seedlings taken at the end of the experiment. Showing significant correlations only ($\alpha = 0.05$).

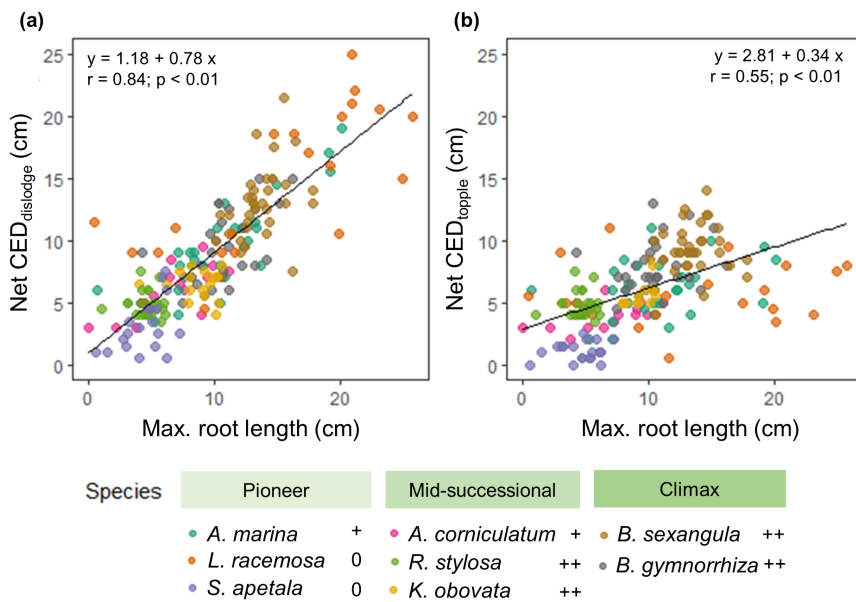


Figure 2.6: Critical erosion depth (CED) versus maximum root length per treatment per species for (a) net $CED_{dislodge}$, (b) net CED_{topple} . Type of embryo development is indicated with 0 = non-viviparous, + = cryptoviviparous, ++ = viviparous.

Seedling establishment

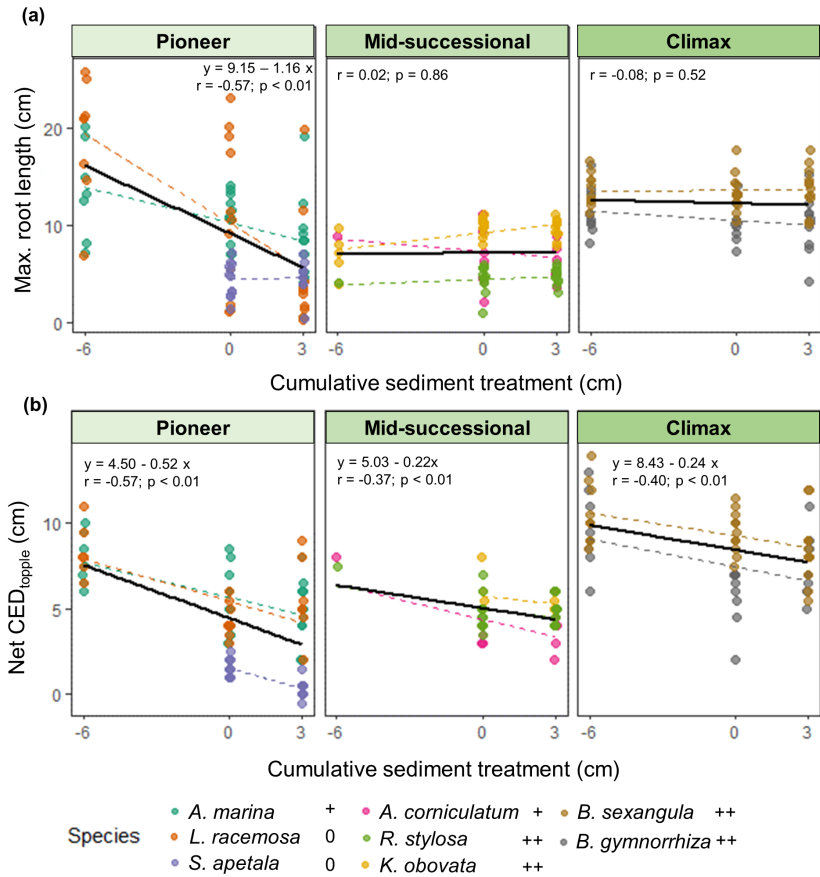


Figure 2.7: Jitterplots of (a) maximum root length and (b) net CED_{topple} at end of experiment per sediment treatment, shown per successional stage and per species. Black solid lines show correlations per successional stage, dashed coloured lines show correlation per species.

2.3.3 Shoot length correlates with propagule size

We analysed which traits correlated most strongly with shoot length after 34 days of growth and found the strongest correlation with initial propagule length ($r = 0.89$, $p < 0.01$; Figure 2.5, 2.8a), followed closely by propagule weight ($r = 0.87$; Figure 2.5). We observed a significant negative, logarithmic correlation between relative shoot growth rate and propagule length ($y = 0.05 + \log(-0.002x)$, $r = -0.89$, $p < 0.01$; Figure 2.8b), such that the smallest species grew relatively fastest. Absolute growth rate is shown in Figure S2.8.

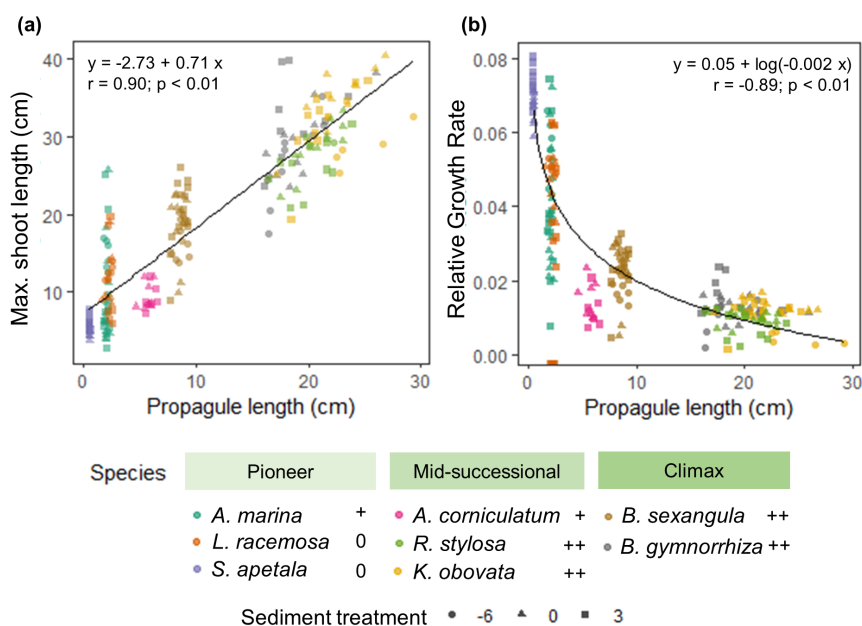


Figure 2.8: (a) Shoot length at day 34 and (b) relative growth rate of shoots, versus propagule length, per species, per treatment. For the regression lines treatments and species are pooled. Type of embryo development is indicated with 0 = non-viviparous, + = cryptoviviparous, ++ = viviparous.

2.4 Discussion

Successful seedling establishment is essential to preserve and restore mangrove ecosystems and their services. Here, the impact of mechanical disturbance on mangrove seedling establishment is studied across a range of species diverging in the traits successional stage, type of embryo development and propagule size. We found a key factor explaining successful seedling establishment under erosion was root length. Climax species had the longest roots overall, while the plasticity of pioneer species allowed them to develop longer roots in response to sediment erosion. Species with small propagules were found to be the most sensitive in that they

Seedling establishment

were buried most easily. Overall, in our 34-day study sediment erosion was more challenging than accretion for mangrove seedling establishment.

2.4.1 Optimal seedling morphology and traits to withstand erosion and accretion

The Window of Opportunity framework on seedling establishment in sedimentary dynamic environments posed that seedlings need to grow fast enough to overcome mechanical disturbance from (1) tides, (2) waves and (3) sediment dynamics (Balke et al., 2011, 2013). Here, we expand on this framework by showing how species with contrasting successional stages, type of embryo developments and propagule sizes, overcome accretion and erosion thresholds by growing fast in general (i.e. regardless of sediment dynamics), being responsive to sediment dynamics or being already tall (Figure 2.9). Sediment erosion can have two consequences for a mangrove

Mechanical disturbance	Potential consequences for seedling	Ideal morphology to avoid burial, toppling or dislodgement	Traits that contribute to ideal morphology	
Accretion	Burial	Tall shoots	Large viviparous propagules: tall if establish vertical	Small pioneer propagules: relatively fast growth
Hydrodynamic forces	Toppling	Short, flexible shoots deep, sturdy roots	Viviparous: establish horizontal, less drag*	Pioneers: increase flexibility*
Erosion	Dislodgement	Deep roots	Climax species: deep roots	Pioneers: increase root length under erosion

Figure 2.9: Summary of ideal seedling morphologies for overcoming accretion and erosion thresholds, and the traits we identified that contribute to such a morphology. Blue arrows indicate hydrodynamic forcing. * indicate expectations based on literature. Figure 1 shows the relevant traits for the eight species studied in this paper; here large viviparous propagules were *R. stylosa*, *K. obovata*, *B. sexangula* and *B. gymnorrhiza*, *A. marina*, *L. racemosa* and *S. apetala* were pioneers, of which *S. apetala* was the smallest, and *B. sexangula* and *B. gymnorrhiza* were climax species.

seedling: (1) loss of stability leading to toppling and (2) complete dislodgement. By analysing more species than previous studies (Balke et al., 2011, 2013), we were able to reveal the optimal seedling morphology to overcome sediment erosion. Root length was a key morphological feature that had a strong correlation with critical dislodgement depth. In other words, propagules with long roots can withstand deeper erosion before being dislodged. Any deviation from this correlation between root length and dislodgement might be explained by waves pushing a seedling further out of the sediment than the erosion depth. That is, these simple seedling root systems do not hold a complex grip in the root-sediment matrix (see Balke et al., 2011). The correlation with root length was however not so obvious for critical toppling depth. In fact, we argue that seedling stability is a function of not only belowground root morphology, but also aboveground shoot morphology. In our experiment we found that critical toppling depth was better explained when we included both root and shoot length. Similarly, Redelstein et al. (2018) found a correlation between critical toppling depth, shoot biomass, and root biomass when they studied seedling stability in saltmarsh species. Research on the stability of mature trees in terrestrial ecosystems may explain our mangrove observations. Here, tall and inflexible trees will experience larger overturning moments than short and flexible trees (Sagi et al., 2019; Urata et al., 2012). For trees to remain stable, they need a wide, strong and inflexible root system with a deep layer of heavy soil above it (Achim & Nicoll, 2009; Coutts, 1983). Though seedlings are much smaller than mature trees, the same physical laws apply. Thus, the most stable seedling would have small, short and flexible shoots, and long and sturdy roots. Moreover, as water is denser than air, these morphological features that increase stability may be more important in aquatic systems (Bouma et al., 2005; Puijalón et al., 2011).

In terms of optimal morphology to avoid toppling or dislodgement, long roots were found in the pioneer species *A. marina* and *L. racemosa*, particularly in response to erosion treatments. This responsiveness is likely a common feature in pioneer species, as increased biomass allocation to roots has also been observed in *A. alba* and *S. alba* after undergoing erosion treatments (Balke et al., 2013), and saltmarsh species developed longer roots compared to shoots after undergoing erosion treatments (Cao et al., 2018). Long roots were also found in the climax species *B. gymnorhiza* and *B. sexangula*, that had highest survival in erosion treatments. The mid-successional species *K. obovata* and *R. stylosa* were less successful in developing long roots. Instead, they developed many short roots (Figure 2.1, S2.6). At least in *R. stylosa*, but possibly also in *K. obovata*, this large number of roots is because their propagules abort their embryonic root and instead have many lateral, sub-apical root primordia (Tomlinson & Cox, 2000). Perhaps these lateral root primordia are useful in earlier

Seedling establishment

stages of seedling establishment, as a larger number of root primordia could provide more opportunities for a seedling to anchor and overcome disturbance from tides and waves (Balke et al., 2011). Furthermore, we found the shortest shoots in the pioneer species and in the mid-successional *A. corniculatum*. In pioneer species, we also expect highest flexibility. Firstly, because increased flexibility in shoots has also been observed in pioneer mangrove and saltmarsh species in response to waves (Balke et al., 2013; Cao et al., 2020). Secondly, because we expect lower flexibility in species with long propagules, as these are quite rigid (Figure 2.1). Although long, rigid viviparous propagules are neither short nor flexible, they may avoid drag forces if they establish from a horizontal position. On the tidal flat they have a roughly 50% chance of stranding horizontally, effectively reducing their length for a few weeks until they have grown upright (Figure S2.9, S2.10; Tomlinson and Cox, 2000).

Most seedlings survived accretion treatments, except for the tiny *S. apetala* seedlings. Thus, to avoid the risks of complete burial it is best to be tall. Indeed, in a similar experiment with small *S. alba* seedlings and larger *A. alba* seedlings, the former had lower survival under sediment accretion (Balke et al., 2013). Seedlings with the tallest shoots after 34 days since sowing, were among the species that had the tallest propagule (Figure 2.8a). These species were all viviparous with long propagules, such that they were already initially tall – though only if they arrive vertically on the tidal flat (Figure S2.9, S2.10). Shorter shoots were observed in the species with smaller propagules, with the shortest shoots observed in *S. apetala*, which had the smallest propagules. To quickly achieve taller shoots as a small propagule, it needs to grow fast. Pioneer species grew relatively fastest, particularly in response to accretion. In many cases, accretion resulted in the tallest shoots observed. However, the mean shoot length of pioneers *A. marina* and *L. racemosa* reduced in accretion treatments because there were several individuals where the shoots failed to develop. In dune species, burial is known to reduce growth rates (Maun, 1998), which may have happened here as well. More detailed studies that compare a larger range of accretion treatments, and thus burial depths, are needed to identify in detail how growth rate reduction and accretion thresholds depend on mangrove species traits. Such burial depths may need to be relative to the seedling height, such that each species can be tested for its response to complete burial. This could uncover wider species differences, such as was observed by Thampanya et al. (2002), who found much higher survival and growth rates in *Sonneratia* species compared to *Avicennia* species (*A. officinalis* vs. *S. caseolaris*). Further burial studies could also include various (complete) burial durations. Complete burial can often be deadly (Maun, 1998; Thampanya et al., 2002), but can be overcome. In dune species, on rare occasions, seedlings of species with large seeds can emerge from complete burial

(Maun, 1998). Furthermore, dune species can survive burial if erosion occurred within a few days after the burial event (Maun, 1998). Cao et al. (2018) found similar results in experiments with saltmarsh species, that can survive higher levels of burial if bed levels fluctuate versus a constant rate of burial. Studying various burial durations could reveal potential differences in species tolerances.

The current study works with a set range of environmental variables that result in growth rates specific to those environmental settings. However, it is well-known that seedling growth rates are determined by a myriad of environmental drivers (Krauss et al., 2008), and the growth we observed in our experiment may differ widely in drier, saltier, darker, or otherwise different environments (e.g. Kodikara, Jayatissa, et al., 2017; Sloey et al., 2022). This could result in shorter shoots or roots than we measured in our experiment and reduce erosion or accretion thresholds. To illustrate, in our study we used a semidiurnal inundation regime of 5 h day^{-1} in total. Previous work has shown that longer inundation can directly reduce establishment success under sediment dynamics (Balke et al., 2013). This could, for example, affect the relative shoot growth rate of *B. gymnorhiza*, which is significantly reduced when growing in a waterlogged environment compared to *K. obovata*, so that *K. obovata* might produce deeper roots and reach higher erosion thresholds than *B. gymnorhiza* (Ye et al., 2003; previously *K. candel*; Sheue et al., 2003). Furthermore, our study was carried out across different seasons with different temperatures, because we used species whose propagules reach maturity in different seasons. Seasonal differences such as temperature can affect the growth rate of seedlings, and even within a season, or across years, different growth rates may be found (e.g. Gillis et al., 2019). Temperature difference may also have an impact on the erodibility of coastal sediment and the resulting critical erosion depth (Nguyen et al., 2019). Therefore, the effect of these and other environmental differences is worthy of further study in the context seedling establishment in sedimentary dynamic environments.

The main aim of the paper was to identify whether one of the traits, or a combination of traits, provides an advantage in establishing in a sedimentary dynamic environment. By doing so, we uncovered various strategies to overcome establishment thresholds in dynamic sedimentary environments (Figure 2.9). We expected that being a pioneer would be advantageous to overcoming erosion and accretion thresholds. Indeed, pioneer species were responsive to erosion, and small pioneers grew relatively fast to avoid complete burial. We also expected that being viviparous would bring an advantage, and found that a horizontal arrival on the tidal flat may potentially reduce the change of toppling. Furthermore, we expected that having a large propagule would be an advantage, and found that large propagules had

Seedling establishment

taller shoots at the end of our experiment. Additionally, our findings contribute to our understanding of what makes pioneer species a pioneer. We initially assigned pioneer status based on location in the intertidal zone in south China, and being described as such in the literature (Table S2.1). Now, we may add that being able to grow roots fast under erosion and, at least in the case of small propagule (*S. apetala*) being able to grow shoots fast under accretion, likely contribute to what makes them successful at growing in the pioneer zone.

2.4.2 Implications for mangrove restoration and modelling of mangrove establishment

Although in our study *Bruguiera*-like climax species were most robust with longest roots and tallest shoots, pioneers were most plastic in response to their environment and were hence also able to reach high root and shoot maxima. Furthermore, pioneer species typically have higher fecundity than climax species (Friess et al., 2012), and smaller propagules that allow them to disperse further away from the mature mangrove forest (Van der Stocken et al., 2015). This provides pioneer species with a larger number of offspring reaching colonisable land. Thus, a lower survival rate at the individual level, may make pioneers seem less successful than they really are. Hence it is useful to mix a broad range of species in restoration projects, especially in exposed sites, but keeping in mind that the inundation frequency should match the successional stage of the species. By including multiple species with diverse traits, the risk of establishment failure is mitigated by the presence of diverse establishment strategies. We argue that the development of the shoot length and root length over time can be used as simple proxies to predict seedling survival in sedimentary dynamic environments. Identifying such simple proxies is valuable for modelling establishment events and restoration measures under global change. This kind of mechanistic modelling approach has for example recently been applied to predict the sensitivity of saltmarsh establishment under global and local stressors (Hu, Borsje, et al., 2021). Using such a mechanistic approach could support the prediction of seedling establishment beyond the limitations of the environmental setting of the current study. Including other factors than sediment dynamics, such as salinity, temperature and light availability can be easily done, by using existing relations between such factors and how they affect the growth rate of seedling roots and shoots (reviewed in Krauss et al., 2008).

S2 Supporting information

S2.1 Trait assignment

Where possible, we used information about south China for the tidal elevation a species generally inhabits (Duke et al., 1998; He et al., 2007; Peng, Diao, et al., 2016; Table S2.1). Then, we assigned a species to a particular successional stage based on the tidal elevation and whether a species is considered a pioneer (sensu Friess et al., 2012). Following tidal elevation, *K. obovata* should be classified as a climax species, but because it has been mentioned in the literature as a pioneer by some (Khan & Kabir, 2017), we assigned it to mid-successional stage. Data on germination type came from Tomlinson 2016, average propagule length (cm) came from our own data (Figure 2.8) and fresh weight (g) was from Hong et al., 2021, Rabinowitz, 1978 and Wang et al., 2019. For background information, propagule shape is also shown in Figure 2.1 (Duke et al., 1998), but we did not use propagule shape as a trait in our analyses because this would have resulted in four groups with only one species, and because it is not an ordinal trait. It is noted that there is some correlation between the traits, for example, *R. stylosa*, *K. obovata*, *B. gymnorrhiza* and *B. sexangula* all belong to the Rhizophoraceae, all have large propagules and are all viviparous, though they inhabit different successional stages (Figure 2.1).

Table S2.1: Studied traits listed for each species, selected such that we had at least two species in each trait group: Am = *Avicennia marina*, Lr = *Laguncularia racemosa*, Sa = *Sonneratia apetala*, Ac = *Aegiceras corniculatum*, Rs = *Rhizophora stylosa*, Ko = *Kandelia obovata*, Bs = *Bruguiera sexangula*, Bg = *Bruguiera gymnorrhiza*. Successional stage is a combination of tidal elevation and whether or not a species is considered a pioneer. Vivipary: ++ = viviparous, + = cryptoviviparous, - = non-viviparous. Variability in propagule fresh weight was reported in different measures: se = standard error, 95%CI = 95% confidence interval, sd = standard deviation, ? = unreported.

Trait	Am	Lr	Sa	Ac	Rs	Ko	Bs	Bg
Tidal elevation ¹	LM	LM	LM	LM	LM	MH	MH	H
Pioneer species ²	Yes	Yes	Yes	No	No	Maybe	No	No
Successional stage	1	1	1	2	2	2	3	3
Vivipary ³	+	-	-	+	++	++	++	++
Propagule length (cm, mean \pm variance) ⁴	2.06	2.26	0.50	5.88	20.80	22.80	8.61	18.8
Propagule fresh weight (g, mean) ⁵	4	0.21	0.03	0.91	16.94	19.5	9.25	23.74
Propagule fresh weight (g, variability) ⁵	1.8 (se)	0.0 (95%CI)	0.0 (?)	0.1 (se)	3.1 (se)	1.2 (sd)	1.1 (se)	2.1 (se)

¹ Duke et al., 1998; Peng, Zheng, et al., 2016

² sensu Friess et al., 2012; Khan and Kabir, 2017

³ Tomlinson, 2016

⁴ Own data, averaged

⁵ Hong et al., 2021; Morrisey et al., 2010; Rabinowitz, 1978; Wang et al., 2019; Weng et al., 2012

Seedling establishment

S2.2 Practical set-up

Mesocosm set-up

We set up mesocosms at an undisturbed place near Sun Yat-Sen University Zhuhai campus, Guangdong, China. Mesocosms were constructed following the same method as in Balke et al. 2013), with two tanks with inside dimensions of 90 x 110 x 43 cm stacked on top of each other and provided with transparent roofing to avoid debris or rain falling into the tanks. The bottom tanks functioned as a water reservoir from which water was pumped to inundate the top tanks. Each mesocosm contained 30-31 pots with one seedling per pot. Pots were made of PVC tubes with a diameter of 15 cm and a height of 25 cm and ribbons were attached to the sides for easy lifting. We placed a sandwich bag filled with sediment in the pots and used a rubber band to keep the bags in place. The bags were perforated at the bottom to allow water to flow out. To avoid sediment leaching, we lined the perforated bag bottoms with a small piece of fabric. At the bottom of each tube, we placed 1 cm PVC discs: for the accretion treatment four discs; for the erosion and control treatments one disc. These discs functioned (1) to allow for an accretion treatment where discs were removed from the bottom so a layer of sediment could be added at the top, and (2) to be consistent across treatments, so that each pot has at least one disc at the bottom. At the start of each phase, the pots were filled to the edge with sediment and then left to rest for 36 hours, inundating every hour to promote consolidation. Extra sediment was then added to fill the pots up to the edge again and create a smooth, level surface. Any further consolidation was measured on day 11 and taken into account when calculating the seedling growth and cumulative sediment treatment.

Sediment treatments

For the erosion treatment (-2 cm week^{-1} , cumulative change: -6 cm), we added two 1 cm PVC disks at the bottom of the pot, then used a putty knife to scrape of the 2 cm excess sediment layer that was created at the top. Water spray was used to spray away sediment between the vulnerable seedling roots. For the accretion treatment ($+1 \text{ cm week}^{-1}$, cumulative change: $+3 \text{ cm}$), we removed a 1 cm PVC disk from the bottom of the pot. This created a 1 cm gap between the sediment layer and the edge of the pot, which we filled up with extra sediment. For both treatments, we ensured that the new sediment layers were smooth and even.

CED wave treatment

Critical erosion depth was measured with a combined treatment of waves and sediment removal to mimic storm conditions. First, we subjected the seedlings to a wave treatment in a flume (Infantes et al., 2021). Then, we removed a 0.5 cm layer of sediment (using the same method as in the erosion treatment) and subjected the seedling to another wave treatment. This procedure was repeated until a seedling

Chapter 2

was first toppled. If a seedling toppled the erosion depth was noted. We then repeated the procedure again until a seedling was dislodged. When a seedling became dislodged, the erosion depth was again noted. We created the wave treatment by placing two pots inside a flume at a water depth of 15 cm and generating waves with a wave height of 7-8 cm for approximately 1 minute (or 7 waves). With a water depth of 0.15 m, wave period of 1.5 s, wave height of 0.07 m and assuming that waves were regular waves, the maximum wave orbital velocity was 0.26 m s^{-1} . The corresponding bed shear stress was 0.26 Pa, calculated following Zhu et al. 2016. The waves were generated by a wave paddle that was fitted inside the flume. The paddle was pneumatically driven by a compressor combined with a pressure regulator to provide a continuous 6-7 bar airflow. The flume was 3.5 m long and 0.6 m wide and had a wave run-up of 1.2 m with a slope of 11.77 degrees. The back of the flume was outfitted with wave damping material to reduce wave reflection.

Seedling establishment

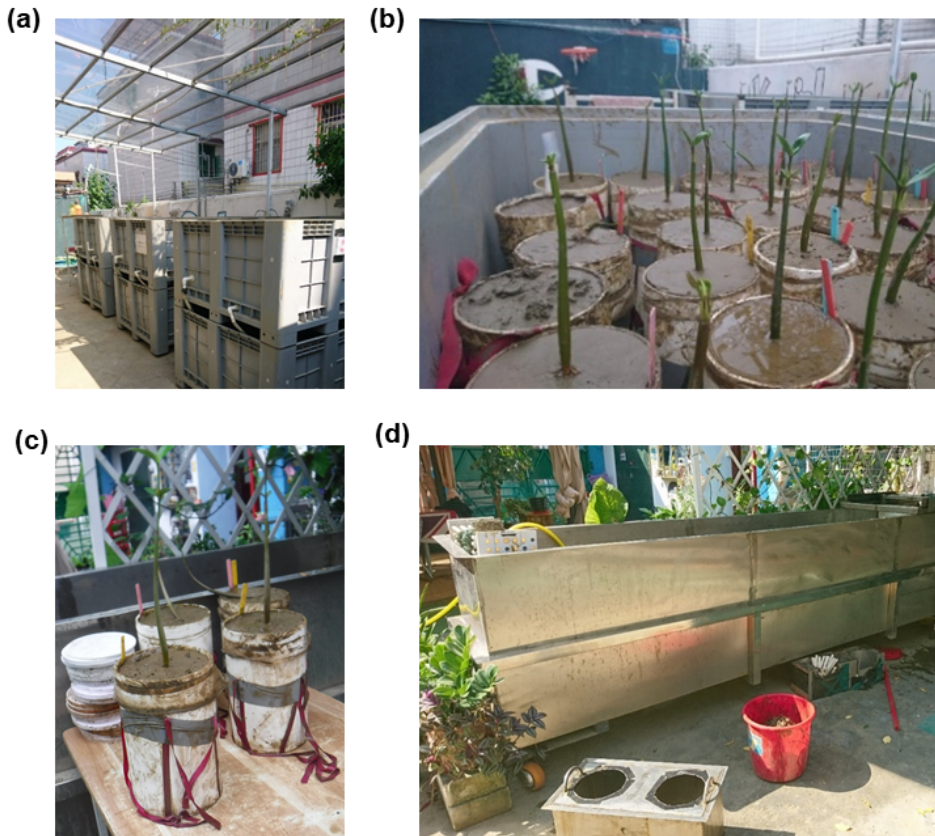


Figure S2.1: Experimental set-up with (a) tidal tanks (top tank was inundated twice daily, bottom tank was reservoir), (b) pots with seedlings in top tidal tanks, (c) pot with seedling and (d) flume with holder for two experimental pots taken out (at the foreground). Photos by Rosanna van Hespén.

Chapter 2

S2.3 Additional results

Table S2.2: Results of the Kaplan–Meier Mantel–Cox log-rank test on survival and toppling of seedlings during the experiment. *A. corniculatum* and *B. sexangula* are excluded from the analysis as they resulted in infinite values; *A. corniculatum* only had 1 germinated propagule and all *B. sexangula* survived.

Dataset	Variable	Assumed toppling = alive			Assumed toppling = dead		
		X ²	d.f.	Sig.	X ²	d.f.	Sig.
All species pooled (except <i>A. corniculatum</i> , <i>B. sexangula</i>), all bed level treatments	Bed level change	418	2	0.00	569	2	0.00
Bed level change = erosion only, all species except	Species	98	5	0.00	85	5	0.00

Table S2.3: Pairwise comparisons of Kaplan-Meier survival curves between species in the erosion treatment, and the survival probabilities at the end of the experiment St=34 for each species. Dataset used includes only the erosion treatments and excludes *A. corniculatum* and *B. sexangula*. A Benjamini-Hochberg correction was used. P-values below a significance level of $\alpha = 0.05$ are printed in bold. Survival probabilities are shown for day 34 (St=34), mean and standard error, the latter if possible. Am = *Avicennia marina*, Lr = *Laguncularia racemosa*, Sa = *Sonneratia apetala*, Rs = *Rhizophora stylosa*, Ko = *Kandelia obovata*, Bg = *Bruguiera gymnorrhiza*.

	Assumed toppling = alive					Assumed toppling = dead					St=34 mean±se	
	Sig.					Sig.						
	Am	Bg	Ko	Lr	Rs	St=34 mean±se	Am	Bg	Ko	Lr	Rs	St=34 mean±se
Am	-	-	-	-	-	0.39±0.09	-	-	-	-	-	0.24±0.08
Bg	0.71	-	-	-	-	0.49±0.09	0.29	-	-	-	-	0.41±0.09
Ko	0.43	0.25	-	-	-	0.19±0.07	0.00	0.00	-	-	-	0.00
Lr	0.67	0.43	0.72	-	-	0.37±0.09	0.36	0.05	0.001	-	-	0.10±0.06
Rs	0.00	0.00	0.01	0.01	-	0.02±0.02	0.00	0.00	0.22	0.03	-	0.02±0.02
Sa	0.00	0.00	0.00	0.00	0.00	0.00	0.00	0.00	0.00	0.00	0.00	0.00

Seedling establishment

Table S2.4: Two-way ANCOVA's for maximum shoot length, maximum root length, shoot growth and relative shoot growth rate for the surviving seedlings.

Model	Df	Type III SS	F	Sig.
Shoot length ~Species * Sediment treatment				
Intercept	1	51452.0	2513.56	0.00
Species	7	18788.0	131.12	0.00
Sediment treatment	1	0.0	0.02	0.90
Species : Sediment treatment	7	494.0	3.45	0.00
Residuals	194	3971.0		
Max. root length ~ Species * Sediment change				
Intercept	1	12622.6	1106.20	0.00
Species	7	1427.8	17.88	0.00
Sediment treatment	1	73.7	6.46	0.01
Species : Sediment treatment	7	761.7	9.54	0.00
Residuals	195	2224.9		
Total shoot growth ~ Species * Sediment treatment				
Intercept	1	8191.1	465.76	0.00
Species	7	821.6	6.82	0.00
Sediment treatment	1	1.3	0.07	0.79
Species : Sediment treatment	7	540.2	4.48	0.00
Residuals	193	3322.8		
Relative shoot growth rate ~Species * Sediment treatment				
Intercept	1	0.11	1595.61	0.00
Species	7	0.05	112.39	0.00
Sediment treatment	1	0.00	0.05	0.83
Species : Sediment treatment	7	0.00	4.61	0.00
Residuals	186	0.01		

Chapter 2

Table S2.5: Estimated mean and standard deviations for each species, sediment treatment and the interaction effect of species and bed level change. Sed. = Sediment treatment. Am = *Avicennia marina*, Lr = *Laguncularia racemosa*, Sa = *Sonneratia apetala*, Ac = *Aegiceras corniculatum*, Rs = *Rhizophora stylosa*, Ko = *Kandelia obovata*, Bs = *Bruguiera sexangula*, Bg = *Bruguiera gymnorrhiza*. P-values below a significance level of $\alpha = 0.05$ are printed in bold.

Variable	Max. shoot length ~ Species * Sediment treatment			Max. root length ~ Species * Sediment treatment			Total shoot growth ~ Species * Sediment treatment			Relative shoot growth rate ~ Species * Sediment treatment		
	Mean	SD	Sig.	Mean	SD	Sig.	Mean	SD	Sig.	Mean	SD	Sig.
Intercept	10.07	0.83	0.00	10.28	0.62	0.00	8.00	0.76	0.00	0.041	0.002	0.00
Lr	-1.60	1.20	0.18	-0.11	0.89	0.90	-1.81	1.10	0.10	0.004	0.002	0.07
Sa	-5.07	1.55	0.00	-5.78	1.16	0.00	-3.50	1.42	0.01	0.026	0.003	0.00
Ac	-0.79	1.53	0.61	-2.93	1.14	0.01	-4.03	1.74	0.02	-	0.003	0.00
Rs	18.07	1.36	0.00	-5.79	1.01	0.00	-0.67	1.24	0.59	0.026	-	0.002
Ko	22.21	1.18	0.00	-1.02	0.88	0.25	1.80	1.08	0.10	0.033	0.002	0.00
Bs	8.69	1.14	0.00	3.35	0.85	0.00	2.17	1.05	0.04	-	0.002	0.00
Bg	19.78	1.20	0.00	0.25	0.89	0.78	2.96	1.10	0.01	0.031	-	0.002
Sed.	-0.49	0.24	0.04	-0.61	0.18	0.00	-0.50	0.22	0.03	-	0.002	0.00
Lr : Sed.	-0.16	0.35	0.65	-0.92	0.25	0.00	-0.16	0.32	0.61	0.001	0.001	0.10
Sa : Sed.	0.88	0.71	0.22	0.65	0.53	0.22	0.89	0.65	0.17	0.004	0.001	0.00
Ac : Sed.	0.53	0.56	0.34	0.40	0.42	0.34	0.22	0.80	0.78	0.001	0.002	0.60
Rs : Sed.	0.05	0.50	0.92	0.70	0.37	0.06	0.32	0.46	0.49	0.002	0.001	0.04
Ko : Sed.	0.87	0.36	0.02	0.89	0.27	0.00	1.25	0.33	0.00	0.003	0.001	0.00
Bs : Sed.	0.79	0.32	0.01	0.63	0.24	0.01	0.81	0.29	0.01	0.002	0.001	0.00
Bg : Sed.	1.13	0.33	0.00	0.45	0.25	0.07	1.00	0.31	0.00	0.002	0.001	0.00

Seedling establishment

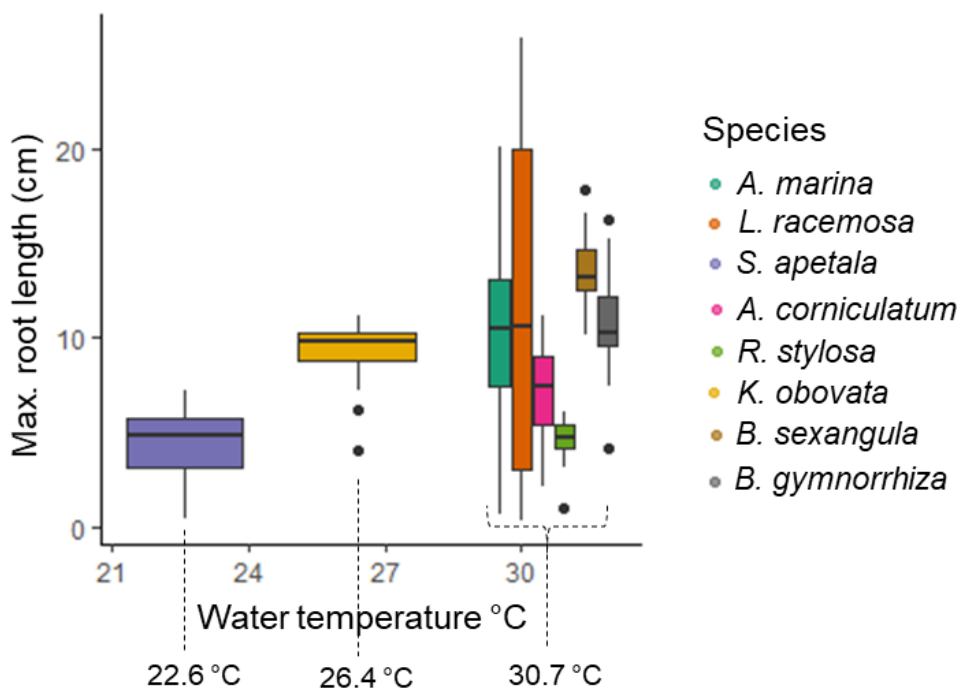


Figure S2.2: Max. root length (cm) per water temperature (°C).

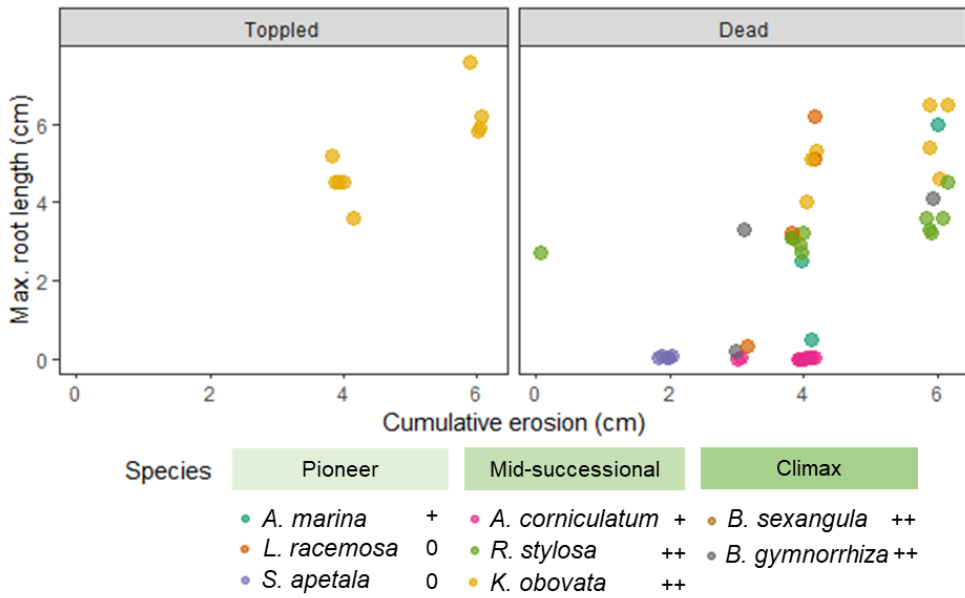


Figure S2.3: Jitterplots of longest root at toppling or death after erosion treatments. For accretion (not shown) only two seedlings died, one *S. apetala* after the first treatment (shoot length 0.3 cm, cumulative accretion 1 cm) and one *S. apetala* after the second treatment (shoot length 3.1 cm, cumulative accretion 2 cm).

Seedling establishment

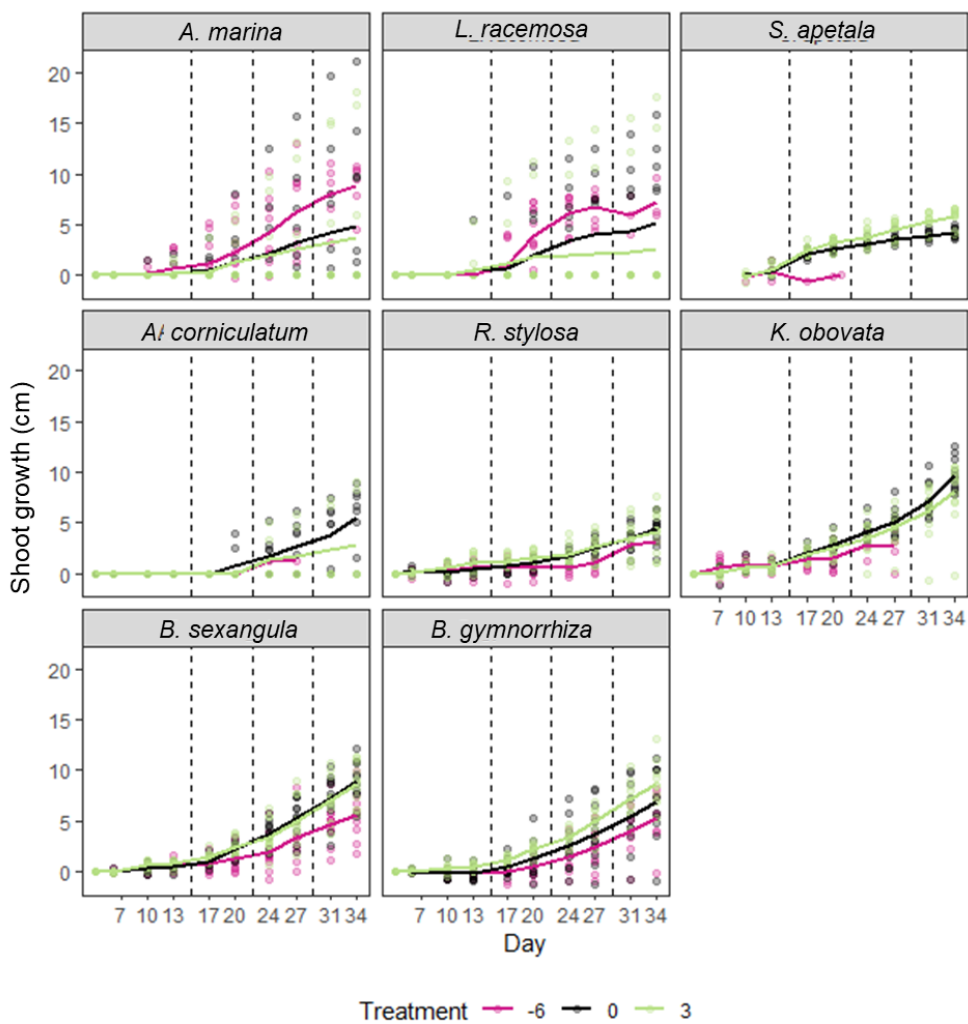


Figure S2.4: Shoot growth per day (shoot growth = shoot length – initial propagule size) over the course of the 34-day experiment per species, per sediment treatment. Dotted vertical lines indicate the timing of the three sediment treatments.

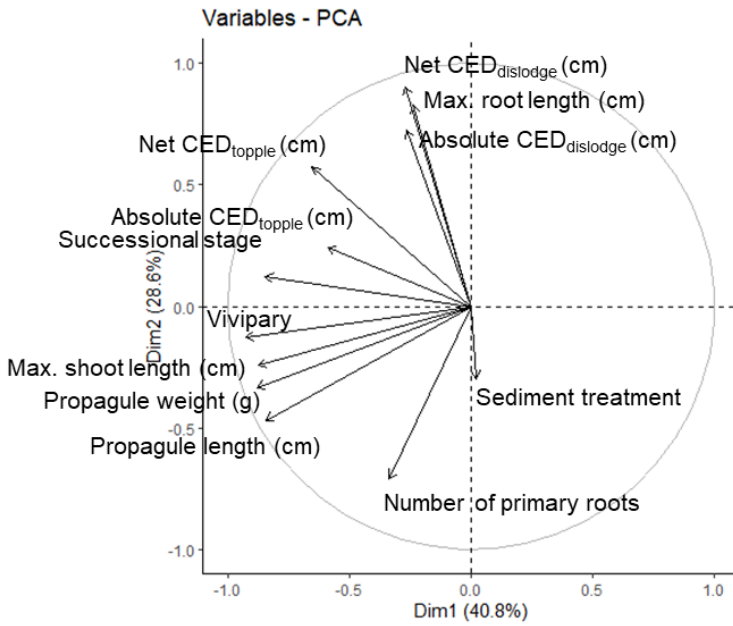


Figure S2.5: Correlation circle showing correlation between Principal Components, traits, and the measurements of the surviving seedlings taken at the end of the experiment.

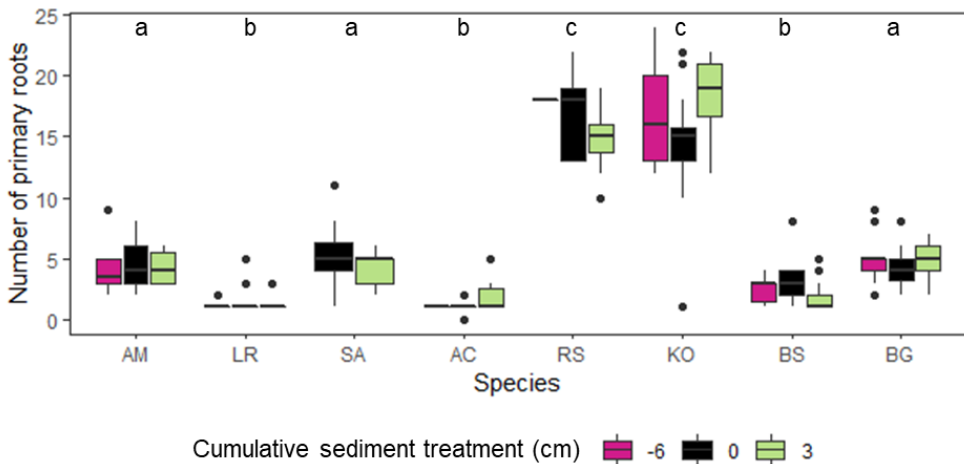


Figure S2.6: Number of roots per species per sediment treatment. There was no significant treatment effect. Significance letters shown per species for Dunn's test with significance level $\alpha = 0.05$.

Seedling establishment

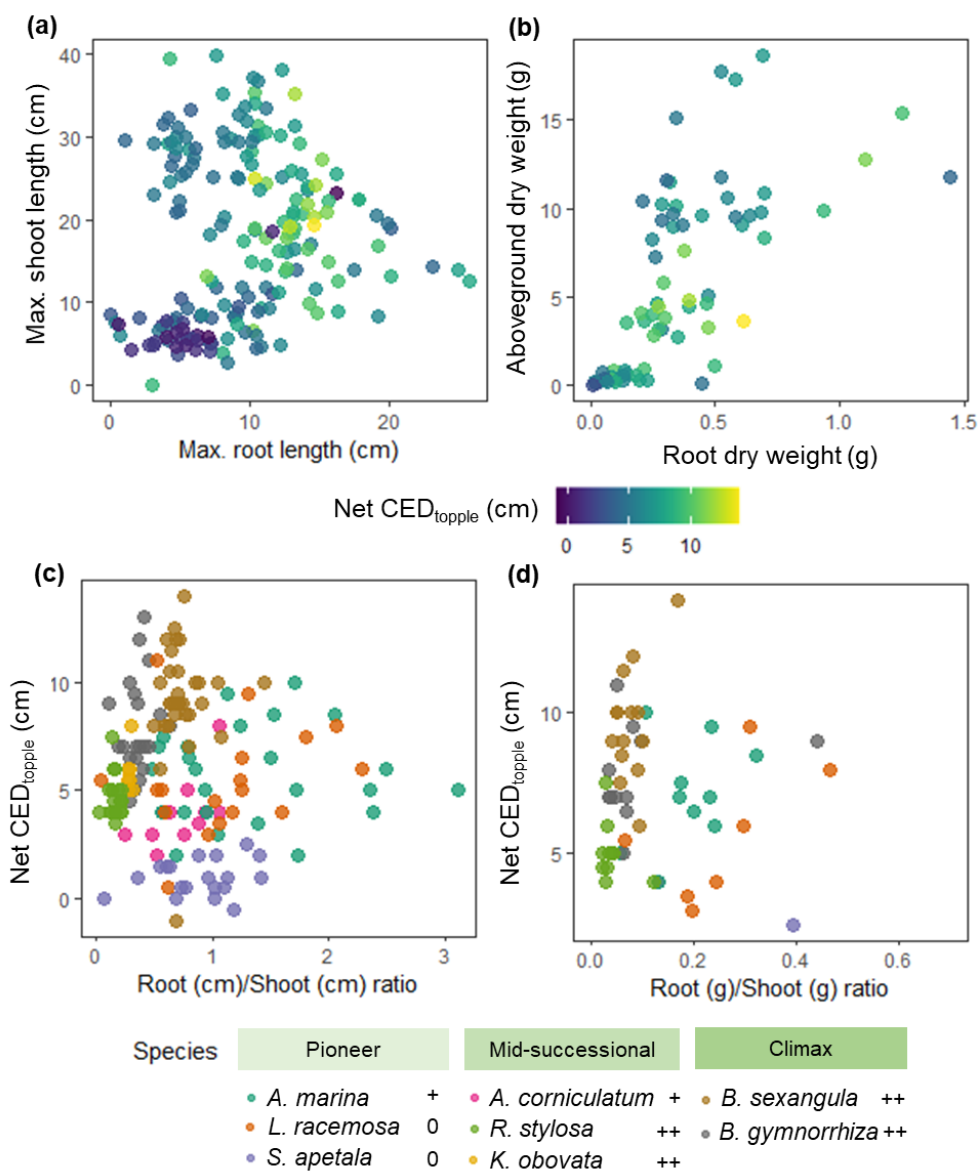


Figure S2.7: Net CED_{topple} versus (a) shoot length and root length of seedlings, (b) aboveground and root dry weight (g), panel (c) shows net CED_{topple} per root/shoot ratio (length, cm) and panel (d) shows net CED_{topple} per root/shoot ratio (dry weight, g). Dry weight was obtained by drying plant parts in the oven at 65 °C for 48 hours.

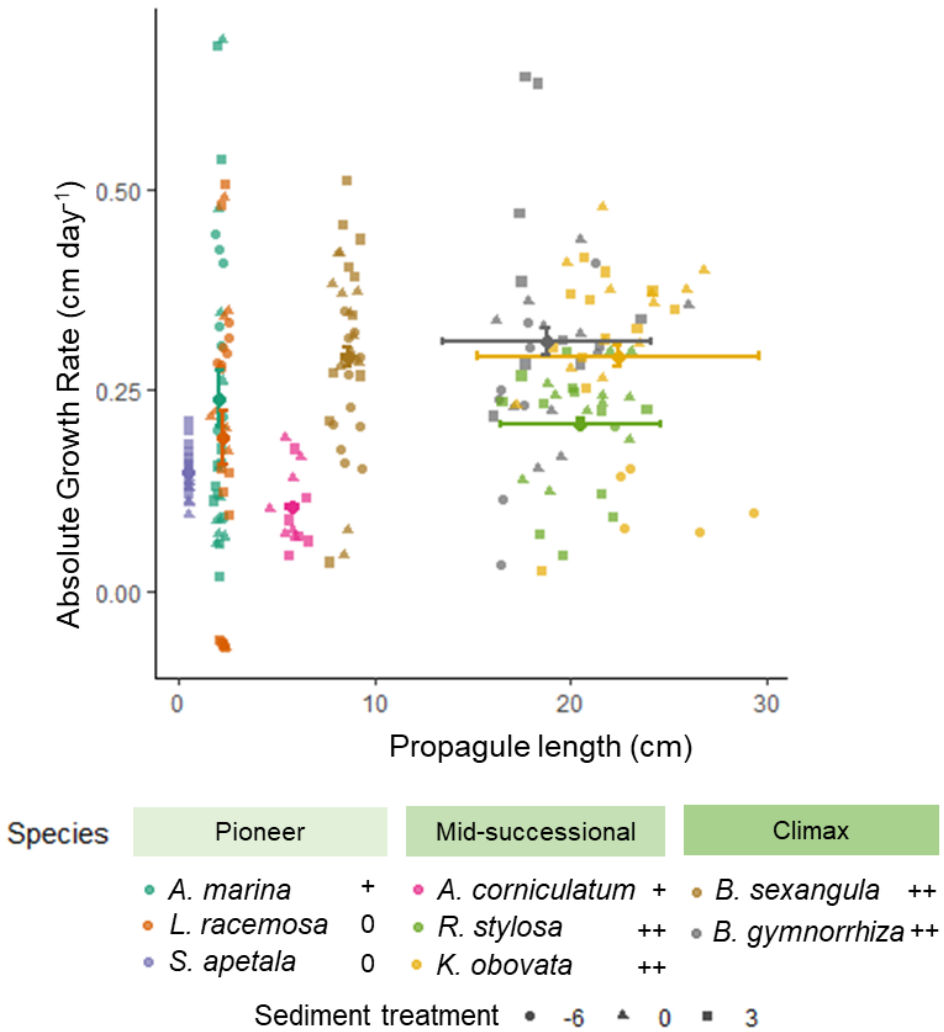


Figure S2.8: Absolute growth rate per species over the 34 days of the experiment, calculated as (max. shoot length - initial propagule size)/34.

Seedling establishment

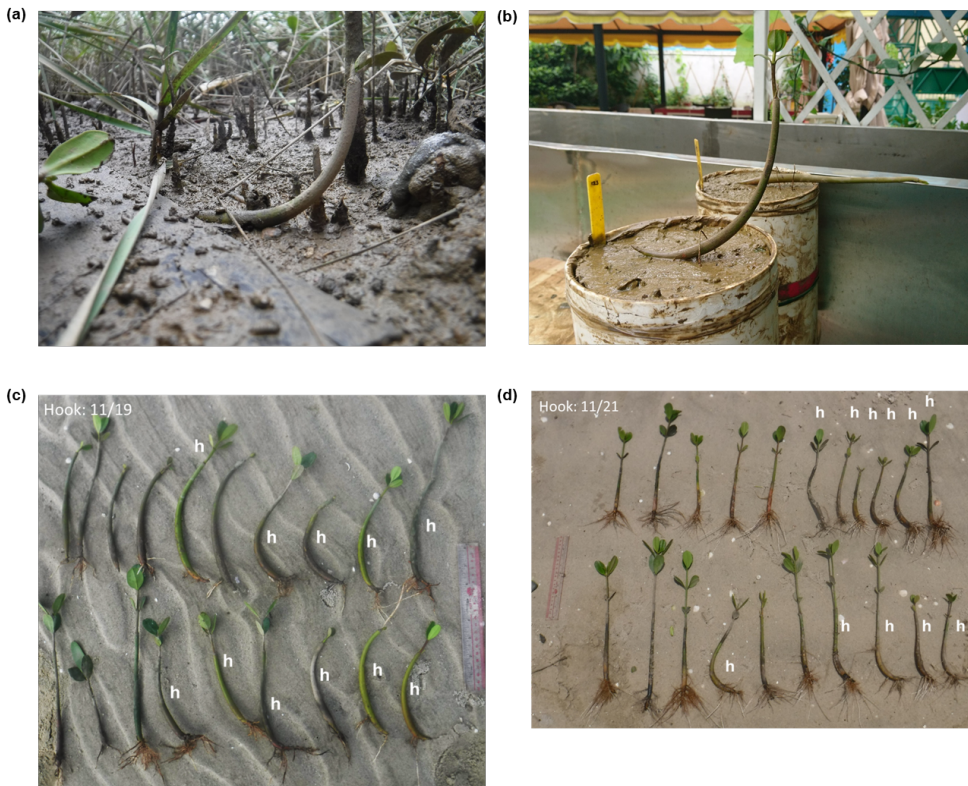


Figure S2.9: Self-erected *K. obovata* seedling with 'hook' inside a mature forest, (b) self-erected *K. obovata* seedling with 'hook' in experimental pot; and number of seedlings that are hooked (arrived horizontally) versus straight (arrived vertically) on (c) bare tidal flat and (d) inside mature forest at Hailing Island field site, Guangdong, China in May 2019. Photos by Rosanna van Hespren.

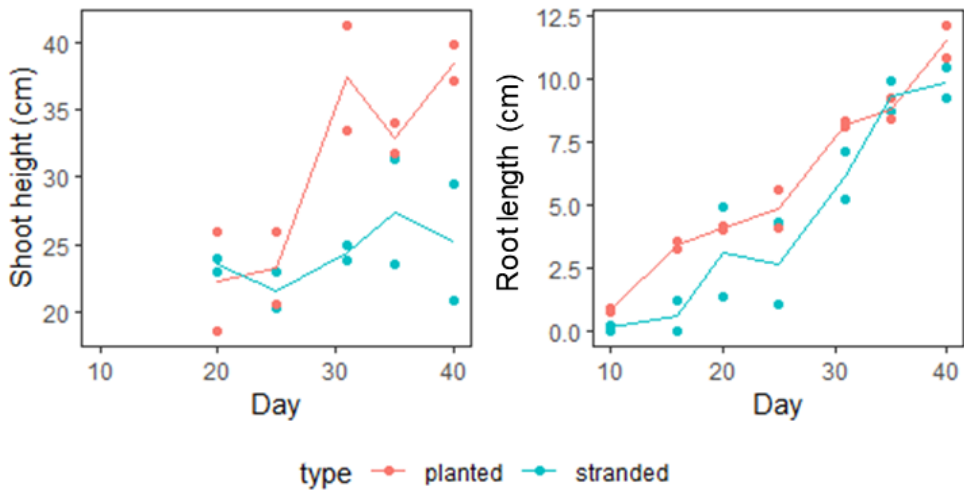
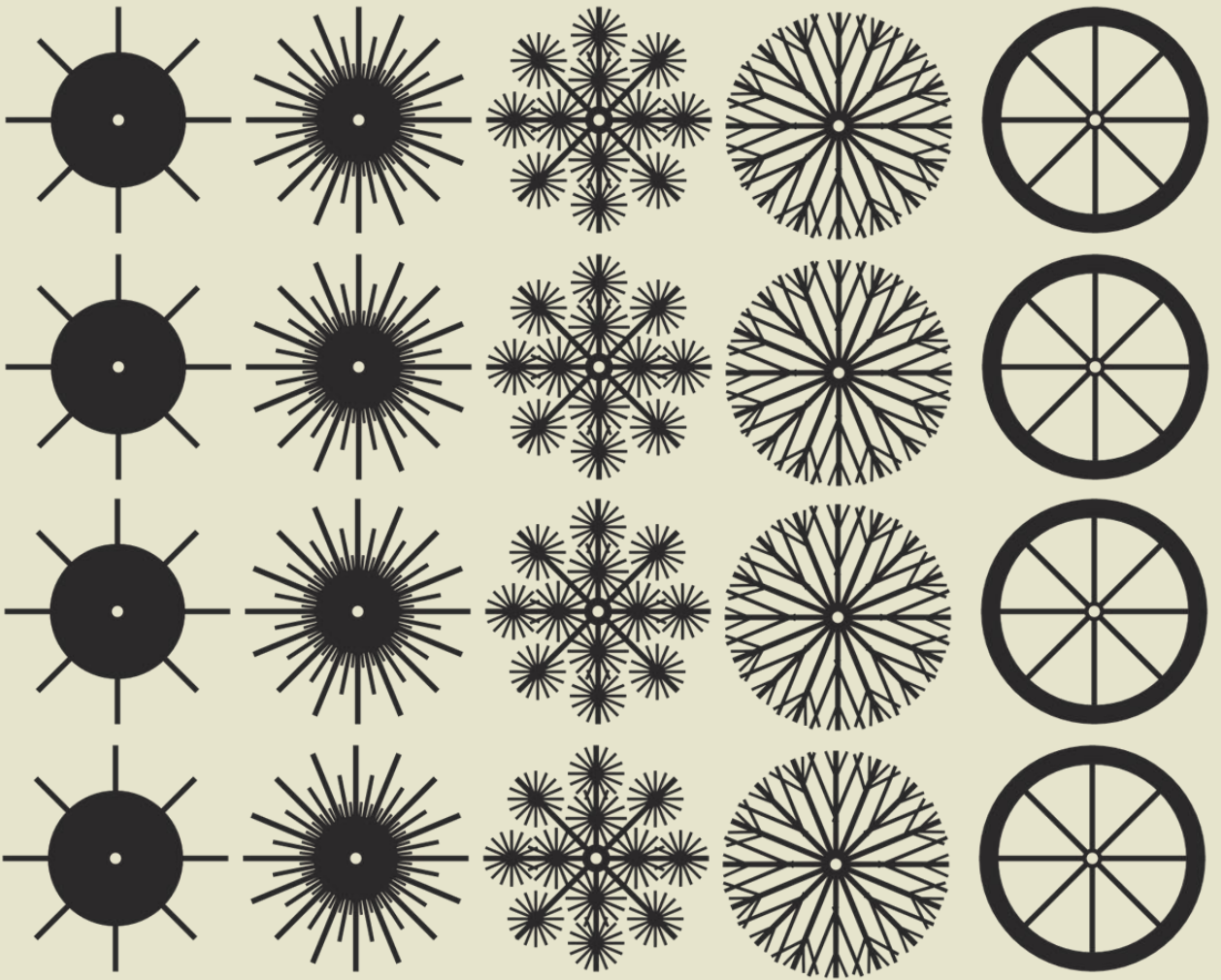


Figure S2.10: Absolute $CED_{dislodge}$ for *Kandelia obovata* seedlings. Corrected for planting depth (vertically 'planted' seedlings went 2.5 cm into the sediment, 'stranded' seedlings were laid horizontally on top of the mud). Shoot height is measured as height from sediment to highest point of seedling.



Chapter 3

Unravelling mangrove tree stability as a function of root morphology and sediment type using 3D-printed mimics

R. van Hespen, M.G. Kleinhans, J. van Belzen, C.E.J. van Bijsterveldt, J.C. de Smit, Z. Hu, B.W. Borsje, T.J. Bouma

Submitted

3 | Unravelling mangrove tree stability as a function of root morphology and sediment type using 3D-printed mimics

Abstract

Mangrove forests provide important ecosystem services globally, yet the processes that affect their persistence are not fully understood. Coastal storms can lead to tree damage and uprooting, causing massive mortality events and reducing forest resilience to repeated stressors. However, the underlying mechanisms of root stability are poorly known. Here, we use 3D-printed, scaled mangrove mimics to study the effect of (i) sediment, (ii) root mass distribution and (iii) root breakage on mangrove stability. We also assess whether a mechanistic anchorage model developed for terrestrial trees can be applied to coastal mangrove trees. We found that higher sediment shear strengths result in substantially higher mimic stability. Interestingly, the optimal root distribution for high mechanical stability depends on the sediment in which a mimic was placed. This suggests that mangroves need to alter their belowground root morphology depending on the sediment they are rooted in to reach the highest possible mechanical stability. Furthermore, we found that the mechanistic anchorage model developed for terrestrial trees provides useful mechanistic principles for estimating mangrove mimic stability, where the specification of sediment resistance through sediment shear strength provided a useful alteration to the existing mechanistic anchorage model. Overall, our findings illustrate the importance of sediment type for mangrove tree stability and consequently minimising storm damage, and highlight the need to map belowground mangrove root morphology. Importantly, this research contributes to a fundamental understanding of mangrove tree stability, which is urgently needed in this era with increasing storminess.

3.1 Introduction

3.1.1 A mechanistic understanding of mangrove tree stability is needed

Mangrove forests provide important ecosystem services such as nature-based flood defence through sediment stabilisation and wave damping (Lee et al., 2014). Although forests provide safety during a storm, they themselves can also be impacted by storms. The strong storm winds, surges and storm waves can cause direct mechanical damage in the form of trunk damage (trunk breakage, branch damage, defoliation), or uprooting, which is exacerbated by the displacement of large volumes of sediment and is most likely fatal (Gardiner, 2021; Krauss & Osland, 2020; Semeniuk, 1980). These storm impacts can cause massive mortality events and lower flood defence capacity (Jimenez et al., 1985), a risk which may be exacerbated over the coming decades as storms potentially increase in frequency and intensity (IPCC, 2022). This forms a barrier to creating or restoring mangrove ecosystems for nature-based flood defence, as it is uncertain if the ecosystem is resilient enough long-term. The consequences of storm damage in mangroves are often mapped in terms of type and extent of damage and recovery rates (e.g. Asbridge et al., 2018; Baldwin et al., 1995; Primavera et al., 2016; Proffitt et al., 2006; Smith et al., 2009). Although the extent of damage (area) can be linked with storm intensity, such a statistical approach makes generalisation of mangrove damage to different geographical and sedimentary settings difficult (Kamimura et al., 2016; Seidl et al., 2011). Hence, a more mechanistic understanding of damage processes is needed. In this study, we focus on understanding the factors protecting mangrove tree stability against uprooting.

3.1.2 Mangrove trees are rooted in marine sediments and have unknown root morphology

Research on terrestrial pine trees has shown that there are two simultaneous processes that affect tree stability (Peltola, 2006). Aboveground, drag forces generated by wind (or waves) acting on the canopy result in an overturning moment (Sagi et al., 2019; Urata et al., 2012). Belowground, this overturning moment is counteracted by an anchorage moment, made up of the tree roots and the root-sediment resistance (Achim & Nicoll, 2009; Coutts, 1986; Fourcaud et al., 2007). While these mechanistic processes have been translated to models, with which the extent of damage during a storm can be estimated for entire forests (Gardiner et al., 2008), it remains uncertain if it works the same way in mangroves. Unlike terrestrial trees that are rooted in terrestrial soils, mangrove trees can grow in sediments ranging from fluid mud, to sandy beaches and even on carbonate reefs (Worthington et al., 2020). These sediments can be dynamic with frequent bed changes and are typically waterlogged (Winterwerp et al., 2020). Furthermore, the belowground morphology of mangrove roots is not well-known. Aboveground, it is well-known what mangrove root system

look like, such as plate roots with pneumatophores, buttresses and stilt roots that allow them to take up oxygen despite living in an anoxic, waterlogged environment (Srikanth et al., 2016; Vovides et al., 2021). Belowground, datasets that describe the size and shape of root systems are sparse (but see Figure 3.1; Njana et al., 2015, 2016; Vovides et al., 2016).

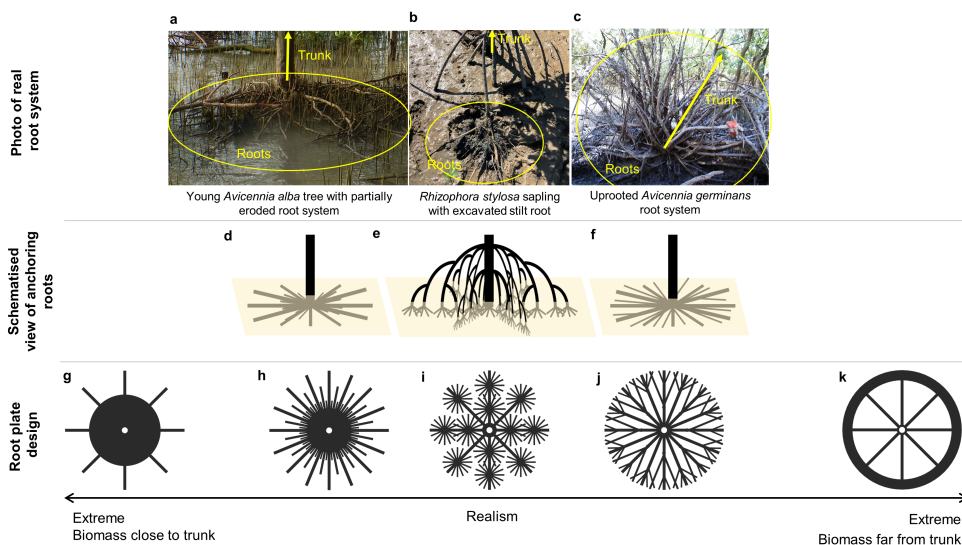


Figure 3.1: Resemblance between real mangrove root systems and the root mimics used in this study. Photos show root systems of mangrove trees, with (a) young *Avicennia alba* trees with root systems partially eroded after the 2017–2018 wet season in Bedono bay, Indonesia, (b) *Rhizophora stylosa* sapling (5yo) with an excavated stilt root in Hailing Island, China in 2021, and (c) an uprooted *Avicennia germinans* tree in central coast of the Gulf of Mexico in 2015. The schematised views (d, e, f) show what the entire anchorage root systems would roughly look like belowground. The bottom row shows the root plate designs that range from extreme (g, k) to more realistic (h, i, j), where the more realistic designs were inspired by the real mangrove root systems, while the extreme root systems allow us to study the extreme ends of the biomass distributions (close or far from the tree trunk). Photos taken by Celine van Bijsterveldt (a), Tianping Xu (b) and Alejandra Vovides (c).

3.1.3 Aims of this research

In this research, we aim to enhance the current mechanistic understanding of mangrove anchorage by carrying out pulling tests with 3D-printed, scaled mangrove mimics – allowing for rapid and reproducible testing. We (1) examine how (a) sediment, (b) root distribution and the (c) breakage of roots affect tree stability, and, upon completion of the pulling tests, we (2) compare the measured mimic stability to predicted mimic stability using a mechanistic model developed for terrestrial trees. Given the wide range of sediments mangroves can grow in, we test stability in five sediments with variable sand:silt ratios and water contents. Furthermore, we design five root plates with hypothetical, idealised root mass distributions. These are (i)

inspired by photos of uprooted and eroded mangrove root systems, (ii) idealised to allow for reproducible testing, and (iii) amplified to allow to test the full extent of root mass distributions: ranging from closely centred around the stem, to evenly spread out, to mostly far away from the stem. As anchorage roots can break under large loads (Coutts, 1986), we design broken versions of the root plates with either half (25% of the complete plate) or complete (45%) breakage at windward, leeward, or both sides of the root plate.

3.2 Methods

3.2.1 Sediment preparation and properties

As mangroves can grow in diverse sedimentary environments, we aimed to cover a range of coastal sediments. We prepared five sediments by mixing various sand, silt and water contents (Table 3.1). An overview of sediment grain sizes in mangrove forests in the literature can be found in Table S3.3. Each sediment was mixed with water, as dry sediment is not usually found at the seaward forest fringe – the zone where most uprooting takes place (Van Loon et al., 2016; Watson, 1928). We mixed homogenous sediments to ensure that our measurements were as consistent as possible. For sand, we used aquarium sand with a grain size of 0.2-0.6 mm (JBL Sansibar, Neuhofen, Germany). For silt, we used kaolin powder with a grain size of 25-35 μm ($\text{Al}_2\text{Si}_2\text{O}_5(\text{OH})_4$, Colpaert – Van Leemputten, Nevele, Belgium). For each mixture, we measured the bulk density ρ_s (kg m^{-3}), penetration resistance pen_s (kPa) and shear strength τ_s (kPa; Table 3.1). Bulk density ρ_s was measured by weighting a disk filled with a known volume of sediment. Penetration resistance pen_s was measured by pushing down a 60° cone with a surface area of 50 mm^2 using a precise automated extenuator (INSTRON, Norwood, US) with a speed of 60 mm min^{-1} . Sediment shear strength τ_s was measured by placing a plate with a diameter of 8 cm below a 0.7 cm layer of sediment (i.e. same size and depth as the mimics in the pulling test; Section 3.2.3), and pulling the plate upward with a speed of 60 mm min^{-1} . The maximum load before failure was used to calculate the sediment shear strength $\tau_{s,r}$, where we first subtracted the weight of the root-sediment plate from the maximum load, and then divided by the surface area of the sediment edge (i.e. perimeter of the plate x depth of the plate). Note that sediment shear strength measured here is not the same as bed shear stress, the latter which is the hydraulic force needed to bring single sediment particles in suspension.

3.2.2 Root plate and mimic design

We designed scaled mangrove mimics with 3D-printed root systems and designed five root mass distributions (Figure 3.1, 3.2a) and various root breakages (Figure 3.2b). The root mass distributions were inspired by photos of uprooted or eroded mangrove roots (Figure 3.1a,b,c). We developed idealised versions for reproducible

Chapter 3

Table 3.1: The five sediment types we mixed and their properties, ordered by shear strength τ_s for easy comparison with figures in the Results section.

Satura- tion state	Sediment	Sand content, (%)	Silt content, (%)	Average grain size (μm)	Water content (% of dry weight)	Bulk density ρ_s (kg m^3)	Pene- tration resis- tance pen_s (kPa)	Shear strength τ_s (kPa)
Undrained	Silt	0	100	30	100	1498	0.5	0.7
Undrained	Sand	100	0	400	30	1732	64.3	7.6
Undrained	Silty Sand	50	50	215	50	1738	6.5	9.1
Drained	Silt	0	100	30	70	1537	20.0	15.0
Drained	Silty Sand	50	50	215	30	1903	53.7	40.7

Table 3.2: Properties of mangrove trees and mimics, and mimics scaled up 100x. Tree data are from Njana et al. 2015, 2016, where root plate radius is based on the length of the belowground (cable) roots.

Tree or mimic	Tree height, m (mean \pm sd)	Root plate radius, m (range)	Root depth, m
<i>Avicennia marina</i>	9.6 \pm 5.4	1.4-16.1	0.2-1.4
<i>Rhizophora stylosa</i>	7.4 \pm 6.4	1.6-5.1	0.3-1.0
Mimic	0.105	0.04	0.007
Upscaled 100x	10.5	4	0.7

testing, with some more realistic and detailed (Figure 3.1h,I,j) and some more extreme and simplified root mass distributions (Figure 3.1g, k) to test along the entire realm of possible root mass distributions, such that some have biomass closely centred around the stem (SimInn), evenly spread out (DetInn, DetMid, DetOut), and some far away from the stem (SimOut). In this naming system, 'Sim' stands for simple and 'Det' stands for detailed. The root plates were designed with equal surface areas A_r (cm^2 ; Figure 3.2a), but differed slightly in actual surface area because of the 3D-printing process (Figure 3.3). Therefore, in this paper, the root plate areas A_r (cm^2) will be represented by the proxy root plate weight W_r (g). To assess the effect of root breakage, we removed a part of the root plate. We did this at two distances from the edge of the root plate, at 25% and 45% of the total diameter of the plate (2 and 3.5 cm of 8 cm diameter, respectively), on the windward (25W, 45W), leeward (25L, 45L) or both sides (25B; Figure 3.2b). As the root distributions varied in the location of their biomass, the reduction in area (proxy weight W_r) was higher for some (e.g. SimOut) than for other root distributions (e.g. SimInn; Figure 3.3).

Mangrove tree stability

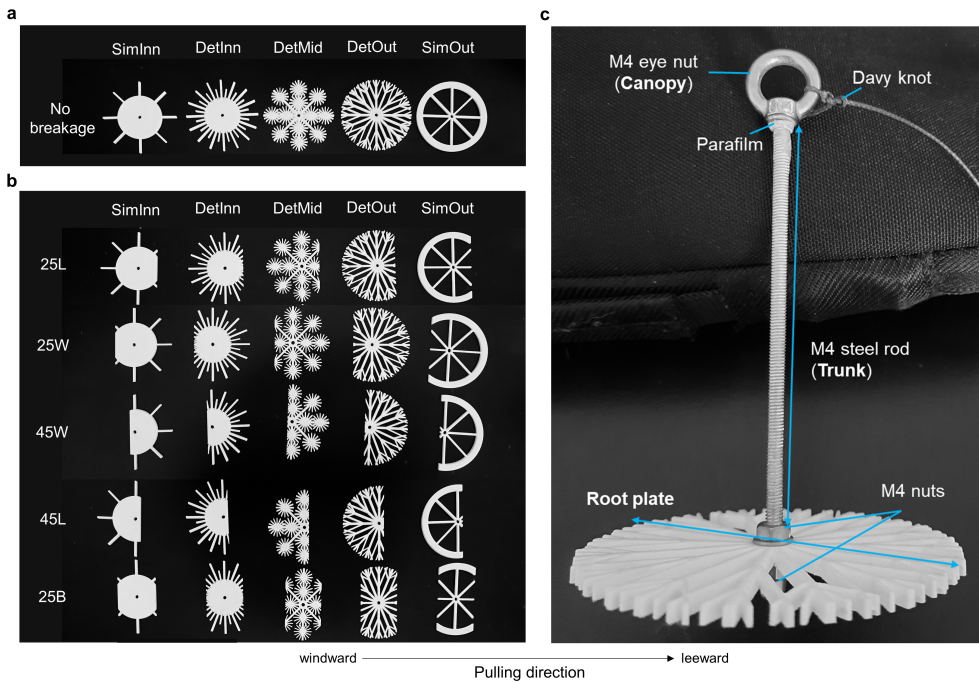


Figure 3.2: The mangrove mimics, with (a) the 3D-printed root plates, showing the five root mass distributions (where Sim = simple and Det = detailed), (b) breakage variations, and (c) the construction of a mangrove mimic, with a tree trunk made of an M4 stainless steel rod, a canopy made of an M4 stainless steel eye nut held firmly in place with parafilm, and a 3D-printed root plate held in place with nuts. Mimic and root plates are shown following the pulling direction used in the pulling tests.

We opted to design mangrove tree mimics that were scaled roughly 1:100 in terms of size compared to real mangrove trees (Table 3.2), resulting in a root plate diameter of 8 cm and a height of 3 mm (we opted for small mimics to facilitate the quick subsequent pulling tests). It was not possible to scale weight in this manner, due to the differences between mangrove root properties and the plastic used for 3D-printing. We drew the root systems using a browser-based 3D modelling program, Tinkercad (Autodesk, San Rafael, USA), and 3D-printed them with Nylon12 plastic using Selective Laser Sintering (Shapeways, Eindhoven, The Netherlands). The mimics were constructed by attaching the 3D-printed root plates with nuts to a tree trunk made of an M4 stainless steel rod and a canopy made of an M4 stainless steel eye nut held firmly in place with parafilm (Figure 3.2c).

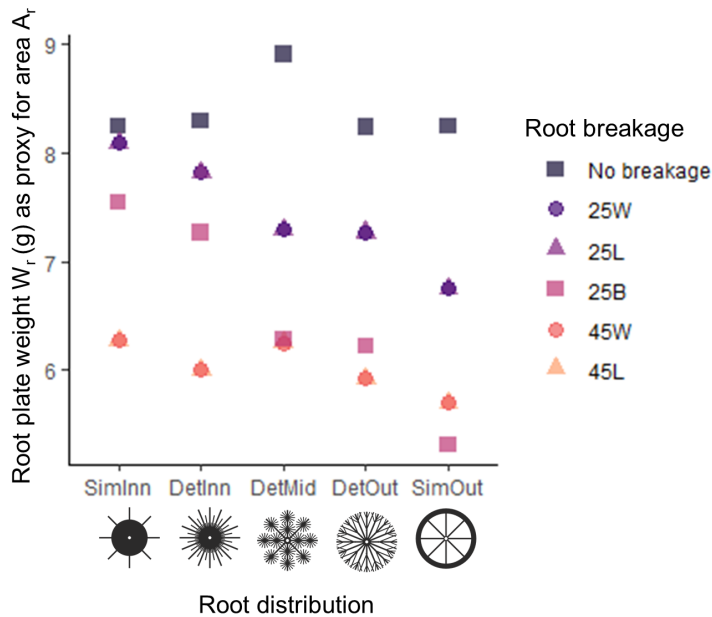


Figure 3.3: Root plate weight W_r (g), as a proxy for area A_r (cm^2), per root mass distribution and root breakage.

3.2.3 Pulling tests to measure overturning moments

We carried out pulling tests with all sediments, root mass distributions and root breakages. In total, 345 pulling tests were conducted. Each test was carried out three times, where we replaced the sediment in the pot after each test and placed the same mimic in it again (explained below). We carried out tests in each sediment type with each root mass distribution with the unbroken root plates (5 sediments \times 5 root distribution \times 3 repetitions = 75 tests). Undrained Silt and Undrained Sand did not provide much stability to the mimics. Therefore, we did not test root breakage (which further reduced stability) in these sediments, as it was practically challenging to keep the mimics upright before pulling. Thus, we carried out tests with root breakage, for each root distribution, only in Drained Silt, Drained Silty Sand and Undrained Silty Sand (3 sediments \times 5 root distributions \times 6 root breakages \times 3 repetitions = 270 tests).

Each pulling test was prepared by 'planting' the mimic in a pot filled with one of the sediments. An 80-micron plastic bag with a watertight seal (to avoid water leakage from sediments) was placed in a 9.6 cm tall pot made out of a PVC pipe with a diameter of 15.5 cm. The plastic bag was filled with sediment and levelled

off evenly at the top. The pot had a 1 cm disk at the bottom that was removed so that the sediment sank 1 cm. The mimic was then placed on top of the sediment and the remaining gap was filled and levelled off evenly at the top, so that the mimic was now 1 cm belowground with an effective sediment depth of 7 mm (as the root plate was 3 mm tall – equal to 0.7 m belowground in the field; Table 3.2). The same steps (filling the bag with sediment, removing the 1 cm disk, placing the mimic and filling and levelling off the top 7 mm) were used for repeat tests (three repetitions per sediment x mimic configuration). Then, we attached the mimics to the pulling mechanism of a universal testing machine fitted with a 10 N load cell (INSTRON, Norwood, US) by tying a polyester string (with a diameter of 0.75 mm and a tensile strength of 17 kg; Paracord Nano, Atwood Rope MFG, Millersport, US) to the ‘crown’ of the mimic (the eye nut) with a Davy knot (Figure 3.2c). The other side of the string was looped through a pulley that was placed at a distance of 45 cm and attached with a bowline knot to the universal testing machine (INSTRON, Norwood, US).

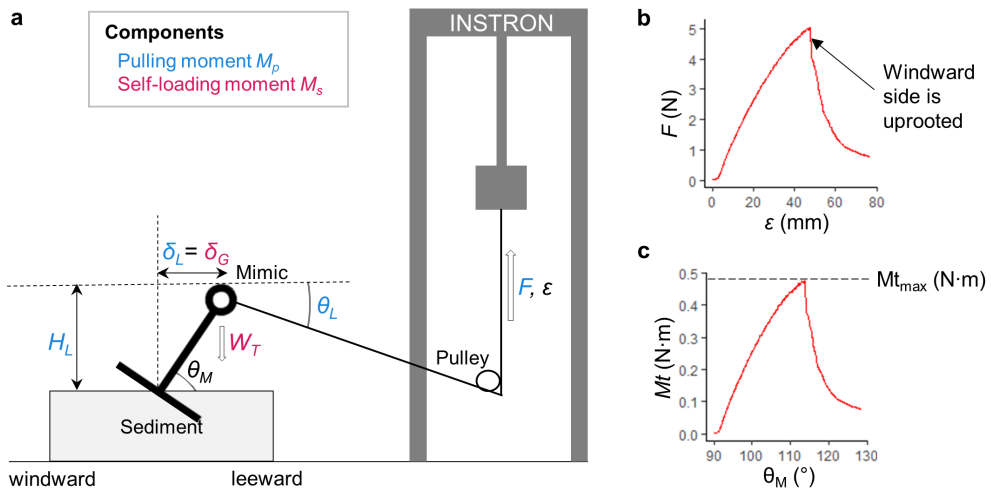


Figure 3.4: Pulling experiment, with (a) the pulling setup (not to scale) used to measure the overturning moment of each mimic using an INSTRON universal testing machine, (b) an example of output of a pulling test with load F (N) per extension ϵ (mm) that illustrates how the load (F) drops after the windward side is uprooted, and (c) an illustration of how we obtained the maximum overturning moment $M_{t_{max}}$ (N·m). Calculation of the overturning moment M_t (N·m) is described in the text.

The pulling test was carried out by moving the pulling mechanism upwards, so that the mimic that was attached moved forward (Figure 3.4a). During each pulling test, we measured the load F (N) per extension ϵ (mm) continuously (Figure 3.4b) and pulled at least until the windward side of the root plate was fully uprooted. The pulling mechanism moved upwards at an extension speed of 60 mm min⁻¹.

Chapter 3

The extension ϵ (mm) was converted to a mimic angle θ_M ($^\circ$), that moved with approximately $0.5^\circ \text{ mm}^{-1}$ (i.e. $30^\circ \text{ min}^{-1}$).

We calculated the overturning moment M_t (N·m) as in Urata et al. 2012:

$$M_t = M_p + M_s \quad (3.1)$$

where M_p (N·m) and M_s (N·m) are the moments of pulling load and self-loading (i.e. the turning moment generated by the weight of the mimic as it topples), respectively. The pulling load is the sum of its horizontal and vertical components:

$$M_p = H_L F \cos \theta_L + \delta_L F \sin \theta_L \quad (3.2)$$

where H_L is the pulling height (m), F is the pulling load (N), θ_L is the angle of pulling (rad) and δ_L is the horizontal displacement of the stem at pulling height (m). We calculated the pulling angle θ_L (rad) and the horizontal displacement of the stem at pulling height δ_L (m) using basic trigonometric calculations (Table S3.2). The self-loading moment M_s (N·m) is defined as

$$M_s = \delta_G W_T g \quad (3.3)$$

wherein δ_G is the horizontal stem displacement at the centre of gravity of the above-ground part (m), which is in our case the same as the horizontal displacement of the stem at pulling height δ_L (m), W_T is the aboveground biomass (kg) and g is the gravity (9.81 N kg^{-1}). An overview of all parameters can be found in Table 3.3.

Mangrove tree stability

Table 3.3: All properties with symbols, units, their meaning and the source where values can be found.

Symbol	Unit	Meaning	Source
Soil parameters			
τ_s	N m^{-2}	Shear strength	Table 3.1
ρ_s	kg m^{-3}	Bulk density	Table 3.1
pen_s	N m^{-2}	Penetration resistance	Table 3.1
Root parameters			
P_r	%	Half surface parameter	Figure 3.9a
piv_b	#	Number of root breakages	Figure 3.2b
A_r	m^2	Root plate area	Figure 3.3; Table S3.3
W_r	kg	Root plate weight, proxy for area A_r	Figure 3.3; Table S3.3
D_s	m	Sediment/rooting depth	0.007; Table 3.2
Overtuning components			
M_t ;	$\text{N}\cdot\text{m}$	(Maximum) overturning moment	$M_t = M_p + M_s$
M_{tmax}			
M_p	$\text{N}\cdot\text{m}$	Pulling moment	$M_p =$ $H_L F \cos \theta_L +$ $\delta_L F \sin \theta_L$
M_s	$\text{N}\cdot\text{m}$	Self-loading moment	$M_s = \delta_G W_T g$
H_L	m	Pulling height	See Figure 3.4a
F	N	Pulling load	See Figure 3.4a
θ_L	rad	Angle of pulling	See Figure 3.4a
δ_L ; δ_G	m	Horizontal displacement of the stem at pulling height	See Figure 3.4a
W_T	kg	Aboveground biomass	0.02
Anchorage components			
M_a	$\text{N}\cdot\text{m}$	Anchorage moment	$M_a = M_w + M_r$
M_w	$\text{N}\cdot\text{m}$	Weight moment	$M_w = y_1 W_s g$
M_r	$\text{N}\cdot\text{m}$	Resistance moment	$M_r = \tau_s D_s C_p y_2$
y_1	m	Distance from hinge to the centre of gravity of root-sediment plate	Figure 3.5; Table S3.3
W_s	kg	Weight of the sediment cylinder above the roots	
g	N kg^{-1}	Gravitational constant	9.81
C_p	m	Perimeter of windward side of the root plate	Figure 3.5; Table S3.3
y_2	m	Distance from hinge to the centre of gravity of the arc	Figure 3.5; Table S3.3

3.2.4 Statistical analysis

We used R (version 4.1.1) with packages *rstatix* (0.7.0), *corrplot* (0.92), *FactoMiner* (2.4), *factoextra* (1.0.7) and *MuMIn* (1.46.0) to carry out all statistical analyses. We calculated the maximum overturning moment $M_{t_{\max}}$ (N·m) as the highest overturning moment M_t (N·m) that was measured during a pulling test before failure, i.e. the moment just before the root plate was uprooted (Figure 3.4b,c). First, we tested the effect of sediment on mimic stability. We used a Kruskal-Wallis test to check if there were any significant differences in the maximum overturning moment $M_{t_{\max}}$ (N·m) between sediments, followed by a post-hoc Dunn's test to compare any differences between sediments. We then tested the effect of root breakage on mimic stability. We normalised the maximum overturning moments $M_{t_{\max}}$ (N·m) for the sediment effect on stability, by dividing the average $M_{t_{\max}}$ per sediment by the $M_{t_{\max}}$. We then fit, per sediment, a linear model between the normalised moments and root breakage, which was represented by root plate weight W_r (g), as a proxy for the change root plate area A_r (cm²), and we also calculated the Pearson correlation coefficient.

To assess the role of root distribution in mimic stability, we calculated a parameter to describe the root distribution; P_r (%). Root distribution P_r was calculated by finding out at what distance from the trunk 50 % of the cumulative biomass was reached. We then fit a polynomial regression model between the maximum overturning moment $M_{t_{\max}}$ (N·m) and the root distribution parameter P_r , per sediment type.

Then, we carried out a Principal Component Analysis and Pearson correlation tests to assess the effect of sediment properties (shear strength τ_s , bulk density ρ_s , penetration resistance pen_s), root distribution (P_r) and root breakage (number of breakages piv_b , root plate area A_r , root plate weight W_r as a proxy for area, C_p , y_1 , y_2) on the maximum overturning moment $M_{t_{\max}}$. Based on this analysis, we selected the best fitting parameters per variable group (sediment, root distribution, root breakage), and fit linear and interaction models to the data. We then used model comparison using the Akaike Information Criterion (AIC) and Akaike weights (W_i) to find the best fitting model (Johnson & Omland, 2004).

3.2.5 Comparing predicted stability to measured stability

We aimed to find out if mangrove (mimic) stability can be modelled mechanistically by adapting a model developed for terrestrial, shallow-rooted pine trees by Achim and Nicoll 2009. We used this model to predict the anchorage moment of our mangrove mimics, and compared this to the measured maximum overturning moment $M_{t_{\max}}$ (i.e. we assume that the maximum overturning moment $M_{t_{\max}}$ before failure is equal to the anchorage moment of the mimic). We have adapted the model at one point. In the original model the resistance moment M_r is the resistance

of the root-sediment matrix, which requires that a resistance constant ' A_1 ' (N m^{-1}) is estimated per sediment type based on pulling tests. There is effectively no root resistance in our setup because the 3D-printed Nylon12 material is too strong to break under the test circumstances, so that the only limiting factor is resistance of the sediment. Hence, we argue that the constant A_1 used in their model can be replaced with sediment resistance, measured as sediment shear strength τ_s (N m^{-2}). Thus, we define the anchorage moment M_a as:

$$M_a = M_w + M_r \quad (3.4)$$

where M_a is the anchorage moment, M_w is the moment of the root-sediment plate weight and M_r is the moment of the root-sediment resistance. The moment representing the root-sediment plate weight is:

$$M_w = y_1 W_s g \quad (3.5)$$

where M_w is the moment of the root-sediment plate, with y_1 the distance from the hinge to the centre of gravity of the root-sediment plate (m; lever arm length, Figure 3.4), and W_s is the weight of the sediment in the root-sediment plate: $W_s = D_s A_r \rho_s$, with A_r the area of the root-sediment plate, D_s the sediment depth, ρ_s the bulk density of the sediment (kg m^{-3}) and g the gravity (9.81 N kg^{-1}). Furthermore,

$$M_r = \tau_s D_s C_p y_2 \quad (3.6)$$

where τ_s (N m^{-2}) is the sediment shear strength (as measured in Section 3.2.1), D_s (m) is the sediment depth, C_p (m) is the circumference/perimeter of the windward edge of the root-sediment plate and y_2 (m) is the distance from the hinge to the centre of gravity of the arc (Figure 3.4, Table S3.3).

To assess the model fit of the anchorage model (Equation 3.4), we compared the predicted anchorage moment M_a to the observed maximum overturning moment $M_{t_{\max}}$ for the full anchorage model M_a (Equation 3.4), the weight model M_w (Equation 3.5) and the resistance model M_r (Equation 3.6). For each of these models, we compared the Akaike information criterion (AIC) and Akaike weight (Johnson and Omland, 2004), correlation r , intercept β_0 (which should be 0 for a perfect prediction) and the slope β_1 (which should be 1 for a perfect prediction). For the best fitting model, we then left out each of the non-constant model components (e.g. for the resistance model leave out τ_s , then C_p , then y_2) to assess the role of each component.

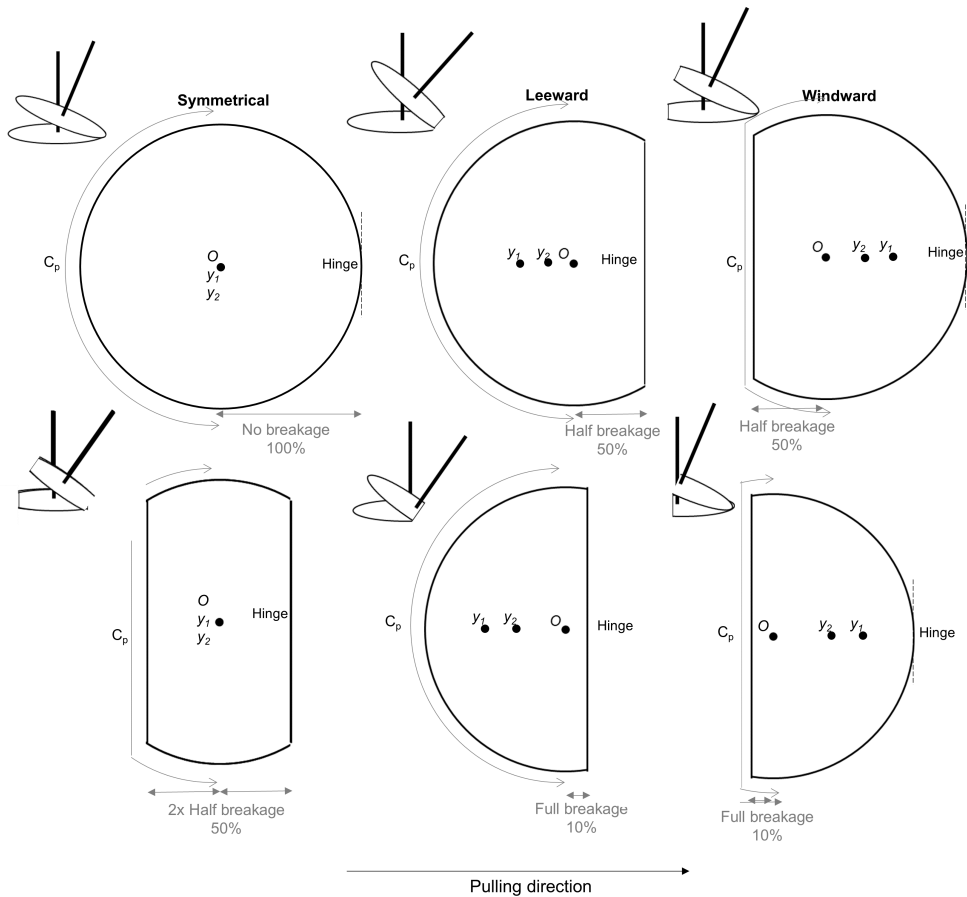


Figure 3.5: Hinges, centroids y_1 and y_2 (where we use the distance from the hinge to the centroids), and windward perimeter C_p for each of the root cuts, where we assume they do not vary between the five different root mass distributions. Values can be found in Table S3.3.

3.3 Results

3.3.1 General patterns in mimic stability

The overturning curves (overturning moment M_t per mimic angle θ_M) varied between sediment types, root mass distributions and root breakage (Figure 3.6). Sediment type strongly affected the maximum overturning moment ($M_{t_{\max}}$; Figure 3.4c), with higher maximum overturning moments $M_{t_{\max}}$ for sediments with stronger sediment shear strengths τ_s (N m^{-2} ; $\alpha = 0.05$; Figure 3.7). Furthermore, root breakage also had a significant effect on mimic stability. We observed a significant decrease in sediment-normalised maximum overturning moment $M_{t_{\max}}$ for more excessive breakage (Figure 3.8a; where maximum overturning moment $M_{t_{\max}}$ ($\text{N}\cdot\text{m}$) is sediment-normalised to exclude the effect of sediment on stability, and breakage

Mangrove tree stability

was represented by root weight W_r as a proxy of root plate area A_r ; Figure 3.3). The strength of this effect depended on sediment type; the decrease in mimic stability was mild in Undrained Silty Sand ($y = 0.13 + 0.19x, r = 0.55, p < 0.001$), steeper in Drained Silt ($y = -0.27 + 0.28x, r = 0.53, p < 0.001$), and steepest in Drained Silty Sand ($y = -0.07 + 0.23x, r = 0.27, p < 0.001$). We found no significant difference between leeward (45L and 25L) and windward breakage (45W and 25W; Dunn's test with $\alpha = 0.05, p = 0.82$). When fitting the linear model ($y = -0.07 + 0.23x$) for each root mass distribution, we found significant differences in residuals between the root mass distributions (Figure 3.8b), indicating that root mass distribution also had an effect on stability. Indeed, using a root distribution parameter P_r (Figure 3.9a) to test the effect of root mass distribution on mimic stability, we fit a polynomial curve to the maximum overturning moment Mt_{\max} across the root mass distributions per sediment. This confirmed the effect of root mass distribution, where optimal root mass distribution depended on sediment type (Figure 3.9b,c).

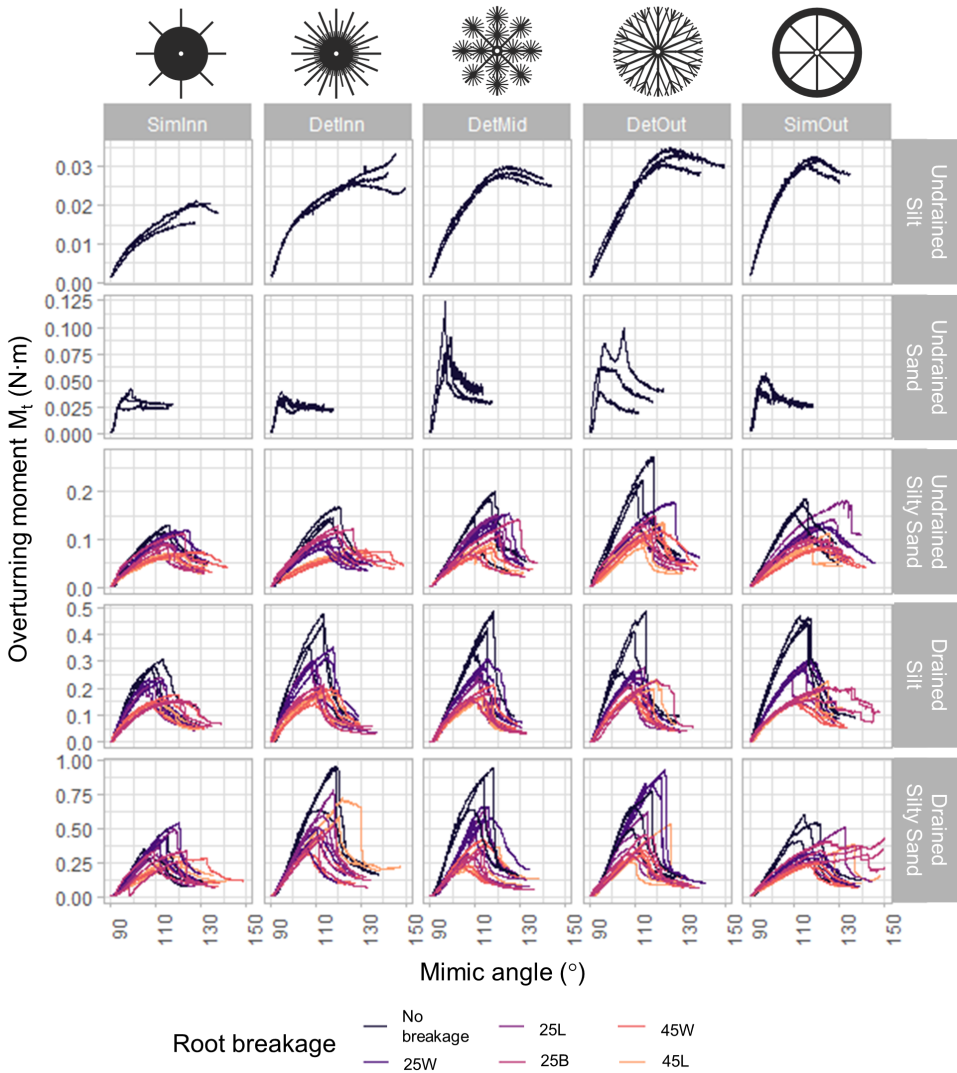


Figure 3.6: Overturning curves, showing overturning moment M_t (N·m) per mimic angle θ_M (degrees) for each root type and sediment. Note different y-axes between sediments.

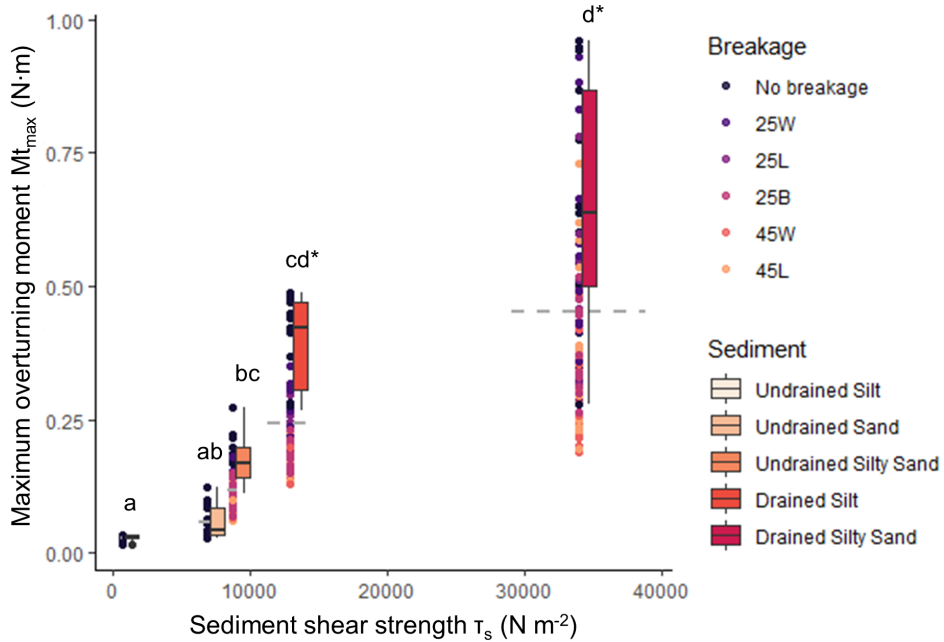


Figure 3.7: Effect of sediment type on mimic stability, showing maximum overturning moment $M_{t_{max}}$ ($N\cdot m$) per sediment shear strength τ_s ($N\ m^{-2}$), shown for all root mass distributions and breakages. Points show all data and are shown at exact mean shear strength τ_s , while boxplots are dodged. The boxplots show data only for the non-broken root systems, as Undrained Silt and Undrained Sand were not tested with broken roots. Significance letters for the boxplots are based on a Dunn's test ($\alpha = 0.01$), where the * indicates no significant difference when testing for all data (same as in points). Dashed line indicates the standard deviation of the shear strength measurements.

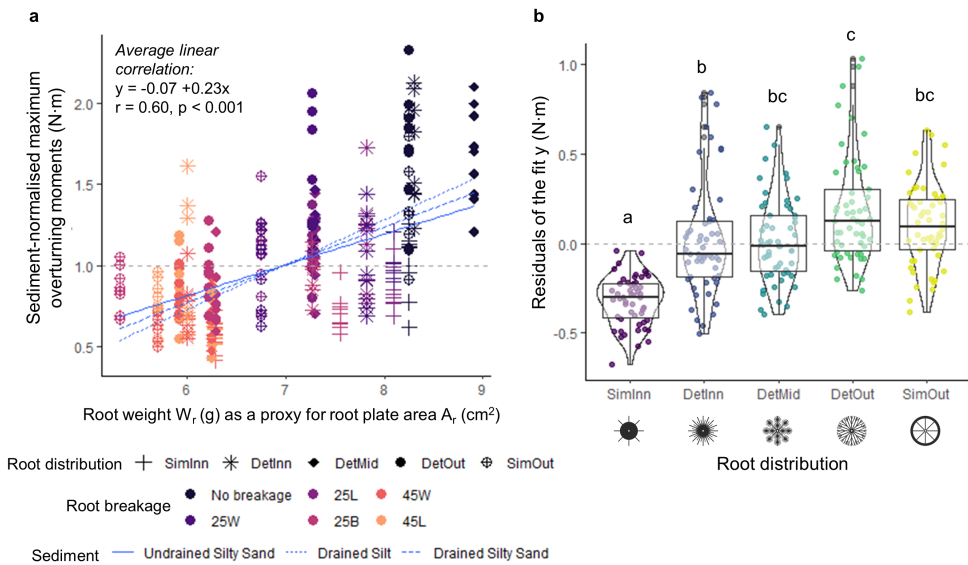


Figure 3.8: Effect of root breakage on mimic stability, with. (a) Sediment-normalised maximum overturning moment $M_{t_{max}}$ (N·m) per root weight W_r (g) as a proxy for surface area A_r (cm²), tested in Undrained Silt Sand, Drained Silt and Drained Silty Sand. Blue lines indicate the Pearson correlation between root weight W_r and the sediment-adjusted maximum overturning moment $M_{t_{max}}$. (b) Residuals (jitterplot with boxplot and violinplot) of the linear regressions from (a). Significance letters ($\alpha = 0.05$) from Dunn's test.

Mangrove tree stability

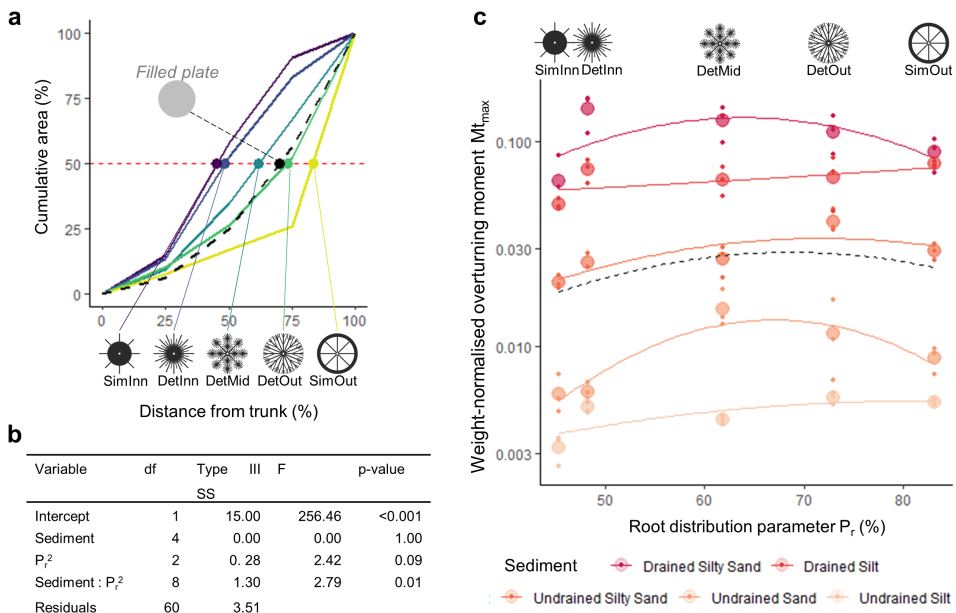


Figure 3.9: Effect of root mass distribution on mimic stability, with (a) root distribution parameter P_r as the point where the cumulative surface area of the root plate reaches 50% (only for unbroken root plates), (b) ANOVA for the polynomial interaction model $Mt_{\max} \sim \text{Sediment} * P_r^2$ (dashed line in c); and (c) weight-normalised maximum overturning moment Mt_{\max} (small dots) and mean moments (large dots) per root distribution P_r (%), shown per sediment for all non-broken roots. Mt_{\max} is normalised for root plate weight W_r as proxy for root plate area A_r , to account for the small variations in surface area from the printing process (Figure 3.3); Mt_{\max}/W_r . Showing only non-broken roots.

3.3.2 Best statistical model to explain the mimic stability data

From the previous section it is apparent that sediment type, root breakage, and root mass distribution each affect mimic stability. To investigate the size of the effect of these stability components and their interactions, we first carried out a principal components analysis and tested linear correlations between all quantitative sediment and root plate variables (Figure 3.10). We found that the first three principal components accounted for 79% of the variation. In Principal Component 1 we observed the strongest correlation between maximum overturning moment Mt_{\max} and root weight W_r (that functions as a proxy for root area, A_r), and in Principal Component 2 we observed the strongest correlation between the maximum overturning moment Mt_{\max} and sediment shear strength τ_s . In Principal Component 3, we did not observe a significant linear correlation between Mt_{\max} and P_r . Then, we carried out a model selection to analyse the role of sediment shear strength τ_s , root weight W_r as proxy for root plate area A_r , the root distribution parameter P_r (as a polynomial), and their potential interactions (Table 3.5). The model with the lowest Akaike Information Criterion was $Mt_{\max} \sim \tau_s + W_r + \tau_s : W_r + P_r^2 + \tau_s : P_r^2 + W_r : P_r^2$ (AIC = -526.62). The parameter that best explained the variation in Mt_{\max} was sediment shear strength τ_s , followed by root weight W_r (proxy for root area), and then an interaction between the two. Thus, if roots break, the change in stability depends on the sediment shear strength.

Mangrove tree stability

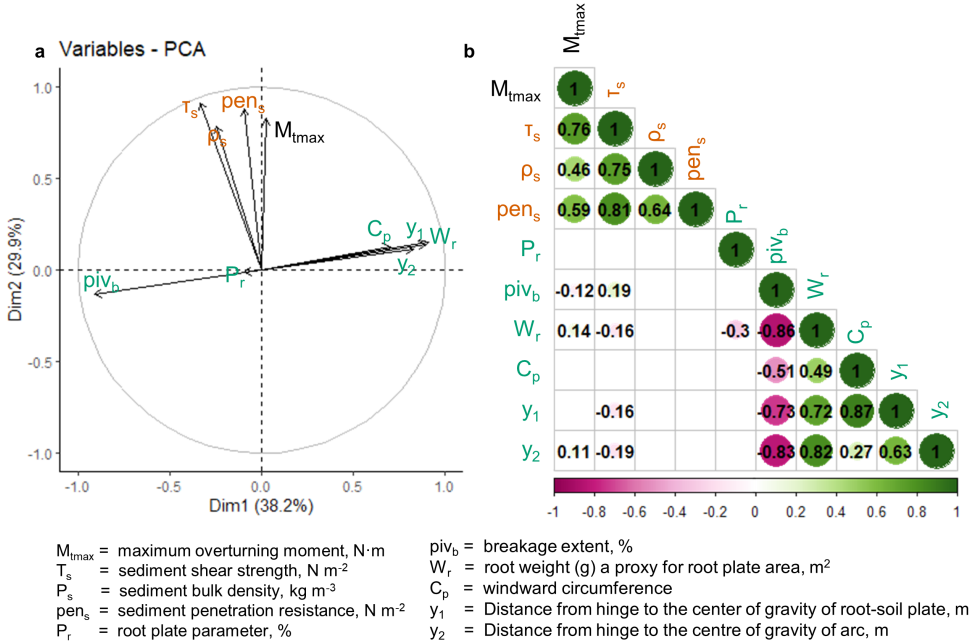


Figure 3.10: (a) Correlation circle showing correlation between variables and Principal Components and (b) all significant ($\alpha = 0.05$) correlations between variables. Symbol colours indicate sediment (brown) and mimic (green) related properties.

Table 3.4: Model comparison, showing model fits with Akaike Information Criterion AIC, Akaike weights W_i and adjusted R^2 with its p-value. Note that root plate weight W_r functions as a proxy for root plate area A_r .

model	df	AIC	W_i	Adj. R^2	p-value
$Mt_{max} \sim 1$	2	-142.78	0	-	-
$Mt_{max} \sim T_s$	3	-399.28	0	0.58	<0.001
$Mt_{max} \sim W_r$	3	-146.58	0	0.02	0.017
$Mt_{max} \sim P_r^2$	4	-142.90	0	0.01	0.13
$Mt_{max} \sim T_s + W_r$	4	-451.16	0	0.64	<0.001
$Mt_{max} \sim T_s + P_r^2$	5	-405.13	0	0.59	<0.001
$Mt_{max} \sim T_s + W_r + T_s : W_r$	5	-490.85	0	0.69	<0.001
$Mt_{max} \sim T_s + W_r + P_r^2$	6	-466.51	0	0.66	<0.001
$Mt_{max} \sim T_s + W_r + T_s : W_r + P_r^2$	7	-513.12	0	0.71	<0.001
$Mt_{max} \sim T_s + W_r + T_s : W_r + P_r^2 + T_s : P_r^2$	9	-519.52	0.03	0.72	<0.001
$Mt_{max} \sim T_s + W_r + T_s : W_r + P_r^2 + W_r : P_r^2$	9	-516.17	0.01	0.72	<0.001
$Mt_{max} \sim T_s + W_r + T_s : W_r + P_r^2 + T_s : P_r^2 + W_r : P_r^2$	11	-526.62	0.97	0.73	<0.001

3.3.3 Anchorage predictions and model fitting

We compared measured maximum overturning moments $M_{t_{\max}}$ (N·m) to anchorage moments M_a (N·m) predicted with the anchorage model (Equation 3.4) and found that the resistance model M_r (Equation 3.6) best fit our data (Table 3.5). Furthermore, we observed that the model overestimated stability slightly in most cases, such that the average ratio $M_{t_{\max}}/M_a = 0.71$ (Figure 3.11). The model's accuracy was quite variable across sediment type, while more consistent for root breakage (Figure 3.11a, b). Across root mass distributions, the model was more accurate for more widespread root mass distributions (Figure 3.11c).

Table 3.5: Parameters of mechanical model variations. Sediment depth D_s and gravitational constant g are constants and not considered in calculated df.

Prediction equation	df	AIC ($M_t \sim M_a$)	W_i	$r(p < 0.01)$	β_0	β_1
$M_a = y_1 W_s g + \tau_s D_s C_p y_2$	5	-507.08	0.06	0.84	0.03	0.53
$M_a = y_1 W_s g$	2	-153.08	0	0.20	0.17	14.07
$M_a = \tau_s D_s C_p y_2$	3	-512.60	0.94	0.84	0.04	0.56
$M_a = \tau_s D_s y_2$	2	-491.76	0	0.83	0.03	0.07
$M_a = D_s C_p y_2$	2	-145.53	0	0.13	0.18	3065.44
$M_a = \tau_s D_s C_p$	2	-433.52	0	0.79	0.03	0.02

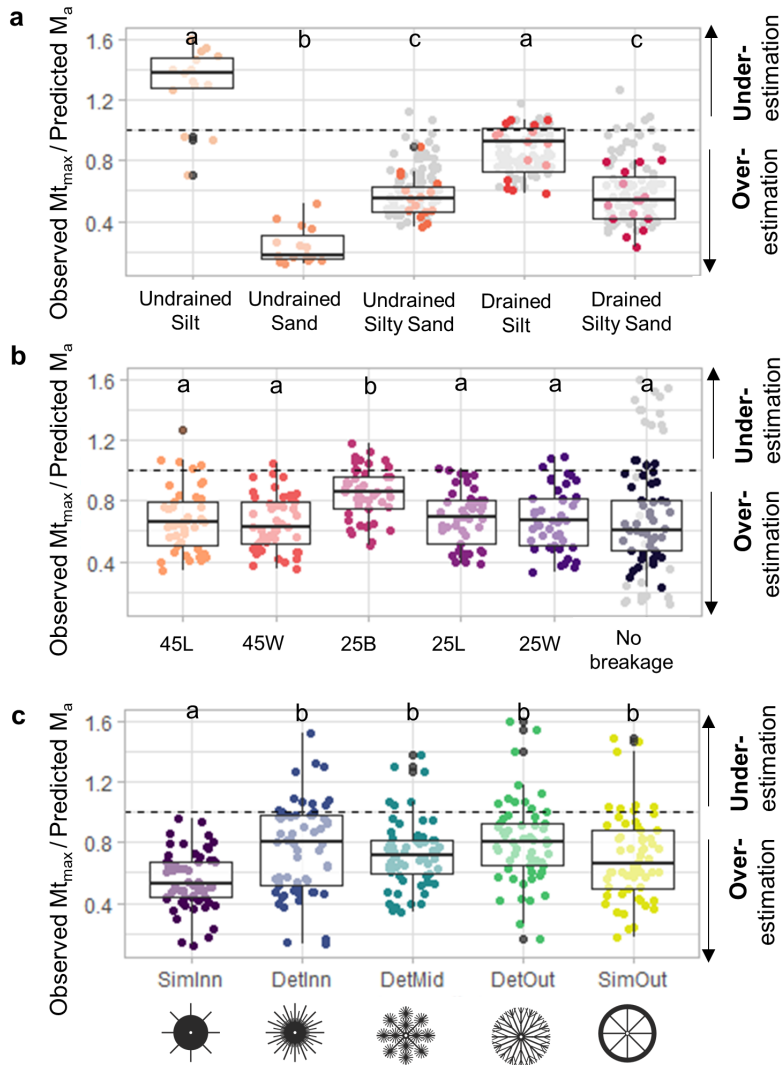


Figure 3.11: Jitterplots and boxplots of model fit for (a) sediment types, (b) root breakage and (c) root distributions. Coloured dots represent the data used in the boxplots. Grey dots represented the entire dataset, but were excluded as not all root breakages were tested in all sediments. Dashed line indicates accurate prediction. Significance letters for boxplots ($\alpha = 0.05$) from Dunn's test.

3.4 Discussion

In this study we aimed to understand the effect of sediment type, root mass distribution and root breakage on mangrove tree stability using 1:100 scaled 3D-printed mimics. We observed higher mimic stability for higher sediment shear strength and larger root plates (i.e. with less mimicked root breakage). Moreover, we found that the optimal root distribution for stability depended on sediment type, and the effect of root breakage on mimic stability also depended on sediment type. Finally, we showed that the mechanistic anchorage model developed for terrestrial trees provided useful mechanistic principles for estimating mangrove tree stability, with the specification of sediment resistance through sediment shear strength as a useful alteration to this model.

3.4.1 Elements of mangrove tree anchorage

Sediment

Sediment likely plays an important role in coastal mangrove tree anchorage, as our experimental data showed a strong effect of shear strength, with higher mimic stability in sediments with higher upward shear strength. A similar result has been confirmed in work with terrestrial trees, be it for a much more narrow range of sediment shear strengths due to the absence of waterlogged soils (Nicoll et al., 2006; Rahardjo et al., 2009). As sediment shear strength is generally lower for waterlogged sediments (Gillen et al., 2021), mangroves could be less stable at the seaward fringe, where sediments are more often waterlogged. Other factors that affect sediment shear strength may also increase a tree's risk of toppling, such as presence of biota (negative effect) or roots (positive effect; Grabowski et al., 2011; Karimi et al., 2022).

Root depth

While not tested experimentally, the mechanistic anchorage model suggests that rooting depth plays a large role in tree stability as well (Equation 3.6). Hence, mangrove trees that are rooted in undrained silty or clayey sediments, which erode more easily (Grabowski et al., 2011), could be at higher risk of toppling than mangrove trees that grow in more sandy sediments. This is particularly a risk during coastal storms that can erode and displace large volumes of sediment (Bhargava & Friess, 2022), placing mangrove trees at heightened risks of overtopping. Over timescales that span beyond the immediate impact of a storm, mangroves can adjust for the root depth. Trees of the *Rhizophora* genus have been observed to produce more prop roots in shallower sediments (0.1 m depth), which could be to increase belowground biomass in depth-restrained environments (Yoshikai et al., 2021). Furthermore, a well-known strategy is sediment trapping, where aboveground (aerial) mangrove roots reduce flow and thereby promote settling of suspended sediment (Krauss

et al., 2003), potentially self-increasing root depth and protecting against erosion and uprooting.

Root morphology

Given the strong effect of sediment on tree stability, it may be expected that mangroves adjust their root morphology depending on the sediment they grow in. At least this is what our data suggest, as we found that optimal root distribution for stability depended on sediment type. Such a growth response has been observed in twelve terrestrial tree species in France, where, independent of species, different root morphologies were found depending on coarser or finer sediments Zanetti et al., 2015. Although to our knowledge, the effect of shear strength on mangrove root morphology has not been studied directly, it has been shown that mangroves can adjust their roots depending on other sediment properties. For example, in a study on sediment bulk density, Ola et al. (2019) showed that denser sediments lead to an increase in total root biomass and primary root diameter, but a decrease in primary root length. Furthermore, we found that a larger root plate (i.e. with less root breakage) offers relatively more stability in some sediments than others, such as Undrained Silty Sand versus Drained Silty Sand (Figure 3.8). Though we only studied root breakage, the effective root plate size may also be increased by growing longer anchorage roots. To develop such a large root plate, mangroves can grow long, strong and sturdy anchorage roots (that together form the root plate, Figure 3.1), that maintain their function and do not bend or break under mechanical loading. Note that mangrove trees that are rooted in sediments with high shear strength could be at higher risk of root breakage, as roots are not able to move freely through the sediment during wind or wave loading. Nevertheless, the higher shear strength will likely increase stability. Given this trade-off, we expect smaller root plates in sediments with high shear strengths.

Variations in root morphology

Our work shows that mangrove tree anchorage depends on an interaction between sediment and the root morphology, which a tree can adjust in response to sediment. However, other drivers can also affect tree root morphology and consequently tree stability. First, trees can respond to wind loading. A study on 46-year-old, shallow-rooted Sitka spruces (*Picea sitchensis*), found that their root systems developed more structural root mass at the leeward side of trees in response to wind loading Nicoll and Ray, 1996. Second, the presence of neighbouring trees can increase stability, as mangrove trees can develop mechanical root grafts with neighbouring trees, potentially increasing their effective root plate size. Indeed, these trees tend to develop more slender (trunk height:diameter ratio) stems, suggesting that this form of belowground root development increases stability (Vovides et al., 2021).

Third, environmental factors such as waterlogging and eutrophication can prompt a shift in biomass allocation from roots to shoots (McKee, 1995; Ye et al., 2003), potentially reducing mechanical tree stability. Finally, the belowground root morphologies may vary between species. The root morphologies mimicked in this study were inspired and simplified representatives of the *Rhizophora* and *Avicennia* genera. While we found small differences between these root mimics (DetInn, DetMid, DetOut; Figure 3.9c), there is little data on the morphology of other species, and the root morphological response of any species to environmental drivers such as waterlogging. Hence, field studies on drivers of belowground root morphology across mangrove species could reveal more about mangrove tree stability in the coastal environment.

3.4.2 Towards estimating storm damage in coastal mangroves forests

To create or restore mangrove ecosystems with the purpose of nature-based flood defence, we must understand how resilient they are to stressors like coastal storms. Here, we discuss to what extent we can currently estimate stability in mangrove trees. We adapted a mechanistic model from Achim and Nicoll (2009) that estimates root anchorage for Sitka spruces. The resistance part of the model fit best with our mimic data, which is in accordance with their findings. Although there was a tendency to overestimate stability, the resistance model provided anchorage estimates with reasonable precision (compare AIC's from Table 3.4 and 3.5). Current study revealed that the specification of sediment resistance through sediment shear strength provides a useful alteration to the model.

Given the general precision and previous field validation with Sitka spruces (Achim & Nicoll, 2009), we argue that the model provides useful, simple mechanistic principles for understanding mangrove tree stability. However, the model does not distinguish between different root distributions, and hence is not able to capture the effective (instead of the modelled) windward perimeter C_p and leeward arm y_2 , which can vary depending on the interaction effect between sediment type and root morphology. Furthermore, the model does not account for root-sediment resistance (instead of only sediment resistance). Consequently, field validation specifically with mangroves is still needed to estimate how reliable anchorage estimates are across sedimentary environments, root morphologies and species. As field measurements with mangrove root structures are destructive in nature, such measurements could be complemented with computer simulations of tree stability using Finite Element Methods, to identify how this interaction affects the accuracy of stability estimates, and how C_p and y_2 can be calibrated depending on the sediment type (Yang et al., 2014).

Mangrove tree stability

If the anchorage moment is known, the critical wind speeds can be estimated by finding the critical overturning moment at which a tree loses its stability, which is a function of the tree height H_T and the drag force F_d acting on the canopy. Following the drag equation ($F_d = 0.5AC_d\rho u^2$; Morison et al., 1950), the drag force acting on the canopy will depend on its surface area A and drag coefficient C_d . The water level will also matter, as this will determine whether the tree is hit by wind or waves, which have different flow velocities u and fluid densities ρ . The critical wind or wave speed is then the point where the overturning moment M_t surpasses the anchorage moment M_a . During a storm, sediment can be eroded, reducing root depth D_s . The anchorage model allows for this, providing more realism to the estimations (Figure 3.12). Ultimately, tree stability could be estimated across an entire forest. This could be combined with other types of damage generated during a storm, such as trunk or branch breakage (Gardiner, 2021), to assess the risk of massive mortality under a range of storm scenarios. Furthermore, such estimates can be calibrated with high-resolution satellite imagery and measured wind speeds from real storm events (Svejkovsky et al., 2020), as well as wind tunnel or flume experiments with real-time erosion and more realistic aboveground morphologies (Figure 3.2c). Ultimately, this allows not only for estimating resilience of a specific forest during a particular storm scenario, but also for evaluating how resilience can change as a restored forest matures. Such approaches can provide highly useful tools in deciding whether creating or restoring a mangrove forest for nature-based flood defence is worthwhile under altering storm regimes.

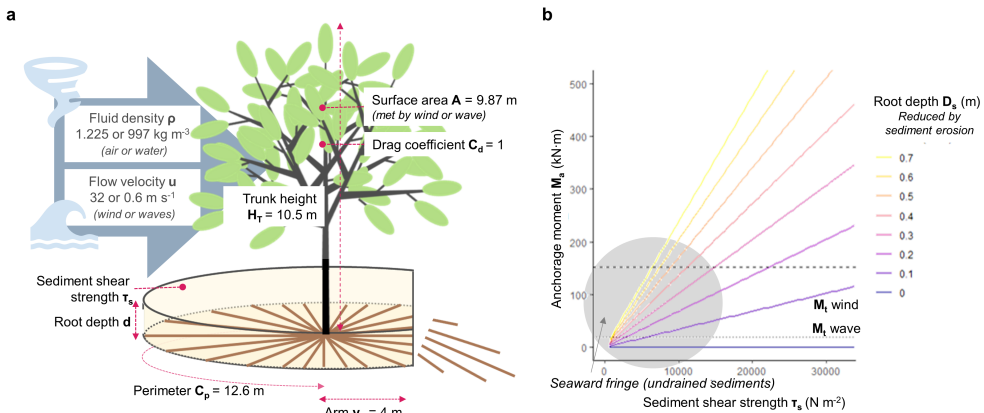


Figure 3.12: Simplified example of mangrove tree stability estimation for various root depths D_s and sediment shear strengths τ_s , assuming that the true parameter values are known. Using the resistance model to estimate anchorage (Achim & Nicoll, 2009) and the drag model to estimate overturning moment (Morison et al., 1950). If the overturning moment M_t becomes larger than the anchorage moment M_a , the tree loses its stability. Value sources are listed in Table S3.4.

3.5 Conclusions

Predicting the impact of storms on a mangrove forest is challenging, yet highly needed to assess a forest's future resilience under altering storm tracks and intensifying coastal storms. In this paper we uncovered the role of sediment and root properties in mangrove tree stability. Furthermore, we have shown that the mechanistic principles applied to terrestrial trees largely hold in mangrove trees, with the extra specification of sediment resistance through sediment shear strength. If tree mechanical and size properties are known, these mechanistic principles can be used estimate the critical wind or wave speed (and erosion depth) required to uproot a tree. Combined with other damages such as breakage of plant parts based on mechanical properties (Chapter 4), the insights in this study contribute to better understanding of mangrove forest resilience and restoration success under altering storm regimes.

S3 Supporting information

S3.1 Mangrove sediments

Table S3.1: Mangrove sediment composition reported in the literature.

Location	Sand %	Silt %	Clay %	Reference
New Zealand*				Bulmer et al., 2015
	29.4±10.6	47.5±7.8	16.6±2.7	
New Zealand 4y**	37(16.7)	46(11.8)	17(5.9)	Stokes and Harris, 2015
New Zealand 6y**	43(13.1)	46(10.0)	9(3.9)	Stokes and Harris, 2015
Bhitarkanika, Odish, India	26.7±14.7	34±8.72	39.14±6.39	Banerjee et al., 2018
Indonesia, rehabilitation	49.7	37.2	13	Dewiyanti et al., 2021
Indonesia, no rehabilitation	54.3	36.4	9.2	Dewiyanti et al., 2021
Futian Shenzhen HVL	9.5±1.2	70.7±1	19.8±0.09	Duan et al., 2020
Futian Shenzhen LVL	0±0	60.6±0.8	39.4±0.8	Duan et al., 2020

* Gravel: 3.7±2.3 %

** 4y: water content 54%, bulk density 500 kg m⁻³, 6y: water content 69%, bulk density 600 kg m⁻³

S3.2 Trigonometric calculations

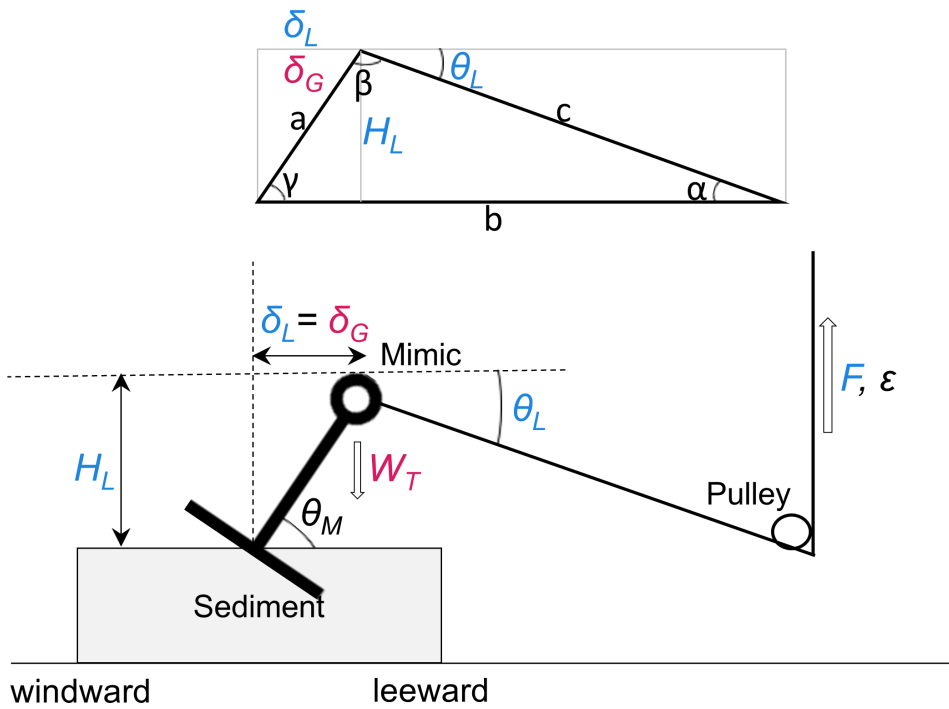


Figure S3.1: Parameters used to calculate H_L and θ_L and δ_L , figure adapted from Figure 3.4.

Mangrove tree stability

Table S3.2: Calculation to obtain parameters values for H_L and θ_L and δ_L , needed for Equations 3.2 and 3.3.

Symbol	Unit	Calculation	Note
θ_L	Rad	$\arccos\left(\frac{b^2+c^2-a^2}{2bc}\right)$	Same as α
δ_L	m	$\sqrt{a^2 H_L^2}$	Same as δ_G
a	m	0.095	
b	m	0.45	
c	m		
γ	rad	$90 - 8.73\epsilon$	$\epsilon =$ extension (m); 8.73 (rad m ⁻¹) converted from 0.5 ° mm ⁻¹ ; see Section 3.2.3
H_L	m	$a \sin \gamma$	

Chapter 3

S3.3 Anchorage moment variable values

Table S3.3: Values used to calculate anchorage (see Equations 3.4, 3.5 and 3.6).

Root type	Breakage	Area A_r (cm ²)	Weight W_r (g)	y_1 (m)	y_2 (m)	C_p (m)
SimInn	None	20.50	8.25	0.04	0.04	0.13
DetInn	None	20.10	8.30	0.04	0.04	0.13
DetMid	None	20.30	8.91	0.04	0.04	0.13
DetOut	None	20.60	8.24	0.04	0.04	0.13
SimOut	None	20.50	8.25	0.04	0.04	0.13
SimInn	25, Wind	19.00	8.09	0.02	0.03	0.11
DetInn	25, Wind	18.10	7.82	0.02	0.03	0.11
DetMid	25, Wind	16.80	7.30	0.02	0.03	0.11
DetOut	25, Wind	15.20	7.27	0.02	0.03	0.11
SimOut	25, Wind	16.80	6.75	0.02	0.03	0.11
SimInn	25, Lee	19.00	8.09	0.04	0.03	0.13
DetInn	25, Lee	18.10	7.82	0.04	0.03	0.13
DetMid	25, Lee	16.80	7.30	0.04	0.03	0.13
DetOut	25, Lee	15.20	7.27	0.04	0.03	0.13
SimOut	25, Lee	16.80	6.75	0.04	0.03	0.13
SimInn	25, Both	17.50	7.55	0.02	0.02	0.11
DetInn	25, Both	16.00	7.27	0.02	0.02	0.11
DetMid	25, Both	13.30	6.29	0.02	0.02	0.11
DetOut	25, Both	12.90	6.22	0.02	0.02	0.11
SimOut	25, Both	9.80	5.31	0.02	0.02	0.11
SimInn	45, Wind	12.90	6.28	0.02	0.03	0.09
DetInn	45, Wind	12.40	6.00	0.02	0.03	0.09
DetMid	45, Wind	12.70	6.25	0.02	0.03	0.09
DetOut	45, Wind	12.20	5.92	0.02	0.03	0.09
SimOut	45, Wind	11.80	5.70	0.02	0.03	0.09
SimInn	45, Lee	12.90	6.28	0.03	0.02	0.13
DetInn	45, Lee	12.40	6.00	0.03	0.02	0.13
DetMid	45, Lee	12.70	6.25	0.03	0.02	0.13
DetOut	45, Lee	12.20	5.92	0.03	0.02	0.13
SimOut	45, Lee	11.80	5.70	0.03	0.02	0.13

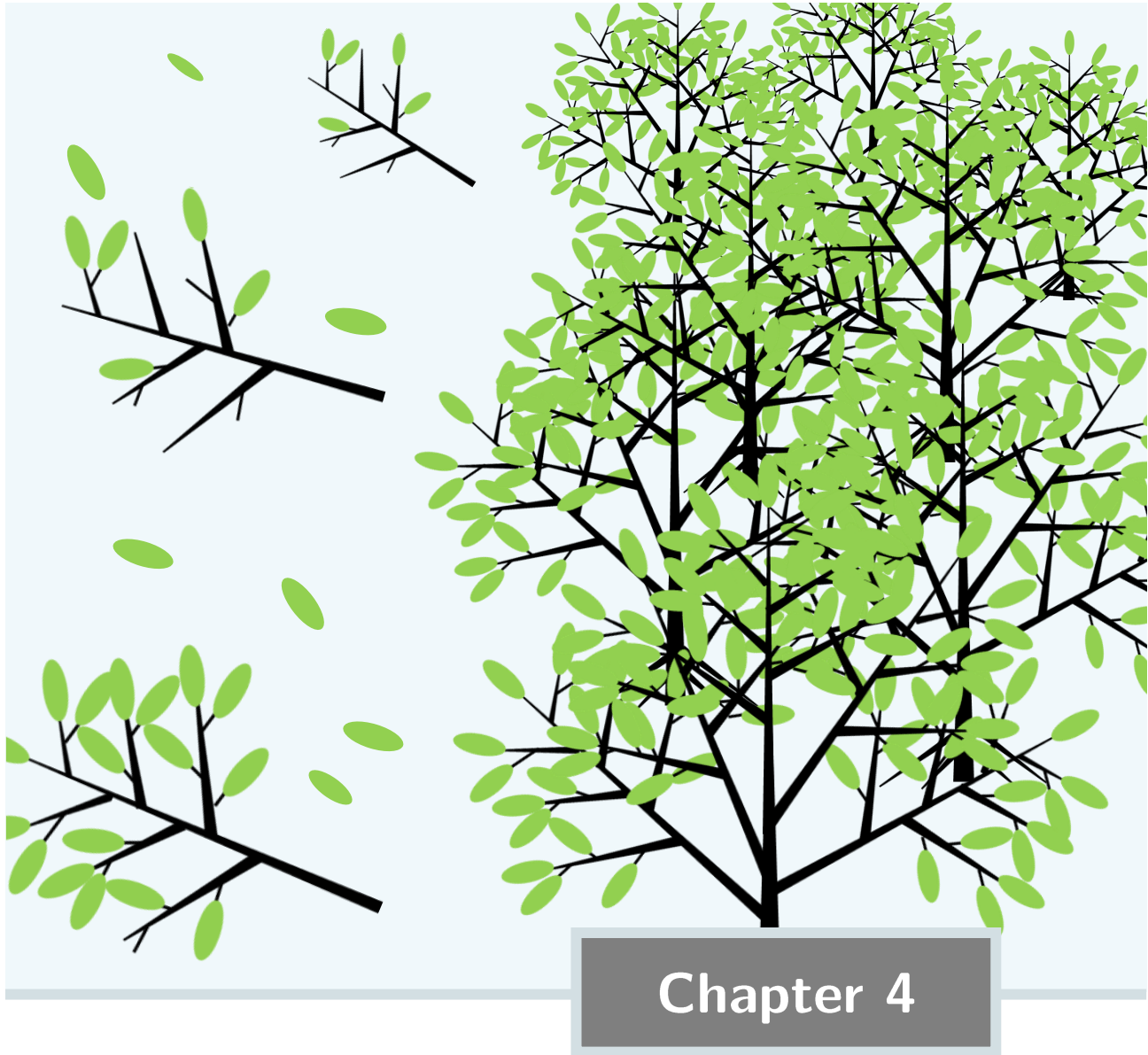
Mangrove tree stability

S3.4 Critical wind and wave speeds calculations for an upscaled mimic

We modelled an 100x upscaled mimic (Table 3.2) as a mangrove tree, such that it had the properties as listed in Table S3.3. We modelled values based on a 25L broken root plate as depicted in Figure 3.12.

Table S3.4: Values used to calculate anchorage (see Equations 3.4, 3.5 and 3.6).

Sym- bol	Unit	Meaning	Value	Source
$F_{wind};$ F_{water}	N	Drag force of wind/water	$0.5C_d A \rho u^2$	Morison et al., 1950
C_d	-	Drag coefficient	1	Chapter 4
A	m ²	Projected surface area		Chapter 4
ρ	kg m ⁻³	Density air/water	1.225; 997	Standard value
u	m s ⁻¹	Wind/wave orbital velocity	48.87; 0.6	Wind: Typhoon Hato (Takagi et al., 2018); Wave: Typhoon Hato (see Chapter 4, Section S4.8)
F_{crit}	N	Critical overturning force	M_a/H_T	-
M_a	N·m	Anchorage moment	$\tau_s D_s C_p y_2$	3.6
τ_s	N m ⁻²	Shear strength	Range	Table 3.1
D_s	m	Root depth	Range	-
C_p	m	Windward perimeter	12.6	Table S3.3 (x100)
y_2	m	Arm	4	Table S3.3 (x100)
H_T	m	Trunk height	10.5	Table 3.2



Chapter 4

Analysis of coastal storm damage resistance in successional mangrove species

R. van Hespen, Z. Hu, Y. Peng, B.W. Borsje, M.G. Kleinhans, T. Ysebaert, T.J. Bouma

Limnology & Oceanography (2021)

4 | Analysis of coastal storm damage resistance in successional mangrove species

Abstract

Use of mangrove ecosystems for coastal flood protection requires reliable predictions of mangrove wave attenuation, especially if this capacity lessens due to storm-induced forest damage. Quantifying and understanding the variation in drag forces and mechanical properties of mangrove vegetation can improve assessment of mangrove protective capacity. We studied five mangrove species common in the subtropical Pearl River Delta, south China. The studied species range from typically landward-occurring to more seaward-occurring pioneer species. We sampled across seven sites in the delta to study the impact of salinity on mechanical properties. We quantified strength and flexibility of branches (branch strength and flexibility related to branch diameter, Modulus of Rupture and Modulus of Elasticity), leaf strength (leaf attachment strength related to leaf size, and Leaf Mass per Area) and drag properties (drag force related to surface area and drag coefficient). For all tested species, larger branch diameters resulted in higher mechanical strength. Larger leaf size resulted in larger peak pulling forces and larger branch surface area resulted in stronger drag forces. Notably, species that generally occur lower in the intertidal zone, where exposure to wind and waves is higher, had relatively stronger branches but more easily detachable leaves. This may be regarded as a damage-avoiding strategy. Across the seven field sites we found no clear effect of salinity on mangrove mechanical properties. This study provides a mechanistic insight into the storm damage process for individual mangrove trees and a solid base for modelling storm (surge) damage at the forest scale.

4.1 Introduction

4.1.1 Reducing cost of flood protection with coastal ecosystems

The urgency for effective and affordable coastal flood defence will increase if sea levels and storm frequency rise as projected over the coming decades (Knutson et al., 2020; Nicholls et al., 2019). This is especially the case in highly urbanised deltas, such as the Pearl River Delta in south China, that harbours megacities like Guangzhou and Shenzhen (De Dominicis et al., 2020). The cost of maintaining coastal safety increases as larger barrier structures are needed. Coastal vegetation can attenuate waves, reducing the required height of barrier structures and resulting in lower construction and maintenance costs (Borsje et al., 2011; Temmerman et al., 2013). Consequently, coastal ecosystems are increasingly considered as an addition to conventional coastal safety structures (Morris et al., 2019; Temmerman et al., 2013; van Wesenbeeck et al., 2017). In subtropical and tropical areas, mangrove forests are known for the large extent of ecosystem services they can provide, and their dense vegetation and high elevation in the intertidal zone make them effective natural wave attenuating structures (Bouma et al., 2014; Lee et al., 2014). Under the right circumstances, they may even attenuate extreme storm waves, provided that vegetation stretches wide and matches the height and length of the waves (Bao, 2011; Horstman et al., 2014; Menéndez et al., 2020). However, mangroves are dynamic, living structures that do not always have the same vegetation width and density. Supplementing conventional coastal safety structures with mangrove ecosystems will require a strong understanding of how mangrove width and density fluctuate, to enable careful prediction and testing of the long-term structural integrity of these ecosystems (Bouma et al., 2014).

4.1.2 Variability in flood protection by mangrove forests

The coastal wave attenuating capacity of mangrove ecosystems is related to surge properties and to the size, height and density of the vegetated area: a larger, denser forest leads to better protection, and vegetation height relative to the storm surge determines what part of the vegetation (pneumatophores, tree trunks, canopy) can attenuate waves (Bouma et al., 2014; Mazda et al., 1997; McIvor et al., 2015). For example, height of native species in the Pearl River Delta in south China is comparable to the seawalls behind them and can thus experience waves over the full height of the tree during storms (Figure S4.1). Naturally, these vegetation properties are variable across species, age and space inside and across forests (i.e. canopy height is globally related to precipitation, temperature and cyclone frequency; (Koch et al., 2009; Simard et al., 2019). Furthermore, large irregular disturbances can strongly impact forest structure and consequently wave attenuation capacity as well as long-term presence. If disturbance regimes such as storm frequency or intensity are

altered under climate change (Hoegh-Guldberg et al., 2018; Knutson et al., 2020), this could drive forests that are already vulnerable from previous disturbances over an ecological tipping point, resulting in substantial narrowing or loss of the ecosystem (Bouma et al., 2014; Scheffer et al., 2001). Even if forest size is relatively stable, recovering will take some time, during which local protection capacity is lowered (Johnstone et al., 2016; Krauss & Osland, 2020). Conventional flood protection structures need to adhere to rigid safety standards, often measured to withstand a storm of particular intensity, that has an estimated return period (e.g. 100 years; CIRIA et al., 2013). To safely integrate mangroves in flood protection schemes, it is essential to understand how mangrove vegetation structure changes under disturbance regimes.

4.1.3 Mechanistic models for storm damage predictions

Storms and accompanying storm surges can cause mangrove tree damage through direct mechanical impact such as branch and trunk damage and complete defoliation, and indirect effects like extensive flooding and displacement of large volumes of sediment (Jimenez et al., 1985; Ouyang et al., 2021; Smith III et al., 1994). Predicting direct mechanical storm damage in forests can be done with models like HWIND, FOREOLE and GALES (Gardiner et al. 2008). Such models can predict tree uprooting and trunk breakage by comparing tree strength with drag force generated in local (storm) wind climates (Peltola et al., 1999). Mangroves can experience damage from both wind and waves during coastal storms. For example, Tanaka (2008) observed tree damage similar to that of damage by tsunamis or river floods after Cyclone Sidr hit Bangladesh in 2007. These existing storm damage models have been developed for trees in terrestrial forests and do not incorporate the impact of water motion, that may impose much larger drag forces (a drag force imposed by water moving at a velocity of 2 m s^{-1} is roughly equivalent to wind speeds of 130 mph or 58.3 m s^{-1} ; Denny and Gaylord, 2002). Still, the basic principle remains: a force is acting on a tree. Thus, the modelling principle may also be applied in the case of storm surge damage on mangroves, where wind is replaced with waves and terrestrial wood properties are replaced by mangrove wood properties.

4.1.4 Variability in storm damage across species and space

When making mechanistic predictions of mangrove tree damage, it should be considered that not all trees are damaged in the same way. For instance, it is known that tree species vary in their mechanical strength (Chave et al., 2009; Santini et al., 2013) and mechanical flexibility (where more flexible wood can reduce storm impact; Kauffman and Cole, 2010). Furthermore, leaf mechanical properties such as leaf size, which increases drag force acting on the tree, and the potential for leaf reorientation and defoliation under influence of wind and waves (which reduce surface area and resulting drag force), vary across plant species (Butler et al., 2012; Onoda et al., 2011;

Vollsinger et al., 2005). These differences often follow drag avoidance or drag tolerance strategies, such that some species, often pioneers, are better equipped to deal with the force of incoming surge waves (e.g. in saltmarshes, seaward pioneers have more flexible stems, which helps to reduce drag; Puijalon et al., 2011; Schoutens et al., 2020). Beyond species differences, environmental factors may also affect the mechanical properties of mangrove trees. Wood density – which correlates positively with mechanical strength (Chave et al., 2009) – differs across intertidal position, countries (Santini et al., 2012), and possibly salinity (Table S4.1). Given these potential sources of variation, predicting storm impact on mangroves requires sufficient knowledge of mechanical and drag properties across mangrove species and environmental variables.

4.1.5 Aims of this research

Safely integrating mangrove forests in coastal protection schemes requires accurate predictions of forest size and structure under the influence of storms. Here, we focus on identifying storm surge resistance of mangrove trees by quantifying the mechanical and drag properties of small branches (0.5-1.75 cm diameter) and leaves of five species. We situate the study in the Pearl River Delta, one of the largest urban deltas in the world that could benefit from nature-based flood protection with mangroves (De Dominicis et al., 2020; Menéndez et al., 2020). The five species studied here are common in the Pearl River Delta and range from typically seaward occurring with pioneer traits to more landward growing species with late-successional traits. We quantify the species' mechanical and drag properties across a salinity gradient along seven sites in the larger delta area. We quantify the following properties:

- strength and flexibility of mangrove branches (branch strength and flexibility related to branch diameter, Modulus of Rupture and Modulus of Elasticity),
- mangrove leaf strength (leaf attachment strength related to leaf size and petiole diameter, and Leaf Mass per Area), and
- drag properties (drag force related to surface area and drag coefficient).

The collected data are analysed to assess: 1) potential damage avoidance strategies for different species and 2) possible salinity impact on mechanical properties. We do this to provide mechanistic insight in storm damages for individual mangrove trees across species and salinities, ultimately supporting the aim to improve predictions of mangrove-based flood safety.

4.2 Methods

We collected data on mechanical and drag properties of five mangrove species to estimate potential storm damage on individual trees (Table 4.1). These data comprise:

1. Strength and flexibility of small mangrove branches (diameters ranging from 0.5-1.75 cm, allowing us to harvest and transport branches from field to the lab without causing unacceptably large damage to trees). We measured strength as the absolute peak force (F_{\max} , N) branches can withstand and flexibility as the amount of force needed to bend a branch a certain amount (e.g. 1 mm; F/x , N mm^{-1}). From this we derived relative material properties independent of branch diameter: Modulus of Rupture (MOR, N mm^{-2}), a relative measure of strength, and Modulus of Elasticity (MOE, N mm^{-2}), a relative measure of flexibility.
2. Leaf attachment strength (F_{pull} , N), where we measured the peak force required to detach a leaf under a static load and compared this to leaf size (leaf surface area A_{leaf} , cm^2), petiole diameter (cm) and cost of leaf production (Leaf Mass per Area LMA, g cm^{-2}).
3. Drag force on mangrove branches (F_D , N), where we measured drag force linked to branch surface area (A_{proj} , m^2) and derived a drag coefficient (C_D , dimensionless).

The mangrove species studied are typical for the subtropical Pearl River Delta. To identify potential differences in storm damage avoidance or resistance traits, we selected species that range from generally more sheltered, landward occurring to generally more exposed, seaward occurring pioneer species: *Acanthus ilicifolius*, *Kandelia obovata*, *Aegiceras corniculatum*, *Avicennia marina* and *Sonneratia apetala*, listed here from landward to seaward, respectively. We selected seven field sites to cover salinities that range from fresh water to seawater (0 to 15 psu) to study the potential effect of salinity on mangrove mechanical properties.

Storm damage resistance

Table 4.1: Mechanical and drag properties used with symbols and their meaning.

Item	Sym- bol	Unit	Name and explanation	Obtained by
Branch	F_{\max}	N	Absolute peak force: maximum load before branch breaks	measured
Branch	F/x	N mm ⁻¹	Flexibility: initial slope of the stress-strain curve, i.e. force needed to bend the branch a certain amount (e.g. 1 mm)	measured
Branch	R, \varnothing	cm	Branch radius, branch diameter	measured
Branch	L	m	Branch arm: length of the part of the branch that experiences load F	measured
Branch	MOR	N mm ⁻²	Modulus of Rupture: a relative, size-independent measure of branch strength	$MOR = \frac{F_{\max}L}{\pi R^3}$
Branch	MOE	N mm ⁻²	Modulus of Elasticity: a relative, size-independent measure of branch rigidity	$MOE = \frac{F}{x} \cdot \frac{L^3}{12\pi R^4}$
Leaf	F_{pull}	N	Leaf attachment strength: peak pulling force at which leaf detaches	measured
Leaf	A_{leaf}	cm ²	Leaf size: leaf surface area	measured
Leaf	M_{leaf}	g	Leaf dry weight	
Leaf	LMA	g cm ⁻²	Cost of leaf production: Leaf Mass per Area, in gram biomass invested to produce 1 m ² leaf, considered a measure of cost of leaf production	
Leaf	MOL_A	N cm ⁻²	Modulus of Leaf loss, area based: force required to detach a leaf for a given leaf size	$MOL_A = \frac{F_{\text{pull}}}{A_{\text{leaf}}}$
Leaf	MOL_M	N g ⁻¹ cm ²	Modulus of Leaf loss, mass based: force required to detach a leaf for a given leaf cost (using LMA as measure of cost)	$MOL_M = \frac{F_{\text{pull}}}{LMA}$
Drag	F_D	N	Drag force experienced by branch	measured
Drag	A_{proj}	m ²	Branch surface area: projected frontal surface area of branch	measured
Drag	u	m s ⁻¹	Wave orbital velocity	measured
Drag	ρ	kg m ⁻³	Fluid density (1000 kg m ⁻³ for fresh water)	known constant
Drag	C_D	-	Drag coefficient	$C_D = \frac{2F_D}{\rho u^2 A_{\text{proj}}}$

4.2.1 Species and site selection

We collected data at seven locations in the Pearl River Delta, Guangdong province, south China. Between 1954 and 2008, 181 typhoons have landed in this province (Jie et al., 2012). During a typhoon, wave height can reach up to 2 m surge height can reach up to 4 m at the coast inside the Pearl River Delta (De Dominicis et al., 2020; Yin et al., 2017). The seven sites have increasing salinity ranging from 0 to 15 psu (Figure 4.1; for salinity estimation see Figure S4.5). We sampled five species commonly found in the subtropical Guangdong province, south China: *A. ilicifolius*, *K. obovata*, *A. corniculatum*, *A. marina* and *S. apetala* listed here as ranging from respectively high intertidal (landward species) to low intertidal (seaward species; based on Peng et al. (2016) and our own field observations). Particularly *A. marina* and *S. apetala* are considered pioneer species in the region, *K. obovata* and *A. corniculatum* less so and *A. ilicifolius* is not considered a pioneer species (Chen et al., 2015; Ren et al., 2008). Note that *A. ilicifolius* is not a woody species, unlike the other four. In the Pearl River Delta, south China, these species do not reach tall heights (2-4 meters max.), except for the non-native species *S. apetala*, that reaches heights of 5-12 m. The native species have heights comparable to the seawalls behind the mangrove forests (i.e. built to resist expected storm water levels), such that they can experience waves over the length of the full tree (Figure S4.1). The non-native species *S. apetala* can be significantly higher than adjacent seawalls and may therefore be less effective in wave attenuation and more sensitive to wind forces. *S. apetala* is an exotic species in China and was introduced from Bangladesh for mangrove afforestation in the mid-1980's Xin et al., 2013. Although some of the selected species have low salinity tolerance (*A. ilicifolius*: low, *K. obovata*: mid, *A. corniculatum*: mid, *A. marina*: high and *S. apetala*: low; (Reef & Lovelock, 2015; Ye et al., 2005), the 0-15 psu range is relatively low for mangroves in general and likely tolerable for all species – indeed, they grow at most sites (Figure 4.1; but note that *S. apetala* trees are often nursery-raised and then planted; Ren et al., 2009).

Storm damage resistance

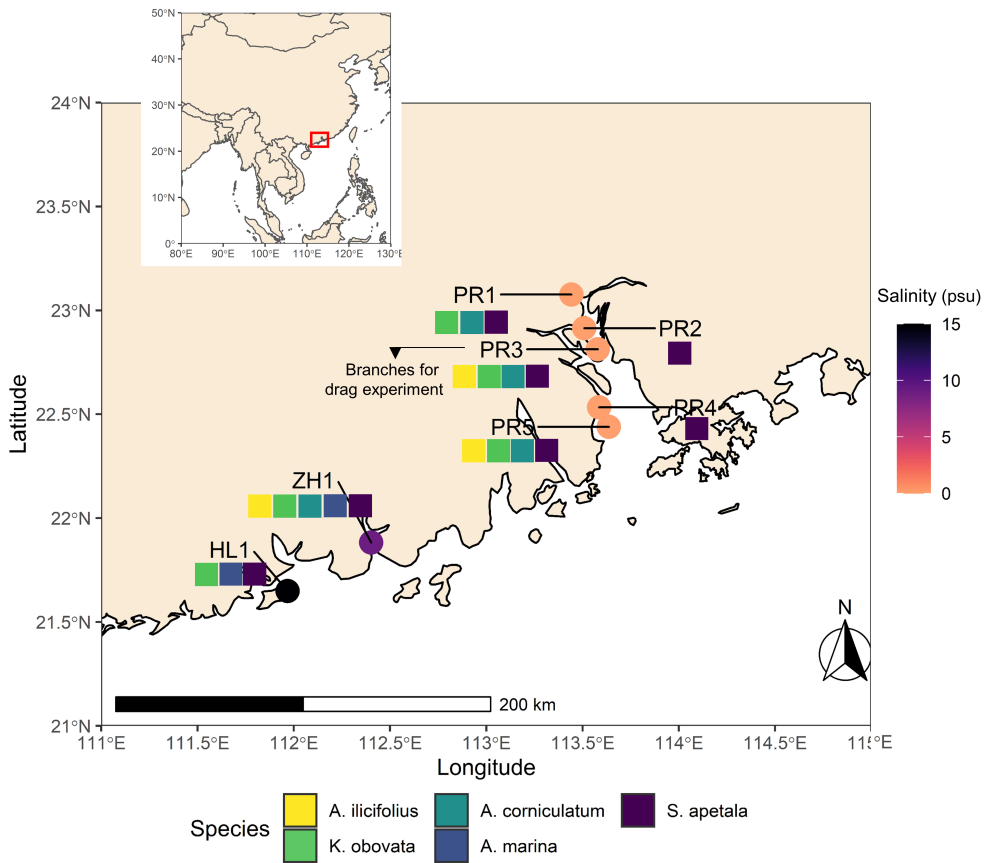


Figure 4.1: Site locations shown with salinity and species sampled. For details on salinity estimation see Figure S4.5

4.2.2 Mechanical properties of mangrove branches

We collected branches at each site for one to five species, depending on availability (Figure 4.1). Sampling was carried out from 9 to 24 January 2019. One or two branches were taken from a tree, with diameters ranging from roughly 0.50 cm to about 1.75 cm (see Figure S4.2 for branch diameters per hierarchy level). We selected this size range and excluded larger sizes for three reasons: *i*) in several cases, taking larger branches would have resulted in destruction of a major part of or even the whole tree, *ii*) large parts of tree biomass can be found in smaller branches (Figure S4.2), as trees likely have more smaller than larger branches, and *iii*) the Modulus of Rupture and Modulus of Elasticity are size-independent measures for which diameter is not relevant (Figure S4.3). Each tree was selected randomly but

opportunistically, considering limited accessibility due to deep creeks or dense vegetation. For each required diameter, the straightest part of a branch was selected and stripped of any side branches such that it approximated a straight cylinder. This need not be the point where a branch will actually break during a storm, but it offered the best place to get reproducible measurements on location-independent tissue properties such as Modulus of Rupture and Modulus of Elasticity (Gere & Goodno, 2012). These properties can then be used to calculate the actual strength at any place of a branch, assuming there are no weaknesses in the branch. Collected branches were then rolled in moist paper towels and stored in airtight bags in cool boxes with ice and transferred to a fridge upon arrival at the lab before analysis. Analysis using a three-point bending test happened within 48 hours after collection of the branches. The three-point bending test was carried out to obtain both absolute tissue properties – maximum load F_{\max} (N) and force to bend F/x (N mm^{-1}) – and relative tissue properties – Modulus of Rupture (MOR, N mm^{-2}) and Modulus of Elasticity (MOE, N mm^{-2} ; Gere and Goodno, 2012). The test was carried out with a universal testing machine (SUST CMT5105, Zhuhai SUST Electrical Equipment Co., Ltd, Zhuhai, China) in which we placed a branch in the load frame, with the cross head set to move at a speed of 25 mm min^{-1} . Maximum load F_{\max} (N) was determined at the point where the applied force was highest before the branch started to weaken and irreversible damage occurred. The size-independent mechanical property Modulus of Rupture (N mm^{-2}) was obtained with:

$$\text{MOR} = \frac{F_{\max}L}{\pi R^3} \quad (4.1)$$

with branches of a radius R (mm) and an arm L (m) undergoing loading F (N). Radius R was measured in the middle of each branch (note that branches tend to tapes), where the cross head met the branch (Figure S4.4). Branches were cut so that they fit an arm of $L = \varnothing \cdot 20 + 2$ (to fit inside the universal testing machine and following Onoda et al., 2010 who used lengths > 20 times longer than the diameter in comparable measurements), but no larger than the load frame maximum width of 38 cm. This means that branches thicker than 1.9 cm were tested with a relatively shorter arm L (68 in total). As such, we excluded these data from absolute force measurements (F_{\max}) as they could not be compared to other branches and only included them in relative, size-independent mechanical property measurements (MOR, MOE).

The force to bend F/x (N mm^{-1}) was determined during the initial bending process where the cross head pushes down the branch before breaking. We used the initial slope of the stress-strain curve to obtain this measure (see Figure S4.4 for an exam-

ple). To obtain the size-independent mechanical property Modulus of Elasticity (N mm⁻²), we used:

$$\text{MOE} = \frac{F}{x} \cdot \frac{L^3}{12\pi R^4} \quad (4.2)$$

4.2.3 Mechanical properties of mangrove leaves

Leaf mechanical properties were measured in the field during the January 2019 field campaign using a static pulling approach. For each tree of which a branch was sampled, at least five healthy, intact leaves were selected semi-randomly (i.e. with a bias for accessible leaf heights). We developed a method where we closed a thin steel wire loop around the petiole or base of the leaf (in case of a very short petiole). The other end of the wire was attached to a dynamometer with a minimum load of 0.2 kg, readability at 0.02 kg intervals and an accuracy of ± 0.08 kg (PCE-HS 50N, PCE Brookhuis, Enschede, the Netherlands). The dynamometer was then pulled at a constant speed until the leaf broke off and the peak load F_{pull} was noted. Pulled leaves were stored in plastic bags in a cool box with ice and transferred to a fridge upon arrival at the lab, and photos and size measurements (petiole diameter, leaf width, height and surface area) were taken within 48 hours. The leaf surface area A_{leaf} (cm²) was analysed with photo analysis software ImageJ (Schindelin et al., 2012). Leaves were oven-dried at 60 °C for 24 hours. Dry weight M_{leaf} (g) of pulled leaves, averaged per tree, was used to calculate the Leaf Mass per Area - considered a measure of investment of biomass per cm² leaf (Onoda et al., 2011) - as the leaf dry mass M_{leaf} per unit leaf area A_{leaf} (LMA = $M_{\text{leaf}} / A_{\text{leaf}}$, g cm⁻²).

A measure of relative leaf attachment strength was obtained by standardizing the attachment strength against the leaf surface area A_{leaf} , where A_{leaf} can be considered a proxy for the drag forces a leaf may be experiencing (i.e. a larger leaf will experience higher drag forces; (Albayrak et al., 2014):

$$\text{MOL}_A = \frac{F_{\text{pull}}}{A_{\text{leaf}}} \quad (4.3)$$

A second measure of relative leaf attachment strength was obtained by standardizing the attachment strength against the leaf mass per area LMA, to observe if leaves that require a higher investment of biomass per cm² (LMA) have more strongly attached leaves (higher F_{pull}):

$$\text{MOL}_M = \frac{F_{\text{pull}}}{\text{LMA}} \quad (4.4)$$

Using relative measures of leaf attachment strength gives insight in whether a species invests more in leaf attachment strength F_{pull} if they have larger leaves

A_{leaf} , that will inherently experience more drag, or if they have more expensive leaves, as reflected by a higher LMA. Petiole diameter was not used for calculating a relative attachment measure, as many leaves broke elsewhere; in a number of pulling attempts the whole twig with multiple leaves broke off (13% of pulling attempts for *A. marina*, 1% *K. obovata* and *S. apetala*), and in successful pulling attempts on average 72% of leaves broke off at the leaf base, such that the petiole remained attached to the tree (98% in *A. ilicifolius*, 84% in *A. corniculatum*, 81% in *A. marina*, 53% in *K. obovata* and 42% in *S. apetala*). This might be an artefact of the pulling method, where force is concentrated in the point where the steel wire meets the leaf – under real wave loading, the interaction will be quite different, though detaching will likely require forces of a similar magnitude.

4.2.4 Drag force on mangrove branches

We obtained absolute (peak drag force F_D , N) and relative (drag coefficient C_D) measurements of the forces experienced by mangrove branches, the latter of which can be used to make comparisons across species. Branches of each mangrove species were sampled at the PR3 field site and tested in June 2019. For each branch, with and without leaves, we cut the branch to fit inside the flume (40 cm high x 60 cm wide). Branches were cut such that the basis of the branch matched the desired diameter; anything sticking out from the 40 x 60 cm frame was cut off. We then took a photo to measure the projected frontal surface area A_{proj} (m^2) with ImageJ (Schindelin et al., 2012). Maximum drag force F_D on branches, with and without leaves, was measured by placing the branch in a flume (located at the School of Marine Sciences, Sun Yat-Sen University, Zhuhai campus) and attaching the base of the branch to a force transducer (Load cell M140, UTILCELL, s.r.o., Ostrovačice, Czech Republic). Drag force F_D was measured for three scenarios: (1) waves without a current, (2) a current of 15 cm s^{-1} without waves, and (3) waves and a 15 cm s^{-1} current, with water height of 33 cm, wave height of 11 cm and a wave period of 1.5 s (achieving the highest possible conditions in this flume, resulting in around max. orbital velocities of 0.25 m s^{-1} for waves and currents combined with Reynolds number of about 2500). We measured current velocity at half of the water depth, which approximates the depth-averaged velocity (Chen, Ni, et al., 2018; Hu et al., 2014). Following basic fluid dynamics (Morison et al., 1950), a wave-averaged drag coefficient C_D was derived from the peak drag measurements for each scenario:

$$C_D = \frac{2F_D}{\rho u^2 A_{\text{proj}}} \quad (4.5)$$

with u = current velocity (m s^{-1}) measured with acoustic doppler velocimeters, ρ = fluid density of fresh water (1000 kg m^{-3}) and A_{proj} = projected frontal surface area

of vegetation (m^2). We used peak drag force instead of average drag force to derive the drag coefficient, as it is the maximum force that a branch experiences that may cause breakage.

4.3 Results

4.3.1 Generic patterns in mangrove mechanical properties

Branch mechanical properties followed generic patterns across species, where thicker branches can withstand larger forces before breaking (F_{max} , Figure 4.2a, adj. $R^2 = 0.78$, $p < 0.05$), as the volume to be broken increases cubically with branch diameter. Thicker branches also tended to be more rigid (F_x , Figure 4.2b, adj. $R^2 = 0.56$, $p < 0.05$). Leaf mechanical properties also followed a generic pattern across species where leaves with a larger surface area A_{proj} or thicker petiole could withstand larger pulling forces (F_{pull} , Figure 4.3c, adj. $R^2 = 0.50$; Figure 4.3d, adj. $R^2 = 0.31$, $p < 0.05$). Contrarily, we did not find a generic pattern between cost of leaf production (i.e. estimated as Leaf Mass per Area LMA) and required pulling force to detach the leaf F_{pull} (Figure 4.3g).

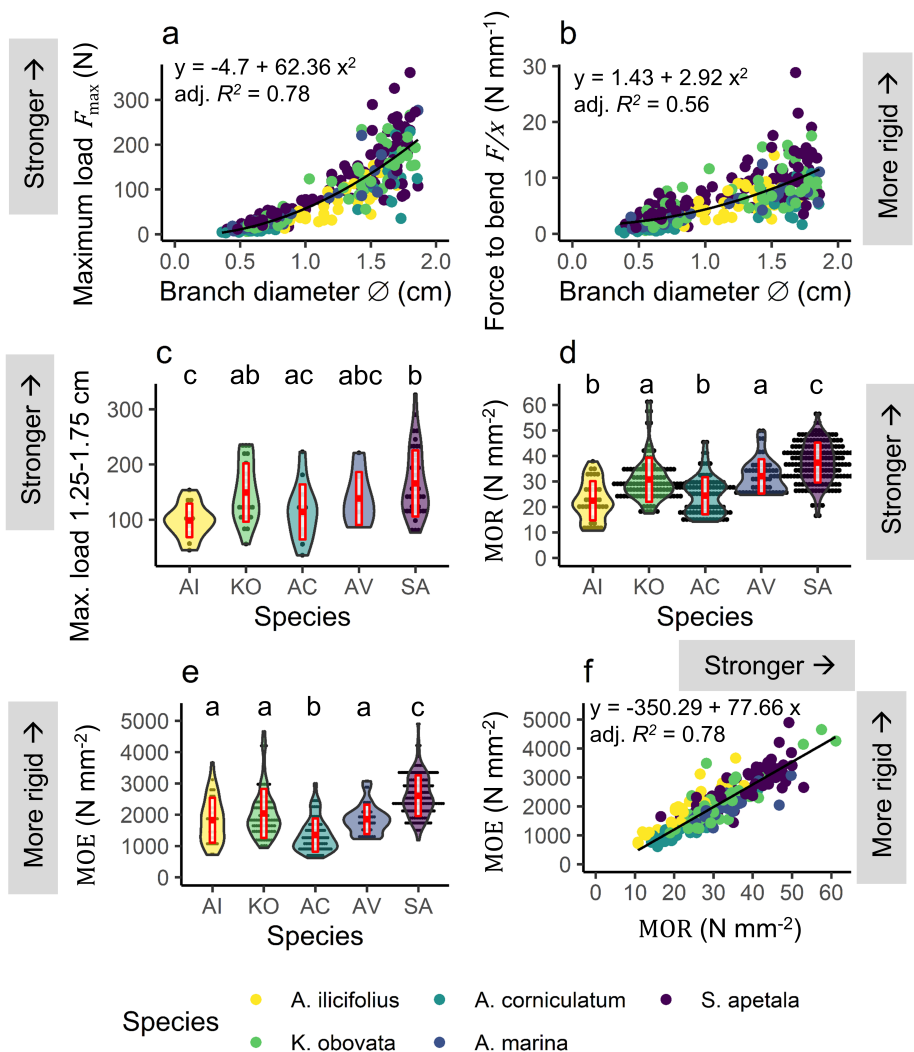


Figure 4.2: Branch mechanical properties of five mangrove species with (a) maximum load before breaking (F_{max} ; N) per diameter \varnothing (cm), (b) force needed to bend the branch (F/x ; $N\ mm^{-1}$) per diameter \varnothing (cm), (c) the maximum load F_{max} (N) for branches ranging from 1.25 to 1.75 cm, (d) average Modulus of Rupture MOR ($N\ mm^{-2}$), (e) average Modulus of Elasticity MOE ($N\ mm^{-2}$) and (f) Modulus of Elasticity MOE vs. Modulus of Rupture MOR. Red crossbars indicate mean and standard deviation. Letters indicate significance following Dunn's test with $\alpha = 0.05$.

Storm damage resistance

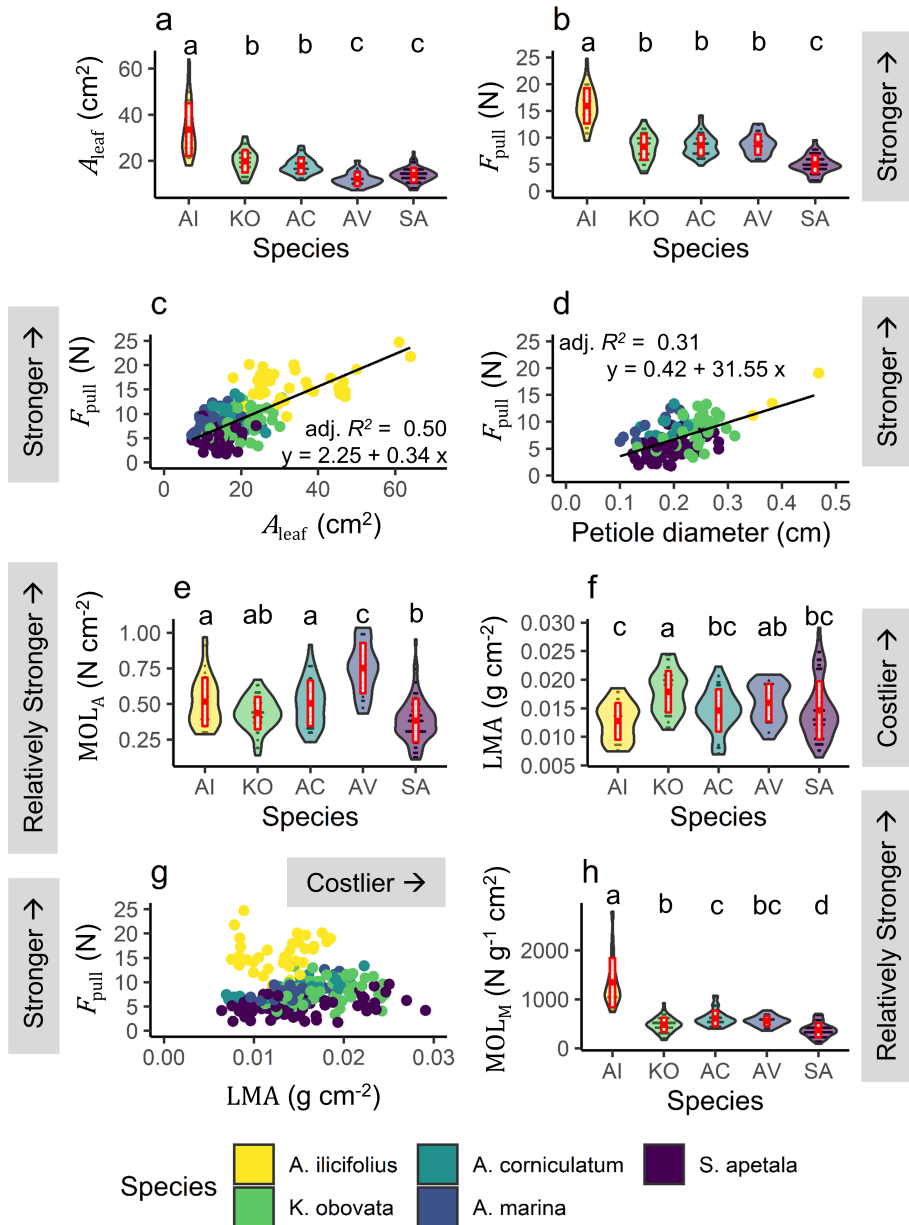


Figure 4.3: Leaf properties of five mangrove species with (a) surface area of the leaf A_{leaf} (m²), (b) force needed to detach a leaf F_{pull} (N), (c) pulling force F_{pull} (N) vs. leaf surface area A_{leaf} (m²), (d) pulling force F_{pull} (N) per petiole diameter (cm; note that *A. ilicifolius* leaves have very short petioles that broke off in 98% of pulling tests), (e) area-based Modulus of Leaf loss MOL_A as $F_{\text{pull}}/A_{\text{leaf}}$ (N cm⁻²), (f) Leaf Mass per Area "LMA" (g cm⁻²), (g) Leaf Mass per Area "LMA" (i.e. considered a measure of investment of biomass per cm² leaf) vs pulling force F_{pull} (N), and (h) Modulus of Leaf loss MOL_M as $F_{\text{pull}} \text{ LMA}$ (N g⁻¹ cm²). Red crossbars indicate mean and standard deviation. Letters indicate significance following Dunn's test with $\alpha = 0.05$.

4.3.2 Variability in mechanical properties across species

We identified a trend where species that occur more seawards had significantly stronger branches but more weakly attached leaves. Firstly, this was observed for branch strength. The maximum load F_{\max} that branches of 1.25 to 1.75 cm diameter can withstand was significantly higher for the most seaward species *S. apetala* (166.0 ± 59.9 N) compared to the most landward species *A. ilicifolius* (98.7 ± 30.4 N; Figure 4.2c). The other three species fell somewhere in the middle (149.0 ± 52.9 N for *K. obovata*, 114.0 ± 50.0 N for *A. corniculatum* and 138.0 ± 47.8 N for *A. marina* branches with diameters of 1.25 to 1.75 cm). This pattern was also observed to some extent for the relative strength of branches, Modulus of Rupture, across species (Figure 4.2d). Secondly, we observed significantly lower values of leaf size A_{leaf} and pulling force F_{pull} for species that generally occur more seaward (A_{leaf} 12.0 ± 2.93 cm² for *A. marina*, 13.7 ± 3.11 cm² for *S. apetala*; F_{pull} 8.73 ± 1.91 N for *A. marina*, 5.04 ± 1.67 N for *S. apetala*) versus more landward species (A_{leaf} 33.5 ± 11.4 cm² and F_{pull} 15.9 ± 3.31 N for *A. ilicifolius*; Figure 4.3a,b). Thirdly, we observed a significantly higher mass-based Modulus of Leaf Loss MOL_M for the landward species *A. ilicifolius* (1341 ± 505 N g⁻¹ cm²) compared to the four other species (478 ± 146 N g⁻¹ cm² for *K. obovata*, 609 ± 159 N g⁻¹ cm² for *A. corniculatum*, 555 ± 103 N g⁻¹ cm² for *A. marina*, 453 ± 758 N g⁻¹ cm² for *S. apetala*), so that *A. ilicifolius* required relatively much higher forces to detach given the investment made to produce the leaf; Figure 4.3h). Finally, the trend where species that occur more seawards had significantly stronger branches but more weakly attached leaves can be observed in Figure 4.4. The relative flexibility, Modulus of Elasticity MOE, followed a less distinct pattern of increase as with distance from the coast (Figure 4.2e), as *A. corniculatum* had slightly lower MOE (1350 ± 534 N mm⁻²), as can also be observed in Figure 4.2f. Further, the relative leaf attachment strength MOL_M , did not follow the seaward to landward species pattern observed above. Rather, when comparing leaf size A_{leaf} to pulling force F_{pull} (Figure 4.3e), we can see that *A. marina* leaves required relatively higher force (0.75 ± 0.18 N cm⁻²) to be detached given their size and may thus withstand higher drag forces than other species (0.51 ± 0.17 N cm⁻² for *A. ilicifolius*, 0.44 ± 0.11 N cm⁻² for *K. obovata*, 0.50 ± 0.16 N cm⁻² or *A. corniculatum*, 0.38 ± 0.15 N cm⁻² for *S. apetala*). Leaf Mass per Area LMA did not follow a distinct pattern across species either (Figure 4.3f).

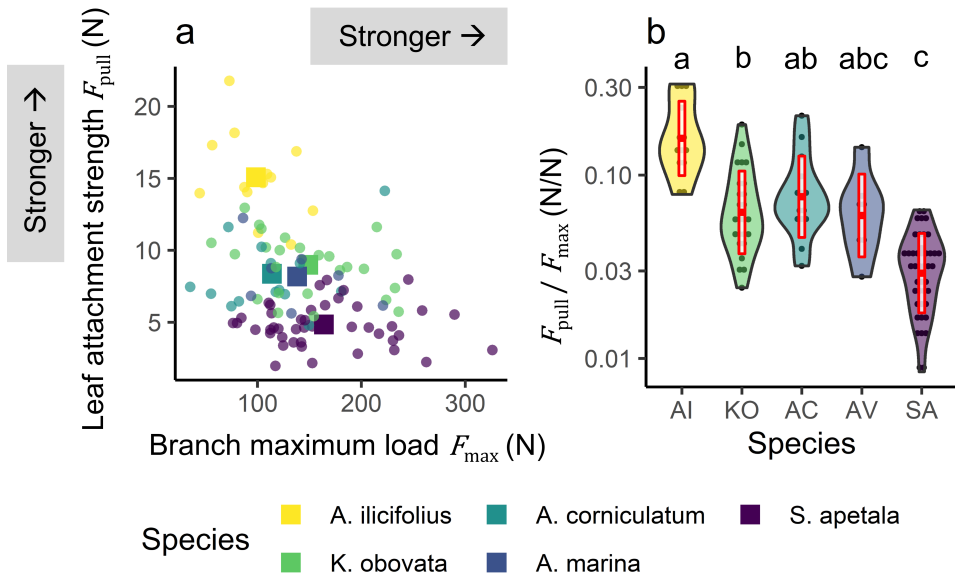


Figure 4.4: Relationship between absolute branch breaking strength F_{\max} (N) and absolute leaf detachment strength F_{pull} (N), and the ratio between F_{pull}/F_{\max} (N/N) sorted per species. Large squares represent mean values, red boxplots indicate mean and standard deviation, letters indicate significance following Dunn's test with $\alpha = 0.05$.

4.3.3 Variability in mechanical properties across salinity

We identified some significant differences of mechanical properties of branches MOR and leaves F_{pull} between sites for *K. obovata*, *A. corniculatum* and *S. apetala* and for leaves of *K. obovata*, *A. corniculatum* and *A. marina* (Figure 4.5), but found no clear correlation between salinity and mechanical properties (MOR, F_{pull}) for any species (Table S4.2). The observed differences between the sites were in general smaller compared to species differences (see Supplemental Information for detailed results).

4.3.4 Drag force on mangrove branches

The absolute drag forces as measured on mangrove branches followed generic patterns, where branches with a larger projected surface area (A_{proj}) experienced larger drag forces F_D than smaller ones (Figure 4.6), as was expected following the general drag force equation (Equation 4.2). Absence of leaves drastically reduced a branch's projected surface area A_{proj} (Figure 4.6), resulting in much lower drag forces F_D (Figure 4.6a). Our data show a significantly higher drag coefficient C_D for *A. marina* branches (averaged across tests: 16 ± 5.99 with leaves, 5.37 ± 2.3 without leaves; Figure 4.6b; Table S4.4), which also required relatively strong forces MOL_A to detach a leaf (Figure 4.3e).

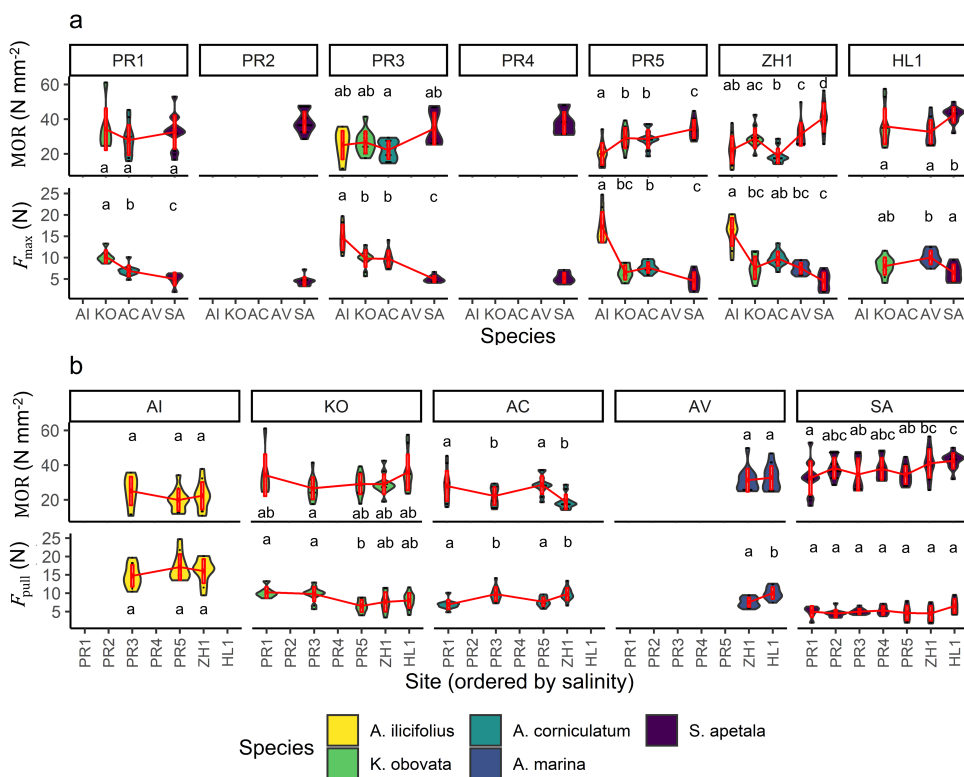


Figure 4.5: Modulus of Rupture MOR (N mm^{-2}) and leaf strength F_{pull} (N) across (a) species per site and (b) sites per species, with sites ordered towards increasing salinity (salinity based on Figure 4.1). Letters indicate significance following Dunn's test with $\alpha = 0.05$ (for *A. marina* a t-test was used), letters should be read per individual plot only (considering 24 plots in total).

Storm damage resistance

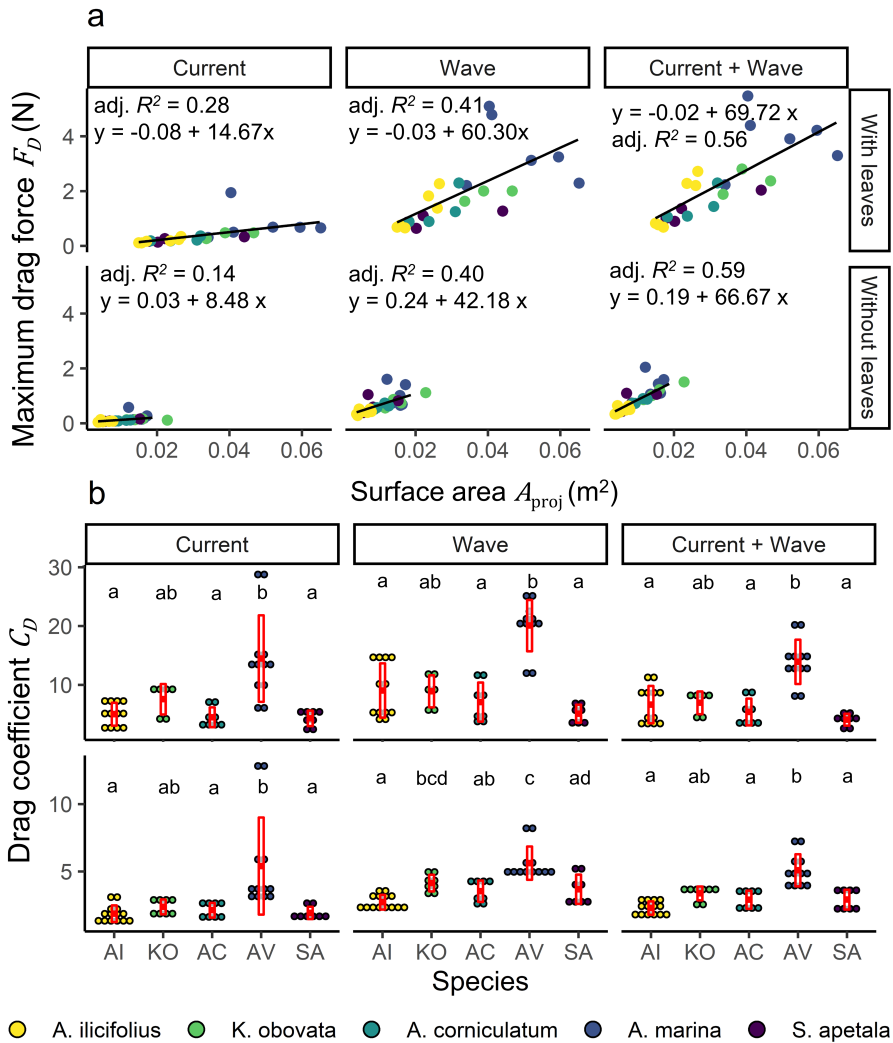


Figure 4.6: Drag forces and coefficients per species, with (a) drag force F_D (N) experienced per with and without leaves per projected surface areas, and (b) drag coefficient C_D with and without leaves. Scenarios tested are: current only, wave only, and current with waves. Letters indicate significance following Dunn's test with $\alpha = 0.05$.

4.4 Discussion

By systematically assessing mangrove mechanical properties, we aim to contribute to the safe integration of mangrove forests in coastal flood protection structures. We measured how much force mangrove branches can experience and withstand and how this differs between mangrove species and across environments with different salinities. We observed a generic pattern across species, where thicker branches are less flexible and can withstand larger forces. We also found that larger leaves withstand larger forces before detaching from the tree. We identified a trend where species that occur more seawards have significantly stronger branches but weaker leaf attachment compared to more landward species. Across sites, we found no clear correlation between salinity and mechanical properties. Finally, drag force experienced by mangrove branches followed a generic pattern, where branches with a larger projected surface area experienced larger drag forces than smaller ones. Leaf removal drastically reduced drag force and might protect branches from breakage during a storm, making easy leaf detachment a good adaptation for pioneer species living near the forest edge.

4.4.1 Mechanical strategies in successional mangrove species

Coastal mangrove forests are disturbance-driven, but not all trees are damaged equally when a storm hits (Krauss & Osland, 2020). Trees that grow at the seaward edge of the forest will likely be hit much harder, as the wave is still in full height. Present results suggest that the seaward dwelling pioneer species are adjusted to these harsh conditions. That is, we identified a pattern where species that generally occur more on the seaward forest edge (*S. apetala*, *A. marina*) have stronger branches yet smaller and more weakly attached leaves than landward species (*A. ilicifolius*, with *A. corniculatum* and *K. obovata* residing in between; Figure 4.4). Such strong wood can resist larger forces, reducing the chance of breakage, while the weaker leaves detach more readily and thus reducing the surface area and drag force on the tree. This pattern is similar to that of intertidal marsh vegetation in temperate zones, where pioneer species also exhibit clear wave-resistance or wave-avoidance strategies (Bouma et al., 2005). We propose two possible explanations for this pattern. The first is that various species have evolved strategies to avoid damage, either through resistance or reduction of drag forces. This was studied and confirmed for 28 freshwater species, with the actual strategy (avoidance vs. tolerance) depending on the type of plant (Puijalon et al., 2011). A second explanation for the seaward vs. landward differences could be thigmomorphogenesis. Thigmomorphogenesis is the process where a plant grows smaller and more compact in response to mechanical stress such as wind or water flow (Gardiner et al., 2016; Jaffe, 1973; Schoelynck et al., 2015). It is likely that plants growing at the exposed seaward edge of a mangrove

forest might grow phenotypes to resist or avoid mechanical stresses. Observations on saltmarsh vegetation support this hypothesis. For example, Cao et al. (2020) observed that seedlings – if they were able to survive the impact of wave exposure – developed shorter and stronger phenotypes under wave exposure. Here, we will not confirm or falsify either the evolutionary or the thigmomorphogenesis hypothesis as a driving factor behind branch and leaf strength, as (1) evolutionary studies require a different approach from our mechanistic angle (see Puijalón et al., 2011), and (2) the species sampling in this study was restricted by accessibility and availability within and across sites (e.g. *A. ilicifolius* was never found at exposed seaward locations). Given the findings of others described here we suspect a combination of the two will be at play.

4.4.2 Salinity impact on mechanical properties

Although salinity can impact wood properties (Table S4.1), we found no clear effect of salinity as an environmental driver of mechanical properties in mangroves across the seven sites we studied. Perhaps the range of salinity across the sites we selected (estimated at 0 to 15 psu, see Supplementary Information) was too small to find an impact on the five species studied, that had various salt tolerances (*A. ilicifolius*: low, *K. obovata*: mid, *A. corniculatum*: mid, *A. marina*: high and *S. apetala*: low; Reef and Lovelock, 2015; Ye et al., 2005). Possibly, seasonal variation in salinity may have disturbed clear spatial patterns. Alternatively, there might be overruling environmental drivers at play that we were not able to identify. For example, mangroves are generally considered oligotrophic ecosystems, and the continuous terrigenous input of nutrients in the Pearl River Delta area may alter wood density (Boland & Woodward, 2019; McKee, 1995). Regardless, this lack of a strong salinity response simplifies modelling storm damage to mangrove forests for the studied region, as the overall patterns across the studied species are dominant.

4.4.3 Drag properties of mangrove branches

Larger branches are stronger, but also bigger and less flexible and experience more drag force. Furthermore, branches with a higher drag coefficient can experience larger drag forces. *A. marina* branches experienced largest drag forces and had largest drag coefficients. Note that the drag coefficients were obtained at relatively low flow velocities (around 0.25 m s^{-1} for waves and currents combined), typical to that of mangroves under normal conditions; typical flow velocities in mangroves reach $0.15\text{-}0.35 \text{ m s}^{-1}$ during a flood tide (Mullarney et al., 2017), whereas (modelled) storm surge conditions can produce velocities around $0.5\text{-}0.7 \text{ m s}^{-1}$ (Figure 4.7; Dasgupta et al., 2019; Roeber and Bricker, 2015). Despite the low flow conditions, the tests are still informative about the drag coefficient, which is known to be reasonably constant when the Reynolds number is above 1000 (2500 in our test; Chen, Ni, et

al., 2018; Hu et al., 2014). However, higher flow conditions would likely result in strong branch realignment, reducing the frontal surface area and thus drag force on the branch (Vollsinger et al., 2005). Thus, the derived drag coefficients can be used as a most conservative estimate for single branches. Furthermore, we looked at drag on single branches, while surrounding vegetation causes turbulence and can increase drag forces more than twofold (Norris et al., 2017; Paul et al., 2016). Ideally, a much larger flume that can encapsulate entire tree canopies would be used to generate realistic currents and waves under variable storm surge heights or up to the point of branch or tree breakage. However, such flumes are expensive to run (Möller et al., 2014; van Wesenbeeck et al., 2022). Regardless of these limitations, *A. marina*'s larger drag coefficients are in line with their branch architecture, that is rather irregular with leaves directly attached to sturdy, inflexible branches (Figure S4.6). Contrarily, *S. apetala* branches experienced much lower drag forces and have more flexible terminal branches that allow for realignment in the water stream. Aside from flexibility of branches, leaf removal also resulted in lower drag forces and drag coefficients for all species. Possibly, leaf loss can mitigate the effects of storm wind and waves, but it is not certain when this occurs. Our static measurements are useful for species comparisons but may be improved upon – to estimate leaf loss, it is necessary to know what drag forces individual leaves experience and how much they are impacted by dynamic loading from turbulent flow, which may be different from static pulling concentrated in a small point (Vogel, 2009).

4.4.4 Mechanical tree damage during storm surges

Following methods used in mechanical storm wind damage models (Gardiner et al., 2008), our measurements of mechanical and drag properties can be used to estimate storm surge damage on idealised branches. Here, we can compare the drag force generated under different wave orbital velocities to the maximum force a branch can withstand. A branch will break if the drag force (F_D) it experiences becomes larger than the maximum force (F_{\max}) it can withstand. This maximum strength will depend on the relative strength of the wood (MOR) and the branch arm the drag force is acting on (L) (Equation 4.1). The drag force the branch experiences will depend on the projected frontal surface area of the branch (A_{proj}), the drag coefficient (C_D) and the flow velocity (u ; Equation 4.2). We show an example of such an estimation for idealised branches that are rigid and completely submerged in Figure 4.7 (see Supplemental Information for the full calculation). When scaling up to full trees, a similar approach may be used where the diameter of the idealised branch becomes the diameter of the idealised trunk. There are a number of steps that can be taken to refine this simple model. First, one can validate that the Modulus of Rupture for branches (0.5-1.75 cm diameter) remains the same for tree trunks (Figure S4.1) by

measuring the MOR of tree trunks directly – but carefully, so that no vulnerable mangrove forests are harmed. Second, one can link drag coefficients more closely to natural conditions by including surrounding vegetation in drag measurements, as discussed in the previous Section (4.4.3), or by measuring drag in the field. Third, one can include how the realignment of branches and leaves impacts the frontal surface area A_{proj} or arm L . In three North American hardwood species placed in a wind tunnel under wind velocities of 20 m s^{-1} , branch realignment resulted in a 50% reduction in projected frontal surface area (Vollsinger et al., 2005). Fourth, one may consider the tree location and average height distribution of branches and leaves per species relative to (variable) storm surge heights. For example, late-successional species are generally located higher in the intertidal zone, where they may be less submerged by a storm surge, and more sheltered from storm waves. However, in the Pearl River Delta, the average height of native trees is comparable to that of the seawalls behind them, and can thus experience waves over the full height of the tree during storms. Depending on whether it is wind or waves that will reach branches during a storm, drag properties in wind will also need to be included in the model. Fifth, trees can experience much larger loads from dynamic loading than static loading (James et al., 2013). Measuring dynamic loads is currently not possible, given the lack of knowledge on motion. Thus, measuring the difference between static versus dynamic loading on mangrove trees and branches should be addressed in future research. Furthermore, aside from breaking mechanisms, uprooting mechanisms should also be included, particularly if storms are accompanied by large erosion events that can result in the loss of a tree's mechanical stability (Gardiner et al., 2016). Last, measuring what drag forces leaves experience under real wind and wave loads and when leaf loss occurs will help us understand if trees will experience complete defoliation, which can be lethal, particularly in species that cannot resprout epicormically (e.g. Rhizophoraceae, Gill and Tomlinson, 1969; Saenger, 2002).

4.4.5 Towards long-term coastal flood safety with mangrove forests

This research provides a basis for understanding the mechanistic processes that take place in mangrove forests during major storms. It provides a comprehensive dataset of mechanical and drag properties of mangrove species in one of the most highly urbanised, at-risk urban deltas in the world. This is a key input to model assessment and an important step in the direction of analytical storm damage modelling in mangroves. This research also produces new insights in damage-resistance strategies across mangrove species. These results may provide guidance on mangrove afforestation efforts for flood protection, suggesting that pioneer species are more suitable to resist the influence of the exposed seaward environment. This amplifies knowledge that pioneer species are generally more suitable to grow in the lower

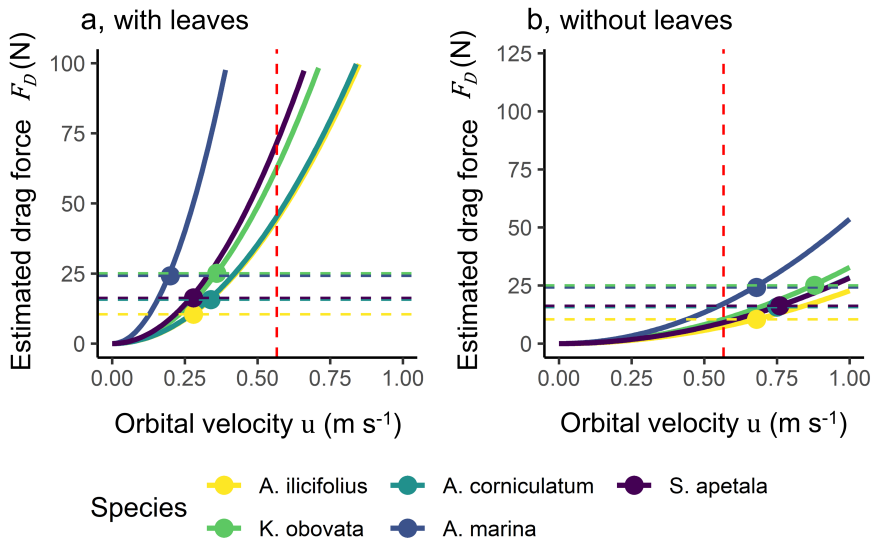


Figure 4.7: Conceptual model with estimations of drag force F_D experienced for idealised branches of 1 cm in diameter \varnothing , (a) with and (b) without leaves. Dashed lines indicated maximum force F_{max} a branch can withstand. Red dotted lines indicate estimated peak orbital velocity during a typhoon (based on Hato, August 2017). See Supplemental Information for calculation.

intertidal zone (Lewis, 2005; Primavera et al., 2016). In the case of the Pearl River Delta, we emphasize that *S. apetala* is an introduced and potentially invasive species and its long-term impact on natural ecosystem functioning is not fully understood (Ren et al., 2009). Thus, care should be taken in species selection when afforesting for long-term flood defence.

Ultimately, long-term flood protection will require scaling up individual tree damage to whole-ecosystem damage and taking into account the indirect impacts of storms such as prolonged flooding and sedimentation (Krauss & Osland, 2020). It should also consider other drivers of variability across species and space, such as regeneration speeds between species (Gill & Tomlinson, 1969; Saenger, 2002) or changes in tidal regime or salinity, which could alter species zonation in the coastal zone and consequently change the storm resistance of the present ecosystem (Zhu et al., 2019). As more knowledge is gained about mechanical tree damage, it will become easier to predict forest structure and size over time and provide reliable long-term flood safety predictions. This will advance the incorporation of nature in flood defence schemes and enable affordable and durable coastal flood safety while preserving one of the most precious ecosystems on earth.

S4 Supporting information

S4.1 Vegetation height in the Pearl River Delta, China

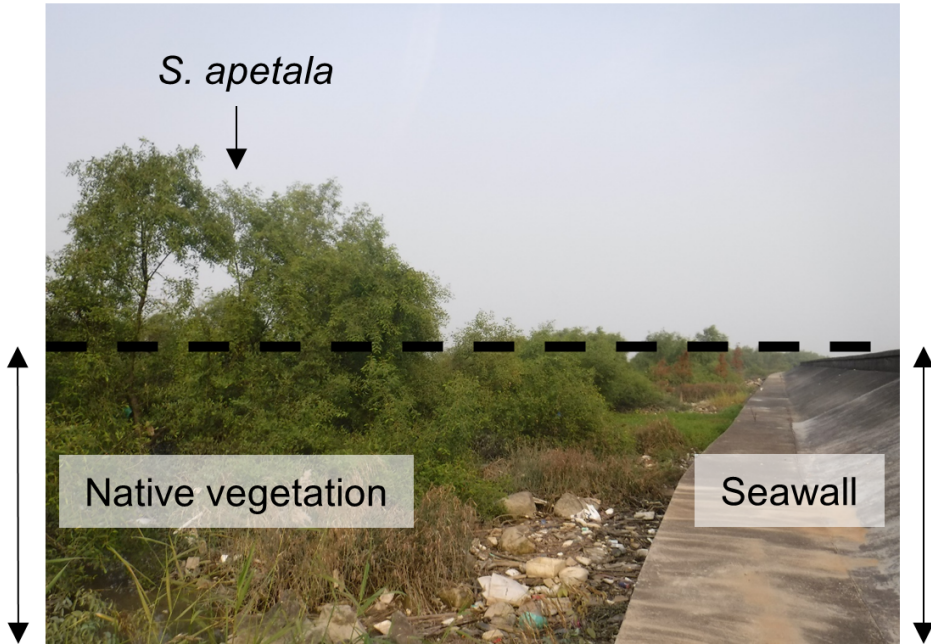


Figure S4.1: Height of vegetation relative to seawall. Picture taken in field site PR1.

S4.2 Literature on impact of salinity on mangrove wood properties

Table S4.1 presents literature on the impact of salinity on wood properties of various mangrove species. Salinity, wood properties and strength are linked as such: salinity can increase the tension in the water column, which imposes mechanical stress on the xylem vessels (Jacobsen et al., 2005). Vessel density in turn may correlate negatively with wood density (Preston et al., 2006), and wood density correlates positively with mechanical strength (Chave et al., 2009). Thus, salinity may potentially impact mechanical strength of mangrove wood.

Table S4.1: Literature on the impact of salinity on wood anatomy for various mangrove species.

Salinity range	Salinity impact	Con-founding factors?	Species	Reference
32 – 48 ppt	"MOE and density of intact mangrove branches increased as fibre wall thickness increased. [...] We did not observe significant increases in fibre wall thickness in <i>A. marina</i> specimens growing in more saline high intertidal environments"	Intertidal zone	<i>Avicennia marina</i>	Santini et al., 2013
3.5 – 23 ‰	"fiber-tracheids [...] under higher soil salinities, they had small diameters and, in general, thicker walls with fewer pits."		<i>Aegiceras corniculatum</i>	Sun and Lin, 1997
26.4 – 49.2 ‰	"Vessel density showed a significant increase with salinity."	Inundation frequency	<i>Rhizophora mucronata</i>	Schmitz et al., 2006
6.7 - 9.8 ppt	"Analyses revealed that in sites with high salinity and flooding levels, there are more abundant vessels and axial parenchyma although the fibres and vessel elements are shorter, suggesting a water stress effect. ... <i>L. racemosa</i> wood harvesting should avoid those sites with [...] high salinity that may modify wood quality"		<i>Laguncularia racemosa</i>	Yanez-Espinosa et al., 2004
0, 15, 30 ‰	"The vessel density increased with salinity"		<i>Laguncularia racemosa</i>	Sobrado, 2007
0, 10.6, 26.7, 42.3, 58.4 ppt	"increasing salinity caused an increase in mortality rate whereas production of new leaves and leaf longevity decreased and, finally, the leaf area was reduced"		<i>Avicennia germi-nans</i>	Suárez and Medina, 2005
0-27 ppt, 9-37 ppt, 45-100 ppt	"Our findings indicate that the inter- and intra-specific variation found in the wood density of the mangrove trees is the result of the different levels of salinity found in the study area"		<i>Avicennia germi-nans</i>	Virgulino-Júnior et al., 2020

Storm damage resistance

S4.3 Branch diameter across the tree

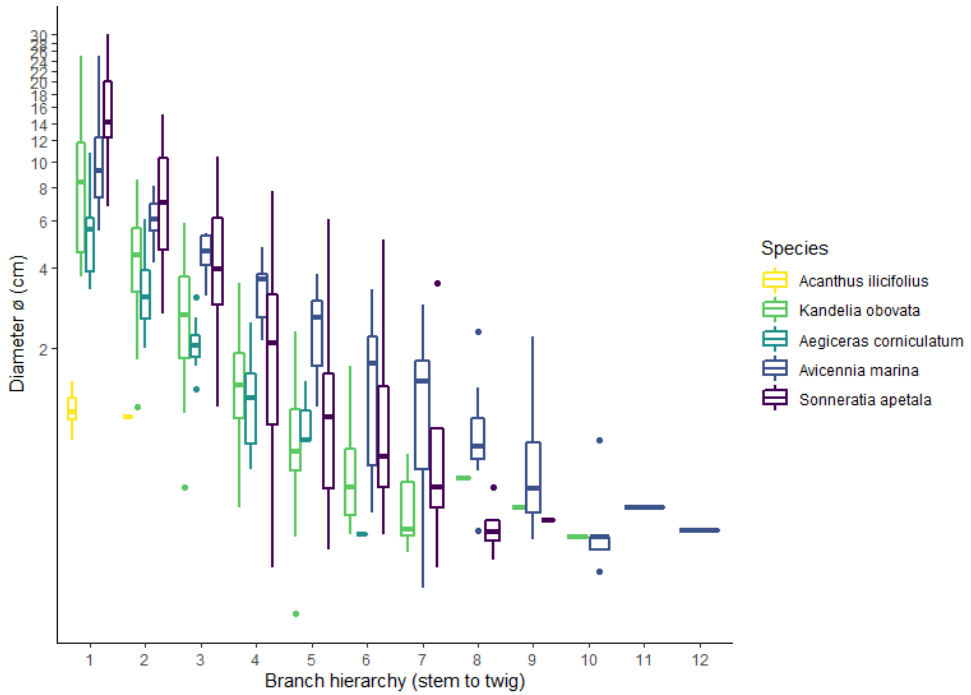


Figure S4.2: Diameter \varnothing (cm) near the base of branches (past the strong initial tapering that occurs at the base of branches), measured for stem to child branches (i.e. branch 3 branches of from branch 2, branch 2 branches from the stem). Data were collected in January 2019 at field site ZH1.

S4.4 MOR and MOE per branch diameter

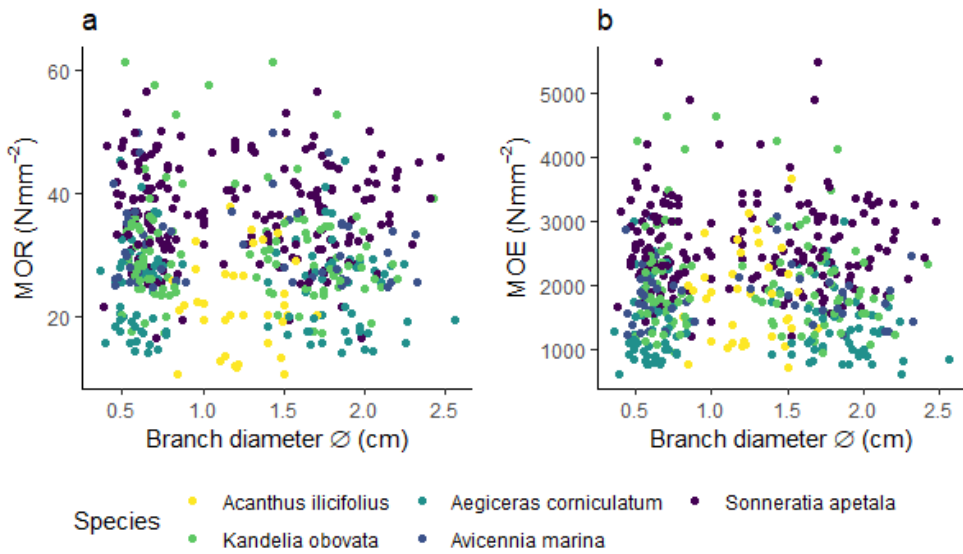


Figure S4.3: Modulus of Rupture MOR (N mm^{-2}) and Modulus of Elasticity MOE (N mm^{-2}) per branch diameter.

Storm damage resistance

S4.5 Three-point bending test and stress-strain curve

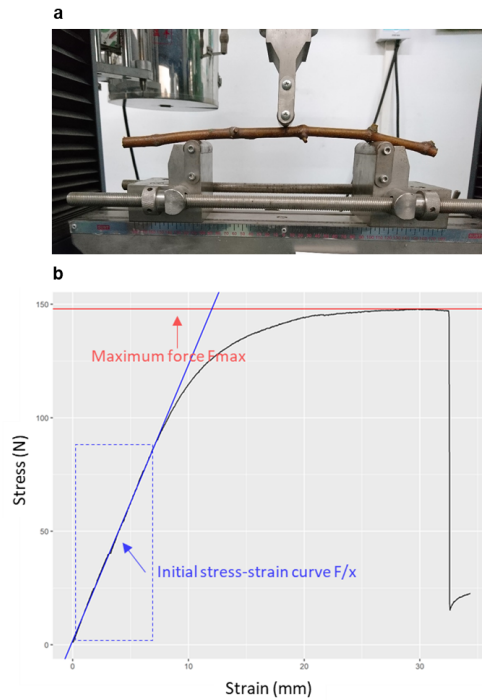


Figure S4.4: (a) universal testing machine performing a three-point bending test on a mangrove branch with the cross head pushing down the middle of the branch and (b) a typical stress-strain curve (black line) for a mangrove branch with the blue line indicating the initial slope of the stress-strain curve F/x and the red line at the maximum force before weakening (F_{\max}).

S4.6 Site salinity and mechanical properties per site

Figure S4.5 shows salinity estimates collected from various sources (literature and output from an FVCOM ocean model, validated for water levels and wave height but not for salinity). It is important to mention here that these are rough estimates, not all taken under the same circumstances (time period, time of sampling, etc.). Regardless, it is logical to say that salinity will be higher towards the coast and lower more inward into the Pearl River Delta, as various rivers empty into the delta. Final salinity that was used is shown in Figure 4.1.

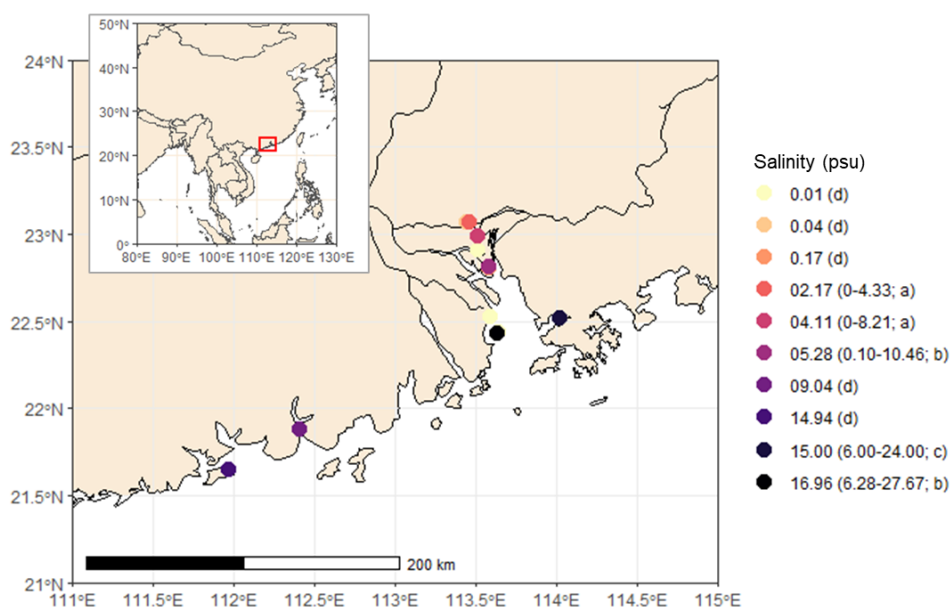


Figure S4.5: Salinity data from various sources: (a) Mingkai Guan et al. 2016 Saltwater intrusion lengths in the Pearl River networks based on one-dimension salinity model, Port & Waterway Engineering 11: 66-7), (b) Song Yang et al. 2011. Acute toxicity effects of salinity stress on the invasive golden apple snails. Journal of South China Agricultural University 2: 142-146), (c) Jiezhong Chen & Liya Wang. 2005. Influence of the diversion of seawater from Dapeng Bay on Shenzhen Bay. Shenzhen SAR Science and Technology), (d) output from an FVCOM ocean model, validated for water levels and wave height but not for salinity (Peng Zheng, personal communication, January 17, 2020).

Looking at Figure 4.5 we cannot observe a clear increase or decrease as a result of salinity across sites, which are ordered by salinity (see Figure 4.1 for salinities used here). Furthermore, we applied a linear model $MOR \sim \text{salinity}$ or $F_{\text{pull}} \sim \text{salinity}$ to each species that results in very minor correlations and slope effects (Table S4.2), such that we cannot conclude that salinity explains the variations in mechanical properties of the five mangrove species studied here. Using the lme4 library in R (lme4 version 1.1-21; R version 3.5.3; Bates et al., 2014; R Core Team, 2021), we

Storm damage resistance

Table S4.2: Correlations between mechanical properties and salinity, per species.

Species	MOR ~ salinity			$F_{\text{pull}} \sim \text{salinity}$		
	slope	p-value	adj. R ²	slope	p-value	adj. R ²
<i>A. ilicifolius</i>	-0.01	0.95	-0.03	0.01	0.90	-0.03
<i>K. obovata</i>	0.34	0.01	0.05	-0.05	0.30	0.00
<i>A. corniculatum</i>	0.82	0.00	0.18	0.01	0.01	0.11
<i>A. marina</i>	0.23	0.45	0.00	0.42	0.00	0.42
<i>S. apetala</i>	0.47	0.00	0.10	0.08	0.02	0.07

fit a linear mixed-model with species as fixed effect, site as a fixed effect, and site as a species-dependent random intercept effect (because we expect that some site variation will be dependent on the species and is not just a global site effect, i.e. to capture species-specific site-variation): $y \sim \text{species} + \text{site} + (1|\text{species}:\text{site})$ to identify if species or site differences were larger. From Table S4.3 one can see that the species effects are much larger than the site and random effects for both mechanical properties MOR and F_{pull} .

Table S4.3: Correlations between mechanical properties and salinity, per species.

Fixed effect	Value of fixed effect, MOR	Value of fixed effect, F_{pull}
intercept	24.33	37.57
Species KO	6.94	-14.34
Species AC	1.47	-17.22
Species AV	6.47	-21.02
Species SA	13.03	-20.45
Site PR2	0.92	-2.96
Site PR3	-2.69	-6.29
Site PR4	0.49	-4.62
Site PR5	-1.59	-0.61
Site ZH1	-1.40	-4.29
Site HL1	3.88	-4.82
Random species- dependent site effect	3.54	4.02
Residual error	7.19	4.38

S4.7 Drag coefficients and branch photos

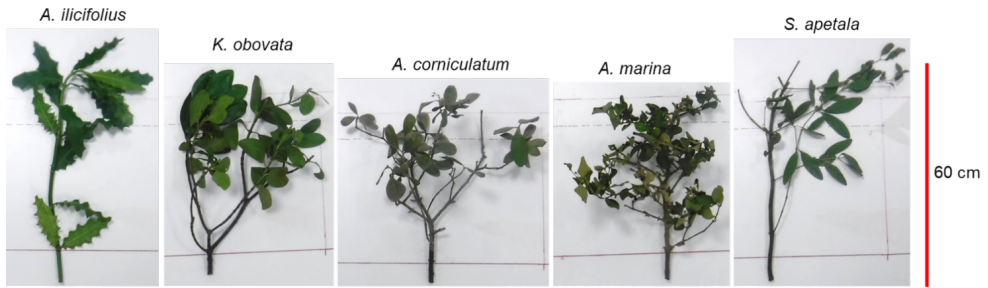


Figure S4.6: Branches of each species that were tested in the flume for drag force and drag coefficient.

Storm damage resistance

Table S4.4: Mean, standard deviation and standard error of the mean of drag coefficients C_D per species. Tests were (1) waves without a current, (2) a current of 15 cm s^{-1} without waves, and (3) waves and a 15 cm s^{-1} current, with water height 33 cm, wave height 11 cm and wave period 1.5 s.

Test	Leave presence	Species	Mean C_D	Standard deviation	Standard error
Current	with	<i>A. ilicifolius</i>	5.01	1.98	0.57
Current	with	<i>K. obovata</i>	7.56	2.97	1.21
Current	with	<i>A. corniculatum</i>	4.49	1.69	0.60
Current	with	<i>A. marina</i>	14.47	7.40	2.13
Current	with	<i>S. apetala</i>	4.30	1.38	0.49
Current	without	<i>A. ilicifolius</i>	1.85	0.64	0.17
Current	without	<i>K. obovata</i>	2.36	1.25	0.44
Current	without	<i>A. corniculatum</i>	2.11	0.55	0.20
Current	without	<i>A. marina</i>	5.40	3.69	1.07
Current	without	<i>S. apetala</i>	1.91	0.81	0.29
Wave	with	<i>A. ilicifolius</i>	9.04	4.75	1.37
Wave	with	<i>K. obovata</i>	8.91	2.78	1.13
Wave	with	<i>A. corniculatum</i>	7.07	3.35	1.19
Wave	with	<i>A. marina</i>	20.07	4.48	1.35
Wave	with	<i>S. apetala</i>	5.09	1.54	0.58
Wave	without	<i>A. ilicifolius</i>	2.71	0.57	0.15
Wave	without	<i>K. obovata</i>	4.13	0.67	0.24
Wave	without	<i>A. corniculatum</i>	3.52	0.80	0.28
Wave	without	<i>A. marina</i>	5.61	1.26	0.36
Wave	without	<i>S. apetala</i>	3.67	1.10	0.39
Current + Wave	with	<i>A. ilicifolius</i>	6.64	3.18	0.92
Current + Wave	with	<i>K. obovata</i>	6.95	1.95	0.80
Current + Wave	with	<i>A. corniculatum</i>	5.40	2.29	0.81
Current + Wave	with	<i>A. marina</i>	13.92	3.78	1.09
Current + Wave	with	<i>S. apetala</i>	4.09	1.02	0.36
Current + Wave	without	<i>A. ilicifolius</i>	2.27	0.50	0.13
Current + Wave	without	<i>K. obovata</i>	3.37	0.52	0.18
Current + Wave	without	<i>A. corniculatum</i>	2.89	0.68	0.24
Current + Wave	without	<i>A. marina</i>	5.08	1.20	0.35
Current + Wave	without	<i>S. apetala</i>	2.90	0.74	0.26

S4.8 Simple estimation of storm damage to idealised branches

Using the quantified mechanical and drag properties and data on branch size, we estimated branch breakage for idealised branches. To support this estimation, we collected field data on length and projected surface area of tree branches (Figure S4.7). We measured the length L (m) of a branch given the diameter \varnothing (cm) at the base of the branch, but after initial strong tapering (Figure S4.7a). We measured the projected frontal surface area A_{proj} of a branch given the diameter \varnothing (cm) at the base of the branch with and without leaves (Figures S4.7b and c, respectively).

We estimated damage as follows: a branch will break if the drag force (F_D) it experiences becomes larger than the maximum strength (F_{max}) it can withstand: $F_D > F_{\text{max}}$. Inverting Equation 4.1, the maximum strength (F_{max}) of a branch will depend on the relative strength of the wood (MOR) and the branch arm the drag force is acting on (L):

$$F_{\text{max}} = \frac{MOR\pi R^3}{L} \quad (4.1)$$

whereas, following basic fluid dynamics, the drag force will depend on the projected frontal surface area of the branch (A_{proj}), the drag coefficient (C_D) and the flow velocity (u):

$$F_D = \frac{1}{2}\rho A_{\text{proj}}C_D u^2 \quad (4.2)$$

We estimated F_{max} and F_D for idealised branches with a diameter of 1 cm for each of the five species using our own data on MOR, L , A_{proj} and C_D and for orbital velocities u ranging from 0–1.5 m s⁻¹ (Table S4.5). The outcomes were compared to the orbital velocities u that were generated during a typhoon that hit the coast of south China in August 2017 (typhoon Hato, orbital velocities from output of a SWAN-model that simulates the typhoon; Peng Zheng, personal communication, January 17, 2020).

Storm damage resistance

Table S4.5: Sources and modelled values used in simple branch breakage estimation. $A_i = A. ilicifolius$, $K_o = K. obovata$, $A_c = A. corniculatum$, $A_m = A. marina$ and $S_a = S. apetala$. Species-specific values for L and A_{proj} with leaves were derived from Figure 4.7a and b respectively, where we assumed a linear(a) or quadratic (b) curve per species where the intercept went through the origin (this was done to avoid unrealistic negative correlations due to small data ranges for some species and is for illustrative purposes only). For area without leaves, we assumed that all species have similar area and used a grouped average.

Variable (unit)	Source	Values per species				
		A_i	K_o	A_c	A_m	S_a
MOR (MPa)	Figure 4.2d	22.4	30.7	24.4	32.0	37.4
L (m)	Figure S4.7a	0.84	0.48	0.61	0.52	0.90
R (cm)	Idealised $\varnothing =$ 1 cm branch	0.5	0.5	0.5	0.5	0.5
A_{proj} with leaves (m^2)	Figure S4.7b	0.04	0.05	0.05	0.08	0.10
A_{proj} without leaves (m^2)	Figure S4.7c	0.02	0.02	0.02	0.02	0.02
ρ ($kg\ m^{-3}$)	$1000\ kg\ m^{-3}$ (fresh water)	1000	1000	1000	1000	1000
u ($m\ s^{-1}$)	$0-1.5\ m\ s^{-1}$	0 to 1.5	0 to 1.5	0 to 1.5	0 to 1.5	0 to 1.5
C_D with leaves	Figure 4.6b	6.90	7.81	5.66	16.0	4.47
C_D without leaves	Figure 4.6b	2.28	3.29	2.84	5.37	2.83

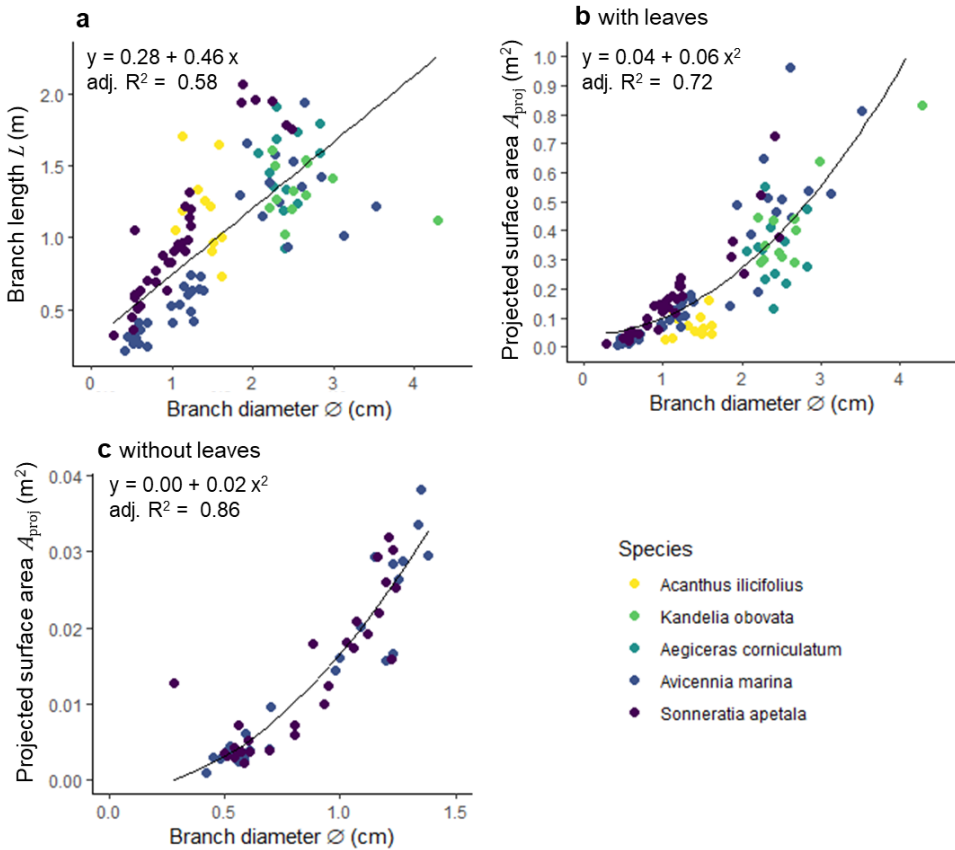
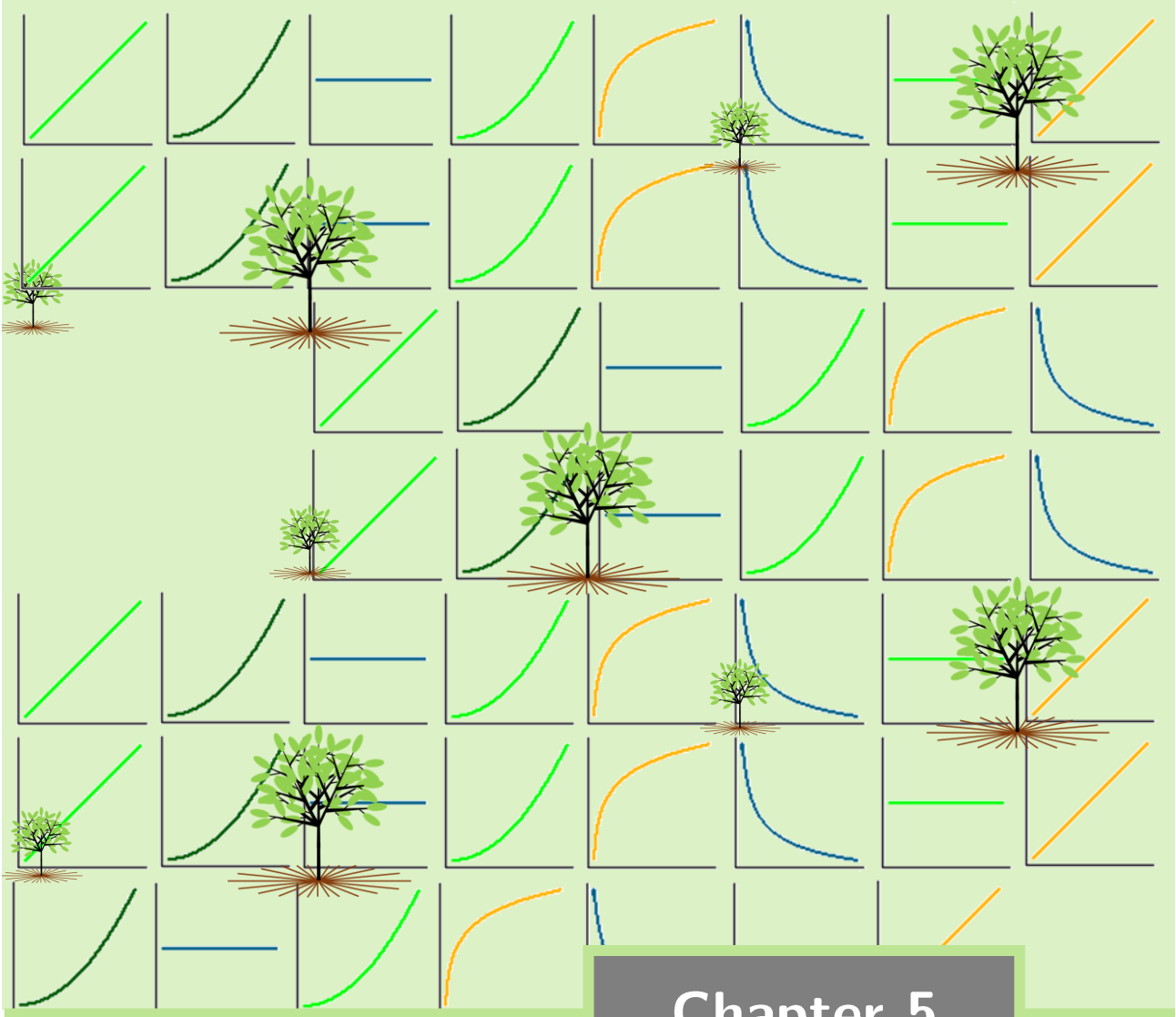


Figure S4.7: Branch dimensions per species with (a) fitted linear relationship between branch diameter \varnothing (cm) and branch length L (m), (b) fitted quadratic relationship between branch diameter \varnothing (cm) and projected surface area A_{proj} (m^2) for branches with leaves (data only available for *A. marina* and *S. apetala*), (c) fitted quadratic relationship between branch diameter \varnothing (cm) and projected surface area A_{proj} (m^2) for branches without leaves. Regression lines shown here are species-independent. Data in panels were collected at different dates and come from different sources: data in (a) and (b) were collected in June 2019 at field site PR3 for all species, and in October 2019 at field site HL1 extra for *A. marina* and *S. apetala*, data in (c) were collected in October 2019 at field site HL1.



Chapter 5

Synthesis

R. van Hespén

5 | *Synthesis*

Implementing nature-based flood defence requires that its safety value over the span of decades is known with reasonable level of certainty. In this thesis, I aimed to uncover how physical drivers affect mangrove forest properties for nature-based flood defence. **Chapter 1** described how biophysical interactions between the environment (such as wind, waves and sediment dynamics) and mangrove seedlings and trees make up a forest's functioning in nature-based flood defence and identified the most urgent unanswered questions. **Chapter 2** used a mesocosm experiment to specifically look at the impact of sediment dynamics on seedling establishment in eight contrasting mangrove species, and uncovered mechanisms with which mangrove seedlings may overcome sediment dynamics. **Chapter 3** studied how mangrove tree stability is determined by its belowground structure, using 3D-printed mimics. It showed that sediment type is a determining characteristic in mangrove tree stability, together with root plate size and root mass distribution. **Chapter 4** presented a field campaign to examine the mechanical strength of aboveground tree structures. Specifically, it tested the mechanical properties of mangrove branches and leaves across five species, showing that thicker branches are stronger, reducing the risk of damage, while leaves that detach easily reduce the effective surface area of the branch and hence also the risk of damage. Here, I combine these findings to show to what extent we now understand the impact of mechanical disturbance on mangrove plants (Figure 5.1), in general and between species.

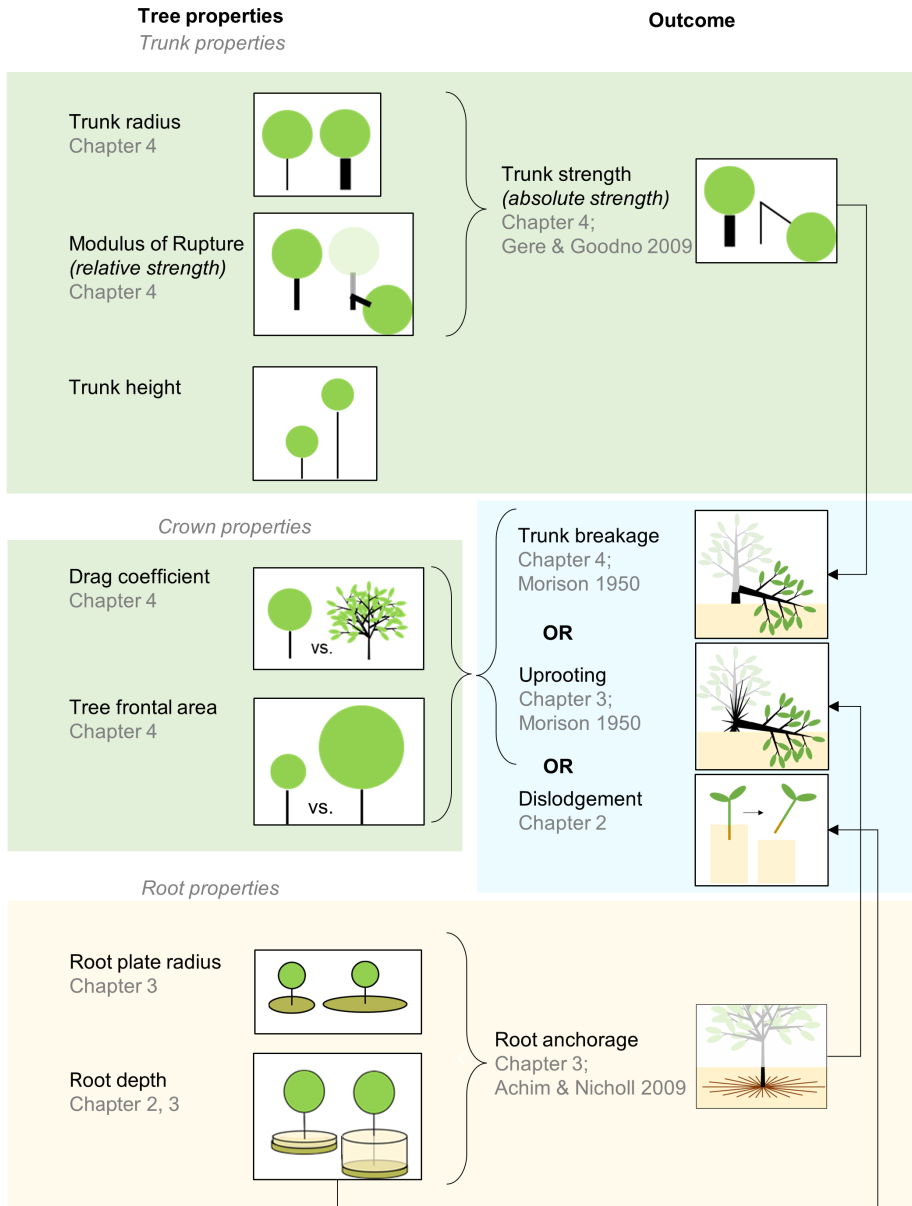


Figure 5.1: Overview of the mechanical disturbances and relevant tree properties studied in this thesis.

5.1 General impact of mechanical disturbance on mangrove plants

Nature-based flood defence with mangroves requires a wide and dense forest to provide optimal flow energy attenuation (Chapter 1). Mechanical damage affects the structural integrity of the forest, reducing the wave attenuation capacity. The mechanical damages most impactful on wave attenuation capacity are seedling dislodgement (which completely inhibits new forest establishment, Chapter 1), belowground tree uprooting and aboveground trunk breakage, which usually leads to tree death and loss of forest biomass (Figure 5.1, Chapter 1). Based on the findings in this thesis, these damages can be roughly estimated (Figure 5.2). Estimating seedlings dislodgement is relatively straightforward. Dislodgement can be considered a special case of uprooting, where the roots have been eroded so deeply that barely any force is needed to dislodge the seedling from the sediment. Hence, deeper roots provide more anchorage (Chapter 2), as the critical erosion depth is closely linked to the root depth (Figure 5.2). Because erosion thresholds will be much larger for saplings and trees (Chapter 3 for trees, Figure S5.1 for saplings), dislodgement is mainly a risk for seedlings (Figure 5.2). For trees, we can roughly estimate critical wind or wave velocities (Figure 5.2). I assume an idealised tree of 5 metres tall (the average maximum height of the mangrove species in south China, that were studied in this thesis). Belowground, this idealised tree would have a root plate with a radius of 1.9 m and a root depth of 0.81 m (Figure 5.2). The anchorage of this root plate is determined by (1) the sediment it is rooted in, (2) the effective size of the root plate (which depends on an interaction with the sediment properties and the distribution and strength of the roots) and (3) the depth of the roots (Chapter 3). For the idealised tree, I assume a sediment shear strength of 5000 Nm^{-2} (equivalent to undrained sediments at the seaward fringe; Chapter 3). Assuming that the roots break on the leeward side of the tree, the idealised tree then has an anchorage moment of $23241 \text{ N}\cdot\text{m}$ if the storm does not erode any sediment. The tree will uproot if the overturning moment acting on its canopy surpasses its anchorage moment. The overturning moment is formed by the drag force acting on the canopy and the height of the tree. Thus, the idealised tree would uproot at a wind speed of 76 m s^{-1} (equivalent to a Category 5 storm), or a wave orbital velocity of 2.7 m s^{-1} . Aboveground, we can roughly estimate when the idealised tree trunk will break. This can be inferred by extrapolating branch mechanical properties (Chapter 4). Then, the idealised trunk would have a trunk with a diameter of 8 cm and Modulus of Rupture of 35 N mm^{-2} and would break if the drag force acting on the tree's canopy surpasses 1442 N. This drag force is determined by the drag coefficient and the effective frontal surface area of the canopy – which can decline as flow velocities increase and branches bend and leaves realign in the wind or water stream. For the idealised tree, the surface area

Synthesis

of the canopy is 1.3 m^2 without leaves (to account for the realignment). Assuming a drag coefficient of 1, the idealised tree trunk would then break at a wind speed of 43 m s^{-1} (equivalent to a Category 1 storm) or a wave orbital velocity of 1.5 m s^{-1} . Consequently, for this idealised tree it is more likely that the trunk will break than that it will uproot. Modelling the critical flow velocities for this idealised tree is a worthwhile exercise, as it illustrates where further quantification of mangrove properties is most urgently needed. For example, in calculating the trunk strength I assumed that mechanical properties for trunks can be extrapolated from branches, yet this assumption is currently unvalidated. Furthermore, the wind and wave velocities required to uproot the idealised tree are high due to the assumptions I made about the root properties – which are largely unknown, illustrating the need for better quantification of belowground mangrove properties. Furthermore, there is need to quantify the allometric relationships between canopy, trunk and root dimensions (e.g. roughly estimated in Figure 5.2). Moreover, long-term monitoring of mechanical, dimensional, morphological and drag properties is needed to estimate risk damage as mangrove plants mature from seedling, to sapling, to adult tree. Finally, it is essential to validate damage estimates in the field, such as defoliation, branch damage, trunk breakage and uprooting. While important, each of these measurements causes harm to mangroves. This is far from ideal, as many mangrove forests are threatened (Friess et al., 2019; Valiela et al., 2001). Hence, careful consideration of such field campaigns is needed (Parris et al., 2010) and should be complemented with less harmful approaches such as lab studies and comparing prevailing wind and waves velocities with high-resolution satellite and LIDAR imagery (e.g. Lagomasino et al., 2021). In the case of field validation of damage, wind tunnel (Vollsinger et al., 2005) or wave flume experiments (de Smit et al., 2020) could be used and initially combined with tree mimics to understand how wind and waves interact with mangrove canopies and lead to tree damage.

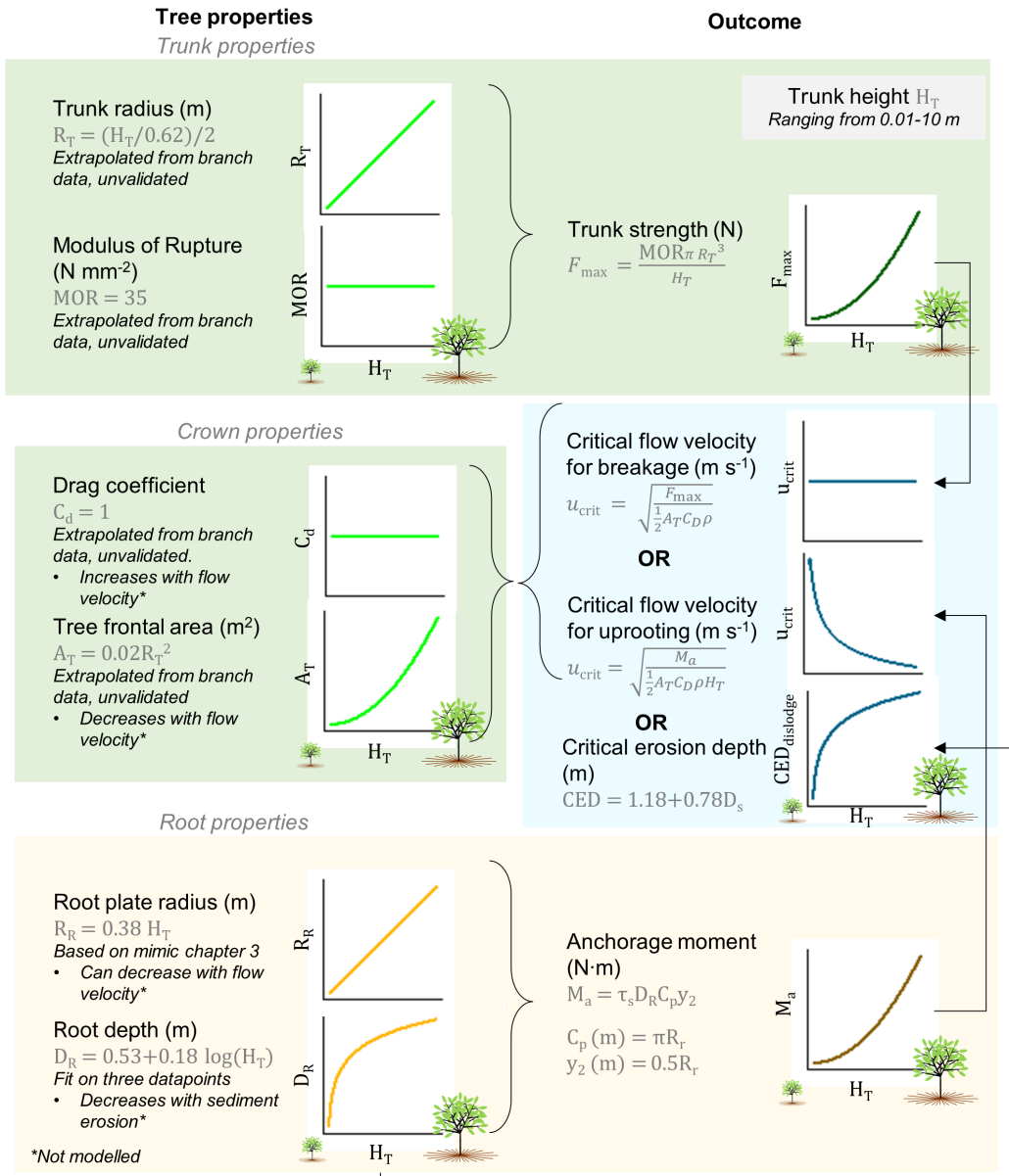


Figure 5.2: Summary of quantified relationships between tree properties and mechanical disturbances presented in this thesis. Seedlings are modelled as tiny trees. The critical flow velocity is that at which the first failure is reached (either breakage, uprooting, or dislodgement). See Table S5.1 for data sources.

5.2 Impact of mechanical disturbance differs between species

The impact of mechanical disturbance will differ between mangrove species. Firstly, there are morphology differences that can alter the impact of mechanical disturbance. For example, *Avicennia marina* branches have much higher drag coefficients than other species (Chapter 4), probably because they have a rather irregular branch architecture with leaves directly attached to relatively sturdy, inflexible branches. This difference is particularly striking when compared to *Sonneratia apetala* branches, which had lower drag forces and flexible terminal branches that allow for realignment in the water stream. In seedlings, the tall shoots of viviparous species likely provide them with high burial tolerance, which could be directly ascribed to the elongated shape of their propagules (Chapter 2). Hence, these morphological differences contribute directly to different impacts of mechanical disturbance. Secondly, mechanical damage is probably not equally deadly for all species. For example, the propagules of *Avicennia* spp. have multiple root primordia, allowing them to establish multiple times and potentially reducing the impact of seedling dislodgement (Farrant et al., 1987). Similarly, recovery studies after hurricanes have shown species differences in regeneration and changes in forest structure after storms (e.g. Baldwin et al., 2001; Kovacs et al., 2001). Indeed, for most species uprooting results in death, yet *Sonneratia* and *Avicennia* spp. can regrow shoots if some root connection remains (Saenger, 2002). On the other hand, *Rhizophora mangle* trees do not have epicormic leaf buds, reducing their ability to regrow leaves after defoliation (Gill & Tomlinson, 1969). Thirdly, the amount of mechanical damage depends highly on the intensity of the mechanical disturbance. At the exposed seaward forest fringe the flow velocity of wind and waves will be higher than deeper in the forest (Dalrymple et al., 1984). Hence, the typical tidal elevation of species (i.e. zonation; the spatial distribution of species across a forest) will affect its proneness to damage. In other words, species that generally occur lower in the intertidal zone (i.e. more seaward) will likely experience stronger mechanical disturbances than species that occur higher in the tidal frame. Thus, even if a more landward species is damaged more easily (e.g. due to a weak trunk), it effectively experiences less damage because the effective mechanical disturbance from for example a storm wave is lower. Finally, environmental factors, such as water availability, temperature, nutrient availability and salinity can significantly reduce growth rates (Chapter 1; Krauss et al., 2008), resulting in smaller or weaker plants that experience more damage from mechanical disturbance. This is particularly a risk for species with low tolerance to a particular stressor. For example, *Sonneratia apetala* seedlings have low salt tolerance and will fail to establish if salinity becomes too high (Hoque et al., 1999), as this impedes their growth rate

and inhibits their ability to grow long enough roots to avoid, for example, toppling or dislodgement (own data, unpublished).

5.3 Thigmomorphogenesis and the implications for restoration

Mangrove species can exhibit a growth response to mechanical disturbance. I observed stronger branches and weaker leaves in mangrove species occurring across an exposure gradient (**Chapter 4**) and the pioneer mangrove seedlings in the mesocosm experiment (**Chapter 2**) had longer root lengths in erosion treatments. These morphological and mechanical changes could potentially be ascribed to thigmomorphogenesis. Thigmomorphogenesis is defined as a response of plants in reaction to mechanical disturbance (Jaffe, 1973), whereby they reduce their height (i.e. reduced growth), increase their width (radial growth, trunk diameter), increase allocation from aboveground to belowground biomass, and alter their mechanical properties (Gardiner et al., 2016; Telewski, 2021). Not all plant species possess this response (Jaffe, 1973), and while such responses have not been studied in mangroves explicitly, it is highly likely that at least some of them possess it. For example, a study on mechanical properties of branches found that *A. marina* trees that grow lower in the intertidal zone (more exposed) develop relatively stronger branches (with a higher Modulus of Rupture) than trees higher in the intertidal zone (Santini et al., 2013). Furthermore, mangroves that grow in regions with more frequent storms have been correlated with shorter tree heights (Simard et al., 2019). Additionally, pioneer saltmarsh and mangrove seedlings have been found to shift biomass allocation from shoots to roots in response to wave disturbance (Balke et al., 2013; Cao et al., 2020). This provides a few important implications for mangrove restoration and nature-based flood defence. First, in the case of degraded ecosystems that have become exposed, pioneer species (that might have a stronger thigmomorphogenesis response) could be used to initially reduce exposure to wind and waves and provide more shelter before a mid or late-successional species is brought in. Second, nursery-raised seedlings may not be adapted enough to mechanical disturbances if the nursery environment is too calm. Third, thigmomorphogenesis may reduce wave attenuation capacity by inducing smaller plants. Hence, more research into the response of mangrove seedlings and saplings to currents, waves and sediment dynamics is needed to understand how mangroves adjust to a mechanically disturbed environment, and particularly which species differences exist.

5.4 The future of mangrove forests in nature-based flood defence

Ultimately, in trying to achieve optimal wave attenuation function, one should be careful to consider mangrove forest width and mangrove forest density as measurement tools rather than end goals. Mangrove forests are complex ecosystems that are affected by numerous physical (Chapter 1), biotic (Biswas et al., 2018; Pranchai

Synthesis

et al., 2022) and anthropogenic drivers (van Bijsterveldt et al., 2021, 2020). Hence, selecting the species with for example the highest drag coefficient or the best establishment success is not a guarantee for an optimal nature-based flood defence in the long run. In fact, using density and width as end goals could result in selecting a non-native and possibly invasive species, as has happened in a similar case with *Sonneratia apetala* in China (Xin et al., 2013). Alternatively, it could result in 'restoring' mangrove forests in areas where they do not naturally occur (i.e. habitat conversion, Erfteimeijer and Lewis III, 2000). While one could choose to do this, such activities can have detrimental effects on the natural functioning of the ecosystem and the surrounding estuary (Carugati et al., 2018; Su et al., 2021). Furthermore, it can potentially drive development towards the flood defence equivalent of agricultural systems or production forests – man-made systems that usually require a substantial amount of maintenance, which defeats the purpose of a self-sustaining nature-based flood defence. Hence, I recommend that the research presented in this thesis is used to understand natural mangrove ecosystem functioning, improve restoration principles, and protect these fascinating intertidal forests.

S5 Supporting information

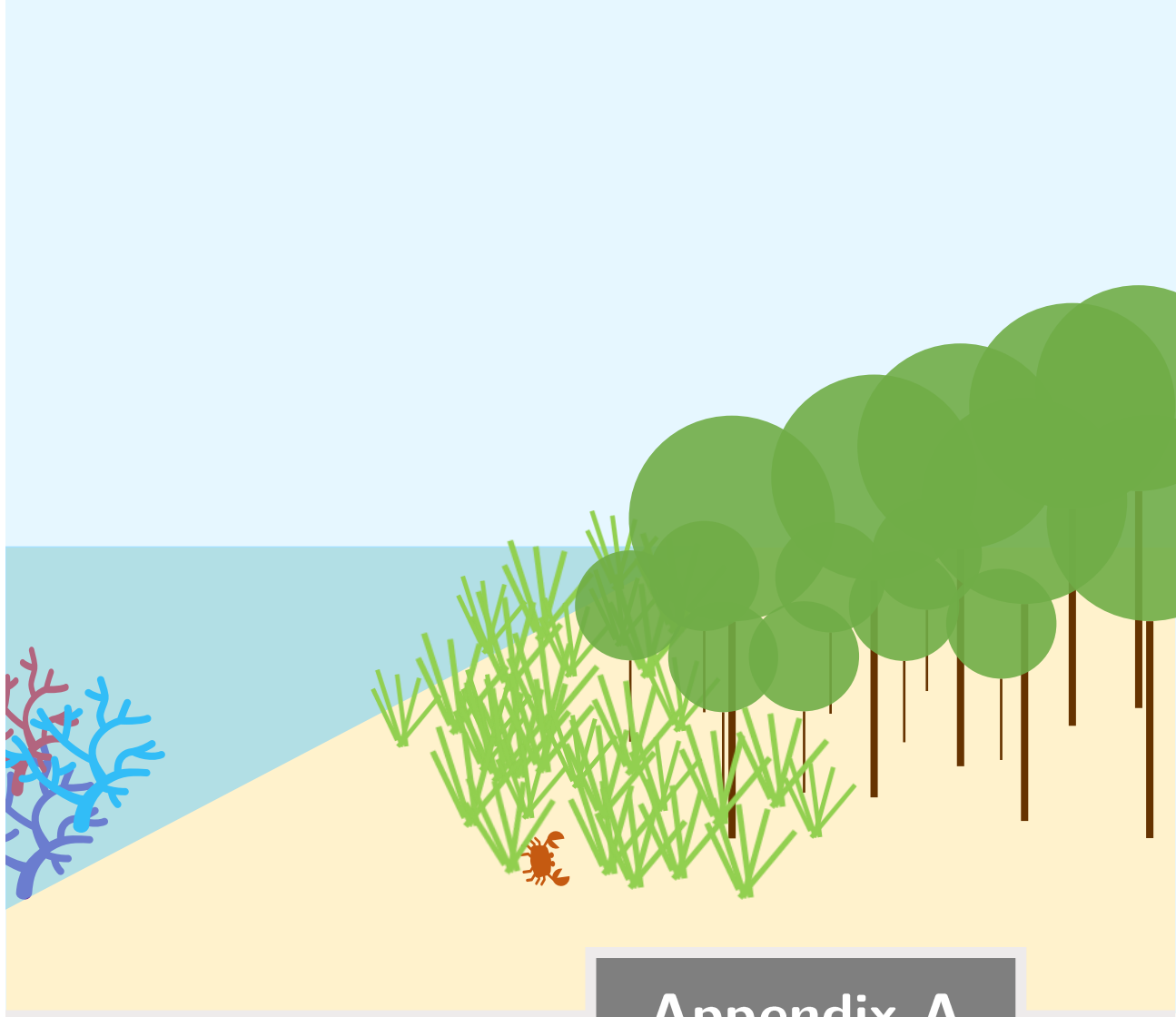
Table S5.1: Data sources for estimating damage for an idealised mangrove tree.

Parameter	Source
Trunk height H_T (m)	Range: 0.01-10 m
Trunk radius R_T (m)	Fit a model on the data from Figure S4.7, forced through the origin to avoid negative values
Modulus of Rupture (N mm ⁻²)	Figure 4.2d, averaged
Trunk strength F (N)	Gere and Goodno, 2012
Drag coefficient C_D	Figure 4.6b, averaged
Tree frontal area A_T m ²	Fit a model on the data from Figure S4.7c, forced through the origin to avoid negative values
Root plate radius (m)	Based on the data in Table 3.2: $4/10.5 = 0.38$
Root depth (m)	Fit a logarithmic model on three datapoints: seedling root depth ($H_T = 0.1$; $D_s = 0.1$; Figure 2.4), sapling root depth ($H_T = 0.6$; $D_s = 0.4$; Figure S5.1) and tree root depth ($H_T = 10$; $D_s = 1$; Table 3.2).
Anchorage moment M_a (N·m)	Equation 3.6; Achim and Nicoll, 2009
Critical flow velocity for breakage u_{crit} (m s ⁻¹)	Based on the drag force equation; Morison et al., 1950
Critical flow velocity for breakage u_{crit} (m s ⁻¹)	Based on the drag force equation; Morison et al., 1950
Critical erosion depth (m)	Figure 2.6a

Synthesis



Figure S5.1: Excavated 3-5 year old saplings in Hailing Island, south China (shoe size 36).



Appendix A

How can nature protect people against sea-level rise?

R. van Hespen, C.E.J. van Bijsterveldt, C.M.L. Camargo, M.M. Stoorvogel, T.J. Bouma

Frontiers for Young Minds (2023)

A | How can nature protect people against sea-level rise?

Abstract

Almost one third of people on Earth live near the coast where they are at risk from floods. Coastal areas are often protected from flooding by human-built flood-protection structures, like dikes and seawalls. Now that Earth's climate is changing, sea-level rise and storms are becoming more intense and frequent, which increases the risk of flooding. Therefore, we need to develop bigger flood defence structures to stay safe from flooding. However, this is very expensive. Is there an alternative? It may sound surprising, but nature can help us out. Around the world, ecosystems like mangrove forests, saltmarshes, and coral reefs can help to protect our coasts from flooding. They can contribute to greener, more natural, biodiverse coasts, and make living along Earth's coastlines safer and more sustainable. Using these natural systems is called nature-based flood defence. In this article, we explain how it works.

Why do we need to protect ourselves against sea-level rise?

The coast is a nice place to live. One third of the people on Earth live along the coast: in small fishing towns, in big cities like New York and Shanghai, or even in entire countries, like the Netherlands. Many of these places lie in areas called river deltas, where a river enters the sea. River deltas are great locations for harbours, agriculture, and fishing, but they are also low-lying areas that can easily flood. Half of the Netherlands, for example, is several meters below sea level and would be flooded today if the country's flood protection failed! Living at the coast is risky, and it's becoming riskier with climate change and its consequences, including sea-level change and more or stronger storms. As global temperature continues to rise, glaciers and ice sheets, like those in Antarctica and Greenland, are melting. The melted ice flows into the oceans, raising sea levels. At the same time, the oceans capture some of the heat from the atmosphere and, as the water gets warmer, it expands — so sea levels rise even more. But that is not all — some cities are literally sinking. One of the main reasons cities sink is because we pump water, gas, and oil from underground. The weight of buildings and houses then pushes the emptied soil downward. This effect is called land subsidence. In some cities, land subsidence makes the water level rise more than ten centimetres per year, making sea-level rise an even bigger threat! The effect of land subsidence and sea-level rise together is called relative sea-level rise (Figure A.1a; Nicholls et al., 2021), and it increases the flood risk to coastal areas. Beyond contributing to relative sea-level rise, climate change also causes more frequent and intense storms. Stronger storm winds can blow more water onto the coast, leading to even higher water levels than are seen with relative sea-level rise alone. Because of this, the waves that reach the coast are also higher. Why? Waves consist of an above-water part and an underwater part (Figure A.1b). Normally, when the underwater part of the wave hits the seafloor or a man-made barrier, it collapses and the whole wave breaks. You can see this at sandy beaches. However, when the water level is too high, waves do not break, so they stay large. Storms with such high waves can cause floods, damage buildings, and sometimes even take human lives. How can we protect ourselves against sea-level rise?

Is it time to update our flood defences?

Coastal cities are protected by concrete structures often called grey flood defences (Figure A.2a). These defences include dikes, seawalls, and breakwaters. A breakwater protects the coast from the force of the waves by forming an elevated barrier in the sea. The underwater parts of waves hit this barrier and lose some of their energy, kind of like stumbling over a curb when you run. Dikes or sea walls are barriers on the shore. They protect the land from flooding, especially when the water level is

Appendix A

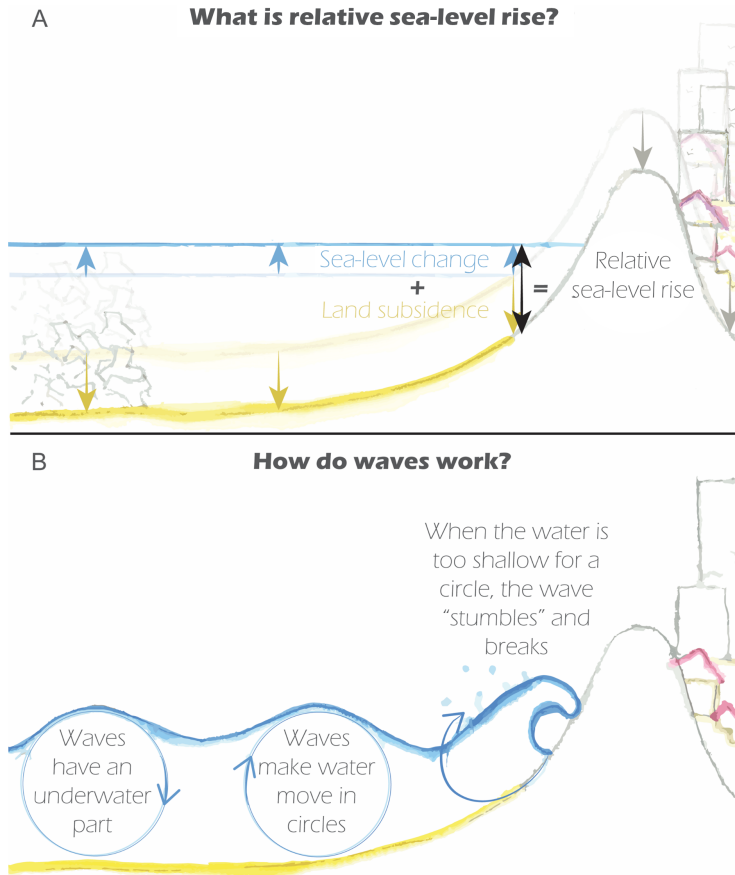


Figure A.1: (a) Relative sea-level rise is a combination of sinking land (land subsidence) and rising sea levels. (b) Waves have an above-water part and an underwater part. When the underwater part of a wave hits a barrier, it collapses and the wave breaks.

higher than normal, which happens during storms in combination with really high tides. Grey defence structures are built to survive heavy storms, but they are not so effective when sea levels rise. For example, breakwaters are less effective against sea-level rise because the underwater parts of waves do not hit the breakwater anymore. Instead, the waves have enough space to travel over the breakwater and break on the shore (Figure A.2a). Dikes and seawalls are also less effective — if relative sea level rises too much, the water level becomes higher than the barrier and the land behind it floods. Also, dikes and seawalls can be damaged by very strong waves and storms, which makes them less effective. Sinking lands, rising seas, and increasing storms mean that we need higher and stronger flood defences, but that will cost lots

of money. What if we could use living systems to help protect the coastline? This is called nature-based flood defence (Figure A.2b; Temmerman et al., 2013).

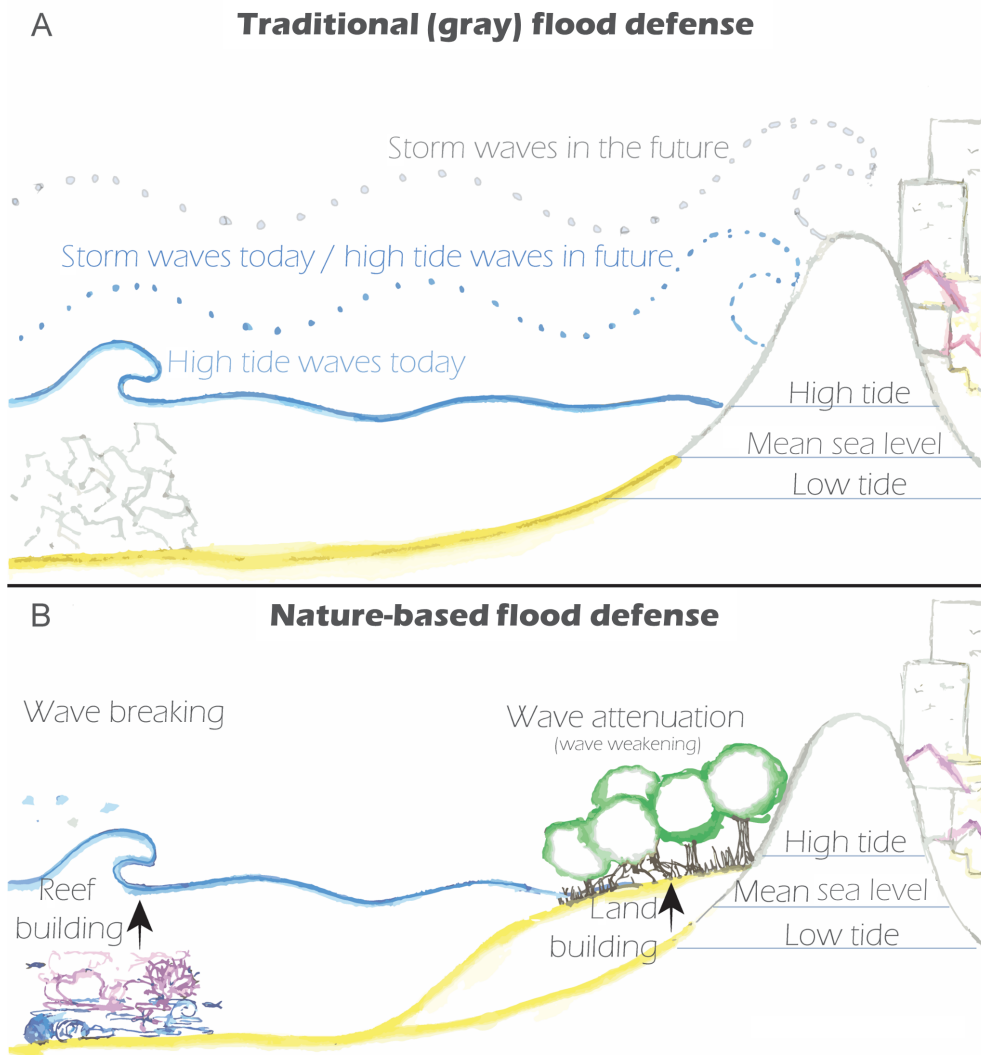


Figure A.2: (a) Traditional grey flood defences protect the land from waves and flooding, but relative sea-level rise makes grey flood defences less effective. (b) Nature-based flood defences use living ecosystems to help protect the coast. Specific plants and animals can be used depending on the geographical location (see Figure A.3).

How nature can protect us from relative sea-level rise

Coastal ecosystems around the world can be used for nature-based flood defence. These ecosystems are made up of plants such as mangrove trees and saltmarsh plants, and animals that build “breakwater-like” reefs including oysters, mussels,

and corals (Figure A.3). These plants and animals are adapted to living in salty seawater. Some can protect us from floods by slowing down waves, others do so by building land, and some can do both! Coral reefs are not just pretty; they are sturdy and grow close to the coast. Their locations are very similar to those of grey concrete breakwaters and they also work the same way — by forming an underwater elevated barrier that breaks waves (Figure A.2b). Oysters and mussels can build shellfish reefs that break waves much like corals do. Although reefs and grey breakwaters protect the coast in the same way, reefs can grow! By growing, reefs can keep up with sea-level rise and stay high enough to keep breaking waves, while breakwaters must be maintained. Mangroves and saltmarshes often grow outside dikes and seawalls. This is helpful, because they can reduce the size of the waves before they reach the grey flood defences. If a wave rolls into a mangrove forest (or saltmarsh), it runs into many obstacles. Every time the wave hits a plant, it weakens and loses a bit of its energy. By hitting all the plants in a marsh or forest, the wave loses so much energy that it becomes a lot smaller. We call this effect wave attenuation. If a mangrove forest or saltmarsh is large enough, it can reduce wave height a lot. This is so effective that we can build a smaller dike, saving a lot of money! Mangroves and saltmarshes can also raise the land on which they grow. Without plants, seawater can flow so fast that it can carry mud and sand particles. But when water flows through coastal plants, it slows down and the particles sink onto the soil. Over time, this makes the soil surface higher. This is very useful for keeping up with sea-level rise (Kirwan et al., 2010), and consequently the area is flooded less often. Since mangrove trees and saltmarshes like to grow in less flooded areas, they keep building land in those areas and the surface level keeps increasing. The elevated surface level can act like a breakwater, protecting the coast even more (Vuik et al., 2016).

More advantages of using coastal ecosystems

Besides providing nature-based flood defence, coastal ecosystems have more advantages. As we mentioned, their surface level can rise with the sea (Zhu et al., 2020). This makes them cheaper because they need less maintenance than grey flood defences do. These ecosystems can also store large amounts of carbon, which lowers the amount of carbon dioxide in the atmosphere. Lower carbon dioxide levels mean less climate change — so less sea-level rise. Finally, these ecosystems provide a nice area for rare plants and animals to live, which supports biodiversity. People can enjoy these coastal ecosystems, too! Unfortunately, coastal ecosystems have been declining over the last 50 years. Therefore, scientists are now learning how to protect and restore them. We can do this by studying the preferences of the plants and animals that live there. How often do they like to get flooded? Can they handle lots of

Appendix A

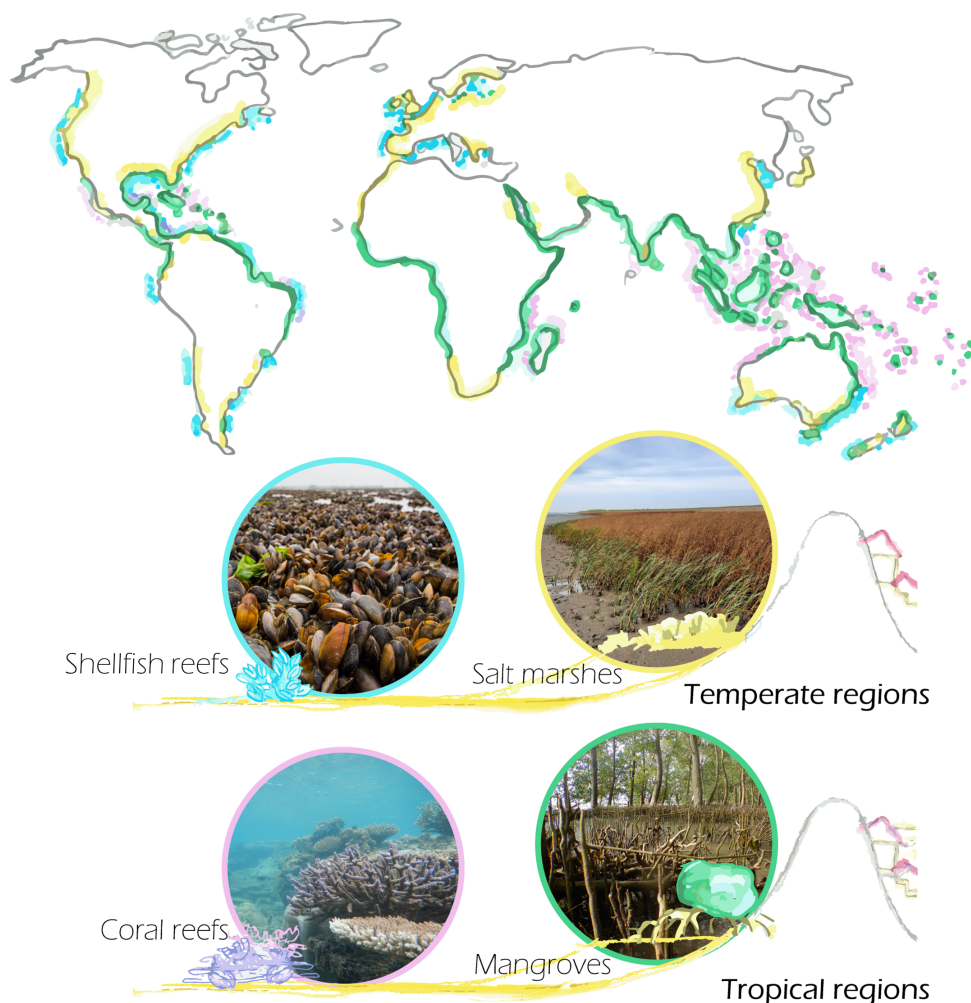


Figure A.3: Global distribution of coastal ecosystems that provide nature-based flood defences. The coloured circles around each picture correspond to the colours on the map. Saltmarshes and shellfish reefs are mostly found in temperate regions, while mangroves and coral reefs are found in the tropics. Photo credits: Jildou Schotanus (mussel reef), Marte Stoorvogel (saltmarsh), and Celine van Bijsterveldt (coral reef and mangrove).

waves? How salty should it be? The more we learn about these plants and animals, the better we can protect them — so they can protect us from floods!

In summary, maintaining grey flood defences will be very expensive with sea-level rise. Coastal ecosystems can also break waves and even build land to keep up with sea-level rise. In this way, they can help us protect our coasts from flooding all around the world. There are a few ways that YOU can help. First, if you are

Appendix A

interested in this topic, you can read more articles¹! You could consider giving a presentation at your school to teach others about nature-based flood defence. To learn even more, you could find and meet your local scientists, or meet them online². Finally, if you want to become a scientist yourself, learn as much as you can about biology, mathematics, and physics! Maybe someday you will help to discover new mechanisms of nature-based flood protection!

Glossary

Ecosystem: Plants and animals that form a distinct piece of nature. This can be the Amazon rain forest, the Great Barrier Reef, or your local forest.

River delta: A low-lying area where rivers empty into the sea. Famous examples are the Nile delta in the Mediterranean Sea and the Mississippi delta in the Gulf of Mexico.

Land subsidence: The sinking cities at the coast. It happens if we pump water, gas or oil from underground, and the weight of buildings and houses pushes the emptied soil downward.

Sea-level change: Sea-level is actually quite variable and can even fall in some places. It also does not rise all the time. But for coastal protection, sea-level rise is most relevant.

Relative sea-level rise: The combined effect of land subsidence and sea-level rise. It increases flood risk more than sea-level rise alone.

Grey flood defences: Concrete structures that protect the coast from flooding, such as dikes, seawalls, and breakwaters.

Nature-based flood defences: These flood defences use both concrete structures and coastal ecosystems such as saltmarshes or coral reefs to protect the coast from flooding.

Wave attenuation: Every time the wave hits a plant, it loses a bit of its energy. By hitting lots of plants, it loses so much energy that the wave becomes smaller.

¹Check out these Frontiers for Young Minds articles, on sea-level change, global ocean climate change, or seagrasses

²For example, Skype a Scientist or Letters to a Pre-Scientist

Summary | Samenvatting

Summary

Coastal flood risk will increase over the coming decades as sea level rise accelerates, storm patterns change and coastal populations grow. This will likely lead to a surge in costs to build and maintain reliable flood safety infrastructure. Hence, innovative nature-based solutions that use coastal ecosystems are gaining attention. Nature-based flood defence is a potentially sustainable and cost-effective solution to reduce coastal flood risk, that can be carried out with ecosystems such as mangrove forests, saltmarshes or coral reefs (**Appendix A**). Mangrove forests are increasingly studied for nature-based flood defence across the subtropical and tropical latitudes, as their sturdy vegetation can effectively attenuate flow energy from waves – surge attenuation with mangroves remains less well understood. Wider and denser forests provide more wave attenuation. As mangroves naturally fluctuate in size, so does their wave attenuation capacity. Consequently, to reliably estimate the safety of a mangrove-based flood defence, it is necessary to understand the long-term development of the mangrove forest (**Chapter 1**).

Mangrove forests grow wider when seedlings establish successfully and develop into healthy mature trees. Similarly, forests grow taller and denser if most trees survive and the ones that die are replaced. These ecological processes of establishment, growth and survival are governed by a myriad of environmental drivers that not only interact with each other, but also differ across species. These drivers are generally more physical in nature at the seaward edge (**Chapter 1**). For example, daily disturbances by tides, waves and sediment dynamics form bottlenecks to seedlings establishment. At larger timescales, mangrove forests can experience strong disturbances from coastal storms and other extreme events that potentially result in massive tree mortality. Hence, mechanical disturbances form important drivers of the establishment and survival of coastal mangrove trees.

During establishment at the seaward fringe, seedlings first need to anchor their small roots strong enough to avoid being washed away by currents and waves during high

Summary

tide. Then, the next obstacle is surviving daily sediment dynamics. Across species, there is variation in traits such as successional stage (pioneer, mid-successional or climax species), type of embryo development (non-viviparous, cryptoviviparous or viviparous) and propagule sizes (0.5 to 22.8 cm). **Chapter 2** studies the impact of sediment dynamics on eight species that diverge in these traits. The pioneer species studied have relatively smaller propagules, but increase their shoot length or root length in response to sediment accretion or erosion, respectively, potentially reducing the chance of burial, toppling or dislodgement. The viviparous climax species on the other hand have large propagules, such that they have a tall shoot immediately if they arrive vertically on the tidal flat. Furthermore, they can grow longer roots and can withstand more erosion.

When a mangrove tree matures, it can no longer be easily dislodged by sediment dynamics. Nevertheless, it remains at risk of uprooting during for example coastal storms, which can cause massive sediment erosion combined with high wind loading. **Chapter 3** tests the stability of 3D-printed, scaled mangrove mimics with five idealised root designs and shows that sediment shear strength is important for mechanical anchorage. Hence, waterlogged sediments, which often have lower shear strength, may provide less stability to mangrove trees, and sediment with high erodibility can increase the risk of uprooting as well. Furthermore, the optimal belowground root morphology of a mangrove mimic depends on the sediment it is rooted in. Hence, it is likely that mangrove trees adjust their belowground root mass distribution and root mechanical strength depending on the sediment type they are rooted in.

Aside from belowground damage, mangrove trees can also experience aboveground damage during coastal storms. This can include canopy damage, such as defoliation and branch breakage, or even breaking of the entire trunk. **Chapter 4** investigates the former two by studying the resistance to leaf and branch damage of five species across seven field sites in the Guangdong province of south China. Generally, thicker branches are stronger, reducing the risk of damage. However, they are also more rigid and have a larger surface area, increasing the risk of damage. Across mangrove species, we can see that species that generally occur at the more exposed seaward fringe have relatively stronger branches yet more easily detachable leaves than species that generally occur more landward.

Overall, the studies presented in this thesis contribute important datasets and mechanistic principles that can be used to advance mangrove forest development models and estimate long-term flood protection capacity with coastal mangroves (**Chapter 5**). Furthermore, mechanical disturbance impacts coastal mangrove trees at all stages

Summary

of life, but the damage will differ between species. The consequence of mechanical disturbance will depend on variations in morphology, the deadliness of damage, the species' typical location in the forest (exposure to mechanical disturbances) and tolerances to other environmental drivers. Furthermore, some mangrove species may exhibit a growth response to mechanical disturbance. If true, this has implications for mangrove restoration and nature-based flood defence: pioneers could be used initially to reduce exposure for mid- or late-successional species, nursery-raised seedlings may not experience enough mechanical disturbance to adapt to conditions in the field, and thigmomorphogenesis can reduce wave attenuation as trees may stay smaller.

Samenvatting

De komende decennia neemt het overstromingsgevaar toe als gevolg van een sneller stijgende zeespiegel, veranderende stormpatronen en groeiende populaties aan de kust. Dit heeft een toename in bouw- en onderhoudskosten van kustbeschermingsinfrastructuur tot gevolg, waardoor de interesse in innovatieve oplossingen zoals *'nature-based flood defence'* toeneemt. Kustbescherming op basis van natuur maakt gebruik van ecosystemen (bijvoorbeeld mangrovebossen, schorren of koraalriffen) om overstromingsrisico's verlagen en is mogelijk duurzaam en kostenbesparend (**Bijlage A**).

Mangrovebossen, die voorkomen in de tropen en subtropen, worden steeds meer bestudeerd voor kustbescherming omdat de stugge structuur van de bomen effectief golven kan dempen (over hun rol in het verlagen van stormvloed is nog minder bekend), waarbij bredere en dichtere bossen golven sterker kunnen dempen. De bossen fluctueren van nature in breedte, waardoor ook de golfdempingscapaciteit door de tijd heen varieert. Om mangroves op een betrouwbare manier in te zetten in kustbescherming, moeten we dus weten hoe ze zich op lange termijn ontwikkelen (**Hoofdstuk 1**).

Mangrovebossen groeien breder als zaailingen zich kunnen vestigen en ontwikkelen tot gezonde volwassen bomen. Tegelijkertijd kunnen mangrovebossen hoger en dichter groeien als de meeste bomen overleven, en de bomen die dood gaan worden vervangen. Deze ecologische processen van vestiging, groei en overleving worden gestuurd door een groot aantal omgevingsfactoren die niet alleen op elkaar inwerken, maar ook verschillen per soort. Aan de zeewaartse kant van het bos zijn deze factoren over het algemeen meer fysisch van aard. Dagelijkse verstoringen door getijden, golven en sedimentdynamiek knelpunten vormen voor de vestiging van zaailingen. Op grotere tijdschalen kunnen mangrovebossen verstoringen ondervinden van storm en andere extreme gebeurtenissen met massale boomsterfte tot gevolg (**Hoofdstuk 1**). Mechanische verstoringen hebben dus grote impact op de vestiging en overleving van mangrovebomen aan de kust.

Tijdens de vestiging moeten zaailingen worteltjes groeien die sterk genoeg zijn verankerd in de bodem dat ze tijdens hoogwater niet worden weggespoeld door golven en de getijdenstroom. Daarna is hun grootste uitdaging het overleven van sedimentdynamiek. Deze tolerantie voor sedimentdynamiek verschilt waarschijnlijk tussen soorten. **Hoofdstuk 2** onderzoekt tolerantieverschillen tussen acht soorten aan de hand van drie propagulekenmerken. De pioniersoorten in deze studie hebben relatief kleinere propagules, maar ontwikkelen langere scheuten of wortels in reactie op respectievelijk accretie of erosie van sediment. Hierdoor vermindert de kans dat

Summary

de zaailing raakt begraven onder sediment, of juist omvalt of volledig loskomt van de bodem en wegspoelt. De levendbarende climaxsoorten daarentegen hebben grote propagules die daardoor direct een lange scheut hebben, mits ze zich rechtop kunnen 'planten'. Daarnaast ontwikkelen ze lange wortels en zijn ze beter bestand tegen erosie. Hoewel de levendbarende middensuccessiesoorten minder stabiel zijn bij sedimenterosie, hebben ze veel zijwortels waardoor ze mogelijk, als ze wegspoelen, opnieuw kunnen proberen om zich te verankeren in de bodem.

Als een mangroveboom volgroeid is, kan hij niet meer zo gemakkelijk worden ontworteld. Toch blijft het risico op ontworteling wel bestaan, bijvoorbeeld tijdens een storm. Daarbij kan op grote schaal sediment wegspoelen terwijl tegelijkertijd sterke windstoten worden gegenereerd, wat voor mangrovebomen fataal kan zijn. **Hoofdstuk 3** onderzoekt hoe sedimenteigenschappen en ondergrondse wortelmorfologie de stabiliteit van mangrovebomen bepalen. Ik maak hier gebruik van 3D-geprinte, geschaalde modellen van mangrovebomen met vijf wortelsystemen. De studie toont aan dat de schuifsterkte van het sediment belangrijk is voor mechanische verankering. Daarom biedt ongedraineerd sediment, dat vaak een lagere schuifsterkte heeft, mogelijk minder stabiliteit aan mangrovebomen, en kan sediment met een hoge erodeerbaarheid ook het risico van ontworteling vergroten. Daarnaast hangt de optimale ondergrondse wortelmorfologie van een mangrove model af van het sediment waarin die wortelt. Het is dus waarschijnlijk dat mangrovebomen hun ondergrondse wortelmassaverdeling en mechanische wortelsterkte aanpassen aan het type sediment waarin ze wortelen.

Behalve ondergronds kunnen mangrovebomen tijdens kuststormen ook bovengronds schade oplopen. Dit kan schade aan het kruin zijn, zoals ontbladering en takbreuk, of zelfs het afbreken van de hele stam. **Hoofdstuk 4** onderzoekt de eerste twee, en kijkt naar de weerstand tegen blad- en takschade van vijf soorten op zeven veldlocaties in de provincie Guangdong in Zuid-China. Over het algemeen zijn dikkere takken sterker, waardoor de kans op schade afneemt. Ze zijn echter ook stijver en hebben een groter oppervlak, waardoor het risico op schade toeneemt. Soorten die over het algemeen voorkomen aan de zeewaartse kant van een bos, waar blootstelling aan mechanische verstoring hoger is, relatief sterkere takken hebben maar blaadjes die makkelijker loslatende dan soorten die over het algemeen meer landwaarts voorkomen.

De studies in dit proefschrift bevatten belangrijke data en mechanistische principes, die helpen bij het voorspellen van mangrovebossen en hun kustbeschermingscapaciteit op lange termijn (**Hoofdstuk 5**). Mechanische verstoring heeft gevolgen voor mangrovebomen aan de kust in alle levensfasen, maar de schade zal verschillen naar

Summary

gelang de boomsoort. Dit hangt af van verschillen in morfologie, dodelijkheid van de schade, de locatie van de soort in het bos (zeewaarts is er meer mechanische verstoring dan landwaarts) en de tolerantie voor andere milieufactoren. Daarnaast vertonen mangrovesoorten waarschijnlijk een veranderde groei als gevolg van mechanische verstoring. Dit heeft mogelijk gevolgen voor mangroveherstel en natuurbescherming: pioniersoorten kunnen aanvankelijk worden ingezet om de mechanische verstoring voor middensuccessie- of climaxsoorten te verminderen, zaailingen uit kwekerijen ervaren misschien niet genoeg mechanische verstoring om zich aan te passen aan de omstandigheden in het veld, en thigmomorfogenese kan de golfdemping verminderen omdat bomen mogelijk kleiner blijven.

Acknowledgements

Researching and writing this thesis wouldn't have been possible without the advice, support, and much needed distractions of many, many wonderful people. Thank you all so much. A special thanks to:

Tjeerd Bouma, for teaching me how to see the bigger picture and giving me the freedom and trust to carry out this research. For believing in me when I was convinced that I couldn't pull off Chapter 1, and for finding a positive twist on every situation. Working with you has been truly inspiring.

Zhan Hu, for sharing your substantial knowledge on coastal dynamics and being the backbone of my Chinese research endeavours. You tirelessly worked to help me get visas, visit numerous field sites, and build an outdoor mesocosm lab from the ground up. Your ambition and support have been invaluable.

Tom Ysebaert, for bringing a balanced and realistic perspective to my research plans and the oyster reef expertise that you brought to our Chinese field visits.

Maarten Kleinhans, for your collaboration and for teaching me so much about sediment during our inspiring and energising meetings.

Bas Borsje, for your thoughtful comments and contributions. They made me a better researcher and always left me feeling supported.

Celine van Bijsterveldt, for sharing your mangrove expertise and teaching me how to jump a pole into the mud, a technique I never thought I'd need. Although we never got to visit the mangroves together, I had a lot of fun building our own version in the Westerschelde. Thank you for your friendship and collaboration.

Michela De Dominicis, Svetlana Jevrejeva, Judith Wolf, Ming Li and Peng Zheng for teaching me a thing or two about large scale modelling and our enjoyable meetings in China, at NIOZ, and in the UK, Yisheng Peng for teaching me about Chinese

Acknowledgements

mangrove species, Jim van Belzen for teaching me some complex statistical analyses, and many other collaborators for taking the time to share their expertise with me.

The NIOZ staff for supporting me, including Jeroen van Dalen, Daniël Blok, and especially Lennart van IJzerloo, for helping me with SED-sensors, field work, ordering obscure items and thinking through experimental setups with me and Joke van Houte, Christine de Zeeuw, Elly van Hulsteijn, and Jan Megens for supporting me with loads of practical questions and always making me feel welcome.

Juangling Zhou, Hong Wang, Simei Lian and Nanyang Chu for making sure I got to all my visa and immigration appointments without getting lost in Zhuhai, for joining me on field and lab work, and taking me out for delicious Chinese meals (I still miss the food!), and Tianping Xu, who helped me get some particularly hard to come by data on mangrove roots.

The students who worked with me, Sebastiaan van Dongen, Yihui Wang, Yuxin Yin, Xinyu Zhang, Xionghui Zhang, Junwen Ruan, Jieming He, Weijie Pan, Olivier Raven, Constance de Vos, Zongyi Wang, and Amy Taylor. Thank you for trusting me and for all the contributions you made to this research. It was a pleasure working with and learning from you.

My friends, family, writing buddies, football team mates, fellow bouldering enthusiasts, sailing crew mates, coffee buddies, and Keete housemates for your kindness, support and loads of fun! Thank you Felix and Anna, for inviting me on your many boat-related adventures, Anna-Carolina for our sporadic but always fun chats and visits, Lauren for our Friday evening cocktail brewing ventures, Greg for always making sure I get my workout in, and, together with Puck, getting me hooked on bouldering, Jette for our many coffee breaks, Roeland for our hilarious Dungleish-speaking nights at the Keete, Tim for being my reliable officemate for many years, Jaco for your advice on sediment and PhD-ing, Carolina for your supportive conversations and hosting so many nice gatherings, Christiaan for always being up for a chat, Chiu for our thoughtful conversations, Justin and Lexie for your sharing your entertaining travel stories, Tim for inviting me on some much welcomed fieldwork in the middle of a long and covidy winter, Dunia for our delicious dinners, Marte for our cheerful lunch breaks in an empty NIOZ, Tori for lots of bouldering fun, and so many other wonderful people and occasions - I'm grateful for all that you did for me.

Jana, for always being there for me when I need someone to talk to. Thank you for our many catch ups over video, coffee, lunches and dinners, and all the good times,

Acknowledgements

even when we were too lazy to leave the house. It's so much fun and I felt super supported. Thank you for being an amazing friend, housemate, and paranymp.

Pim, for your enthusiasm and humour, they always cheer me up. Thank you for our many entertaining evenings discussing life and code over beers, and also to Thyrsa, for your delightful and supportive presence at all our family gatherings over the past five years. Thanks Pim, for always getting me and wholeheartedly being on my side, and thank you for being an awesome brother and paranymp.

My parents, for being the best cheerleaders I could have possibly wished for. Thank you for all your advice, and for listening to what I'm sure must have been countless hours of rants about my excitements and frustrations. Pappa, thank you for sharing your unique insights in research life, and for inspiring me to do a PhD so many years ago. Our many phone calls got me through the hardest and loneliest time of my PhD - thank you for letting me lean on you. It means the world to me. Mamma, thank you for all your love and support and for teaching me to be brave. Thank you for reminding me to keep my feet on the ground, and for our many cosy Sunday morning coffees, chatting and watching the squirrels and birds in the garden.

Mo, for your unwavering support through food and love. Man, am I lucky that I met you! Thank you for listening to my often vague ramblings about mangrove roots and mechanical stability, and for saving me a lot of time with some tricky calculations. Thank you for also reminding me (sometimes daily) to do one thing at a time. I've had so much fun with you finding creative ways to travel during covid and going on spontaneous road trips in the middle of winter. Our many attempts to find delicious food and beautiful hikes have been amazing breaks from all that writing.

شُكْرًا لِكُلِّ شَيْءٍ فَعَلْتُهُ مِنْ أَجْلِي، حَبِيبِي مُحَمَّدٌ.

Rollo, for being the most fluffy, adorable, and annoying little creature. Your demands for head rubs and playtime were a wonderful distraction during that hazy thesis write-up year. You can't read this, so I'll make sure to give you some extra delicious treats.

Finally, I want to thank the mangrove forests that I visited. This research would simply have been impossible without them, supplying hundreds of branches, leaves, and propagules. While this research focuses on the flood defence they offer to humans, I find these ecosystems magical in and of itself and walking among these crazy trees inspired me deeply. I hope I can visit them again one day!



Curriculum Vitae



Rosanna van Hespen was born in Enschede, the Netherlands, on Friday the 13th, March 1992. She joined the local girl's carpenter club at age 8, which would prove helpful in building the experimental setups presented in this thesis. In 2009, she started her bachelor's degree at Utrecht University to become a biologist and write a thesis on peatland degradation. She completed her degree in 2013 with an exchange semester at Griffith University, Gold Coast, Australia, and decided to stick around for a master's. She conducted this degree at the University of Melbourne, Australia, as a member of the Quantitative and Applied Ecology research group from 2014 to 2015. There, she simulated invasive fox populations to design a camera trap monitoring program to measure changes in fox population size. In 2016 she returned to the Netherlands. After a brief stint as a consultant for insurance software, she decided to return to ecological research and started her PhD in 2018. She worked at the NIOZ Royal Netherlands Institute for Sea Research at the Department of Estuarine and Delta systems and spent most of 2019 as a guest researcher at the Sun Yat-sen University in Zhuhai, China. Upon submitting this thesis, she took a four-month intensive course on science journalism, and she is currently setting up a business as an academic writing coach.

List of Publications

R. van Hespén, Z. Hu, B.W. Borsje, M. De Dominicis, D.A. Friess, S. Jevrejava, M.G. Kleinhans, M. Maza, C.E.J. van Bijsterveldt, T. Van der Stocken, B. van Wesenbeeck, D. Xie & T.J. Bouma (In Press) *Mangrove forests as a nature-based solution for coastal flood protection: Biophysical and ecological considerations*, Water Science and Engineering.

T. Xu, Z. Hu, W. Gong, P.W.J.M. Willemsen, B.W. Borsje, **R. van Hespén** & T.J. Bouma (In Press) *A comparison and coupling of two novel sensors for intertidal bed-level dynamics observation*, Limnology and Oceanography: Methods.

R. van Hespén, C.E.J. van Bijsterveldt, C.M.L. Camargo, M.M. Stoorvogel & T.J. Bouma (2023) *How can nature protect people against sea-level rise?*, Frontiers for Young Minds 11:910803.

M. De Dominicis, J. Wolf, **R. van Hespén**, P. Zheng & Z. Hu (2023) *Mangrove forests can be an effective coastal defence in the Pearl River Delta, China*, Communications Earth & Environment 4(1):13.

R. van Hespén, Z. Hu, Y. Peng, Z. Zhu, T. Ysebaert & T.J. Bouma (2022) *Identifying trait-based tolerance to sediment dynamics during seedling establishment across eight mangrove species*, Limnology and Oceanography 67(10):2281-2295.

R. van Hespén, Z. Hu, Y. Peng, B.W. Borsje, M.G. Kleinhans, T. Ysebaert & T.J. Bouma (2021) *Analysis of coastal storm damage resistance in successional mangrove species*, Limnology and Oceanography 66(8):3221-3236.

C.E. Hauser, D. Southwell, J.J. Lahoz-Monfort, L. Rumpff, J. Benshemesh, T. Burnard, **R. van Hespén**, J. Wright, B. Wintle & M. Bode (2019) *Adaptive management informs conservation and monitoring of Australia's threatened malleefowl*, Biological Conservation 233:31-40.

R. van Hespén, C.E. Hauser, J. Benshemesh, L. Rumpff & J.J. Lahoz-Monfort (2019) *Designing a camera trap monitoring program to measure efficacy of invasive predator management*, Wildlife Research 46(2):154-164.

References

- Achim, A., & Nicoll, B. C. (2009). Modelling the anchorage of shallow-rooted trees. *Forestry*, 82(3), 273–284. <https://doi.org/10.1093/forestry/cpp004>
- Albayrak, I., Nikora, V., Miler, O., & O'Hare, M. T. (2014). Flow–plant interactions at leaf, stem and shoot scales: Drag, turbulence, and biomechanics. *Aquatic Sciences*, 76(2), 269–294. <https://doi.org/10.1007/s00027-013-0335-2>
- Alleman, L. K., & Hester, M. W. (2011). Reproductive ecology of black mangrove (*avicennia germinans*) along the louisiana coast: Propagule production cycles, dispersal limitations, and establishment elevations. *Estuaries and Coasts*, 34(5), 1068. <https://doi.org/10.1007/s12237-011-9404-8>
- Alongi, D. M. (2008). Mangrove forests: Resilience, protection from tsunamis, and responses to global climate change. *Estuarine, Coastal and Shelf Science*, 76(1), 1–13. <https://doi.org/10.1016/j.ecss.2007.08.024>
- Alongi, D. M. (2015). The impact of climate change on mangrove forests. *Current Climate Change Reports*, 1(1), 30–39. <https://doi.org/10.1007/s40641-015-0002-x>
- Asbridge, E., Bartolo, R., Finlayson, C., Lucas, R., Rogers, K., & Woodroffe, C. (2019). Assessing the distribution and drivers of mangrove dieback in kakadu national park, northern australia. *Estuarine, Coastal and Shelf Science*, 228, 106353. <https://doi.org/10.1016/j.ecss.2019.106353>
- Asbridge, E., Lucas, R., Accad, A., & Dowling, R. (2015). Mangrove response to environmental changes predicted under varying climates: Case studies from australia. *Current Forestry Reports*, 1(3), 178–194. <https://doi.org/10.1007/s40725-015-0018-4>
- Asbridge, E., Lucas, R., Rogers, K., & Accad, A. (2018). The extent of mangrove change and potential for recovery following severe tropical cyclone yasi, hinchinbrook island, queensland, australia. *Ecology and Evolution*, 8(21), 10416–10434. <https://doi.org/10.1002/ece3.4485>
- Aung, T. T., Mochida, Y., & Than, M. M. (2013). Prediction of recovery pathways of cyclone-disturbed mangroves in the mega delta of myanmar. *Forest Ecology*

References

- and Management*, 293, 103–113. <https://doi.org/https://doi.org/10.1016/j.foreco.2012.12.034>
- Azman, M. S., Sharma, S., Shaharudin, M. A. M., Hamzah, M. L., Adibah, S. N., Zakaria, R. M., & MacKenzie, R. A. (2021). Stand structure, biomass and dynamics of naturally regenerated and restored mangroves in malaysia. *Forest Ecology and Management*, 482, 118852. <https://doi.org/10.1016/j.foreco.2020.118852>
- Baldwin, A., Egnotovich, M., Ford, M., & Platt, W. (2001). Regeneration in fringe mangrove forests damaged by hurricane andrew. *Plant Ecology*, 157(2), 151–164.
- Baldwin, A. H., Platt, W. J., Lessmann, J. M., & Rauch, T. J. (1995). Hurricane damage and regeneration in fringe mangrove forests of southeast florida, USA. *Journal of Coastal Research*, (21), 16.
- Balke, T., Bouma, T., Horstman, E., Webb, E., Erfteimeijer, P., & Herman, P. (2011). Windows of opportunity: Thresholds to mangrove seedling establishment on tidal flats. *Marine Ecology Progress Series*, 440, 1–9. <https://doi.org/10.3354/meps09364>
- Balke, T., Swales, A., Lovelock, C. E., Herman, P. M., & Bouma, T. J. (2015). Limits to seaward expansion of mangroves: Translating physical disturbance mechanisms into seedling survival gradients. *Journal of Experimental Marine Biology and Ecology*, 467, 16–25. <https://doi.org/10.1016/j.jembe.2015.02.015>
- Balke, T., Webb, E. L., van den Elzen, E., Galli, D., Herman, P. M. J., & Bouma, T. J. (2013). Seedling establishment in a dynamic sedimentary environment: A conceptual framework using mangroves (C. Frid, Ed.). *Journal of Applied Ecology*, 50(3), 740–747. <https://doi.org/10.1111/1365-2664.12067>
- Ball, M. C., & Pidsley, S. M. (1988). Establishment of mangrove seedlings in relation to salinity. *Proceedings of a workshop on research and management held in Darwin.*, 123–134.
- Banerjee, K., Bal, G., & Mitra, A. (2018). How soil texture affects the organic carbon load in the mangrove ecosystem? a case study from bhitarkanika, odisha. In *Environmental pollution* (pp. 329–341). Springer.
- Bao, T. Q. (2011). Effect of mangrove forest structures on wave attenuation in coastal vietnam. *Oceanologia*, 53(3), 807–818.
- Baptist, M. J., Gerkema, T., van Prooijen, B. C., van Maren, D. S., van Regteren, M., Schulz, K., Colosimo, I., Vroom, J., van Kessel, T., Grasmeijer, B., Willemsen, P., Elschot, K., de Groot, A. V., Cleveringa, J., van Eekelen, E. M. M., Schuurman, F., de Lange, H. J., & van Puijenbroek, M. E. B. (2019). Beneficial use of dredged sediment to enhance salt marsh development by applying a ‘mud

References

- motor'. *Ecological Engineering*, 127, 312–323. <https://doi.org/10.1016/j.ecoleng.2018.11.019>
- Barbier, E. B., Koch, E. W., Silliman, B. R., Hacker, S. D., Wolanski, E., Primavera, J., Granek, E. F., Polasky, S., Aswani, S., Cramer, L. A., Stoms, D. M., Kennedy, C. J., Bael, D., Kappel, C. V., Perillo, G. M. E., & Reed, D. J. (2008). Coastal ecosystem-based management with nonlinear ecological functions and values. *Science*, 319(5861), 321–323. <https://doi.org/10.1126/science.1150349>
- Bates, D., Mächler, M., Bolker, B., & Walker, S. (2014). Fitting linear mixed-effects models using lme4. *arXiv preprint arXiv:1406.5823*.
- Berger, U., Rivera-Monroy, V. H., Doyle, T. W., Dahdouh-Guebas, F., Duke, N. C., Fontalvo-Herazo, M. L., Hildenbrandt, H., Koedam, N., Mehlig, U., Piou, C., & Twilley, R. R. (2008). Advances and limitations of individual-based models to analyze and predict dynamics of mangrove forests: A review. *Aquatic Botany*, 89(2), 260–274. <https://doi.org/10.1016/j.aquabot.2007.12.015>
- Bhargava, R., & Friess, D. A. (2022). Previous shoreline dynamics determine future susceptibility to cyclone impact in the sundarban mangrove forest. *Frontiers in Marine Science*, 9. <https://doi.org/10.3389/fmars.2022.814577>
- Biswas, S. R., Biswas, P. L., Limon, S. H., Yan, E.-R., Xu, M.-S., & Khan, M. S. I. (2018). Plant invasion in mangrove forests worldwide. *Forest Ecology and Management*, 429, 480–492. <https://doi.org/10.1016/j.foreco.2018.07.046>
- Bland, J. M., & Altman, D. G. (1998). Survival probabilities (the kaplan-meier method). *BMJ (Clinical research ed.)*, 317(7172), 1572. <https://doi.org/10.1136/bmj.317.7172.1572>
- Bland, J. M., & Altman, D. G. (2004). The logrank test [Publisher: British Medical Journal Publishing Group]. *Bmj*, 328(7447), 1073.
- Boland, J. M., & Woodward, D. L. (2019). Impacts of the invasive shot hole borer (*Euwallacea kuroshio*) are linked to sewage pollution in southern california: The enriched tree hypothesis. *PeerJ*, 7, e6812. <https://doi.org/10.7717/peerj.6812>
- Borsje, B. W., van Wesenbeeck, B. K., Dekker, F., Paalvast, P., Bouma, T. J., van Katwijk, M. M., & de Vries, M. B. (2011). How ecological engineering can serve in coastal protection. *Ecological Engineering*, 37(2), 113–122. <https://doi.org/10.1016/j.ecoleng.2010.11.027>
- Bouma, T. J., De Vries, M. B., Low, E., Peralta, G., Tánčzos, I. C., van de Koppel, J., & Herman, P. M. J. (2005). Trade-offs related to ecosystem engineering: A case study on stiffness of emerging macrophytes. *Ecology*, 86(8), 2187–2199. <https://doi.org/10.1890/04-1588>

References

- Bouma, T. J., van Belzen, J., Balke, T., Zhu, Z., Airoidi, L., Blight, A. J., Davies, A. J., Galvan, C., Hawkins, S. J., Hoggart, S. P., Lara, J. L., Losada, I. J., Maza, M., Ondiviela, B., Skov, M. W., Strain, E. M., Thompson, R. C., Yang, S., Zanuttigh, B., ... Herman, P. M. (2014). Identifying knowledge gaps hampering application of intertidal habitats in coastal protection: Opportunities & steps to take. *Coastal Engineering*, *87*, 147–157. <https://doi.org/10.1016/j.coastaleng.2013.11.014>
- Bryan-Brown, D. N., Connolly, R. M., Richards, D. R., Adame, F., Friess, D. A., & Brown, C. J. (2020). Global trends in mangrove forest fragmentation. *Scientific Reports*, *10*(1), 7117. <https://doi.org/10.1038/s41598-020-63880-1>
- Bulmer, R. H., Lundquist, C., & Schwendenmann, L. (2015). Sediment properties and CO₂ efflux from intact and cleared temperate mangrove forests. *Biogeosciences*, *12*(20), 6169–6180.
- Butler, D. W., Gleason, S. M., Davidson, I., Onoda, Y., & Westoby, M. (2012). Safety and streamlining of woody shoots in wind: An empirical study across 39 species in tropical Australia. *New Phytologist*, *193*(1), 137–149. <https://doi.org/10.1111/j.1469-8137.2011.03887.x>
- Cao, H., Feng, W., Hu, Z., Suzuki, T., & Stive, M. J. F. (2015). Numerical modeling of vegetation-induced dissipation using an extended mild-slope equation. *Ocean Engineering*, *110*, 258–269. <https://doi.org/https://doi.org/10.1016/j.oceaneng.2015.09.057>
- Cao, H., Zhu, Z., Balke, T., Zhang, L., & Bouma, T. J. (2018). Effects of sediment disturbance regimes on *Spartina* seedling establishment: Implications for salt marsh creation and restoration: Sediment dynamics affect seedling establishment. *Limnology and Oceanography*, *63*(2), 647–659. <https://doi.org/10.1002/lno.10657>
- Cao, H., Zhu, Z., James, R., Herman, P. M. J., Zhang, L., Yuan, L., & Bouma, T. J. (2020). Wave effects on seedling establishment of three pioneer marsh species: Survival, morphology and biomechanics. *Annals of Botany*, *125*(2), 345–352. <https://doi.org/10.1093/aob/mcz136>
- Carugati, L., Gatto, B., Rastelli, E., Lo Martire, M., Coral, C., Greco, S., & Danovaro, R. (2018). Impact of mangrove forests degradation on biodiversity and ecosystem functioning. *Scientific reports*, *8*(1), 1–11.
- Castañeda-Moya, E., Twilley, R. R., Rivera-Monroy, V. H., Marx, B. D., Coronado-Molina, C., & Ewe, S. M. L. (2011). Patterns of root dynamics in mangrove forests along environmental gradients in the Florida coastal everglades, USA. *Ecosystems*, *14*(7), 1178–1195. <https://doi.org/10.1007/s10021-011-9473-3>

References

- Chave, J., Coomes, D., Jansen, S., Lewis, S. L., Swenson, N. G., & Zanne, A. E. (2009). Towards a worldwide wood economics spectrum. *Ecology Letters*, 12(4), 351–366. <https://doi.org/10.1111/j.1461-0248.2009.01285.x>
- Chen, H., Ni, Y., Li, Y., Liu, F., Ou, S., Su, M., Peng, Y., Hu, Z., Uijttewaal, W., & Suzuki, T. (2018). Deriving vegetation drag coefficients in combined wave-current flows by calibration and direct measurement methods. *Advances in Water Resources*, 122, 217–227. <https://doi.org/10.1016/j.advwatres.2018.10.008>
- Chen, Q., Li, J., Zhang, L., Lu, H., Ren, H., & Jian, S. (2015). Changes in the macrobenthic faunal community during succession of a mangrove forest at zhanjiang, south china. *Journal of Coastal Research*, 300, 315–325. <https://doi.org/10.2112/JCOASTRES-D-13-00019.1>
- Chen, Q., Li, J., Zhao, Q., Jian, S., & Ren, H. (2018). Changes in the benthic protozoan community during succession of a mangrove ecosystem in zhanjiang, china. *Ecosphere*, 9(4). <https://doi.org/10.1002/ecs2.2190>
- CIRIA, Ministere de l'Ecologie, d. D. d. e. d. l., & of Engineers, U. A. C. (2013). *The international levee handbook* [OCLC: 882967920].
- Clarke, P. J. (1992). Predispersal mortality and fecundity in the grey mangrove (avicennia marina) in southeastern australia. *Australian Journal of Ecology*, 17(2), 161–168. <https://doi.org/10.1111/j.1442-9993.1992.tb00794.x>
- Clarke, P. J. (1995). The population dynamics of the mangrove avicennia marina; demographic synthesis and predictive modelling. *Hydrobiologia*, 295(1), 83–88. <https://doi.org/10.1007/BF00029114>
- Clough, B. F., Dixon, P., & Dalhaus, O. (1997). Allometric relationships for estimating biomass in multi-stemmed mangrove trees [Publisher: CSIRO PUBLISHING]. *Australian Journal of Botany*, 45(6), 1023–1031. <https://doi.org/10.1071/bt96075>
- Coutts, M. P. (1983). Root architecture and tree stability. *Plant and Soil*, 71, 171–188.
- Coutts, M. P. (1986). Components of tree stability in sitka spruce on peaty gley soil. *Forestry*, 59(2), 173–197. <https://doi.org/10.1093/forestry/59.2.173>
- Crase, B., Liedloff, A., Vesk, P. A., Burgman, M. A., & Wintle, B. A. (2013). Hydroperiod is the main driver of the spatial pattern of dominance in mangrove communities [eprint: <https://onlinelibrary.wiley.com/doi/pdf/10.1111/geb.12063>]. *Global Ecology and Biogeography*, 22(7), 806–817. <https://doi.org/10.1111/geb.12063>
- Dalrymple, R. A., Kirby, J. T., & Hwang, P. A. (1984). Wave diffraction due to areas of energy dissipation [Publisher: American Society of Civil Engineers]. *Journal of waterway, port, coastal, and ocean engineering*, 110(1), 67–79.

References

- Dasgupta, S., Islam, M. S., Huq, M., Huque Khan, Z., & Hasib, M. R. (2019). Quantifying the protective capacity of mangroves from storm surges in coastal bangladesh (I. A. Kimirei, Ed.). *PLOS ONE*, *14*(3), e0214079. <https://doi.org/10.1371/journal.pone.0214079>
- De Dominicis, M., Wolf, J., van Hespén, R., Zheng, P., & Hu, Z. (In Review). Effectiveness of mangroves as nature-based coastal defences in the pearl river delta.
- De Dominicis, M., Wolf, J., Jevrejeva, S., Zheng, P., & Hu, Z. (2020). Future interactions between sea level rise, tides, and storm surges in the world's largest urban area. *Geophysical Research Letters*, *47*(4). <https://doi.org/10.1029/2020GL087002>
- Debrot, A. O., Plas, A., Boesono, H., Prihantoko, K., Baptist, M. J., Murk, A. J., & Tonneijck, F. H. (2022). Early increases in artisanal shore-based fisheries in a nature-based solutions mangrove rehabilitation project on the north coast of java. *Estuarine, Coastal and Shelf Science*, *267*, 107761. <https://doi.org/10.1016/j.ecss.2022.107761>
- Del Valle, A., Eriksson, M., Ishizawa Escudero, O. A., & Miranda, J. J. (2019). Mangroves for coastal protection: Evidence from hurricanes in central america. *World Bank Policy Research Working Paper*, (8795).
- Denny, M., & Gaylord, B. (2002). The mechanics of wave-swept algae, 8.
- de Smit, J. C., Kleinhans, M. G., Gerkema, T., Timmermans, K. R., & Bouma, T. J. (2020). Introducing the TiDyWAVE field flume: A method to quantify natural ecosystem resilience against future storm waves. *Limnology and Oceanography: Methods*, *18*(10), 585–598. <https://doi.org/10.1002/lom3.10386>
- Dewiyanti, I., Darmawi, D., Muchlisin, Z., Helmi, T., Imelda, I., & Defira, C. (2021). Physical and chemical characteristics of soil in mangrove ecosystem based on differences habitat in banda aceh and aceh besar. *IOP Conference Series: Earth and Environmental Science*, *674*(1), 012092.
- Duan, J., Han, J., Zhou, H., Lau, Y. L., An, W., Wei, P., Cheung, S. G., Yang, Y., & Tam, N. F.-y. (2020). Development of a digestion method for determining microplastic pollution in vegetal-rich clayey mangrove sediments. *Science of the Total Environment*, *707*, 136030.
- Duke, N., Kathiresan, K., Salmo III, S., Fernando, E. S., Peras, J., Sukardjo, S., & Miyagi, T. (2010). *Bruguiera sexangula*. Retrieved May 27, 2021, from dx.doi.org/10.2305/IUCN.UK.2010-2.RLTS.T178843A7624351.en.
- Duke, N. C. (1990). Phenological trends with latitude in the mangrove tree *avicennia marina* [Publisher: [Wiley, British Ecological Society]]. *Journal of Ecology*, *78*(1), 113–133. <https://doi.org/10.2307/2261040>

References

- Duke, N., Mackenzie, J., Hutley, L., Staben, G., & Brouke, A. (2021). Assessing the gulf of carpentaria mangrove dieback 2017–2019. *Field studies*, 150.
- Duke, N. C. (2001). Gap creation and regenerative processes driving diversity and structure of mangrove ecosystems. *Wetlands Ecology and Management*, 9(3), 267–279. <https://doi.org/10.1023/A:1011121109886>
- Duke, N. C., Ball, M. C., & Ellison, J. C. (1998). Factors influencing biodiversity and distributional gradients in mangroves. *Global Ecology and Biogeography Letters*, 7, 27–47.
- Ellison, J. C. (1999). Impacts of sediment burial on mangroves. *Marine Pollution Bulletin*, 37(8), 420–426. [https://doi.org/10.1016/S0025-326X\(98\)00122-2](https://doi.org/10.1016/S0025-326X(98)00122-2)
- Ellison, J. C., Buffington, K. J., Thorne, K. M., Gesch, D., Irwin, J., & Danielson, J. (2022). Elevations of mangrove forests of pohnpei, micronesia. *Estuarine, Coastal and Shelf Science*, 268, 107780. <https://doi.org/10.1016/j.ecss.2022.107780>
- Erfteimeijer, P. L., & Lewis III, R. R. (2000). Planting mangroves on intertidal mudflats: Habitat restoration or habitat conversion? *Proceedings of the ECOTONE VIII Seminar “En—hancing Coastal Ecosystems Restoration for the 21st Century, Ranong, Thailand. Royal Forest Department of Thailand, Bang—kok, Thailand*, 156–165.
- Eswar, D., Karuppusamy, R., & Chellamuthu, S. (2021). Drivers of soil salinity and their correlation with climate change. *Current Opinion in Environmental Sustainability*, 50, 310–318. <https://doi.org/10.1016/j.cosust.2020.10.015>
- Eyring, V., Bony, S., Meehl, G. A., Senior, C. A., Stevens, B., Stouffer, R. J., & Taylor, K. E. (2016). Overview of the coupled model intercomparison project phase 6 (CMIP6) experimental design and organization [Publisher: Copernicus GmbH]. *Geoscientific Model Development*, 9(5), 1937–1958. <https://doi.org/10.5194/gmd-9-1937-2016>
- Facelli, J. M. (2008). Specialized seedling strategies i: Seedlings in stressful environments. In M. A. Leck, V. T. Parker, & R. L. Simpson (Eds.), *Seedling ecology and evolution* (pp. 56–78). Cambridge University Press. <https://doi.org/10.1017/CBO9780511815133.005>
- Farrant, J. M., Pammenter, N. W., & Berjak, P. (1987). Ecological significance of three-phase production of roots during germination and establishment of the recalcitrant propagules of *avicennia marina*. *South African Journal of Science*, 85, 236–237.
- Fourcaud, T., Ji, J.-N., Zhang, Z.-Q., & Stokes, A. (2007). Understanding the impact of root morphology on overturning mechanisms: A modelling approach. *Annals of Botany*, 101(8), 1267–1280. <https://doi.org/10.1093/aob/mcm245>

References

- Friess, D. A., Adame, M. F., Adams, J. B., & Lovelock, C. E. (2022). Mangrove forests under climate change in a 2° c world. *Wiley Interdisciplinary Reviews: Climate Change*, e792.
- Friess, D. A., Krauss, K. W., Horstman, E. M., Balke, T., Bouma, T. J., Galli, D., & Webb, E. L. (2012). Are all intertidal wetlands naturally created equal? bottle-necks, thresholds and knowledge gaps to mangrove and saltmarsh ecosystems. *Biological Reviews*, 87(2), 346–366. <https://doi.org/10.1111/j.1469-185X.2011.00198.x>
- Friess, D. A., Rogers, K., Lovelock, C. E., Krauss, K. W., Hamilton, S. E., Lee, S. Y., Lucas, R., Primavera, J., Rajkaran, A., & Shi, S. (2019). The state of the world's mangrove forests: Past, present, and future. *Annual Review of Environment and Resources*, 44(1), 89–115. <https://doi.org/10.1146/annurev-environ-101718-033302>
- Fromard, F., Puig, H., Mougin, E., Marty, G., Betoulle, J. L., & work(s): L. C. R. (1998). Structure, above-ground biomass and dynamics of mangrove ecosystems: New data from french guiana. *Oecologia*, 115(1), 39–53. <http://www.jstor.org/stable/4221977>
- Gardiner, B. (2021). Wind damage to forests and trees: A review with an emphasis on planted and managed forests [Publisher: Taylor & Francis _eprint: <https://doi.org/10.1080/13416979.2021.1940665>]. *Journal of Forest Research*, 26(4), 248–266. <https://doi.org/10.1080/13416979.2021.1940665>
- Gardiner, B., Berry, P., & Moulia, B. (2016). Review: Wind impacts on plant growth, mechanics and damage. *Plant Science*, 245, 94–118. <https://doi.org/10.1016/j.plantsci.2016.01.006>
- Gardiner, B., Byrne, K., Hale, S., Kamimura, K., Mitchell, S. J., Peltola, H., & Ruel, J.-C. (2008). A review of mechanistic modelling of wind damage risk to forests, 17.
- GBIF. (2021). *Bruguiera sexangula* (lour.) poir. in GBIF secretariat. Retrieved May 18, 2021, from <https://doi.org/10.15468/39omei>
- Gere, J. M., & Goodno, B. J. (2012). *Mechanics of materials*. Cengage learning.
- Gijsman, R., Horstman, E. M., van der Wal, D., Friess, D. A., Swales, A., & Wijnberg, K. M. (2021). Nature-based engineering: A review on reducing coastal flood risk with mangroves. *Frontiers in Marine Science*, 8. Retrieved May 27, 2022, from <https://www.frontiersin.org/article/10.3389/fmars.2021.702412>
- Gijsman, R., Horstman, E. M., van der Wal, D., & Wijnberg, K. M. (2021). Biophysical responses of mangroves to variations in hydrodynamic forcing, 21.
- Gill, A., & Tomlinson, P. (1969). Studies on the growth of red mangrove (*Rhizophora mangle* L.) i. habit and general morphology. *Biotropica*, 1–9.

References

- Gillen, M. N., Messerschmidt, T. C., & Kirwan, M. L. (2021). Biophysical controls of marsh soil shear strength along an estuarine salinity gradient. *Earth Surface Dynamics*, 9(3), 413–421.
- Gillis, L., Bouma, T., Jones, C., van Katwijk, M., Nagelkerken, I., Jeuken, C., Herman, P., & Ziegler, A. (2014). Potential for landscape-scale positive interactions among tropical marine ecosystems. *Marine Ecology Progress Series*, 503, 289–303. <https://doi.org/10.3354/meps10716>
- Gillis, L. G., Jones, C. G., Ziegler, A. D., van der Wal, D., Breckwoldt, A., & Bouma, T. J. (2017). Opportunities for protecting and restoring tropical coastal ecosystems by utilizing a physical connectivity approach. *Frontiers in Marine Science*, 4, 374. <https://doi.org/10.3389/fmars.2017.00374>
- Gillis, L. G., Hortua, D. A. S., Zimmer, M., Jennerjahn, T. C., & Herbeck, L. S. (2019). Interactive effects of temperature and nutrients on mangrove seedling growth and implications for establishment. *Marine Environmental Research*, 151, 104750. <https://doi.org/10.1016/j.marenvres.2019.104750>
- Goessens, A., Satyanarayana, B., Van der Stocken, T., Quispe Zuniga, M., Mohd-Lokman, H., Sulong, I., & Dahdouh-Guebas, F. (2014). Is matang mangrove forest in malaysia sustainably rejuvenating after more than a century of conservation and harvesting management? (M. Heil, Ed.). *PLoS ONE*, 9(8), e105069. <https://doi.org/10.1371/journal.pone.0105069>
- Grabowski, R. C., Droppo, I. G., & Wharton, G. (2011). Erodibility of cohesive sediment: The importance of sediment properties. *Earth-Science Reviews*, 105(3), 101–120. <https://doi.org/10.1016/j.earscirev.2011.01.008>
- Guannel, G., Arkema, K., Ruggiero, P., & Verutes, G. (2016). The power of three: Coral reefs, seagrasses and mangroves protect coastal regions and increase their resilience [Publisher: Public Library of Science]. *PLOS ONE*, 11(7), e0158094. <https://doi.org/10.1371/journal.pone.0158094>
- Gutowski, W. J., Giorgi, F., Timbal, B., Frigon, A., Jacob, D., Kang, H.-S., Raghavan, K., Lee, B., Lennard, C., Nikulin, G., O'Rourke, E., Rixen, M., Solman, S., Stephenson, T., & Tangang, F. (2016). WCRP COordinated regional down-scaling EXperiment (CORDEX): A diagnostic MIP for CMIP6 [Publisher: Copernicus GmbH]. *Geoscientific Model Development*, 9(11), 4087–4095. <https://doi.org/10.5194/gmd-9-4087-2016>
- Hallé, F., Oldeman, R. A. A., & Tomlinson, P. B. (1978). Elements of tree architecture. In F. Hallé, R. A. A. Oldeman, & P. B. Tomlinson (Eds.), *Tropical trees and forests: An architectural analysis* (pp. 13–73). Springer. https://doi.org/10.1007/978-3-642-81190-6_2

References

- He, B., Lai, T., Fan, H., Wang, W., & Zheng, H. (2007). Comparison of flooding-tolerance in four mangrove species in a diurnal tidal zone in the beibu gulf. *Estuarine, Coastal and Shelf Science*, 74(1), 254–262. <https://doi.org/10.1016/j.ecss.2007.04.018>
- Hermans, T. H. J., Tinker, J., Palmer, M. D., Katsman, C. A., Vermeersen, B. L. A., & Slangen, A. B. A. (2020). Improving sea-level projections on the northwestern european shelf using dynamical downscaling. *Climate Dynamics*, 54(3), 1987–2011. <https://doi.org/10.1007/s00382-019-05104-5>
- Hinkel, J., Lincke, D., Vafeidis, A. T., Perrette, M., Nicholls, R. J., Tol, R. S. J., Marzeion, B., Fettweis, X., Ionescu, C., & Levermann, A. (2014). Coastal flood damage and adaptation costs under 21st century sea-level rise [Publisher: Proceedings of the National Academy of Sciences]. *Proceedings of the National Academy of Sciences*, 111(9), 3292–3297. <https://doi.org/10.1073/pnas.1222469111>
- Hoegh-Guldberg, O., Jacob, D., Bindi, M., Brown, S., Camilloni, I., Diedhiou, A., Djalante, R., Ebi, K., Engelbrecht, F., Guiot, J., et al. (2018). Impacts of 1.5 c global warming on natural and human systems [Publisher: IPCC Secretariat]. *Global warming of 1.5 C. An IPCC Special Report*.
- Hoffmann, W. A., & Poorter, H. (2002). Avoiding bias in calculations of relative growth rate [Publisher: Oxford University Press]. *Annals of botany*, 90(1), 37–42. <https://doi.org/10.1093/aob/mcf140>
- Hong, P., Wen, Y., Xiong, Y., Diao, L., Gu, X., Feng, H., Yang, C., & Chen, L. (2021). Latitudinal gradients and climatic controls on reproduction and dispersal of the non-native mangrove *Sonneratia apetala* in china. 248, 106749.
- Hoppe-Speer, S., Adams, J., & Rajkaran, A. (2013). Response of mangroves to drought and non-tidal conditions in st lucia estuary, south africa [Publisher: Taylor & Francis _eprint: <https://doi.org/10.2989/16085914.2012.759095>]. *African Journal of Aquatic Science*, 38(2), 153–162. <https://doi.org/10.2989/16085914.2012.759095>
- Hoque, A., Alam, M., Kabir, M., & Islam, M. (1999). Effect of salinity on the germination of *Sonneratia apetala* buch.-ham. *Bangladesh Journal of Forest Science*, 28(1), 32–37.
- Horstman, E. M., Bryan, K. R., Mullarney, J. C., Pilditch, C. A., & Eager, C. A. (2018). Are flow-vegetation interactions well represented by mimics? a case study of mangrove pneumatophores. *Advances in Water Resources*, 111, 360–371. <https://doi.org/10.1016/j.advwatres.2017.11.018>
- Horstman, E., Dohmen-Janssen, C., Narra, P., van den Berg, N., Siemerink, M., & Hulscher, S. (2014). Wave attenuation in mangroves: A quantitative approach

References

- to field observations. *Coastal Engineering*, 94, 47–62. <https://doi.org/10.1016/j.coastaleng.2014.08.005>
- Hu, J., Hu, Z., & Liu, P. L.-F. (2019). Surface water waves propagating over a submerged forest. *Coastal Engineering*, 152, 103510. <https://doi.org/10.1016/j.coastaleng.2019.103510>
- Hu, K., Chen, Q., & Wang, H. (2015). A numerical study of vegetation impact on reducing storm surge by wetlands in a semi-enclosed estuary. *Coastal Engineering*, 95, 66–76. <https://doi.org/10.1016/j.coastaleng.2014.09.008>
- Hu, Z., Lian, S., Zitman, T., Wang, H., He, Z., Wei, H., Ren, L., Uijtewaal, W., & Suzuki, T. (2022). Wave breaking induced by opposing currents in submerged vegetation canopies. *Water Resources Research*, 58(4), e2021WR031121. <https://doi.org/10.1029/2021WR031121>
- Hu, Z., Zhou, J., Wang, C., Wang, H., He, Z., Peng, Y., Zheng, P., Cozzoli, F., & Bouma, T. J. (2020). A novel instrument for bed dynamics observation supports machine learning applications in mangrove biogeomorphic processes [eprint: <https://agupubs.onlinelibrary.wiley.com/doi/pdf/10.1029/2020WR027257>]. *Water Resources Research*, 56(7), e2020WR027257. <https://doi.org/https://doi.org/10.1029/2020WR027257>
- Hu, Z., Borsje, B. W., Belzen, J., Willemsen, P. W. J. M., Wang, H., Peng, Y., Yuan, L., De Dominicis, M., Wolf, J., Temmerman, S., & Bouma, T. J. (2021). Mechanistic modeling of marsh seedling establishment provides a positive outlook for coastal wetland restoration under global climate change. *Geophysical Research Letters*, 48(22). <https://doi.org/10.1029/2021GL095596>
- Hu, Z., Lenting, W., van der Wal, D., & Bouma, T. J. (2015). Continuous monitoring bed-level dynamics on an intertidal flat: Introducing novel, stand-alone high-resolution SED-sensors. *Geomorphology*, 245, 223–230. <https://doi.org/10.1016/j.geomorph.2015.05.027>
- Hu, Z., Lian, S., Wei, H., Li, Y., Stive, M., & Suzuki, T. (2021). Laboratory data on wave propagation through vegetation with following and opposing currents [Publisher: Copernicus GmbH]. *Earth System Science Data*, 13(10), 4987–4999. <https://doi.org/10.5194/essd-13-4987-2021>
- Hu, Z., Suzuki, T., Zitman, T., Uijtewaal, W., & Stive, M. (2014). Laboratory study on wave dissipation by vegetation in combined current–wave flow. *Coastal Engineering*, 88, 131–142. <https://doi.org/10.1016/j.coastaleng.2014.02.009>
- Hu, Z., van Belzen, J., van der Wal, D., Balke, T., Wang, Z. B., Stive, M., & Bouma, T. J. (2015). Windows of opportunity for salt marsh vegetation establishment on bare tidal flats: The importance of temporal and spatial variability in hydrodynamic forcing: WINDOWS OF OPPORTUNITY FOR SALT MARSH.

References

- Journal of Geophysical Research: Biogeosciences*, 120(7), 1450–1469. <https://doi.org/10.1002/2014JG002870>
- Infantes, E., de Smit, J. C., Tamarit, E., & Bouma, T. J. (2021). Making realistic wave climates in low-cost wave mesocosms: A new tool for experimental ecology and biogeomorphology. *Limnology and Oceanography: Methods*, 10(3), 10425. <https://doi.org/10.1002/lom3.10425>
- IPCC. (2022). *Climate change 2022: Impacts, adaptation, and vulnerability. contribution of working group ii to the sixth assessment report of the intergovernmental panel on climate change* (H.-O. Pörtner, D. C. Roberts, M. Tignor, E. S. Poloczanska, K. Mintenbeck, A. Alegría, M. Craig, S. Langsdorf, S. Löschke, V. Möller, A. Okem, & B. Rama, Eds.). Cambridge University Press.
- Jacobsen, A. L., Ewers, F. W., Pratt, R. B., Paddock, W. A., & Davis, S. D. (2005). Do xylem fibers affect vessel cavitation resistance? *Plant Physiology*, 139(1), 546–556. <https://doi.org/10.1104/pp.104.058404>
- Jaffe, M. J. (1973). Thigmomorphogenesis: The response of plant growth and development to mechanical stimulation: With special reference to bryonia dioica. *Planta*, 114(2), 143–157. <https://doi.org/10.1007/BF00387472>
- James, K., Hallam, C., & Spencer, C. (2013). Measuring tilt of tree structural root zones under static and wind loading. *Agricultural and Forest Meteorology*, 168, 160–167. <https://doi.org/10.1016/j.agrformet.2012.09.009>
- Jevrejeva, S., Frederikse, T., Kopp, R. E., Le Cozannet, G., Jackson, L. P., & van de Wal, R. S. W. (2019). Probabilistic sea level projections at the coast by 2100. *Surveys in Geophysics*, 40(6), 1673–1696. <https://doi.org/10.1007/s10712-019-09550-y>
- Jie, Y., Shaohong, W., & Erfu, D. (2012). Assessment of economic damage risks from typhoon disasters in guangdong, china. *Journal of Resources and Ecology*, 3(2), 144–150.
- Jimenez, J. A., Lugo, A. E., & Cintron, G. (1985). Tree mortality in mangrove forests. *Biotropica*, 17(3), 177. <https://doi.org/10.2307/2388214>
- Johnson, J. B., & Omland, K. S. (2004). Model selection in ecology and evolution. *Trends in Ecology & Evolution*, 19(2), 101–108. <https://doi.org/10.1016/j.tree.2003.10.013>
- Johnstone, J. F., Allen, C. D., Franklin, J. F., Frelich, L. E., Harvey, B. J., Higuera, P. E., Mack, M. C., Meentemeyer, R. K., Metz, M. R., Perry, G. L., Schoennagel, T., & Turner, M. G. (2016). Changing disturbance regimes, ecological memory, and forest resilience. *Frontiers in Ecology and the Environment*, 14(7), 369–378. <https://doi.org/10.1002/fee.1311>

References

- Kalloe, S. A., Hofland, B., Antolínez, J. A. A., & van Wesenbeeck, B. K. (2022). Quantifying frontal-surface area of woody vegetation: A crucial parameter for wave attenuation. *Frontiers in Marine Science*, 9. Retrieved June 16, 2022, from <https://www.frontiersin.org/article/10.3389/fmars.2022.820846>
- Kamimura, K., Gardiner, B., Dupont, S., Guyon, D., & Meredieu, C. (2016). Mechanistic and statistical approaches to predicting wind damage to individual maritime pine (*Pinus pinaster*) trees in forests. *Canadian Journal of Forest Research*, 46(1), 88–100. <https://doi.org/10.1139/cjfr-2015-0237>
- Karimi, Z., Abdi, E., Deljouei, A., Cislaghi, A., Shirvany, A., Schwarz, M., & Hales, T. C. (2022). Vegetation-induced soil stabilization in coastal area: An example from a natural mangrove forest. *CATENA*, 216, 106410. <https://doi.org/10.1016/j.catena.2022.106410>
- Kauffman, J. B., & Cole, T. G. (2010). Micronesian mangrove forest structure and tree responses to a severe typhoon. *Wetlands*, 30(6), 1077–1084. <https://doi.org/10.1007/s13157-010-0114-y>
- Khan, M. N. I., & Kabir, M. E. (2017). Ecology of kandelia obovata (s., l.) yong: A fast-growing mangrove in okinawa, japan. In R. DasGupta & R. Shaw (Eds.), *Participatory mangrove management in a changing climate* (pp. 287–301). Springer Japan. https://doi.org/10.1007/978-4-431-56481-2_18
- Kiesel, J., MacPherson, L. R., Schuerch, M., & Vafeidis, A. T. (2022). Can managed realignment buffer extreme surges? the relationship between marsh width, vegetation cover and surge attenuation. *Estuaries and Coasts*, 45(2), 345–362. <https://doi.org/10.1007/s12237-021-00984-5>
- Kirwan, M. L., Guntenspergen, G. R., d'Alpaos, A., Morris, J. T., Mudd, S. M., & Temmerman, S. (2010). Limits on the adaptability of coastal marshes to rising sea level. *Geophysical research letters*, 37(23).
- Kirwan, M. L., Temmerman, S., Skeehan, E. E., Guntenspergen, G. R., & Fagherazzi, S. (2016). Overestimation of marsh vulnerability to sea level rise. *Nature Climate Change*, 6(3), 253–260. <https://doi.org/10.1038/nclimate2909>
- Knutson, T., Camargo, S. J., Chan, J. C. L., Emanuel, K., Ho, C.-H., Kossin, J., Mohapatra, M., Satoh, M., Sugi, M., Walsh, K., & Wu, L. (2020). Tropical cyclones and climate change assessment: Part II: Projected response to anthropogenic warming. *Bulletin of the American Meteorological Society*, 101(3), E303–E322. <https://doi.org/10.1175/BAMS-D-18-0194.1>
- Koch, E. W., Barbier, E. B., Silliman, B. R., Reed, D. J., Perillo, G. M., Hacker, S. D., Granek, E. F., Primavera, J. H., Muthiga, N., Polasky, S., Halpern, B. S., Kennedy, C. J., Kappel, C. V., & Wolanski, E. (2009). Non-linearity in ecosys-

References

- tem services: Temporal and spatial variability in coastal protection. *Frontiers in Ecology and the Environment*, 7(1), 29–37. <https://doi.org/10.1890/080126>
- Kodikara, K. A. S., Jayatissa, L. P., Huxham, M., Dahdouh-Guebas, F., & Koedam, N. (2017). The effects of salinity on growth and survival of mangrove seedlings changes with age. *Acta Botanica Brasilica*, 32(1), 37–46. <https://doi.org/10.1590/0102-33062017abb0100>
- Kodikara, K. A. S., Mukherjee, N., Jayatissa, L. P., Dahdouh-Guebas, F., & Koedam, N. (2017). Have mangrove restoration projects worked? an in-depth study in sri lanka: Evaluation of mangrove restoration in sri lanka. *Restoration Ecology*, 25(5), 705–716. <https://doi.org/10.1111/rec.12492>
- Kovacs, J. M., Blanco-Correa, M., & Flores-Verdugo, F. (2001). A logistic regression model of hurricane impacts in a mangrove forest of the mexican pacific. *Journal of Coastal Research*, 30–37.
- Krauss, K. W., Allen, J. A., & Cahoon, D. R. (2003). Differential rates of vertical accretion and elevation change among aerial root types in micronesia mangrove forests, 9.
- Krauss, K. W., Keeland, B. D., Allen, J. A., Ewel, K. C., & Johnson, D. J. (2007). Effects of season, rainfall, and hydrogeomorphic setting on mangrove tree growth in micronesia [eprint: <https://onlinelibrary.wiley.com/doi/pdf/10.1111/j.1744-7429.2006.00259.x>]. *Biotropica*, 39(2), 161–170. <https://doi.org/10.1111/j.1744-7429.2006.00259.x>
- Krauss, K. W., Lovelock, C. E., McKee, K. L., López-Hoffman, L., Ewe, S. M., & Sousa, W. P. (2008). Environmental drivers in mangrove establishment and early development: A review. *Aquatic Botany*, 89(2), 105–127. <https://doi.org/10.1016/j.aquabot.2007.12.014>
- Krauss, K. W., & Osland, M. J. (2020). Tropical cyclones and the organization of mangrove forests: A review. *Annals of Botany*, 125(2), 213–234.
- Kulp, S. A., & Strauss, B. H. (2019). New elevation data triple estimates of global vulnerability to sea-level rise and coastal flooding. *Nature Communications*, 10(1), 4844. <https://doi.org/10.1038/s41467-019-12808-z>
- Lagomasino, D., Fatoyinbo, T., Castañeda-Moya, E., Cook, B. D., Montesano, P. M., Neigh, C. S., Corp, L. A., Ott, L. E., Chavez, S., & Morton, D. C. (2021). Storm surge and ponding explain mangrove dieback in southwest florida following hurricane irma. *Nature Communications*, 12(1), 1–8.
- Leck, M. A., Simpson, R. L., & Parker, V. T. (2008). Why seedlings? In M. A. Leck, V. T. Parker, & R. L. Simpson (Eds.), *Seedling ecology and evolution* (pp. 3–14). Cambridge University Press. <https://doi.org/10.1017/CBO9780511815133.003>

References

- Lee, S. Y., Hamilton, S., Barbier, E. B., Primavera, J., & Lewis, R. R. (2019). Better restoration policies are needed to conserve mangrove ecosystems. *Nature Ecology & Evolution*, 3(6), 870–872. <https://doi.org/10.1038/s41559-019-0861-y>
- Lee, S. Y., Primavera, J. H., Dahdouh-Guebas, F., McKee, K., Bosire, J. O., Cannicci, S., Diele, K., Fromard, F., Koedam, N., Marchand, C., Mendelssohn, I., Mukherjee, N., & Record, S. (2014). Ecological role and services of tropical mangrove ecosystems: A reassessment: Reassessment of mangrove ecosystem services. *Global Ecology and Biogeography*, 23(7), 726–743. <https://doi.org/10.1111/geb.12155>
- Lee, W. K., Tay, S. H. X., Ooi, S. K., & Friess, D. A. (2021). Potential short wave attenuation function of disturbed mangroves. *Estuarine, Coastal and Shelf Science*, 248, 106747. <https://doi.org/https://doi.org/10.1016/j.ecss.2020.106747>
- Leong, R. C., Friess, D. A., Crase, B., Lee, W. K., & Webb, E. L. (2018). High-resolution pattern of mangrove species distribution is controlled by surface elevation. *Estuarine, Coastal and Shelf Science*, 202, 185–192. <https://doi.org/10.1016/j.ecss.2017.12.015>
- Lewis, H. W., Castillo Sanchez, J. M., Arnold, A., Fallmann, J., Saulter, A., Graham, J., Bush, M., Siddorn, J., Palmer, T., Lock, A., Edwards, J., Bricheno, L., Martínez-de la Torre, A., & Clark, J. (2019). The UKC3 regional coupled environmental prediction system [Publisher: Copernicus GmbH]. *Geoscientific Model Development*, 12(6), 2357–2400. <https://doi.org/10.5194/gmd-12-2357-2019>
- Lewis, R. R., & Brown, B. (2014). Ecological mangrove rehabilitation—a field manual for practitioners. *Mangrove Action Project, Canadian International Development Agency, and OXFAM*.
- Lewis, R. R. (2005). Ecological engineering for successful management and restoration of mangrove forests. *Ecological Engineering*, 24(4), 403–418. <https://doi.org/10.1016/j.ecoleng.2004.10.003>
- Lewis III, R. R., & Estevez, E. (1988, September 1). *The ecology of tampa bay, florida: An estuarine profile*.
- Li, C. W., & Yan, K. (2007). Numerical investigation of wave–current–vegetation interaction [Publisher: American Society of Civil Engineers]. *Journal of Hydraulic Engineering*, 133(7), 794–803.
- Liu, H., Zhang, K., Li, Y., & Xie, L. (2013). Numerical study of the sensitivity of mangroves in reducing storm surge and flooding to hurricane characteristics in southern florida. *Continental Shelf Research*, 64, 51–65. <https://doi.org/10.1016/j.csr.2013.05.015>

References

- Liu, P. L.-F., Chang, C.-W., Mei, C. C., Lomonaco, P., Martin, F. L., & Maza, M. (2015). Periodic water waves through an aquatic forest. *Coastal Engineering*, *96*, 100–117. <https://doi.org/10.1016/j.coastaleng.2014.11.002>
- Losada, I. J., Maza, M., & Lara, J. L. (2016). A new formulation for vegetation-induced damping under combined waves and currents. *Coastal Engineering*, *107*, 1–13. <https://doi.org/https://doi.org/10.1016/j.coastaleng.2015.09.011>
- Lovelock, C. E., Ball, M. C., Choat, B., Engelbrecht, B. M. J., Holbrook, N. M., & Feller, I. C. (2006). Linking physiological processes with mangrove forest structure: Phosphorus deficiency limits canopy development, hydraulic conductivity and photosynthetic carbon gain in dwarf rhizophora mangle. *Plant, Cell & Environment*, *29*(5), 793–802. <https://doi.org/10.1111/j.1365-3040.2005.01446.x>
- Lovelock, C. E., Cahoon, D. R., Friess, D. A., Guntenspergen, G. R., Krauss, K. W., Reef, R., Rogers, K., Saunders, M. L., Sidik, F., Swales, A., Saintilan, N., Thuyen, L. X., & Triet, T. (2015). The vulnerability of indo-pacific mangrove forests to sea-level rise. *Nature*, *526*(7574), 559–563. <https://doi.org/10.1038/nature15538>
- Lovelock, C. E., Feller, I. C., Reef, R., Hickey, S., & Ball, M. C. (2017). Mangrove dieback during fluctuating sea levels [Number: 1 Publisher: Nature Publishing Group]. *Scientific Reports*, *7*(1), 1680. <https://doi.org/10.1038/s41598-017-01927-6>
- Lovelock, C. E., Krauss, K. W., Osland, M. J., Reef, R., & Ball, M. C. (2016). The physiology of mangrove trees with changing climate. In G. Goldstein & L. S. Santiago (Eds.), *Tropical tree physiology* (pp. 149–179, Vol. 6). Springer International Publishing. https://doi.org/10.1007/978-3-319-27422-5_7
- Ma, W., Wang, W., Tang, C., Chen, G., & Wang, M. (2020). Zonation of mangrove flora and fauna in a subtropical estuarine wetland based on surface elevation [eprint: <https://onlinelibrary.wiley.com/doi/pdf/10.1002/ece3.6467>]. *Ecology and Evolution*, *10*(14), 7404–7418. <https://doi.org/10.1002/ece3.6467>
- Maun, M. A. (1998). Adaptations of plants to burial in coastal sand dunes. 76, 26.
- Maza, M., Lara, J. L., Losada, I. J., Ondiviela, B., Trinogga, J., & Bouma, T. J. (2015). Large-scale 3-d experiments of wave and current interaction with real vegetation. part 2: Experimental analysis. *Coastal Engineering*, *106*, 73–86. <https://doi.org/10.1016/j.coastaleng.2015.09.010>
- Maza, M., Adler, K., Ramos, D., Garcia, A. M., & Nepf, H. (2017). Velocity and drag evolution from the leading edge of a model mangrove forest [Publisher: Wiley Online Library]. *Journal of Geophysical Research: Oceans*, *122*(11), 9144–9159.

References

- Maza, M., Lara, J. L., & Losada, I. J. (2019). Experimental analysis of wave attenuation and drag forces in a realistic fringe rhizophora mangrove forest. *Advances in Water Resources*, *131*, 103376. <https://doi.org/10.1016/j.advwatres.2019.07.006>
- Maza, M., Lara, J. L., & Losada, I. J. (2021). Predicting the evolution of coastal protection service with mangrove forest age. *Coastal Engineering*, *168*, 103922. <https://doi.org/10.1016/j.coastaleng.2021.103922>
- Mazda, Y., Magi, M., Ikeda, Y., Kurokawa, T., & Asano, T. (2006). Wave reduction in a mangrove forest dominated by *Sonneratia* sp. *Wetlands Ecology and Management*, *14*(4), 365–378. <https://doi.org/10.1007/s11273-005-5388-0>
- Mazda, Y., Wolanski, E., King, B., Sase, A., Ohtsuka, D., & Magi, M. (1997). Drag force due to vegetation in mangrove swamps. *Mangroves and Salt Marshes*, *1*(3), 193–199. <https://doi.org/10.1023/A:1009949411068>
- McIvor, A., Spencer, T., Spalding, M., Lacambra, C., & Möller, I. (2015). Mangroves, tropical cyclones, and coastal hazard risk reduction. In *Coastal and marine hazards, risks, and disasters* (pp. 403–429). Elsevier. <https://doi.org/10.1016/B978-0-12-396483-0.00014-5>
- McIvor, A. L., Spencer, T., Möller, I., & Spalding, M. (2012). Storm surge reduction by mangroves [Publisher: The Nature Conservancy and Wetlands International]. *Natural Coastal Protection Series: Report 2. Cambridge Coastal Research Unit Working Paper 35. ISSN 2050-7941.*
- McKee, K. L. (1995). Interspecific variation in growth, biomass partitioning, and defensive characteristics of neotropical mangrove seedlings: Response to light and nutrient availability. *American Journal of Botany*, *82*(3), 299–307.
- Mendez, F. J., & Losada, I. J. (2004). An empirical model to estimate the propagation of random breaking and nonbreaking waves over vegetation fields [Publisher: Elsevier]. *Coastal Engineering*, *51*(2), 103–118.
- Menéndez, P., Losada, I. J., Torres-Ortega, S., Narayan, S., & Beck, M. W. (2020). The global flood protection benefits of mangroves. *Scientific Reports*, *10*(1), 4404. <https://doi.org/10.1038/s41598-020-61136-6>
- Möller, I., Kudella, M., Rupprecht, F., Spencer, T., Paul, M., van Wesenbeeck, B. K., Wolters, G., Jensen, K., Bouma, T. J., Miranda-Lange, M., & Schimmels, S. (2014). Wave attenuation over coastal salt marshes under storm surge conditions. *Nature Geoscience*, *7*(10), 727–731. <https://doi.org/10.1038/ngeo2251>
- Montgomery, J. M., Bryan, K. R., Horstman, E. M., & Mullarney, J. C. (2018). Attenuation of tides and surges by mangroves: Contrasting case studies from new zealand [Number: 9 Publisher: Multidisciplinary Digital Publishing Institute]. *Water*, *10*(9), 1119. <https://doi.org/10.3390/w10091119>

References

- Morison, J., Johnson, J., & Schaaf, S. (1950). The force exerted by surface waves on piles. *Journal of Petroleum Technology*, 2(5), 149–154. <https://doi.org/10.2118/950149-G>
- Morris, R., Strain, E. M. A., Konlechner, T. M., Fest, B. J., Kennedy, D. M., Arndt, S. K., & Swearer, S. E. (2019). Developing a nature-based coastal defence strategy for australia. *Australian Journal of Civil Engineering*, 17(2), 167–176. <https://doi.org/10.1080/14488353.2019.1661062>
- Morrisey, D. J., Swales, A., Dittmann, S., Morrison, M. A., Lovelock, C. E., & Beard, C. M. (2010). The ecology and management of temperate mangroves. *Oceanography and marine biology*, 48, 43.
- Mullarney, J. C., Henderson, S. M., Reyns, J. A., Norris, B. K., & Bryan, K. R. (2017). Spatially varying drag within a wave-exposed mangrove forest and on the adjacent tidal flat. *Continental Shelf Research*, 147, 102–113. <https://doi.org/10.1016/j.csr.2017.06.019>
- Naidoo, G. (2009). Differential effects of nitrogen and phosphorus enrichment on growth of dwarf avicennia marina mangroves. *Aquatic Botany*, 90(2), 184–190. <https://doi.org/10.1016/j.aquabot.2008.10.001>
- Nguyen, H. M., Bryan, K. R., Pilditch, C. A., & Moon, V. G. (2019). Influence of ambient temperature on erosion properties of exposed cohesive sediment from an intertidal mudflat. *Geo-Marine Letters*, 39(4), 337–347. <https://doi.org/10.1007/s00367-019-00579-x>
- Nicholls, R. J., Lincke, D., Hinkel, J., Brown, S., Vafeidis, A. T., Meyssignac, B., Hanson, S. E., Merckens, J.-L., & Fang, J. (2021). A global analysis of subsidence, relative sea-level change and coastal flood exposure. *Nature Climate Change*, 11(4), 338–342.
- Nicholls, R. J., Hinkel, J., Lincke, D., & van der Pol, T. (2019). Global investment costs for coastal defense through the 21st century. *World Bank Policy Research Working Paper*, (8745).
- Nicoll, B. C., & Ray, D. (1996). Adaptive growth of tree root systems in response to wind action and site conditions. *Tree Physiology*, 16(11), 891–898. <https://doi.org/10.1093/treephys/16.11-12.891>
- Nicoll, B. C., Gardiner, B. A., Rayner, B., & Peace, A. J. (2006). Anchorage of coniferous trees in relation to species, soil type, and rooting depth. *Canadian Journal of Forest Research*, 36(7), 1871–1883.
- Njana, M. A. (2020). Structure, growth, and sustainability of mangrove forests of mainland tanzania. *Global Ecology and Conservation*, 24, e01394. <https://doi.org/10.1016/j.gecco.2020.e01394>

References

- Njana, M. A., Bollaerts, O. M., Eid, T., Zahabu, E., & Malimbwi, R. E. (2016). Above- and belowground tree biomass models for three mangrove species in Tanzania: A nonlinear mixed effects modelling approach. *Annals of Forest Science*, 73(2), 353–369. <https://doi.org/10.1007/s13595-015-0524-3>
- Njana, M. A., Eid, T., Zahabu, E., & Malimbwi, R. (2015). Procedures for quantification of belowground biomass of three mangrove tree species. *Wetlands Ecology and Management*, 23(4), 749–764. <https://doi.org/10.1007/s11273-015-9417-3>
- Norris, B. K., Mullarney, J. C., Bryan, K. R., & Henderson, S. M. (2017). The effect of pneumatophore density on turbulence: A field study in a sonneratia-dominated mangrove forest, Vietnam. *Continental Shelf Research*, 147, 114–127. <https://doi.org/10.1016/j.csr.2017.06.002>
- Ola, A., Gauthier, A. R. G., Xiong, Y., & Lovelock, C. E. (2019). The roots of blue carbon: Responses of mangrove stilt roots to variation in soil bulk density [Publisher: Royal Society]. *Biology Letters*, 15(4), 20180866. <https://doi.org/10.1098/rsbl.2018.0866>
- Onoda, Y., Richards, A. E., & Westoby, M. (2010). The relationship between stem biomechanics and wood density is modified by rainfall in 32 Australian woody plant species. *New Phytologist*, 185(2), 493–501.
- Onoda, Y., Westoby, M., Adler, P. B., Choong, A. M. F., Clissold, F. J., Cornelissen, J. H. C., Díaz, S., Dominy, N. J., Elgart, A., Enrico, L., Fine, P. V. A., Howard, J. J., Jalili, A., Kitajima, K., Kurokawa, H., McArthur, C., Lucas, P. W., Markesteijn, L., Pérez-Harguindeguy, N., ... Yamashita, N. (2011). Global patterns of leaf mechanical properties: Global patterns of leaf mechanical properties. *Ecology Letters*, 14(3), 301–312. <https://doi.org/10.1111/j.1461-0248.2010.01582.x>
- Ouyang, X., Guo, F., & Lee, S. Y. (2021). The impact of super-typhoon mangkhut on sediment nutrient density and fluxes in a mangrove forest in Hong Kong. *Science of The Total Environment*, 766, 142637. <https://doi.org/10.1016/j.scitotenv.2020.142637>
- Parris, K. M., McCall, S. C., McCarthy, M. A., Minter, B. A., Steele, K., Bekessy, S., & Medvecky, F. (2010). Assessing ethical trade-offs in ecological field studies. *Journal of Applied Ecology*, 47(1), 227–234.
- Paul, M., Bouma, T., & Amos, C. (2012). Wave attenuation by submerged vegetation: Combining the effect of organism traits and tidal current. *Marine Ecology Progress Series*, 444, 31–41. <https://doi.org/10.3354/meps09489>
- Paul, M., Rupprecht, F., Möller, I., Bouma, T. J., Spencer, T., Kudella, M., Wolters, G., van Wesenbeeck, B. K., Jensen, K., Miranda-Lange, M., & Schimmels, S.

References

- (2016). Plant stiffness and biomass as drivers for drag forces under extreme wave loading: A flume study on mimics. *Coastal Engineering*, 117, 70–78. <https://doi.org/10.1016/j.coastaleng.2016.07.004>
- Peltola, H., Kellomäki, S., & Väisänen, H. (1999). A mechanistic model for assessing the risk of wind and snow damage to single trees and stands of scots pine, norway spruce, and birch. 29, 15.
- Peltola, H. M. (2006). Mechanical stability of trees under static loads. *American Journal of Botany*, 93(10), 1501–1511. <https://doi.org/10.3732/ajb.93.10.1501>
- Peng, Y., Diao, J., Zheng, M., Guan, D., Zhang, R., Chen, G., & Lee, S. Y. (2016). Early growth adaptability of four mangrove species under the canopy of an introduced mangrove plantation: Implications for restoration. *Forest Ecology and Management*, 373, 179–188. <https://doi.org/10.1016/j.foreco.2016.04.044>
- Peng, Y., Zheng, M., Zheng, Z., Wu, G., Chen, Y., Xu, H., Tian, G., Peng, S., Chen, G., & Lee, S. Y. (2016). Virtual increase or latent loss? a reassessment of mangrove populations and their conservation in guangdong, southern china. *Marine Pollution Bulletin*, 109(2), 691–699. <https://doi.org/10.1016/j.marpolbul.2016.06.083>
- Peters, R., Vovides, A. G., Luna, S., Grütters, U., & Berger, U. (2014). Changes in allometric relations of mangrove trees due to resource availability – a new mechanistic modelling approach. *Ecological Modelling*, 283, 53–61. <https://doi.org/10.1016/j.ecolmodel.2014.04.001>
- Peters, R., Walther, M., Lovelock, C., Jiang, J., & Berger, U. (2020). The interplay between vegetation and water in mangroves: New perspectives for mangrove stand modelling and ecological research. *Wetlands Ecology and Management*, 28(4), 697–712. <https://doi.org/10.1007/s11273-020-09733-0>
- Peterson, J. M., & Bell, S. S. (2012). Tidal events and salt-marsh structure influence black mangrove (*avicennia germinans*) recruitment across an ecotone [eprint: <https://onlinelibrary.wiley.com/doi/pdf/10.1890/11-1430.1>]. *Ecology*, 93(7), 1648–1658. <https://doi.org/10.1890/11-1430.1>
- Peterson, J. M., & Bell, S. S. (2015). Saltmarsh boundary modulates dispersal of mangrove propagules: Implications for mangrove migration with sea-level rise [Publisher: Public Library of Science]. *PLOS ONE*, 10(3), e0119128. <https://doi.org/10.1371/journal.pone.0119128>
- Pinsky, M. L., Guannel, G., & Arkema, K. K. (2013). Quantifying wave attenuation to inform coastal habitat conservation. *Ecosphere*, 4(8), art95. <https://doi.org/10.1890/ES13-00080.1>

References

- Pranchai, A., Jenke, M., Pokavanich, T., Puangchit, L., & Berger, U. (2022). Aerial surveys reveal biotic drivers of mangrove expansion along a thai salt flat ecotone. *Restoration Ecology*, e13640.
- Preston, K. A., Cornwell, W. K., & DeNoyer, J. L. (2006). Wood density and vessel traits as distinct correlates of ecological strategy in 51 california coast range angiosperms. *New Phytologist*, 170(4), 807–818.
- Primavera, J. H., & Esteban, J. M. A. (2008). A review of mangrove rehabilitation in the philippines: Successes, failures and future prospects. *Wetlands Ecology and Management*, 16(5), 345–358. <https://doi.org/10.1007/s11273-008-9101-y>
- Primavera, J., dela Cruz, M., Montilijao, C., Consunji, H., dela Paz, M., Rollon, R., Maranan, K., Samson, M., & Blanco, A. (2016). Preliminary assessment of post-haiyan mangrove damage and short-term recovery in eastern samar, central philippines. *Marine Pollution Bulletin*, 109(2), 744–750. <https://doi.org/10.1016/j.marpolbul.2016.05.050>
- Proffitt, C. E., Milbrandt, E. C., & Travis, S. E. (2006). Red mangrove (rhizophora mangle) reproduction and seedling colonization after hurricane charley: Comparisons of charlotte harbor and tampa bay [Publisher: Coastal and Estuarine Research Federation]. *Estuaries and Coasts*, 29(6), 972–978. Retrieved May 25, 2022, from <https://www.jstor.org/stable/4124828>
- Puijalon, S., Bouma, T. J., Douady, C. J., van Groenendael, J., Anten, N. P. R., Martel, E., & Bornette, G. (2011). Plant resistance to mechanical stress: Evidence of an avoidance-tolerance trade-off. *New Phytologist*, 191(4), 1141–1149. <https://doi.org/10.1111/j.1469-8137.2011.03763.x>
- Putz, F. E., & Chan, H. T. (1986). Tree growth, dynamics, and productivity in a mature mangrove forest in malaysia. *Forest Ecology and Management*, 17(2), 211–230. [https://doi.org/10.1016/0378-1127\(86\)90113-1](https://doi.org/10.1016/0378-1127(86)90113-1)
- Quadros, A., & Zimmer, M. (2017). Dataset of “true mangroves” plant species traits [Publisher: Pensoft Publishers]. *Biodiversity Data Journal*, 5, e22089. <https://doi.org/10.3897/BDJ.5.e22089>
- Quang Bao, T. (2011). Effect of mangrove forest structures on wave attenuation in coastal vietnam. *Oceanologia*, 53(3), 807–818. <https://doi.org/10.5697/oc.53-3.807>
- R Core Team. (2021). *R: A language and environment for statistical computing*. R Foundation for Statistical Computing. Vienna, Austria. <https://www.R-project.org/>
- Rabinowitz, D. (1978). Mortality and initial propagule size in mangrove seedlings in panama. *The Journal of Ecology*, 66(1), 45. <https://doi.org/10.2307/2259180>

References

- Rahardjo, H., Harnas, F., Leong, E. C., Tan, P., Fong, Y., & Sim, E. (2009). Tree stability in an improved soil to withstand wind loading. *Urban Forestry & Urban Greening*, 8(4), 237–247.
- Rahman, M. M. (2020). Impact of increased salinity on the plant community of the sundarbans mangrove of bangladesh. *Community Ecology*, 21(3), 273–284. <https://doi.org/10.1007/s42974-020-00028-1>
- Record, S., Charney, N. D., Zakaria, R. M., & Ellison, A. M. (2013). Projecting global mangrove species and community distributions under climate change [eprint: <https://onlinelibrary.wiley.com/doi/pdf/10.1890/ES12-00296.1>]. *Ecosphere*, 4(3), art34. <https://doi.org/10.1890/ES12-00296.1>
- Redelstein, R., Zotz, G., & Balke, T. (2018). Seedling stability in waterlogged sediments: An experiment with saltmarsh plants. *Marine Ecology Progress Series*, 590, 95–108. <https://doi.org/10.3354/meps12463>
- Reef, R., & Lovelock, C. E. (2015). Regulation of water balance in mangroves. *Annals of Botany*, 115(3), 385–395. <https://doi.org/10.1093/aob/mcu174>
- Ren, H., Jian, S., Lu, H., Zhang, Q., Shen, W., Han, W., Yin, Z., & Guo, Q. (2008). Restoration of mangrove plantations and colonisation by native species in leizhou bay, south china. *Ecological Research*, 23(2), 401–407. <https://doi.org/10.1007/s11284-007-0393-9>
- Ren, H., Lu, H., Shen, W., Huang, C., Guo, Q., Li, Z., & Jian, S. (2009). *Sonneratia apetala* buch.ham in the mangrove ecosystems of china: An invasive species or restoration species? *Ecological Engineering*, 35(8), 1243–1248. <https://doi.org/10.1016/j.ecoleng.2009.05.008>
- Rennenberg, H., Loreto, F., Polle, A., Brilli, F., Fares, S., Beniwal, R. S., & Gessler, A. (2006). Physiological responses of forest trees to heat and drought [eprint: <https://onlinelibrary.wiley.com/doi/pdf/10.1055/s-2006-924084>]. *Plant Biology*, 8(5), 556–571. <https://doi.org/10.1055/s-2006-924084>
- Robert, E. M., Oste, J., Van der Stocken, T., De Ryck, D. J., Quisthoudt, K., Kairo, J. G., Dahdouh-Guebas, F., Koedam, N., & Schmitz, N. (2015). Viviparous mangrove propagules of *Ceriops tagal* and *Rhizophora mucronata*, where both rhizophoraceae show different dispersal and establishment strategies. *Journal of Experimental Marine Biology and Ecology*, 468, 45–54. <https://doi.org/10.1016/j.jembe.2015.03.014>
- Roeber, V., & Bricker, J. D. (2015). Destructive tsunami-like wave generated by surf beat over a coral reef during typhoon haiyan. *Nature Communications*, 6(1), 7854. <https://doi.org/10.1038/ncomms8854>
- Roskoden, R. R., Bryan, K. R., Schreiber, I., & Kopf, A. (2020). Rapid transition of sediment consolidation across an expanding mangrove fringe in the firth of

References

- thames new zealand. *Geo-Marine Letters*, 40(2), 295–308. <https://doi.org/10.1007/s00367-019-00589-9>
- Rovai, A. S., Twilley, R. R., Castañeda-Moya, E., Midway, S. R., Friess, D. A., Trettin, C. C., Bukoski, J. J., Stovall, A. E., Pagliosa, P. R., Fonseca, A. L., Mackenzie, R. A., Aslan, A., Sasmito, S. D., Sillanpää, M., Cole, T. G., Purbopuspito, J., Warren, M. W., Murdiyarto, D., Mofu, W., ... Riul, P. (2021). Macroecological patterns of forest structure and allometric scaling in mangrove forests. *Global Ecology and Biogeography*, 30(5), 1000–1013. <https://doi.org/10.1111/geb.13268>
- Saenger, P. (2002). *Mangrove ecology, silviculture and conservation* [OCLC: 864683625]. Retrieved March 27, 2019, from <http://dx.doi.org/10.1007/978-94-015-9962-7>
- Sagi, P., Newson, T., Miller, C., & Mitchell, S. (2019). Stem and root system response of a norway spruce tree (*picea abies* l.) under static loading. *Forestry: An International Journal of Forest Research*, 92(4), 460–472. <https://doi.org/10.1093/forestry/cpz042>
- Saintilan, N., Khan, N. S., Ashe, E., Kelleway, J. J., Rogers, K., Woodroffe, C. D., & Horton, B. P. (2020). Thresholds of mangrove survival under rapid sea level rise [Publisher: American Association for the Advancement of Science]. *Science*, 368(6495), 1118–1121. <https://doi.org/10.1126/science.aba2656>
- Sánchez-Núñez, D. A., Bernal, G., & Mancera Pineda, J. E. (2019). The relative role of mangroves on wave erosion mitigation and sediment properties. *Estuaries and Coasts*, 42(8), 2124–2138. <https://doi.org/10.1007/s12237-019-00628-9>
- Santini, N. S., Schmitz, N., Bennion, V., & Lovelock, C. E. (2013). The anatomical basis of the link between density and mechanical strength in mangrove branches. *Functional Plant Biology*, 40(4), 400. <https://doi.org/10.1071/FP12204>
- Santini, N. S., Schmitz, N., & Lovelock, C. E. (2012). Variation in wood density and anatomy in a widespread mangrove species. *Trees*, 26(5), 1555–1563. <https://doi.org/10.1007/s00468-012-0729-0>
- Scheffer, M., Carpenter, S., Foley, J. A., Folke, C., & Walker, B. (2001). Catastrophic shifts in ecosystems. *Nature*, 413(6856), 591–596. <https://doi.org/10.1038/35098000>
- Schindelin, J., Arganda-Carreras, I., Frise, E., Kaynig, V., Longair, M., Pietzsch, T., Preibisch, S., Rueden, C., Saalfeld, S., Schmid, B., et al. (2012). Fiji: An open-source platform for biological-image analysis. *Nature methods*, 9(7), 676–682.
- Schmitz, N., Verheyden, A., Beeckman, H., Kairo, J. G., & Koedam, N. (2006). Influence of a salinity gradient on the vessel characters of the mangrove species *rhizophora mucronata*. *Annals of Botany*, 98(6), 1321–1330. <https://doi.org/10.1093/aob/mcl224>

References

- Schoelynck, J., Puijalon, S., Meire, P., & Struyf, E. (2015). Thigmomorphogenetic responses of an aquatic macrophyte to hydrodynamic stress. *Frontiers in Plant Science*, 6. <https://doi.org/10.3389/fpls.2015.00043>
- Schoutens, K., Heuner, M., Fuchs, E., Minden, V., Schulte-Ostermann, T., Belliard, J.-P., Bouma, T. J., & Temmerman, S. (2020). Nature-based shoreline protection by tidal marsh plants depends on trade-offs between avoidance and attenuation of hydrodynamic forces. *Estuarine, Coastal and Shelf Science*, 236, 106645. <https://doi.org/10.1016/j.ecss.2020.106645>
- Schuerch, M., Spencer, T., Temmerman, S., Kirwan, M. L., Wolff, C., Lincke, D., McOwen, C. J., Pickering, M. D., Reef, R., Vafeidis, A. T., Hinkel, J., Nicholls, R. J., & Brown, S. (2018). Future response of global coastal wetlands to sea-level rise [Number: 7722 Publisher: Nature Publishing Group]. *Nature*, 561(7722), 231–234. <https://doi.org/10.1038/s41586-018-0476-5>
- Scoffin, T. P. (1970). The trapping and binding of subtidal carbonate sediments by marine vegetation in bimini lagoon, bahamas. *Journal of Sedimentary Research*, 40(1), 249–273. <https://doi.org/10.1306/74D71F28-2B21-11D7-8648000102C1865D>
- Seidl, R., Fernandes, P. M., Fonseca, T. F., Gillet, F., Jönsson, A. M., Merganičová, K., Netherer, S., Arpaci, A., Bontemps, J.-D., Bugmann, H., González-Olabarria, J. R., Lasch, P., Meredieu, C., Moreira, F., Schelhaas, M.-J., & Mohren, F. (2011). Modelling natural disturbances in forest ecosystems: A review. *Ecological Modelling*, 222(4), 903–924. <https://doi.org/10.1016/j.ecolmodel.2010.09.040>
- Semeniuk, V. (1980). Mangrove zonation along an eroding coastline in king sound, north-western australia. *The Journal of Ecology*, 68(3), 789. <https://doi.org/10.2307/2259456>
- Sheng, Y. P., Lapetina, A., & Ma, G. (2012). The reduction of storm surge by vegetation canopies: Three-dimensional simulations. *Geophysical Research Letters*, 39(20). <https://doi.org/10.1029/2012GL053577>
- Sherman, R. E., Fahey, T. J., & Battles, J. J. (2000). Small-scale disturbance and regeneration dynamics in a neotropical mangrove forest. *Journal of Ecology*, 88(1), 165–178. <https://doi.org/10.1046/j.1365-2745.2000.00439.x>
- Sheue, C.-R., Liu, H.-Y., & Yong, J. W. H. (2003). *Kandelia obovata* (rhizophoraceae), a new mangrove species from eastern asia. *TAXON*, 52(2), 287–294. <https://doi.org/10.2307/3647398>
- Sillanpää, M., Vantellingen, J., & Friess, D. A. (2017). Vegetation regeneration in a sustainably harvested mangrove forest in west papua, indonesia. *Forest*

References

- Ecology and Management*, 390, 137–146. <https://doi.org/10.1016/j.foreco.2017.01.022>
- Simard, M., Fatoyinbo, L., Smetanka, C., Rivera-Monroy, V. H., Castañeda-Moya, E., Thomas, N., & Van der Stocken, T. (2019). Mangrove canopy height globally related to precipitation, temperature and cyclone frequency. *Nature Geoscience*, 12(1), 40–45. <https://doi.org/10.1038/s41561-018-0279-1>
- Sippo, J. Z., Lovelock, C. E., Santos, I. R., Sanders, C. J., & Maher, D. T. (2018). Mangrove mortality in a changing climate: An overview. *Estuarine, Coastal and Shelf Science*, 215, 241–249. <https://doi.org/10.1016/j.ecss.2018.10.011>
- Sloey, T. M., Lim, K. E., Moore, J., Heng, J. M., Heng, J. M., & van Breugel, M. (2022). Influence of abiotic drivers on 1-year seedling survival of six mangrove species in southeast asia [Publisher: Wiley Online Library]. *Restoration Ecology*, e13694.
- Smith, T. J., Anderson, G. H., Balentine, K., Tiling, G., Ward, G. A., & Whelan, K. R. T. (2009). Cumulative impacts of hurricanes on florida mangrove ecosystems: Sediment deposition, storm surges and vegetation. *Wetlands*, 29(1), 24–34. <https://doi.org/10.1672/08-40.1>
- Smith III, T. J., Robblee, M. B., Wanless, H. R., & Doyle, T. W. (1994). Mangroves, hurricanes, and lightning strikes: Assessment of hurricane andrew suggests an interaction across two differing scales of disturbance. *BioScience*, 44(4), 256–262.
- Sobrado, M. A. (2007). Relationship of water transport to anatomical features in the mangrove *Laguncularia racemosa* grown under contrasting salinities. *New Phytologist*, 173(3), 584–591. <https://doi.org/10.1111/j.1469-8137.2006.01927.x>
- Srikanth, S., Lum, S. K. Y., & Chen, Z. (2016). Mangrove root: Adaptations and ecological importance. *Trees*, 30(2), 451–465. <https://doi.org/10.1007/s00468-015-1233-0>
- Stokes, D. J., & Harris, R. J. (2015). Sediment properties and surface erodibility following a large-scale mangrove (*avicennia marina*) removal. *Continental Shelf Research*, 107, 1–10. <https://doi.org/10.1016/j.csr.2015.07.011>
- Su, J., Friess, D. A., & Gasparatos, A. (2021). A meta-analysis of the ecological and economic outcomes of mangrove restoration. *Nature communications*, 12(1), 1–13.
- Suárez, N., & Medina, E. (2005). Salinity effect on plant growth and leaf demography of the mangrove, *avicennia germinans* l. *Trees*, 19(6), 722–728. <https://doi.org/10.1007/s00468-005-0001-y>

References

- Sun, Q., & Lin, P. (1997). Wood structure of *aegiceras corniculatum* and its ecological adaptations to salinities. *Asia-Pacific Conference on Science and Management of Coastal Environment*, 61–66.
- Suzuki, T., Hu, Z., Kumada, K., Phan, L. K., & Zijlema, M. (2019). Non-hydrostatic modeling of drag, inertia and porous effects in wave propagation over dense vegetation fields. *Coastal Engineering*, 149, 49–64. <https://doi.org/https://doi.org/10.1016/j.coastaleng.2019.03.011>
- Suzuki, T., Zijlema, M., Burger, B., Meijer, M. C., & Narayan, S. (2012). Wave dissipation by vegetation with layer schematization in SWAN. *Coastal Engineering*, 59(1), 64–71. <https://doi.org/10.1016/j.coastaleng.2011.07.006>
- Svejkovsky, J., Ogurcak, D. E., Ross, M. S., & Arkowitz, A. (2020). Satellite image-based time series observations of vegetation response to hurricane irma in the lower florida keys. *Estuaries and Coasts*, 43(5), 1058–1069.
- Taillie, P. J., Roman-Cuesta, R., Lagomasino, D., Cifuentes-Jara, M., Fatoyinbo, T., Ott, L. E., & Poulter, B. (2020). Widespread mangrove damage resulting from the 2017 atlantic mega hurricane season [Publisher: IOP Publishing]. *Environmental Research Letters*, 15(6), 064010.
- Takagi, H., Xiong, Y., & Furukawa, F. (2018). Track analysis and storm surge investigation of 2017 typhoon hatsu: Were the warning signals issued in macau and hong kong timed appropriately? *Georisk: Assessment and Management of Risk for Engineered Systems and Geohazards*, 12(4), 297–307.
- Tanaka, K. (2008, June). *Effectiveness and limitation of the coastal vegetation for storm surge disaster mitigation*. Investigation Team of Japan Society of Civil Engineering. http://www.jsce.or.jp/report/46/files/Bangladesh_Investigation.pdf
- Telewski, F. W. (2021). Mechanosensing and plant growth regulators elicited during the thigmomorphogenetic response. *Frontiers in Forests and Global Change*, 3, 147.
- Temmerman, S., Meire, P., Bouma, T. J., Herman, P. M. J., Ysebaert, T., & De Vriend, H. J. (2013). Ecosystem-based coastal defence in the face of global change. *Nature*, 504(7478), 79–83. <https://doi.org/10.1038/nature12859>
- Temmink, R. J. M., Lamers, L. P. M., Angelini, C., Bouma, T. J., Fritz, C., van de Koppel, J., Lexmond, R., Rietkerk, M., Silliman, B. R., Joosten, H., & van der Heide, T. (2022). Recovering wetland biogeomorphic feedbacks to restore the world's biotic carbon hotspots [Publisher: American Association for the Advancement of Science]. *Science*, 376(6593), eabn1479. <https://doi.org/10.1126/science.abn1479>
- Terrados, J., Thampanya, U., Srichai, N., Kheowvongsri, P., Geertz-Hansen, O., Boromthanarath, S., Panapitukkul, N., & Duarte, C. (1997). The effect of

References

- increased sediment accretion on the survival and growth of *Rhizophora apiculata* Seedlings. *Estuarine, Coastal and Shelf Science*, 45(5), 697–701. <https://doi.org/10.1006/ecss.1997.0262>
- Thampanya, U., Vermaat, J. E., & Terrados, J. (2002). The effect of increasing sediment accretion on the seedlings of three common thai mangrove species. *Aquatic Botany*, 11.
- Tomlinson, P. B. (2016). *The botany of mangroves*. [OCLC: 961059425]. Cambridge University Press. Retrieved April 12, 2021, from <https://doi.org/10.1017/CBO9781139946575>
- Tomlinson, P. B., & Cox, P. A. (2000). Systematic and functional anatomy of seedlings in mangrove rhizophoraceae: Vivipary explained? *Botanical Journal of the Linnean Society*, 134(1), 215–231. <https://doi.org/10.1111/j.1095-8339.2000.tb02352.x>
- Uddin, M. M., Hossain, M. M., Aziz, A. A., & Lovelock, C. E. (2022). Ecological development of mangrove plantations in the bangladesh delta. *Forest Ecology and Management*, 517, 120269. <https://doi.org/10.1016/j.foreco.2022.120269>
- UNEP. (2020). *The triple planetary crisis: Forging a new relationship between people and the earth*. <https://www.unep.org/news-and-stories/speech/triple-planetary-crisis-forging-new-relationship-between-people-and-earth>
- Urata, T., Shibuya, M., Koizumi, A., Torita, H., & Cha, J. (2012). Both stem and crown mass affect tree resistance to uprooting. *Journal of Forest Research*, 17(1), 65–71. <https://doi.org/10.1007/s10310-011-0249-6>
- Valiela, I., Bowen, J. L., & York, J. K. (2001). Mangrove forests: One of the world's threatened major tropical environments: At least 35% of the area of mangrove forests has been lost in the past two decades, losses that exceed those for tropical rain forests and coral reefs, two other well-known threatened environments. *Bioscience*, 51(10), 807–815.
- Van Coppenolle, R., Schwarz, C., & Temmerman, S. (2018). Contribution of mangroves and salt marshes to nature-based mitigation of coastal flood risks in major deltas of the world. *Estuaries and Coasts*, 41(6), 1699–1711. <https://doi.org/10.1007/s12237-018-0394-7>
- Van der Stocken, T., De Ryck, D., Vanschoenwinkel, B., Deboelpaep, E., Bouma, T., Dahdouh-Guebas, F., & Koedam, N. (2015). Impact of landscape structure on propagule dispersal in mangrove forests. *Marine Ecology Progress Series*, 524, 95–106. <https://doi.org/10.3354/meps11206>
- Van der Stocken, T., Wee, A. K. S., De Ryck, D. J. R., Vanschoenwinkel, B., Friess, D. A., Dahdouh-Guebas, F., Simard, M., Koedam, N., & Webb, E. L. (2019). A general framework for propagule dispersal in mangroves: A general

References

- framework for propagule dispersal in mangroves. *Biological Reviews*, 94(4), 1547–1575. <https://doi.org/10.1111/brv.12514>
- van Bijsterveldt, C. E. J., Debrot, A. O., Bouma, T. J., Maulana, M. B., Pribadi, R., Schop, J., Tonneijck, F. H., & van Wesenbeeck, B. K. (2022). To plant or not to plant: When can planting facilitate mangrove restoration? *Frontiers in Environmental Science*, 9. Retrieved June 14, 2022, from <https://www.frontiersin.org/article/10.3389/fenvs.2021.690011>
- van Bijsterveldt, C. E. J., van Wesenbeeck, B. K., Ramadhani, S., Raven, O. V., van Gool, F. E., Pribadi, R., & Bouma, T. J. (2021). Does plastic waste kill mangroves? a field experiment to assess the impact of macro plastics on mangrove growth, stress response and survival. *Science of The Total Environment*, 756, 143826. <https://doi.org/10.1016/j.scitotenv.2020.143826>
- van Bijsterveldt, C. E., van Wesenbeeck, B. K., van der Wal, D., Afiati, N., Pribadi, R., Brown, B., & Bouma, T. J. (2020). How to restore mangroves for greenbelt creation along eroding coasts with abandoned aquaculture ponds. *Estuarine, Coastal and Shelf Science*, 235, 106576. <https://doi.org/10.1016/j.ecss.2019.106576>
- van Veelen, T. J., Fairchild, T. P., Reeve, D. E., & Karunarathna, H. (2020). Experimental study on vegetation flexibility as control parameter for wave damping and velocity structure. *Coastal Engineering*, 157, 103648. <https://doi.org/10.1016/j.coastaleng.2020.103648>
- van Veelen, T. J., Karunarathna, H., & Reeve, D. E. (2021). Modelling wave attenuation by quasi-flexible coastal vegetation. *Coastal Engineering*, 164, 103820. <https://doi.org/10.1016/j.coastaleng.2020.103820>
- van Wesenbeeck, B. K., IJff, S., Jongman, B., Balog, S. A. B., Kaupa, S. M., Bosche, L. V., Lange, G.-M., Holm-Nielsen, N. B., Nieboer, H., Taishi, Y., et al. (2017). Implementing nature based flood protection: Principles and implementation guidance.
- van Wesenbeeck, B. K., Wolters, G., Antolínez, J. A. A., Kalloe, S. A., Hofland, B., de Boer, W. P., Çete, C., & Bouma, T. J. (2022). Wave attenuation through forests under extreme conditions. *Scientific Reports*, 12(1), 1884. <https://doi.org/10.1038/s41598-022-05753-3>
- van Zelst, V. T. M., Dijkstra, J. T., van Wesenbeeck, B. K., Eilander, D., Morris, E. P., Winsemius, H. C., Ward, P. J., & de Vries, M. B. (2021). Cutting the costs of coastal protection by integrating vegetation in flood defences [Number: 1 Publisher: Nature Publishing Group]. *Nature Communications*, 12(1), 6533. <https://doi.org/10.1038/s41467-021-26887-4>

References

- Virgulino-Júnior, P. C. C., Gardunho, D. C. L., Silva, D. N. C., & Fernandes, M. E. B. (2020). Wood density in mangrove forests on the Brazilian Amazon coast. *Trees*, 34(1), 51–60. <https://doi.org/10.1007/s00468-019-01896-5>
- Vogel, S. (2009). Leaves in the lowest and highest winds: Temperature, force and shape. *New Phytologist*, 183(1), 13–26. <https://doi.org/10.1111/j.1469-8137.2009.02854.x>
- Vollinger, S., Mitchell, S. J., Byrne, K. E., Novak, M. D., & Rudnicki, M. (2005). Wind tunnel measurements of crown streamlining and drag relationships for several hardwood species. *Canadian Journal of Forest Research*, 35(5), 1238–1249. <https://doi.org/10.1139/x05-051>
- Vovides, A. G., Berger, U., & Balke, T. (2021). Morphological plasticity and survival thresholds of mangrove plants growing in active sedimentary environments. In *Dynamic sedimentary environments of mangrove coasts* (pp. 121–140). Elsevier.
- Vovides, A. G., Marín-Castro, B., Barradas, G., Berger, U., & López-Portillo, J. (2016). A simple and cost-effective method for cable root detection and extension measurement in estuary wetland forests. *Estuarine, Coastal and Shelf Science*, 183, 117–122. <https://doi.org/10.1016/j.ecss.2016.10.029>
- Vuik, V., Jonkman, S. N., Borsje, B. W., & Suzuki, T. (2016). Nature-based flood protection: The efficiency of vegetated foreshores for reducing wave loads on coastal dikes. *Coastal Engineering*, 116, 42–56. <https://doi.org/10.1016/j.coastaleng.2016.06.001>
- Walcker, R., Gandois, L., Proisy, C., Corenblit, D., Mougin, É., Laplanche, C., Ray, R., & Fromard, F. (2018). Control of “blue carbon” storage by mangrove ageing: Evidence from a 66-year chronosequence in French Guiana [eprint: <https://onlinelibrary.wiley.com/doi/pdf/10.1111/gcb.14100>]. *Global Change Biology*, 24(6), 2325–2338. <https://doi.org/10.1111/gcb.14100>
- Walters, C. J. (1986). *Adaptive management of renewable resources*. Macmillan Publishers Ltd.
- Wang, B., Guo, X., & Mei, C. C. (2015). Surface water waves over a shallow canopy [Publisher: Cambridge University Press]. *Journal of Fluid Mechanics*, 768, 572–599. <https://doi.org/10.1017/jfm.2015.110>
- Wang, W., Li, X., & Wang, M. (2019). Propagule dispersal determines mangrove zonation at intertidal and estuarine scales. *Forests*, 10(3), 245. <https://doi.org/10.3390/f10030245>
- Ward, R. D., Friess, D. A., Day, R. H., & Mackenzie, R. A. (2016). Impacts of climate change on mangrove ecosystems: A region by region overview [Publisher:

References

- Taylor & Francis _eprint: <https://doi.org/10.1002/ehs2.12111>]. *Ecosystem Health and Sustainability*, 2(4), e01211. <https://doi.org/10.1002/ehs2.12111>
- Waryszak, P., Palacios, M. M., Carnell, P. E., Yilmaz, I. N., & Macreadie, P. I. (2021). Planted mangroves cap toxic petroleum-contaminated sediments. *Marine Pollution Bulletin*, 171, 112746. <https://doi.org/10.1016/j.marpolbul.2021.112746>
- Watson, J. G. (1928). Mangrove forests of the malay peninsula. *Malayan forest records*, 6.
- Weng, B., Xie, X., Weiss, D. J., Liu, J., Lu, H., & Yan, C. (2012). *Kandelia obovata* (s. l.) yong tolerance mechanisms to cadmium: Subcellular distribution, chemical forms and thiol pools. *Marine Pollution Bulletin*, 64(11), 2453–2460. <https://doi.org/https://doi.org/10.1016/j.marpolbul.2012.07.047>
- Willemsen, P. W. J. M., Borsje, B. W., Hulscher, S. J. M. H., Van der Wal, D., Zhu, Z., Oteman, B., Evans, B., Möller, I., & Bouma, T. J. (2018). Quantifying bed level change at the transition of tidal flat and salt marsh: Can we understand the lateral location of the marsh edge? *Journal of Geophysical Research: Earth Surface*, 123(10), 2509–2524. <https://doi.org/10.1029/2018JF004742>
- Winterwerp, J. C., Erfteimeijer, P. L. A., Suryadiputra, N., van Eijk, P., & Zhang, L. (2013). Defining eco-morphodynamic requirements for rehabilitating eroding mangrove-mud coasts. *Wetlands*, 33(3), 515–526. <https://doi.org/10.1007/s13157-013-0409-x>
- Winterwerp, J. C., Albers, T., Anthony, E. J., Friess, D. A., Mancheño, A. G., Moseley, K., Muhari, A., Naipal, S., Noordermeer, J., Oost, A., et al. (2020). Managing erosion of mangrove-mud coasts with permeable dams—lessons learned. *Ecological Engineering*, 158, 106078.
- Woodroffe, C., Rogers, K., McKee, K., Lovelock, C., Mendelssohn, I., & Saintilan, N. (2016). Mangrove sedimentation and response to relative sea-level rise. *Annual Review of Marine Science*, 8(1), 243–266. <https://doi.org/10.1146/annurev-marine-122414-034025>
- Worthington, T. A., zu Ermgassen, P. S. E., Friess, D. A., Krauss, K. W., Lovelock, C. E., Thorley, J., Tingey, R., Woodroffe, C. D., Bunting, P., Cormier, N., Lagomasino, D., Lucas, R., Murray, N. J., Sutherland, W. J., & Spalding, M. (2020). A global biophysical typology of mangroves and its relevance for ecosystem structure and deforestation [Number: 1 Publisher: Nature Publishing Group]. *Scientific Reports*, 10(1), 14652. <https://doi.org/10.1038/s41598-020-71194-5>
- Xie, D., Schwarz, C., Brückner, M. Z. M., Kleinhans, M. G., Urrego, D. H., Zhou, Z., & van Maanen, B. (2020). Mangrove diversity loss under sea-level rise

References

- triggered by bio-morphodynamic feedbacks and anthropogenic pressures. *Environmental Research Letters*, 15(11), 114033. <https://doi.org/10.1088/1748-9326/abc122>
- Xie, D., Schwarz, C., Kleinhans, M. G., Zhou, Z., & van Maanen, B. (2022). Implications of coastal conditions and sea-level rise on mangrove vulnerability: A bio-morphodynamic modeling study. *Journal of Geophysical Research: Earth Surface*, 127(3), e2021JF006301. <https://doi.org/10.1029/2021JF006301>
- Xin, K., Zhou, Q., Arndt, S., & Yang, X. (2013). Invasive capacity of the mangrove *Sonneratia apetala* in hainan island, china. *Journal of Tropical Forest Science*, 9.
- Xu, H., Zhang, K., Shen, J., & Li, Y. (2010). Storm surge simulation along the u.s. east and gulf coasts using a multi-scale numerical model approach [ADS Bibcode: 2010OcDyn..60.1597X]. *Ocean Dynamics*, 60, 1597–1619. <https://doi.org/10.1007/s10236-010-0321-3>
- Yanez-Espinosa, L., Terrazas, T., Lopez-Mata, L., & Valdez-Hernandez, J. I. (2004). Wood variation in laguncularia racemosa and its effect on fibre quality. *Wood Science and Technology*, 38(3), 217–226.
- Yang, M., Défossez, P., Danjon, F., & Fourcaud, T. (2014). Tree stability under wind: Simulating uprooting with root breakage using a finite element method. *Annals of Botany*, 114(4), 695–709. <https://doi.org/10.1093/aob/mcu122>
- Yang, S. L., Shi, B. W., Bouma, T. J., Ysebaert, T., & Luo, X. X. (2012). Wave attenuation at a salt marsh margin: A case study of an exposed coast on the yangtze estuary. *Estuaries and Coasts*, 35(1), 169–182. <https://doi.org/10.1007/s12237-011-9424-4>
- Yang, S.-C., Shih, S.-S., Hwang, G.-W., Adams, J. B., Lee, H.-Y., & Chen, C.-P. (2013). The salinity gradient influences on the inundation tolerance thresholds of mangrove forests. *Ecological Engineering*, 51, 59–65. <https://doi.org/10.1016/j.ecoleng.2012.12.049>
- Yao, P., Chen, H., Huang, B., Tan, C., Hu, Z., Ren, L., & Yang, Q. (2018). Applying a new force–velocity synchronizing algorithm to derive drag coefficients of rigid vegetation in oscillatory flows. *Water*, 10(7), 906. <https://doi.org/10.3390/w10070906>
- Ye, Y., Tam, N. F., Wong, Y., & Lu, C. (2003). Growth and physiological responses of two mangrove species (*bruguiera gymnorrhiza* and *kandelia candel*) to waterlogging. *Environmental and Experimental Botany*, 49(3), 209–221. [https://doi.org/10.1016/S0098-8472\(02\)00071-0](https://doi.org/10.1016/S0098-8472(02)00071-0)
- Ye, Y., Tam, N. F.-Y., Lu, C.-Y., & Wong, Y.-S. (2005). Effects of salinity on germination, seedling growth and physiology of three salt-secreting mangrove

References

- species. *Aquatic Botany*, 83(3), 193–205. <https://doi.org/10.1016/j.aquabot.2005.06.006>
- Yin, K., Xu, S., Huang, W., & Xie, Y. (2017). Effects of sea level rise and typhoon intensity on storm surge and waves in pearl river estuary. *Ocean Engineering*, 136, 80–93. <https://doi.org/10.1016/j.oceaneng.2017.03.016>
- Yoshikai, M., Nakamura, T., Suwa, R., Argamosa, R., Okamoto, T., Rollon, R., Basina, R., Primavera-Tirol, Y. H., Blanco, A. C., Adi, N. S., & Nadaoka, K. (2021). Scaling relations and substrate conditions controlling the complexity of rhizophora prop root system. *Estuarine, Coastal and Shelf Science*, 248, 107014. <https://doi.org/10.1016/j.ecss.2020.107014>
- Ysebaert, T., Yang, S.-L., Zhang, L., He, Q., Bouma, T. J., & Herman, P. M. J. (2011). Wave attenuation by two contrasting ecosystem engineering salt marsh macrophytes in the intertidal pioneer zone. *Wetlands*, 31(6), 1043–1054. <https://doi.org/10.1007/s13157-011-0240-1>
- Zanetti, C., Vennetier, M., Mériaux, P., & Provansal, M. (2015). Plasticity of tree root system structure in contrasting soil materials and environmental conditions. *Plant and Soil*, 387(1), 21–35. <https://doi.org/10.1007/s11104-014-2253-z>
- Zhang, K., Liu, H., Li, Y., Xu, H., Shen, J., Rhome, J., & Smith, T. J. (2012). The role of mangroves in attenuating storm surges. *Estuarine, Coastal and Shelf Science*, 102–103, 11–23. <https://doi.org/10.1016/j.ecss.2012.02.021>
- Zhang, X., Chua, V. P., & Cheong, H.-F. (2015). Hydrodynamics in mangrove prop roots and their physical properties. *Journal of hydro-environment research*, 9(2), 281–294.
- Zhang, X., & Nepf, H. (2021). Wave damping by flexible marsh plants influenced by current [Publisher: American Physical Society]. *Phys. Rev. Fluids*, 6(10), 100502. <https://doi.org/10.1103/PhysRevFluids.6.100502>
- Zhao, C., Tang, J., Shen, Y., & Wang, Y. (2021). Study on wave attenuation in following and opposing currents due to rigid vegetation. *Ocean Engineering*, 236, 109574. <https://doi.org/https://doi.org/10.1016/j.oceaneng.2021.109574>
- Zhong, C., Li, S., Yang, Y., Zhang, Y., & Lin, Z. (2011). Analysis of the introduction effect of a mangrove species laguncularia racemosa. *Journal of Fujian Forestry Science and Technology*, 38(3), 96–99.
- Zhu, Q., van Prooijen, B. C., Wang, Z. B., Ma, Y. X., & Yang, S. L. (2016). Bed shear stress estimation on an open intertidal flat using in situ measurements. *Estuarine, Coastal and Shelf Science*, 182, 190–201. <https://doi.org/10.1016/j.ecss.2016.08.028>
- Zhu, Z., Vuik, V., Visser, P. J., Soens, T., van Wesenbeeck, B., van de Koppel, J., Jonkman, S. N., Temmerman, S., & Bouma, T. J. (2020). Historic storms and

References

- the hidden value of coastal wetlands for nature-based flood defence. *Nature Sustainability*, 3(10), 853–862. <https://doi.org/10.1038/s41893-020-0556-z>
- Zhu, Z., Yang, Z., & Bouma, T. J. (2019). Biomechanical properties of marsh vegetation in space and time: Effects of salinity, inundation and seasonality. *Annals of Botany*, mcz063. <https://doi.org/10.1093/aob/mcz063>